PhD Thesis

Granulation of Hydrophobic Particles: Production of Hollow Granules from Liquid Marbles

By

Nicky Eshtiaghi
M. Eng. (Chem. Eng.), B. Sc. (Chem. Eng.) (1st Hons)

Supervisor: Dr Karen Hapgood

Department Of Chemical Engineering
Faculty of Engineering
Monash University
Australia
December 2009

Errata:

P. VIII Line 11: "Ψ_a" for "Ψa"

P. VIII Line 13, P.221 Line 10, and P.227 Line 4: "110 °" for "110 °C"

P. 29 Line 5: "Re" for "N_{Re}"

P. 29 Line 7: "m/s^2" for "m^2/s"

P. 33 Line 6: "ρ_L" for "ρ" and "γ_{LV}" for "γ"

P. 88 Table 1 column 2: "17" for "0.17", "33" for "0.33", "50" for "0.5", "67" for" 0.67", and "83" for "0.83".

Addendum:

P. III: Add another paragraph at the end of declaration page:
The last paragraph of the Page 98 in the Chapter 4 changed from "... the *b* represents the ease of liquid marble formation (%coverage/ unit energy) and the *E* is the kinetic energy of impact." to "... the *b* represents the ease of liquid marble formation (1/μJ) and the *E* is the kinetic energy of impact (μJ)." . The unit for *b* in Table 4 on Page 100 also changed from (%coverage/ unit energy) to (1/μJ).

P. VIII Line 4: Delete "$d_d > 25\ d_p$" and read "droplet diameter (d_d)> 25 particle diameter (d_p)"

P. VIII Line 7: Delete "(Ψ_a <<1)" and read "(Ψ_a <<1, the dimension spray flux ($\Psi_a = \frac{3\dot{V}}{2\dot{A}d_d}$) is a measure of spray density and drop overlap in the spray zone where $\dot{V}$ (m^3/s) is a volumetric spray flow rate, d_d is an average drop size, and $\dot{A}$ (m^2/s) is powder flux through wetted spray area)"

P. 33 Line 4: Delete "(We>10 and Re>10)" and read "($We = \frac{\rho_L d_d v^2}{\gamma_{LV}} > 10$ and $Re = \frac{\rho_L v d_d}{\mu} > 10$, d_d the droplet diameter, *v* the impact velocity)".

P. 36 Line 12: Delete "contact zone radius" and read "contact zone length"

P. 36 Line 17: Delete "These formulas are independent of drop volume."

P. 96 Line 7: Delete "proportional" and read "exponential"

P. 98 Line 7: Delete "(coverage/unit energy)" and read" (1/μJ)"

P. 100 Table 4: Delete "*b* (%/μJ)" and read "*b* (1/μJ)"

P. 102 Table 5: Delete "*b* (%/μJ)" and read "*b* (1/μJ)"

Comment:
P. VIII Line 4: see the nomenclature of Chapter 3 for definition We and Re.
$\lambda_{SL}, \lambda_{S/L}$ is the same all through chapters.

MONASH UNIVERSITY

Monash Research Graduate School

Declaration for thesis based or partially based on co-jointly published or unpublished work

General Declaration:

In accordance with Monash University Doctorate Regulation 17/ Doctor of Philosophy and Master of Philosophy (MPhil) regulations the following declarations are made:

I hereby declare that this thesis contains no material which has been accepted for the award of any other degree or diploma at any university or equivalent institution and that, to the best of my knowledge and belief, this thesis contains no material previously published or written by another person, except where due reference is made in the text of the thesis.

This thesis includes four published and one submitted original papers in peer reviewed journals. The core theme of the thesis is the granulation of hydrophobic powders. The ideas, development and writing up of all the papers in the thesis were the principal responsibility of me, the candidate, working within the Monash Advanced Particle Engineering Laboratory, Department of Chemical Engineering, Monash University, under the supervision of Dr. Karen P. Hapgood.

The inclusion of co-authors reflects the fact that the work came from active collaboration between researchers and acknowledges input into team-based research.

In the case of listed below, my contribution to the work involved the following:

Thesis chapter	Publication title	Publication status	Nature and extent of candidate's contribution
3	Granulation of hydrophobic powders	Published	Initiations, Key ideas, Experimental works, Analysis works, Development and writing up
4	Liquid marble formation: spreading coefficients or kinetic energy?	Published	
5	An analysis of the thermodynamic conditions for solid powder particles spreading over liquid surface	Submitted	
6	Formation of hollow granules from liquid marbles: small scale experiments	Published	
7	Producing hollow granules from hydrophobic powders in high-shear mixer granulators	Published	

I have renumbered sections of submitted or published papers in order to generate a consistent presentation within the thesis. There is also a post-publication correction on Chapter 4 and Chapter 6.

The last paragraph of the Page 98 in the Chapter 4 changed from "… the *b* represents the ease of liquid marble formation (%coverage/ unit energy) and the *E* is the kinetic energy of impact." to "… the *b* represents the ease of liquid marble formation (1/μJ) and the *E* is the kinetic energy of impact (μJ)." . The unit for *b* in Table 4 on Page 100 also changed from (%coverage/ unit energy) to (1/μJ).

The last paragraph of the page 134 in the Chapter 6 changed from "… is extended by using small particles (e.g. graphite 10-20 μm) rather than larger particles (e.g. PTFE 5-7 μm)" to "…extended by using large particles (e.g. graphite 10-20 μm) rather than smaller particles (e.g. PTFE 7-12 μm)".

Signed: ……

Date: ……

Acknowledgments:

My humble thanks go to Almighty God for the merciful care.

I wish to express my sincere appreciation to my supervisor, Dr Karen Hapgood, for her kind guidance and support throughout of this research study. Indeed, the support given by reviewing the publications and the thesis is invaluable.

Many thanks go to Dr Wei Shen and Dr Leslie Yeo who have contributed toward my understanding and thought. I would like to thank all friends and the academic and administrative staff in Chemical Engineering Department who have provided assistance at various occasions.

I am grateful to Monash University for providing the financial support for my study, and many thanks go to Australian Research Council (ARC) to support this study though the Discovery Projects program (DP0770462).

I acknowledge with gratitude the assistance in experimental work given by Dr Benedicta Arahatari, Mr Jacques Liu, Mr David Barling, and Dr Shyamal Das.

Finally, but most importantly, my sincere gratitude also goes to my husband and my daughter for their moral support and love.

List of publications from this research:

- **Peer-Reviewed Journal Papers**

The following publications are included in this thesis:

1. **Eshtiaghi, N**., Liu, Jacques S., Hapgood, Karen P., "*Formation of Hollow granules from liquid marbles: Small Scale experiments*", Powder Technology, (2010), Vol. 197, P. 184-195.
2. **Eshtiaghi, N**., Liu, Jacques S., Shen, Wei, Hapgood, Karen P., "*Liquid marble formation: Spreading coefficient or Kinetic energy?*", Powder Technology, (2009), Vol. 196, P. 126-132.
3. **Eshtiaghi, N**., Arhtari B., Hapgood K., "*Producing hollow granules from hydrophobic powders in high-shear mixer granulators*", Advanced Powder Technology, (2009), Vol. 20, P. 558-566.
4. Hapgood, K., **Khanmohammadi, B.***, "*Granulation of hydrophobic powders*", Powder Technology, special issue on granulation, (2009), Vol. 189, P. 253-262.
5. Nguyen, T.H., **Eshtiaghi, N.**, Hapgood, K.P., Wei, S., "*An analysis of the thermodynamic conditions for solid powder particles spreading over liquid surface*", submitted to Powder Technology.
6. Arhtari B., Gates, W. P., **Eshtiaghi, N.**, Peele, A.G., "*Phase retrieval tomography in the presence of noise*", Journal of Applied Physics, 2010, Vol.107, P.034904/1-7.

- **Peer-Reviewed Conference Papers**

The following conference papers were presented in international conferences during this research but not included in the thesis:

7. **Eshtiaghi, N**., Liu, Jacques S., Hapgood, K., "*Key Factors in stable Formation of Liquid marble and Hollow Granules*", CHEMECA Conference, 28 Sep. - 1 Oct., 2008, Newcastle, Australia.
8. **Khanmohammadi, B.***, Leslie, Y., Hapgood, K., "*Formation of Hollow Granule from Hydrophobic Powders*", CHEMECA Conference, 23-26 September, 2007, Melbourne, Australia.
9. Hapgood, K., **Khanmohammadi, B.***, "*Nucleation and Granulation of Hydrophobic Powders*", Third International Granulation Workshop, 27-29 June, 2007, Sheffield, England.

* Previous Name "Batool Khanmohammadi" (changed by Deed Poll on July 2008)

Summary:

This thesis investigates granulation of hydrophobic powders. Recently discovered hollow granules formed via spreading of hydrophobic particles around a liquid droplet appear promising to solve the problematic wetting behavior of hydrophobic powders. This new way of granulating hydrophobic powders has not been previously investigated. This thesis focuses on the nucleation stage of hydrophobic powders and investigates the spreading mechanism of particles around a liquid droplet, which is known as liquid marble. The formation of hollow granules from liquid marbles, and the mass production of hollow granules in a mixer granulator are also a main point in this thesis.

An entirely physical flow mechanism for the nucleation stage of liquid marbles was proposed instead of the spreading coefficient theory. Experimental work for testing this mechanism was carried out by studying the effect of binder and powder properties as well as the effect of kinetic energy of impact on powder coverage of the drop. Based on experimental results, a proportional relationship was found between increasing kinetic energy and the percentage of liquid marble coverage. Moreover, calculation of the solid-liquid spreading coefficient and thermodynamic analysis of the existing solid-liquid spreading coefficient revealed that the existing solid-liquid spreading coefficient theory is not a predictive approach. This analysis also pointed out some serious flaws in the assumptions used in definition of the solid-liquid spreading coefficient (Rowe, 1989) in terms of simply exchanging the solid-liquid subscript in liquid-solid spreading coefficient equation, as the thermodynamic conditions taking place during spreading solid over a liquid are quite different to spreading liquid over a solid substrate.

Drying of liquid marbles and the formation of hollow granules was investigated in small scale experiments by employing several types of binder with different concentrations as well as various types of powder with different particle sizes at two selected drying temperatures. Higher drying temperature, smaller or nano-sized particles and higher binder concentration tend to promote the formation of perfect hollow granules. It was found that the survival rate was directly proportional to binder viscosity for HPMC and PVP. However for HPC binder, the survival rate was essentially constant regardless of HPC concentration due to precipitation of the HPC binder above the cloud point temperature.

In the next step, the insight gained in small scale experiments helped to successfully produce hollow granules in large scale experiments using a 4 L laboratory scale granulator. The optimum liquid to solid ratio (L:S) ratio for Aerosil and 5% HPC was found by studying the effect of different liquid to solid ratio on the morphology of formed granules. At the optimum L:S ratio, more of the raw fine particles were granulated and fewer flattened or stretched hollow granules were produced. In addition, the experimental observations of different granule morphologies revealed the importance of performing X-ray tomography during hollow granule formulation. If the nucleation process starts with a preformed template droplet (e.g. spraying liquid), the final granule size increases as the L:S ratio increases as well as the amount of un-granulated fine particles decreases.

Finally, a framework for liquid marble formation via solid spreading nucleation (droplet template) and via mechanical dispersion was proposed by outlining the sequential steps and possible controlling groups for each step. The first step of the framework via droplet template starts with droplet diameter (d_d)> 25 particle diameter (d_p) then it follows with Bo^*<1 and We^*<1000 in order to produce a spherical cap without shattering on powder bed. The next step requirement is that the contact angle of the liquid on the powder must be above 90º. If spray flux is low enough (Ψ_a<<1, the dimension spray flux ($\Psi_a=3\dot{V}/2\dot{A}d_d$) is a measure of spray density and drop overlap in the spray zone where $\dot{V}$ (m^3/s) is a volumetric spray flow rate, d_d is an average drop size, and $\dot{A}$ (m^2/s) is powder flux through wetted spray area) and there is enough kinetic energy, an individual spherical liquid marble will be formed, providing that the energetic contribution E_p of system is within the acceptable range. The main difference between droplet template and mechanical dispersion frameworks are contact angle and spray flux requirement. When spray flux becomes greater than one (Ψ_a>1), granulation switches from droplet template regime to mechanical dispersion regime. Liquid marble can form successfully in mechanical dispersion regime if the contact angle is above 110 º.

A framework for hollow granule formation from liquid marbles was also developed. In this framework, the importance of presence of compatible polymeric binder at the optimum concentration was emphasized as the first requirement for hollow granule formation. The optimum L:S ratio and drying temperature are additional criteria for a successful formation of single cavity hollow granule.

*see the nomenclature of Chapter 3 for definition

These frameworks give a better understanding of the controlling mechanisms in granulation of hydrophobic particles and provide guidance on how to mass produce liquid marbles and hollow granules.

Table of contents:

1

Introduction

Chapter 1: Introduction

Wet granulation is a unit operation which is widely used in a range of industries such as the cosmetic, pharmaceutical, food and mineral industries in order to enlarge the particle size using a liquid binder. The reasons for granulation are: to densify the material, to enhance the flow, to reduce dust and material segregation (Litster and Ennis, 2004). In the pharmaceutical industry, a tablet with good characteristic such as uniform concentration of active ingredients and excipients is not made on a tablet press; it is made in granulation process (Tousey, 2002).

Among all existing size enlargement operations, wet granulation in high shear mixers has generated a lot of interest because it allows regular shaped granules with a high degree of compaction to be obtained. High shear mixers have been extensively used in the pharmaceutical and chemical industries since 1970 (Parikh, 1997). High shear mixers work by agitating the powder using an impeller while liquid (binder) is sprayed onto the powder from above. A number of books and review papers are available, which summarize the state of knowledge in this field (Parikh, 1997; Litster and Ennis, 2004, etc).

Wet granulation can be divided in three major phenomena occurring simultaneously in a granulator: wetting and nucleation, consolidation and growth, and attrition and breakage (Iveson *et al.,* 2001a). Over the last decade, great progress has been made on understanding and controlling wet granulation mechanisms as well as producing granules with a consistent, reproducible size distribution (Iveson *et al.,* 2001a). The granulation

process can be very simple or very complex depending on the characteristics of the powders. If the active ingredient represents a high percentage of the blended material and is also hydrophobic as is the case for many drugs in the pharmaceutical industry, then problems may begin. Granulation of non-wetting (hydrophobic) particles is a common problem in pharmaceutical, minerals and fertilizer granulation; however, there are few studies on how to control the hydrophobic granulation process.

Although it is possible to add a surfactant to the binder fluid to compensate for the poor wetting characteristics of hydrophobic powder, this method is not applicable for certain pharmaceutical formulations and iron ore granulation. Therefore, the current state of knowledge of granulation is not sufficient to slove this problem (Iveson *et al.,* 2001a; Iveson *et al.,* 2001b; Mort, 2005).

Hollow granule formation is a new way to solve the problematic granulating behavior of hydrophobic powders. The nucleation process of hydrophobic particles proceeds by spreading solid over liquid drop surface instead of wetting of the powder by the liquid, and has recently been discovered. The nuclei formed in this process is named "Solid Spreading Nuclei" (Farber *et al.,* 2006), or "liquid marble" (Aussillous and Quere, 2001; 2006) or "dry water" (Forny *et a.,l* 2009). The porous and hollow structure of granules formed by this mechanism has excellent compression properties for the tabletting process, and good drug release and dissolution rates due to the thin shell thickness (Hapgood *et al.,* 2009). It may be possible to create "designer granules" with a controlled size distribution and pre-defined granule structure by controlling the solid shell thickness.

1.1 Thesis objectives

This study aims to build on the recent advances in granulation theory and extend them to include the mechanisms controlling granulation of hydrophobic and non-wetting systems. This study focuses on the nucleation stage of hydrophobic particles and then by gaining knowledge into physical phenomenon occurring in the nucleation stage, it will be possible to control the granulation process. Experimental investigations were designed to understand the mechanism of solid spreading over liquid droplets and liquid marble formation. This research investigates the required conditions to form a stable, spherical, liquid marble from a single drop via solid spreading nucleation and the conditions required to form hollow granules from these liquid marbles.

This study aims to understand:

- The mechanism of liquid marble formation.
- The effect of fluid and powder properties on formation of liquid marbles.
- The effect of binder viscosity and binder type and powder properties (especially particle size) on the formation of hollow granule and liquid marbles.
- The effect of drying conditions on formulation of hollow granules from liquid marbles.
- The effect of changing the liquid to solid mass ratio in a high-shear mixer granulator on granule size and structure.

1.2 Thesis outline

To achieve these aims, Chapter 2 gives the summary of the current understanding of non-wetting granulation and other areas of knowledge which are applicable to hollow granule formation. Literature related to the phenomena of liquid drop impact on solid surface was

reviewed in order to describe the desired regime for producing spherical liquid marbles. Then, in order to understand the mechanism by which particles remain on the surface of droplet, the motion of fluid inside of droplet after impinging on a surface was reviewed.

In chapter 3, the nucleation behavior of a single drop on a bed of hydrophobic powder is investigated and a preliminary framework for liquid marble formation is proposed by outlining the sequential steps and possible controlling groups for each step. The results of this study have been published in Powder Technology (V.189, P: 253-262, 2009).

Chapter 4 investigates in more detail the final step of the proposed framework presented in Chapter 3. This chapter presents the solid-liquid spreading coefficient (λ_{SL}) calculations and studies the effect of the kinetic energy of impact on liquid marble formation for various fluids and particles in order to show whether or not the spreading coefficients predict liquid marble formation. Finally, this chapter discusses how the powder coverage of the drop is driven entirely by a physical flow mechanism and is related to the applied kinetic energy, where the degree of surface coverage is proportional to the size of the bulk flow generated within the drop due either to rolling or impact and is not due to the spreading coefficient. This work has been accepted for publication in Powder Technology (V. 196, P: 126-132, 2009).

A more rigorous thermodynamic analysis on the existing solid-spreading coefficient has been presented in Chapter 5. By examining the fundamental surface chemistry and thermodynamic conditions taking place during solid spreading over a liquid surface, this

chapter shows why the existing solid-liquid spreading coefficient theory is not a predictive approach. The analysis points out some serious flaws in the assumptions used in the definition of the solid-spreading coefficient (Rowe, 1989), in terms of exchanging the solid-air interface for a solid-liquid interface. This work has been submitted to Powder Technology and is under review.

Chapter 6 investigates the formation of hollow granules by drying liquid marbles. A variety of powder-fluid combinations and a range of drying temperatures are tested at laboratory scale to investigate what happens to the liquid marble as the template drop is removed during drying. The aim is to identify the optimal drying conditions to produce stable hollow granules from liquid marble nuclei at small scale. This work has been accepted for publication in Powder Technology (V. 197, P: 184-195, 2010).

Chapter 7 introduces the mass production of hollow granules in a high-shear mixer granulator. Based on the knowledge gained in Chapter 6, a successful combination of powder, binder and drying conditions were chosen as the conditions for the large scale experiments. The effect of changing the liquid/solid mass ratio on hollow granule size and structure were investigated. The granule morphology and structure were investigated using SEM and X-ray tomography (XRT). The optimal liquid to solid mass ratio was determined for the powder and binder chosen in this study. This work has been accepted for publication in Advanced Powder Technology Journal (V. 20, P: 558-566, 2009).

In Chapter 8, the preliminary proposed framework for liquid marble formation presented in Chapter 3 is validated and extended to cover additional required steps for formation of hollow granules from liquid marbles. A framework for formation of liquid marble via mechanical dispersion regime is also introduced.

Conclusions are in Chapter 9, followed by the Appendices which contain the published format of papers, scanning electron microscopy (SEM) images and X-ray tomography (XRT) images of hollow granules for different liquid/solid mass ratios. The appendices also contain a paper on the benefits of phase retrieval tomography which was triggered by our experimental work but it is not directly relevant to the main direction of this thesis. This work has been accepted for publication in Journal of Applied Physics (V. 107, P: 034904-034904-7, 2010).

1.3 References:

Aussillous, P., D. Quere (2001). "Liquid marbles". Nature **411**: 924-927.

Aussillous, P., D. Quere (2006). "*Properties of liquid marbles*". Proceedings of Mathematical, physical, and engineering sciences **462**:973-999.

Farber, L., K. Hapgood, JN.Michaels (2006). "*Hydrophobic nucleation in particle agglomeration*". World Congress of Particle Technology 5, Lake Buena Vista FL USA.

Forny, L., K. Saleh, I.Pezron, P. Guigon, L. Komunjer (2009)." Encapsulation: a way to produce dry water". Powder Technology, special issue on granulation **189**: 263-269.

Hapgood, K. P., L. Farber, J.N. Michaels (2009)."Agglomeration of hydrophobic powders via solid spreading nucleation". Powder Technology **188**: 248-254.

Hapgood, K. P., B. Khanmohammadi (2009)."Granulation of hydrophobic powders". Powder Technology, special issue on granulation **188**: 248-254.

Iveson, S., J. Litster, K. Hapgood (2001a). "Nucleation, growth and breakage phenomena in agitated wet granulation processes: a review". Powder Technology 117: 3-39.

Iveson, S., M. Wauters, P.A. Forrest, S. Litster, J.D. Meesters, B. Scarlett (2001b). "Growth regime map for liquid-bound granules: further development and experimental validation". Powder Technology **117**: 83-97.

Litster , J. and B. Ennis (2004). "The science and engineering and granulation processes". Dordrecht, Kluwer Academic Publishers.

Mort, P. (2005)."Scale-up of binder agglomeration processes". Powder Technology **150**: 86-103.

Parikh, D. M. (1997). Handbook of pharmaceutical Granulation Technology. New York, USA, Marcel dekker, Inc.

Rowe , R. (1989). "Binder-substrate interactions in granulation, a theoretical approach based on surface free energy and polarity". Int. J. Pharm. **52**: 149-154.

Tousey, M. D. (2002)."The granulation process 101, basic technologies for tablet making". Pharmaceutical Technology Journal, Tableting & Granulation Yearbook P.8.

2

Literature review

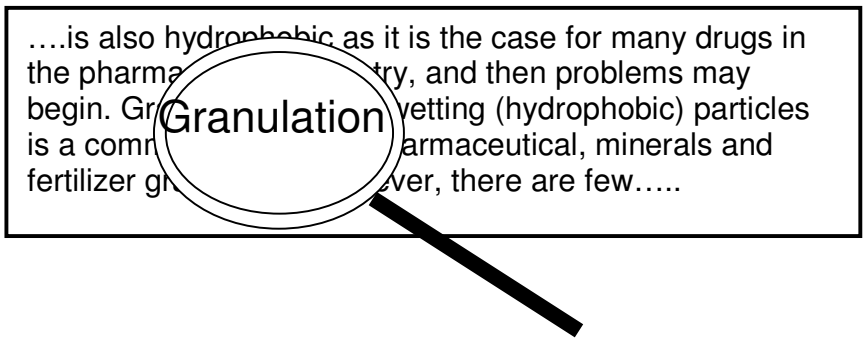

Chapter 2: Literature Review

2.1 Granulation of hydrophobic powders

Wet granulation is the process of collecting particles together by creating bonds between them using a binding agent. The granulation process combines one or more powders and forms granules. Wet granulation is one of the most common ways to granulate. The granulation process can be very simple or very complex depending on the characteristics of the powders. If the active ingredient represents a high percentage of the blended material and is also hydrophobic like many drugs in the pharmaceutical industry, problems may then begin. In many processes a surfactant is added to overcome the problematic characteristics of hydrophobic powders, but in some cases the surfactant is either not compatible or too expensive to be used.

Conventional granulation theory assumes that the liquid spreads over the solid particles. However, it is known that hydrophobic powders may spread around the drop during agitation and or rolling of fluid drops on a hydrophobic powder to form a liquid marble (Aussillous and Quere, 2001; 2006). This has not previously been understood or exploited as a method for forming granules.

There are a few studies investigating solid spreading nucleation, but they have investigated powder compacts (Zajic and Buckton, 1990) or large particles (Rowe, 1989b; 1990) rather than loose powders of small particle size and in those cases the particles are not free to move and spread over the droplet. Solid spreading nucleation where the powder is fine compared to the size of the liquid drops has been observed

experimentally (Hapgood, 2000; Simons and Fairbrother, 2000). It has also been published recently that hydrophobic powder can be used in combination with water to produce stable and structurally strong spherical structures known as liquid marble (Aussillous and Quere, 2001; 2006).

2.2 Liquid marble formation

All surfaces in a natural environment become contaminated. In nature, by a simple rain shower several plants leaves are completely cleaned from dust pollutions. These super hydrophobic leaves are cleaned by water droplets with very little adhesion to the surface which roll off very quickly even at small inclinations (Fürstner and Barthlott, 2005). This effect is called the "Lotus Effect" (Barthlott and Neinhuis, 1997). Spreading solid particles around liquid droplets is common in nature, as shown in Figure 2.1.

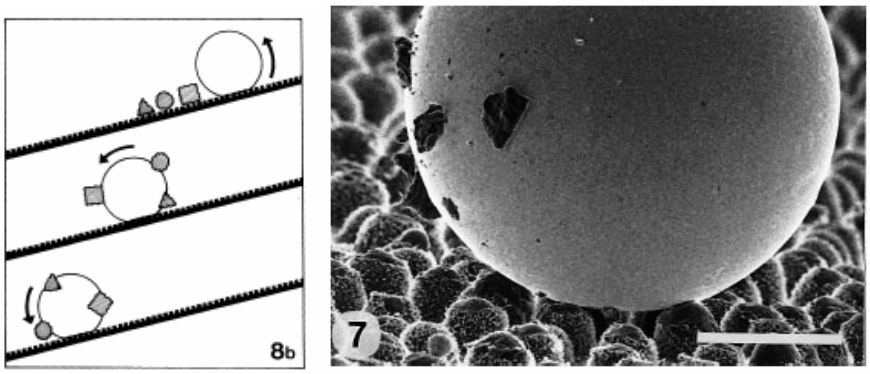

Figure 2.1: Lotus effect, contaminations adhere to the droplets surfaces and are removed from the leaves when the droplets roll off (Barthlott and Neinhuis, 1997)

Liquid marbles can be used as micro reservoirs, which can move quickly without any leakage. Non-stick liquid marbles have attracted significant attention of researchers in the past decade, due to their promising technological applications in medicine,

biotechnology, chemical and mechanical engineering. Recently, Wang *et al.* (2008) reported that liquid marbles are effective in methane storage applications. They showed a great increase in the rate of methane uptake in methane gas hydrate by forming the hydrate in preformed dry water powders, compared with storage in bulk water.

Liquid marbles literally repel water, rebound after an impact and slip on a surface. The force needed to move these marbles on solid surfaces is extremely small because of the diminished area of liquid-solid contact (de Gennes *et al.,* 2003; Quéré, 2005; Bromashenko and Musin, 2009; Dandan and Erbil, 2009; McHale *et al.,* 2009).

Aussillous and Quere (2001; 2006) describe "liquid marbles" formed from water droplets covered with hydrophobic lycopodium grains (see Figure 2.2), which roll and bounce like glass marbles but deform and flex like a fluid. The hydrophobic particles sit at the air-water interface due to the high contact angle, and lateral capillary forces (created by deformation of the liquid surface) cause the particles to self assemble into a powder film on the drop surface (Kralchevsky and Nagayama, 2000; Aussillous and Quere, 2001, 2006; Forny *et al.*, 2007). This powder shell of particles around a droplet prevents liquid leakage and allows two liquid marbles to collide and rebound without coalescence. Aussillous and Quere (2006) focused on liquid marble properties and robustness and possible ways for putting marbles into motion.

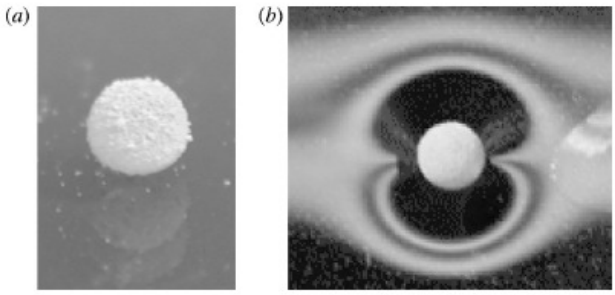

Figure 2.2: Liquid Mable of water and lycopodium grains on (a) solid or (b) on a water pool (Aussillous and Quere, 2006)

Dovrvee *et al.* (2004) used magnetic grains to drive the marbles using a magnetic fluid. McHale *et al.* (2007) investigated the electro-wetting of liquid marbles. McEleney *et al* (2009) studied the effect of powder density and particle size and shape on the stability of the liquid marbles and reported the lower powder particle size, forms more stable liquid marble. They also found a more complete coverage of liquid marble occurs when particle density is lower and/or particles shape is more spherical. The more spherical particles also have a smaller particle-liquid contact and thus less resistance to flow over the liquid surface. Also, the lower particle density means less force would be required to move these particles along the surface of the droplet (McEleney *et al* , 2009).

Liquid marbles are also promising candidates to be applied in the biomedical and genetic analysis fields where very small amounts of materials must be analyzed in short durations so that 2D micro fluidics and lab-on-chip methods are used (Dandan and Erbil, 2009; McHale *et al.*, 2009). In these processes, the powder is used after drying the interior liquid, therefore the evaporation rate of the liquid marble is an important parameter to to ensure that liquid remains in the marble until it reaches its target location. If the liquid is very volatile and evaporates easily, the liquid marble will deform and collapse. The life

time of a liquid marble depends the chemical nature and particle size of the hydrophobic powder as well as the liquid used to form it. Dandan and Erbil (2009) used chemically inert graphite particles to form a liquid marble and they studied the life time of the liquid marble in comparison with the same size water droplet. They found that graphite liquid marbles had a much longer (more than twice) life time than a pure water droplet since graphite is insensitive to chemical reaction. Using graphite liquid marble in many industries such as microfluidics and genetic analysis looks promising.

Ionic liquid marbles also attracted attention recently due to solvent unique characteristics such as thermal stability and ionic conductivity. Gao and McCarthy (2007) formed ionic liquid marbles by using fluoride containing polymers (OTFE, PTFE), and these ionic liquid marbles remained floating on water surface for a week, compared to a hydrophobised silica liquid marble which floated for a minute before coalescing.

Nguyen (2009) investigated the internal liquid marble structure using confocal microscopy. They reported that the liquid marble wall is composed of a combination of mono and multi layers of particles. Coarse particles (above 50 micron in size) formed mono layers, while fine particles formed a multi layered powder shell. They also found that the extent of penetration of coarse particles into the liquid core was much less than fine particles. Larger particles tend to float on the top of the liquid core instead of submerging into the liquid core. Bhosale *et al*., (2008) also reported that cohesive powders were more likely to form a multi-layer of particles on the liquid surface. This

provides flexibility to the liquid marble, and helps to withstand compression forces (Bhosale *et al*., 2008).

Bink and Murakami (2006) studied the transformation of particle-stabilized aqueous foam into water-in-air powder (dry water) and vice versa. These transitions can be achieved in a single system comprising of air, water and fumed silica nanoparticles, which have been hydrophobised to different degrees. The inversion of the air-water-particles system can be achieved in two ways: (i) changing the silica particle hydrophobicity at constant air/water ratio; or (ii) changing the air/water ratio at fixed particles wettability (Figure 2.3). Partially hydrophobic particles with contact angle close to 90º can act as a foam stabilizer, whereas the hydrophobic particles (θ >90º) act in the opposite way and are used as antifoams (Bink and Murakami, 2006). Very hydrophobic particles can stabilize water droplets in air, therefore a free flowing material containing up to 98 w/w% water could be produced (Forny *et al.,* 2006; 2007; 2009). The mechanism behind the phase inversion and liquid marble formation is still unclear and requires further investigation. This study will focus on the mechanism of formation of liquid marble.

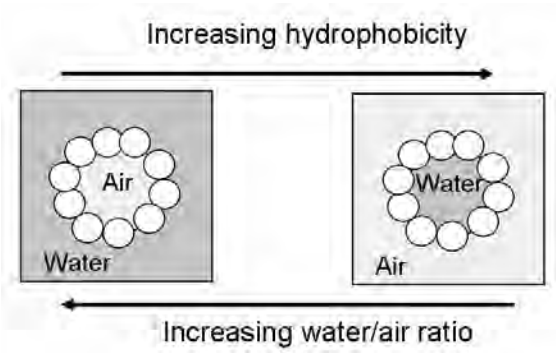

Figure 2.3: Phase inversion of foams (air-in-water) to Liquid Marble (water-in-air) (Adapted from Bink and Murakami, 2006)

There are no studies currently published on *why* liquid marbles form. Two different mechanisms have been tentatively proposed to date in the literature:

- The first proposed mechanism is that kinetic energy (Forny *et al.*, 2009b) is responsible, based on observations of the role of mixing intensity during the manufacture of a large quantity of liquid marbles. At pilot scale of liquid marble formation, Forny *et al.* (2009) used a higher mixer impeller speed to increase the level of agitation and found that the overall kinetic energy applied during mixing was crucial to effectively encapsulate the water in a shell of hydrophobic powder.
- The second suggested mechanism is that liquid marble formation is a surface energy phenomenon, driven by the solid-over-liquid spreading coefficient (λ_{SL}) (Hapgood *et al.*, 2009). The solid-liquid spreading coefficient has been proposed as a quantitative method to predict whether a given powder-liquid combination will form a liquid marble (Hapgood *et al.*, 2009).

None of these proposed mechanisms have been confirmed. It is necessary to test these hypotheses to find out whether liquid marble formation via solid spreading nucleation is a surface energy phenomenon or physical phenomenon occurring due to kinetic energy. To do this, the solid-over-liquid spreading coefficient (λ_{SL}) must be calculated and compared to experimental observations (discussed in more detail in Chapter 4). The next section introduces the equations for calculating the solid spreading coefficient and its implications in the food and pharmaceutical industries.

2.3 Spreading coefficient and thermodynamics of wetting

When a liquid contacts a solid surface, an area of solid-vapor interface is exchanged for an equivalent area of solid-liquid interface and the liquid forms a spherical cap at the solid/liquid interface, which restricted by three-phase contact line (Litster and Ennis, 2003). The angle formed at a point on three-phase contact line between the solid/liquid interface and liquid/vapor interface is known as the contact angle, θ, that can vary between 0º and 180º (Figure 2.4). The relationship between surface energy and the contact angle is given by the classical Young equation (Litster and Ennis, 2003).

$$\text{Cos}\ \theta = \frac{\gamma_{SV} - \gamma_{SL}}{\gamma_{LV}} \tag{2.1}$$

Low contact angles (<90º) imply that the liquid wets surface and will spread readily across it, whereas high contact angles (>90º) imply that the liquid does not wet the surface. The solid substrate is called "hydrophobic" when the contact angle is greater than 90º. There are a variety of methods to assess the contact angle and hydrophobicity of powders and these were reviewed recently (Lazghab *et al.*, 2005).

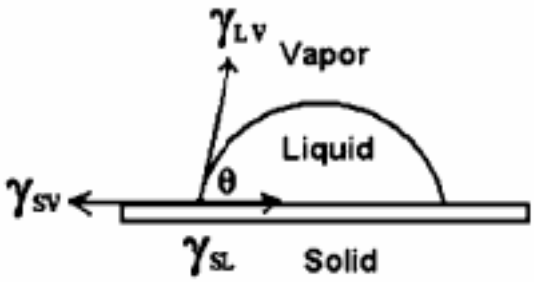

Figure 2.4: Contact angle on a powder surface, where γ_{SV}, γ_{SL}, γ_{LV} are the solid-vapor, solid-liquid, and liquid-vapor interfacial energies, and θ is the contact angle (Litster and Ennis, 2003)

Spreading coefficient equations can be explained from first principles. The energy required to create a contact interface unit between phase S and L, initially separated completely, is represented by the interfacial adhesion γ_{SL}, (Eq. 2.2). The work of cohesion for a solid W_S (Eq. 2.3) or a liquid W_L (Eq. 2.4) is the work required to seperate a unit cross-sectional area of a material from itself. The subscripts S, L and V refer to solid, liquid and vapor, respectively.

Work of interface adhesion: $W_{SL} = \gamma_S + \gamma_L - \gamma_{SL} = \gamma_L(1+\cos\theta)$ (2.2)

Work of solid cohesion: $W_S = 2\ \gamma_S$ (2.3)

Work of liquid cohesion: $W_L = 2\,\gamma_L$ (2.4)

The result for extreme value of $\theta = 0^o$ in Eq. (2.2) will be Eq. (2.3). For $\theta = 180^o$ $W_{SL} = 0$, which means there is no interaction between phases (Hiemenz and Rajagopalan, 1997).

The ability for one phase to spread over another phase can be quantitatively measured by the difference between the works of adhesion and cohesion, known as the spreading coefficient. Spreading coefficients have been used by the pharmaceutical industry for many years to predict whether adequate wetting of the pharmaceutical powders will occur. Hiemenz and Rajagopalan (1997) defined spreading coefficient as the difference between the final and initial states of the spreading process. The spreading coefficient indicates whether spreading (i.e. further replacement of the solid-vapor interface with a solid-liquid interface) is thermodynamically favorable. There are two possible spreading coefficients - liquid over solid (λ_{LS}) or solid over liquid (λ_{SL}).

$$\lambda_{SL} = -\Delta G_{SL} = \gamma_{SL} + \gamma_S - \gamma_L \qquad (2.5)$$

$$\lambda_{LS} = - \Delta G_{LS} = \gamma_{SL} + \gamma_L - \gamma_S \quad (2.6)$$

A negative value for ΔG and a corresponding positive value for λ mean that the process occurs spontaneously and one phase can freely spread over other phase. The solid over liquid spreading coefficient λ_{SL} (Eq. 2.5) is of particular interest in this work.

Although conventional granulation theory assumes that the liquid spreads over the solid particles; there are three possibilities in the interaction between binder and substrate in granulation (Parfitt, 1981; Rowe, 1989).

- Liquid spreading over the solid and creating a liquid film when $\lambda_{LS} > 0$
- Solid spreading over the liquid when $\lambda_{SL} > 0$ (this case is possible if solid is in powdered form and physically moveable)
- No spreading because of high work of liquid and solid cohesion

By combining Eq. 2.2, 2.3, and 2.5, the solid spreading coefficient can also be written:

$$\lambda_{SL} = W_{SL} - W_S \quad (2.7)$$

- If $W_{SL} > W_S$, which means $\lambda_{SL} > 0$ and the solid liquid interaction is sufficiently strong to promote the spreading of solid over liquid
- If $W_{SL} < W_S$, which means $\lambda_{SL} < 0$, and solid will not spread over liquid.

Spontaneous spreading occurs when the coefficients are positive, but in practice, spreading occurs when the coefficients are closest to zero (Krycer and Pope, 1983). Spreading coefficients for each phase can be calculated using the following relationships (Rowe, 1989; Rowe, 1989b). The simplest expression for spreading coefficients is:

$$\lambda_{LS} = \gamma_L(\cos\theta - 1) \tag{2.8}$$

$$\lambda_{SL} = -2\gamma_S + \gamma_L(\cos\theta + 1) \tag{2.9}$$

Rowe (1989) used the harmonic mean interfacial energy developed by Wu (1973) in combination with the Young-Dupre equation and the difference between the work of adhesion and cohesion to derive a spreading coefficient for the spreading of liquid over a solid surface and vice versa. Spreading coefficient equations and interfacial adhesion energy based on dispersive component (indicated by superscript *d*) and polar component (indicated by superscript *p*) of the total surface energy were presented as follows (Rowe, 1989):

$$\lambda_{SL} = 4\left[\frac{\gamma_L^d \gamma_S^d}{\gamma_L^d + \gamma_S^d} + \frac{\gamma_L^p \gamma_S^p}{\gamma_L^p \gamma_S^p} - \frac{\gamma_S}{2}\right] \tag{2.10}$$

$$\lambda_{LS} = 4\left[\frac{\gamma_L^d \gamma_S^d}{\gamma_L^d + \gamma_S^d} + \frac{\gamma_L^p \gamma_S^p}{\gamma_L^p \gamma_S^p} - \frac{\gamma_L}{2}\right] \tag{2.11}$$

$$\gamma_{LS} = \gamma_L + \gamma_S - 4\left[\frac{\gamma_L^d \gamma_S^d}{\gamma_L^d + \gamma_S^d} + \frac{\gamma_L^p \gamma_S^p}{\gamma_L^p \gamma_S^p}\right] \tag{2.12}$$

The ability for the solid particles to spread over the liquid surface has important implications including the selection of a binder or excipient for granulation (Zajic and Buckton, 1990; Planinsek *et al.*, 2000; Tuske *et al.*, 2005), dispersion rate of the cocoa powder into water *(Galet et al.*, 2004) and the prediction of the granule strength (Rowe, 1989). Therefore there is a significant proportion of work that have incorporated the solid spreading coefficient of λ_{SL}, the spreading of solid over liquid surface, into their criteria or predictions into the effect of wettability of the formulation systems.

However, there is a fundamental flaw in the solid spreading coefficient derivation that has not been previously reported. Rowe (1989) simply interchanged the subscripts of solid and liquid in Wu's (1973) equation when deriving the solid spreading coefficient. The spreading coefficient for liquid spreading over solid surfaces λ_{LS} accurately describes the thermodynamic conditions present in liquid spreading coefficient; however interchanging the subscripts to represent solid spreading oversimplifies the thermodynamic conditions for solid spreading. More detail and explanation of an improved model of the solid spreading phenomenon will be discussed in Chapter 5.

2.4 Implications of spreading coefficients in nuclei formation

Wetting, spreading and the contact angle are particularly important during the nucleation stage of granulation. Spreading coefficients can be used to explain the differences in the structure of nuclei formed. Schæfer and Mathiesen (1996), and Tardos *et al.* (1997) proposed two different mechanisms of agglomerate formation in melt pelletization which depended on the relative size of the droplet to the primary particle size. Afterward, Scott *et al.* (2000) expanded these mechanisms in order to cover wet granulation. " Immersion nucleation" occurs when the smaller particles immersed into a molten binder drop. This occurs when the droplet size is larger than the particles (see Figure 2.5). This produces nuclei with saturated pores. "Distribution nucleation" occurs when the drops are distributed on the surface of the solid. This occurs when the binder droplets are small or comparable to the particle size. In this case, particles coated by binder will form granules by coalescence. This will produce nuclei which may have air trapped inside and the granule subsequently will not be fully saturated (< 100%). The distribution mechanism

produces uniform distribution of the binder within the granules compared to the immersion mechanism.

The immersion-distribution hypothesis assumes that the thermodynamics of the wetting process are favorable which means that the binder will always spread over the powder surface. This is not necessarily true depending on the values of the thermodynamic spreading coefficients values, since sometimes the value of λ_{LS} is negative. In addition, the possibility of the solid spreading over the liquid must be included (Hapgood *et al.*, 2009).

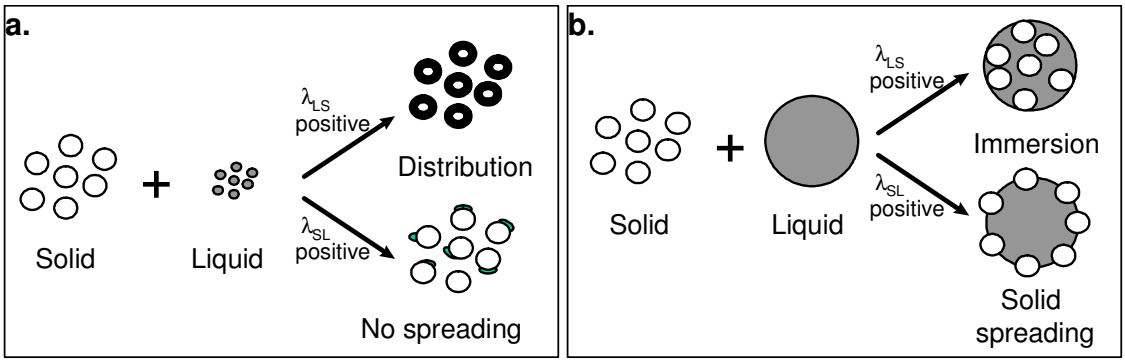

Figure 2.5: Nucleation formation mechanisms (Schæfer and Mathiesen, 1996) as a function of spreading coefficients (Rowe, 1989) when a) the liquid drops are smaller than the solid and b) when the solid particles are smaller than the liquid droplets (solid spreading part proposed by Farber *et al.*, 2006)

All four possible formation mechanisms have been summarized in Figure 2.5 as a function of the ratio of particle to drop size and spreading coefficients. Each nucleation mechanism produces different nuclei morphologies, but ultimately they all depend on the

same thermodynamic properties (contact angle and spreading coefficient) of the feed formulation during the nuclei formation stage. Litster and Ennis (2004) discuss definitions of these thermodynamic properties and measurement techniques for typical granulation formulations in detail. Four articles discuss the effect of spreading coefficients on wet granulation and relationship between spreading coefficient and final granule properties (Krycer and Pope, 1983, Rowe, 1989b, Planinsek *et al.*, 2000, and Zhang *et al.*, 2002). These studies represent only case (a) in Figure 2.5.

Krycer and Pope (1983) granulated paracetamol with six common binders. They used the λ_{LS} spreading coefficient to evaluate the binder efficiency, but they could not correlate their experimental measurements of granule friability and tablet strength with the predicted spreading coefficients due to lack of the λ_{LS} spreading coefficient data. Rowe (1989) calculated spreading coefficients for the paracetamol system that Krycer and Pope (1983) used with six binders; these were Povidone (PVP), hydroxypropylmethylcellulose (HPMC), polyethylene glycol 6000, PEG 6000, acacia gum powder and sucrose. Rowe (1989) concluded that if λ_{LS} is positive, there is a strongly adhering film of binder around the substrate and a strong dense granule will be formed. However, if λ_{LS} is negative and λ_{SL} is positive, the substrate adheres to the binder at isolated points. In this case, the binder does not form a film around the substrate particles, which causes the formation of more open porous structure of granules (see "No spreading" in Figure 2.5a).

Planinsek *et al.* (2000) prepared granules in a fluidized be granulator from lactose, pentoxyfilline and acyclovir and sprayed 5 to 10 wt% HPMC and PVP binder. They

calculated spreading coefficients and correlated these with granule properties. They reported that the spreading coefficients showed a good correlation with the friability of granules. Higher friability results correlates with lower spreading coefficient of liquid over solid (λ_{LS}).

Zhang *et al.* (2002) assessed the wettability of several pharmaceutical powders with water and 20% ethanol using the λ_{LS} spreading coefficient. This prediction for granulating solvent performance based on solvent-drug spreading coefficient was in good agreement with the characteristics of the resulting granules in terms of density, porosity and friability. Their spreading coefficient calculation showed the higher value for 20 vol% Ethanol which was in good agreement with the higher bulk density and lower porosity of formed granule with 20% ethanol.

Hapgood *et al.* (2009) suggested that the liquid marble formation mechanism shown in Figure 2.5, where the droplet is covered by a powder to form a liquid marble could be described by the solid spreading coefficient, λ_{SL}. However, this was not tested and this is one of the main aims of this thesis.

2.5 Hollow granule formation

Hollow granule formation from liquid marbles is a new way to solve the problematic granulating behavior of hydrophobic powders where the powder spreads around a template drop in the nucleation process and the interior liquid is subsequently dried to form a hollow granule. Nuclei formed by powder spreading over the liquid can produce some highly desirable granule properties, such as (Hapgood *et al.*, 2009):

- Simultaneous control of granule size and structure – granule size is controlled by the drop size under low spray flux conditions and the liquid marble structure is self-assembled during the granulation process.
- Ability to easily handle a high loading of a hydrophobic drug.
- Spherical granules with excellent flow properties.
- Fast, mass-transfer limited drying due to the thin powder shell structure, which eliminates the diffusion-controlled, falling rate drying period.
- Highly porous granules due to hollow interior which suggests good compression characteristics for tabletting and fast, reproducible dissolution.
- Potential to load one soluble drug in the fluid interior and granulate with a second hydrophobic drug to form the outer shell.

The nuclei formed by solid spreading (Hapgood *et al.*, 2009) are also known as "liquid marbles" (Aussillous and Quere, 2001; 2006) or "dry water" (Forny *et al.*, 2009), and are used in cosmetic and pharmaceutical formulations. Liquid marbles and dry powder encapsulation are examples of particle design.

There are now two studies on producing liquid marbles and hollow granules at laboratory scale. McEleney *et al*. (2009) reported the formation of a hollow granule shell after drying poly-methylmethacralate (PMMA) liquid marbles. Bhosale *et al*. (2008) investigated the strength of liquid marbles formed with PTFE (7-12 μm) and two types of treated fumed silica powder. High surface area of nanoparticle materials (eg. Aerosil) created more uniform powder shells through uniform coverage of the liquid–vapor interface. They found that nano-powder shells form an "elastic" membrane that makes

these liquid marbles mechanically robust in comparison with conventional liquid marbles made from larger particles, and that these liquid marbles formed from nano-particles are able to withstand higher compressive stresses during drying, and may be more likely to form hollow granules. In these studies, there is no systematic attempt to understand what happens to the liquid marble as the template drop is removed during drying, and investigation to identify the optimal drying conditions to produce stable hollow granules from liquid marble nuclei is necessary.

In addition to two reported studies on the production of liquid marbles and hollow granules via laboratory techniques (McEleney *et al.,* 2009; Bhosale *et al*., 2008), only two methods of mass producing hollow granules are reported in the literature- melt granulation (Ansari and Stepanek, 2006) and mixer granulation (Hapgood *et al.*, 2009; Forny *et al.*, 2009).

The first method for mass production of hollow granules is melt granulation (Ansari and Stepanek, 2006) where a single granule is formed from a binder particle by sequential deposition of hydrophilic primary particles on its molten surface. If the first layer of particles forms a stable arch and does not collapse as the binder liquid from the core is drawn by capillary force to the shell region, a hollow core granule is formed. They performed granulation in a fluidized bed granulator with a 200g batch composed of mannitol and PEG as a melt binder. They found that the granule size directly depended on the core volume size inside of the granule, which was proportional to un-melted binder particle size. In addition, the shell thickness could be controlled by binder/solid ratio.

This work suggested the possibility of controlling melt granule structure with the binder particle size.

The second method of mass production is via solid spreading nucleation in high shear mixers. Two groups (Hapgood *et al.*, 2009; Forny *et al.*, 2009) have independently applied the liquid marble approach to produce designer particle assemblies for industrial applications.

Forny *et al.* (2006; 2007; 2009a,b) reported "powder encapsulation" of fluid, where a hydrophobic fumed silica powder (Aerosil R972, R812S) forms a powder shell encapsulating a water droplet core. They used two different vertical axis mixers – a high shear mixer with knife blades and a Triaxe mixer with rotating gyrating paddles. Two alternate methods were used to add water to the silica powder: direct loading of the liquid and powder into the mixer prior to commencing mixer operation; and by atomization over 3-4 minutes. In the lower shear Triaxe mixer, atomization was required to form liquid marbles but they collapsed quickly to form a foam or mousse. The high shear mixer was more successful and liquid marbles formed very quickly (approximately 10 seconds) without atomization. Using the more hydrophobic silica powder (R812S) and high shear processing conditions, up to 98% w/w water was able to be encapsulated with powder in the high-shear mixer. Formation of stable silica covered drops was most effective at the speeds of 12000 min^{-1} or higher in a high shear mixer with knife-edged impeller blades. Below this speed, the water formed a puddle at the base of the bowl and could not be

successfully dispersed through the powder. Atomization into the high-shear mixer was not attempted.

As the hydrophobicity of the silica powder decreased, the system became less stable, requiring lower impeller speed and more powder to encapsulate the same volume of liquid. Less hydrophobic silica powders were also more sensitive to shear conditions and collapse of the liquid marbles into a foam or mousse was reported (Forny *et al.*, 2007). The time for collapse reduced as the impeller speed and applied shear increased. They investigated the effect of powder hydrophobicity and several process variables on the formation of the powder encapsulated liquid and developed a regime map (Forny *et al.,* 2009a) shown in Figure 2.6. In these studies, the liquid marbles were the desired end product.

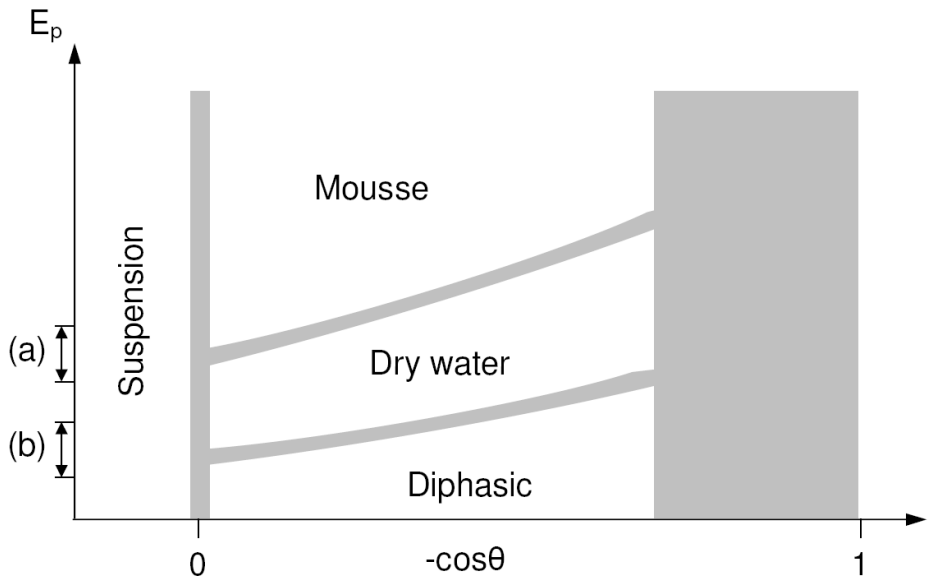

Figure 2.6. State diagram for liquid marble formation as a function of the contact angle and the energetic contribution E_p of the process (a) the position of E_p for blenders, (b) the position of E_p for granulators (Forny *et al.,* 2009a)

Forny *et al.,* (2009a) developed a qualitative state diagram for liquid marble/ dry water formation for blender and granulators as a function of the contact angle and the energetic contribution of the process, E_P, (see Figure 2.6). The amount of energy delivered (E_P) to materials can be defined as (Forny *et al.*, 2009b):

$$E_P = \phi[\frac{g}{N^2 d}]^{-(\frac{a-\log \mathrm{Re}}{b})}[\rho N^3 d^5] \tag{2.13}$$

where, E_P is the energetic contribution of the process (kJ), ϕ is the corresponding value of Power numbers, g is the gravitational acceleration (9.8 m/s^2), N is the rotational speed (rpm), d is the impeller diameter (m), Re is Reynolds number, a and b are constants depending on geometric dimensions, and ρ is the density of fluid (kg/m^3).

Qualitative positioning of the energetic contribution of the process is shown in Figure 2.6, region (a) for high shear mixers such as blenders; and region (b) for atomization process such as granulators. They predicted the formation of three types of final products- mousse, liquid marble and diphasic- during liquid marble formation process. For liquid marble formation E_p should be between $(E_p)_{min}$ and $(E_p)_{max}$. If (E_p) is below $(E_p)_{min}$, a hydrophobic-liquid system will produce two separate phases. If (E_p) is above $(E_p)_{max}$, a mousse will form instead of liquid marbles. The quality of the final product in the right part of the diagram is uncertain. They also summarized that liquid marble formation in highly energetic processes such as blenders requires highly hydrophobic particles, while low energetic processes such as granulators can use moderately hydrophobic particles to form liquid marbles.

Stable hollow granules (Hapgood *et al.*, 2009) were successfully produced by drying liquid marbles which were formed via solid spreading nucleation. In this case, the formation of liquid marbles represents an intermediate product. The end product of hollow granules was obtained by drying the liquid marbles to remove the drop template. Figure 2.7 shows an example structure which has been taken by X-ray tomography (Hapgood *et al.*, 2009).

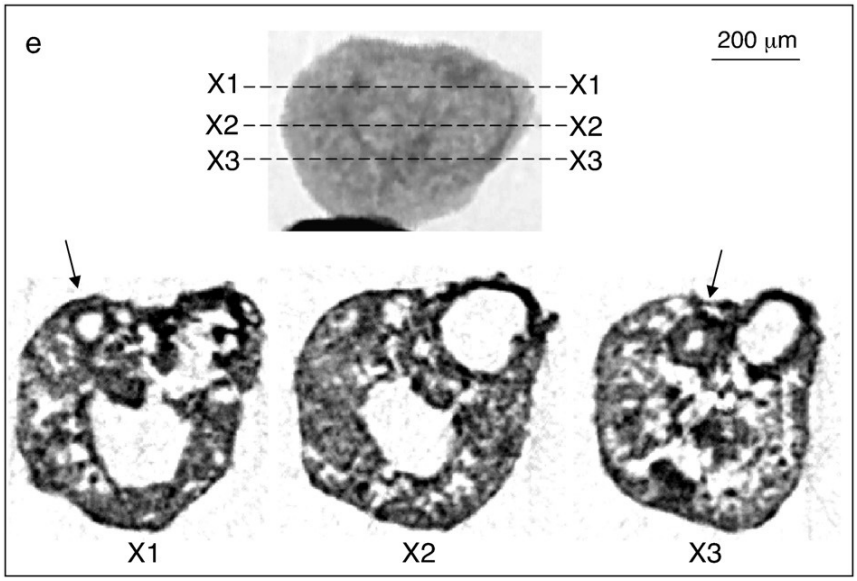

Figure 2.7: Top image: X-ray transmission image of a single hydrophobic fine powder nucleus, formed by powder spreading over the drop surface. Bottom images are reconstructed cross-sections. Dotted line on a side view image indicates position of the reconstructed cross-section (Hapgood *et al.*, 2009)

The granules were produced in a 2L granulator by using a formulation of 70 wt% hydrophobic drug powder (contact angle >90°), 20% microcrystalline cellulose and 4% hydroxypropyl cellulose binder as hydrophilic excipients and 1% sodium lauryl sulfate surfactant. The hollow granules were strong enough to withstand the downstream milling process as the excipients stabilized the powder shell to allow the hollow structure to be

preserved during drying. Hapgood *et al.* (2009) studied the effect of 1 minute and 7 minutes wet massing time on granule structure for two different liquid ratios (70 and 78 wt%). They found that at 70% fluid level the granule size distribution was independent of wet massing and the morphology of granules did not change. However there was deformation in the shape of granules at 7 minutes wet massing in this fluid level. By increasing the fluid level to 78%, at 1 minute wet massing there was no change in the granule size distribution but at 7 minutes the granule size distribution became unimodal and the external microstructure changed significantly. There are no further studies on the effect of changing the process variables such as binder-powder ratio on morphology of the hollow granules. More work is needed to understand the effect of the binder fluid to powder mass ratio on the particle size distribution and internal microstructure of hollow granules formed by a high shear mixer granulation process.

The work by Hapgood *et al.* (2009), and Forny *et al.* (2009) suggests how liquid marbles convert a normally problematic physicochemical property of hydrophobicity into a particle design advantage and show that liquid marbles can be produced using conventional granulation equipment. The work by Hapgood *et al.* (2009) demonstrates that liquid marbles can be exploited as a precursor to hollow granules. This opens the way for a new generation of "designer granules", and unique properties of hollow granules make the design of hollow granules ideal for high-value applications in the pharmaceutical, food and cosmetics industries.

2.6 Droplet impact phenomenon

In this section, literature on drop impact on hydrophobic solid surfaces will be reviewed in order to investigate the mechanism of particle entrainment on liquid droplet surface and also to find the governing dimensionless groups that determine droplet shape and droplet shattering and splashing on impact. If the liquid droplet breaks up during impact, then this will increase the number of drops and decrease the size of granule nuclei produced (Agland and Iveson, 1999).

The phenomena of liquid drop impacts is of interest in a wide range of applications including ink-jet printing, spray painting, spray cooling, application of pesticides, erosion in steam turbines and examining the splatter of blood stains (Kannangara *et al.,* 2006). There is a large body of literature concerning the study of liquid drop impacts with solid surfaces, but there are few papers related to dynamics of water drops upon impact on non-wetting surfaces (Fukai *et al.*, 1995; Mao *et al.*, 1997; Bartolo *et al.*, 2005; Kannangara *et al.,* 2006). There are no papers related to the impact of liquid drops on hydrophobic powder bed surfaces.

In general, three forces play an important role: the capillary, viscous, and the inertia forces of the droplets. Kannangara *et al.* (2006) have studied the spreading and rebounding of water drops on paper surfaces. They investigated the impact of water droplet on a hydrophobic paper surface and reported that the maximum drop recoil on hydrophobic substrates is stronger than hydrophilic substrates. Fukai *et al.* (1995) and Mao *et al.* (1997) investigated the effect of impact velocity and contact angle on the

spread and retraction of a spherical liquid droplet upon collision with a flat surface. They reported that rebounding of the droplet depended on impact velocity. Bartolo *et al.* (2005) showed that the drop retraction rate (the retraction speed divided by maximum radius) does not depend on the impact velocity for strong enough impacts ($We = \frac{\rho_L d_d v^2}{\gamma_{LV}} > 10$ and $\mathrm{Re} = \frac{\rho_L v d_d}{\mu} > 10$, d_d the droplet diameter, v the impact velocity). The dimensionless number that governs the retraction rate was found to be the Ohnesorge number (Eq. 2.14) (with μ the viscosity, ρ_L the liquid density, R the impacting drop radius, and γ_{LV} the surface tension).

$$Oh = \frac{\mu}{(\rho_L \gamma_{LV} R)^{0.5}} \tag{2.14}$$

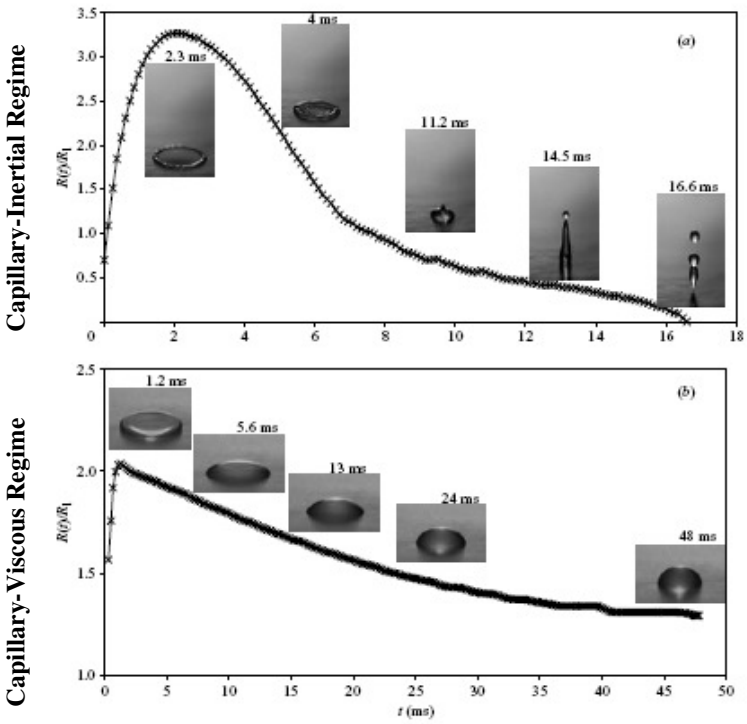

Figure 2.8: The shape of the droplets at the different stages of retraction. Droplet radius is 1 mm, impact speed is 2 ms^{-1}: (a) pure water, (b) viscous water–glycerol mixture, viscosity 50 mPa s (Bartolo *et al.*, 2005)

The Ohnesorge number compares the dissipative (viscous) forces to the non-dissipative (capillary and inertial) forces. Bartolo *et al.* (2005) proposed two distinct drop retraction regimes – the capillary-inertial regime O*h* < 0.05 and the capillary-viscous regime O*h*>0.05 (Figure 2.8). In both regimes, capillary forces are the driver behind the droplet retraction, which is countered by inertial forces in the capillary-inertial regime. In the capillary-viscous regime when $Oh > 0.05$, the main force slowing the retraction is the viscous force. The capillary-viscous regime would be the desired regime in producing spherical hollow granule in non-wetting granulation process as there is less chance of breakage and shattering in this area.

Based on Bartolo *et al.* (2005) studies, at $Oh \geq 0.05$ the droplet recoils into a spherical shape after impact on solid surface. This area is expected to be favorable for producing spherical hollow granules.

The phenomena of liquid droplets impacting on powder bed surfaces plays an important role in wetting and non-wetting granulation processes. Agland and Iveson (1999) studied drop impacts on a static powder surface. They studied liquid drops landing on a hydrophilic powder bed, where the drops form nuclei by binding particles together through a combination of viscous and capillary forces. They considered both drop spreading across surface and soaking into the pores during impact on powder beds. They found that the behavior of droplets impacting on a powder surface is analogous to behavior reported previously for drop impacts with both liquid and solid surfaces (Agland and Iveson, 1999). A critical Weber number ($We = \frac{\rho_L d_d v^2}{\gamma_{LV}}$) was required for drop

breakage. For We < 1000 breakage did not occur (Agland and Iveson, 1999). In principle, these results are also expected to apply to hydrophobic powders, although the fluid does not soak into the pores in this case.

Chouk *et al.* (2009) studied the motion and behavior of a single drop of PEG 200 on the moving hydrophilic powder bed (Durcal) in a high-shear granulator. In a powder bed, drops are subjected to centripetal and gravitational forces. These forces may affect the size and shape of the drop as it is incorporated into the bed. Initially a drop has its own kinetic energy due to falling, giving it sufficient momentum to overcome the localized powder surface motion shortly after impact. As the initial momentum of the droplet is dissipated, it begins to adjust to the surrounding powder bed motion. Eventually the initial droplet kinetic energy is dissipated, and its motion is completely influenced by the localized powder bed motion. Inclination of the bed causes deviation from above mentioned regime for droplet impact on powder bed. It depends on the relative position of the drop with respect to the impeller blade. As the inclination of the powder bed increases, gravitational forces cause the droplet to flow faster in a downward direction compared to the surrounding powder which is also moving downward. Due to this downward flow, the liquid drop becomes elongated in shape. When a droplet is added away from the edge of the mixer, it is more prone to deformation because the droplets have a higher kinetic energy on impact as they land further down the inclined bed. Due to wetting, part of the drop remained attached to the powder bed while the other part retained its momentum and moved downward. This resulted in deformation and breakage

of the drop. Retention of the momentum by the drop is due to its slow deceleration and high impact energy. This causes deformation and breakage.

Achieving a static spherical shape of the liquid drop after impinging on the surface is also important for forming a robust liquid marble. The effects of gravity and surface tension on the drop shape are described by the Bond number (Eq. 2.15):

$$Bo = \frac{\rho g R^2}{\gamma} \tag{2.15}$$

By comparing droplet radius with capillary length (Eq. 2.16) the droplet shape after impinging can be explained (Mahadevan and Pomeau, 1999).

$$\kappa^{-1} = \sqrt{\gamma / \rho g} \tag{2.16}$$

When $B_0 \ll 1$, which corresponds to $R \ll \kappa^{-1}$, gravity is negligible and the drop looks like a sphere with contact zone length (see Figure 2.9) equal to

$$\ell = \sqrt{\frac{2}{3}}\, R\kappa \tag{2.17}$$

Above the capillary length, which means $R \gg \kappa^{-1}$, gravity dominates and the drop becomes a 'puddle' with thickness $h=2\kappa^{-1}$ and contact length equal to

$$\ell = \sqrt{\frac{2}{3}}\, R^{3/2}\kappa^{1/2} \tag{2.18}$$

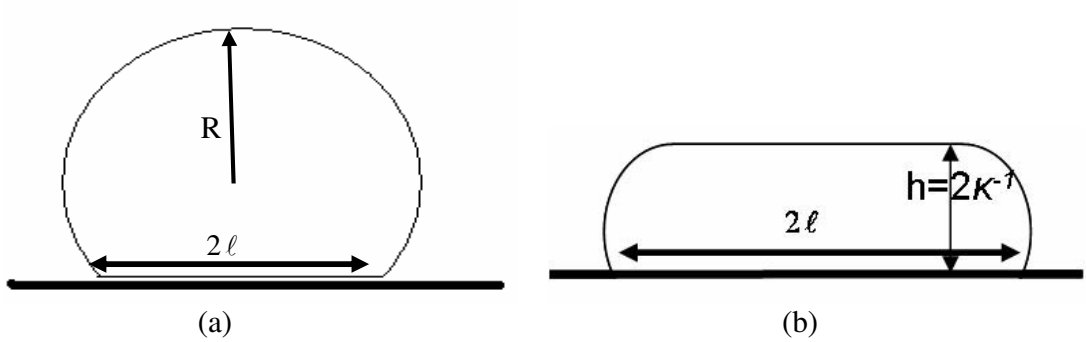

Figure 2.9: Sketch of a small non-wetting drop, (a) below the capillary length ($R \ll \kappa^{-1}$) (Aussillous and Quere, 2006), (b) above the capillary length ($R \gg \kappa^{-1}$)

2.6.1 Mechanism of particle entrainment on liquid droplet surface

When a droplet impacts onto a solid surface, it spreads radially, then deforms into a thin circular disk. The rate of spreading is "driven" by the inertia of the drop, and opposed by viscous effects. When the inertial energy is dissipated, the drop reaches its maximum radius. During this process air bubbles entrap between liquid and solid and cause a depression in the circular liquid disk, and flow circulation begins in the central region of the liquid (Tong *et al.,* 2004). Later, an upward swelling is formed because of the reverse flow from the edge to the center (Mahadevan and Pomeau, 1999; Fujimoto *et al.*, 2005). This bulk motion creates a corresponding surface flow. If the liquid does not wet the surface, surface tension forces will cause the drop to retract to an equilibrium sessile (sitting) drop shape (see Figure 2.10).

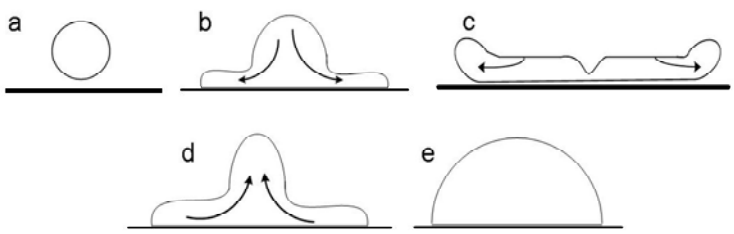

Figure 2.10: Sketch of droplet impact on a hydrophobic solid surface (a) before impact (b) after impact (c) maximum spreading (d) recoil state (e) equilibrium state

2.7 Literature conclusion

Although granulation of hydrophobic powders is a significant problem in industry, there is no research on how to successfully design and control these granulation processes. This thesis proposes a unique approach to address this problem with an entirely new philosophy – solid spreading nucleation – which transforms the normally problematic hydrophobicity into a powerful tool for creating "designer pharmaceutical granules". Extension of current granulation theory to include hydrophobic granulation behavior will represent a significant advance for a variety of industries not currently addressed by current granulation theory.

Therefore, a sound understanding of the following questions is of great interest:

- What is the mechanism of formation of liquid marble and does the spreading coefficient thermodynamically describe the condition taking place in solid spreading over liquid interface?
- What is the effect of binder and powder on liquid marble formation?
- What are the optimal drying conditions to produce stable hollow granules from liquid marbles?
- What is the effect of changing binder to powder mass ratio in mass production of hollow granules?
- What is the optimum binder to powder mass ratio in high shear mixer granulators?

2.8 References

Agland, S. and S. M. Iveson (1999). "*The Impact of Liquid Drops on Powder Bed Surfaces*". CHEMECA, Newcastle, Australia, IEAust/IChemE/RACI.

Ansari, M. A. and F. Stepanek (2006). "Formation of hollow core granules by fluid bed in-situ melt granulation: Modelling and experiments". International Journal of Pharmaceutics **321**: 108-118.

Aussillous, P. and D. Quere (2001). "Liquid marbles". Nature **411**(6840): 924-927.

Aussillous, P. and D. Quere (2006). "*Properties of liquid marbles*". Proceedings. Mathematical, physical, and engineering sciences **462**(2067): 973-999.

Barthlott, W. and C. Neinhuis (1997). "Purity of the sacred lotus, or escape from contamination in biological surfaces". Planta **202**: 1-8.

Bartolo, D., C. Josserand, D.Bonn (2005). "Retraction dynamics of aqueous drops upon impact on non-wetting surfaces". J.Fluid Mech. **545**: 329-338.

Bhosale, P. S., M. V. Panchgnula, H. A. Stretz, (2008). "Mechanically robust nanoparticle stabilized transparent liquid marbles". Applied Physics Letters **93**: 034109/1- 034109/3.

Binks, B., R. Murakami (2006). "Phase inversion of particle-stabilized materials from foams to dry water". Nature Materials Letters **5**:865-869.

Bromashenko, E., and A. Musin (2009). "Revealing of water surface pollution with liquid marbles". Applied Surface Science **255**(12): 6429-6431.

Chouk , V., G. Reynolds, et al. (2009). "Single drop behaviour in a high shear granulator". Powder Technology **189**: 357-364.

de Gennes P.G., F. Brochard-Wyart, D. Quéré (2003). Capillarity and Wetting Phenomena, Springer, Berlin.

Dorvee, J.R., A.M. Derfus, S.N. Bhatia, M.J. Sailor (2004). "Manipulation of liquid droplets using amphiphilic, magnetic one-dimensional photonic crystal chaperones". Nature Materials **3**(12):896-899.

Dandan, M., H.Y. Erbil (2009). "Evaporation rate of graphite liquid marbles: comparison with water droplets". Langmuir **25**(14):8362-7.

Farber, L., K. Hapgood, JN.Michaels (2006). "*Hydrophobic nucleation in particle agglomeration*". World Congress of Particle Technology 5, Lake Buena Vista FL USA.

Forny, L., I. Pezron, K. Saleh (2009a). "Dry water: From physico-chemical aspects to process related parameters". 9th International Symposium on Agglomeration and 4th International Granulation Workshop, Sheffield, UK

Forny, L., K. Saleh, I. Pezron, L. Komunjer, P. Guigon (2009b). "Influence of mixing characteristics for water encapsulation by self-assembling hydrophobic silica nanoparticles". Powder Technology, special issue on granulation **189**: 263-269.

Forny, L., I. Pezron, K. Saleh, P. Guigon, L. Komunjer (2007). "Storing water in powder form by self-assembling hydrophobic silica nanoparticles". Powder Technology **171**(1): 15-24.

Forny, L., K. Saleh, I. Pezron, L. Komunjer, P. Guigon (2006). "*Influence of mixing process characteristics for aqueous encapsulation by silica nanoparticles*". World Congress Particle Technology 5, Lake Buena Vista, Florida, USA.

Fu¨rstner, R. and W. Barthlott (2005). "Wetting and Self-Cleaning Properties of Artificial Superhydrophobic Surfaces". Langmuir **21**: 956-961.

Fujimoto, H., A. Tong, Y. Shiotani, H.Takuda (2005). "*Numerical and experimental study on oblique collision of water droplet with a solid substrate*". 2005ASME International Mechanical Engineering Congress and Exposition,IMECE05.ASME.

Fukai, J., Y. Shiiba, T. Yamamoto,O. Miyatake (1995). "Wetting effects on the spreading of a liquid droplet colliding with a flat surface: Experiment and modeling". Phys.Fluids **7**(2): 236-247.

Galet, L., T. O. Vu, D. Oulahna, J. Fages (2004). "The Wetting Behaviour and Dispersion Rate of Cocoa Powder in Water". Food and Bioproducts Processing **82**(4): 298-303.

Gao, L., T.J. McCarthy (2007). "Ionic Liquid Marbles". Langmuir **23**:10445-10447.

Hapgood, K. P. (2000). "Nucleation and Binder Dispersion in Wet Granulation". Chemical Engineering. Brisbane, Australia, University of Queensland. PhD thesis.

Hapgood, K. P. L. Farber, JN. Michaels (2009). "Agglomeration of hydrophobic powders via solid spreading nucleation". Powder Technology **188**: 248-254.

Hiemenz, P. C. and R. Rajagopalan (1997). Principles of colloid and surface chemistry. New York,USA, Marcel Dekker.

Iveson, S., J. Litster, K. Hapgood (2001a). "Nucleation, growth and breakage phenomena in agitated wet granulation processes: a review". Powder Technology **117**: 3-39.

Kannangara, D., H. Zhang, W. Shen (2006). "Liquid-paper interactions during liquid drop impact and recoil on paper surfaces". Colloid and Surfaces A: Physicochemical and Engineering Aspects **280**: 203-215.

Kralchevsky, P. A. and K. Nagayama (2000). "Capillary intractions between particles bound to interfaces, liquid films and biomembranes". Advance Colloid Interface Science **85**: 145-192.

Krycer, I. and D. G. Pope (1983). "An Evaluation of Tablet Binding Agents. Part I. Solution Binders". Powder Technology **34**: 39-51.

Lazghab, M., K. Saleh, I. Pezron, P. Guigon, L. Komunjer (2005). "Wettability assessment of finely divided solids". Powder Technology **157**: 79-91.

Litster, J. and B. Ennis (2003). The science and engineering granulation processes. Dordrecht,Netherlands, Kluwer Academic Publisher.

Mahadevan, L. and Y. Pomeau (1999). "Rolling droplets". Phys.Fluids **11**: 2449-2453.

Mao, T., D. C. S. Kuha, H. Tran (1997). "Spread and rebound of liquid droplets upon impact on flat surfaces". AIChE Journal **43**(9): 2169-2180.

McEleney, P.G., M. Walker, I. A.Larmour, S. E. J. Bell (2009). "Liquid marble formation using hydrophobic powders". Chemical Engineering Journal, **147**, PP. 373-382 (2009), doi:10.1016/j.cej.2008.11.026.

McHale, G., Herbertson, D.L. Elliot, S.J., Shirtcliff, N.J., Newtn, M.I.(2007). "Electrowetting of Nonwetting Liquids and Liquid Marble". Langmuir **23**(2): 918-924

McHale, G., S.J. Elliot, M.I. Newtn, D. L. Herbertson, K. Esmer, (2009). "Levitation-Free Vibrated Droplets: Resonant Oscillations of Liquid Marbles". Langmuir **25** (1): 529-533.

Nguyen T.H. (2009). Fundamental effects of hydrophobic powders on nucleation and wet granulation, Monash University, Master of Engineering Science thesis.

Parfitt, G. D. (1981). Dispersions of Powders in Liquids. London and New Jersey, Applied Science Publishers.

Planinsek, O., R. Pisek, A.Trojak, S. Srcic (2000). "The utilization of surface free-energy parameters for the selection of a suitable binder in fluidized bed granulation". International Journal of Pharmaceutics **207**(1-2): 77-88.

Quéré D. (2005). "Non-sticking drops". Rep. Prog. Phys. **68**: 2495–2532.

Rowe , R. (1989). "Binder-substrate interactions in granulation, a theoretical approach based on surface free energy and polarity". International Journal of Pharmaceutics **52**: 149-154.

Rowe , R. (1989b). "Surface free energy and polarity effects in the granulation of a model system". International Journal of Pharmaceutics **53**(75-78).

Rowe, R. (1990). "Correlation between predicted binder spreading coefficients and measured granule and tablet properties in the granulation of paracetamol". International Journal of Pharmaceutics **58**: 209-213.

Schæfer, T. and C. Mathiesen (1996). "Melt Pelletization in a high shear mixer IX. Effects of binder particle size". International Journal of Pharmaceutics **139**: 139-148.

Scott, A. C., M. J. Hounslow, T. Instone (2000). "Direct evidence of heterogeneity during high-shear granulation". Powder Technology **113**: 205-213.

Simons, S. J. R. and R. J. Fairbrother (2000). "Direct observations of liquid binder particle interactions: the role of wetting behaviour in agglomerate growth". Powder Technology **110**: 44-58.

Tardos, G. I., M. I. Khan, P.R. Mort (1997). "Critical Parameters and limiting conditions in binder granulation of fine powders". Powder Technology **94**: 245-258.

Tong, A., H. Fujimoto, S. Kasliwal, H. Takuda (2004). "*A numerical study on the successive impingement of droplets onto a substrate*". 2004 ASME International Mechanical Engineering Congress and Exposition,IMECE04. Anaheim, California USA, ASME.

Tuske, Z., G. Regdon Jr, I. Ero, S. Srcic, Pintye-Hodi (2005). "The role of the surface free energy in the selection of a suitable excipient in the course of a wet-granulation method". Powder Technology **155**(2): 139-144.

Wu, S. (1973). "Polar and non polar interactions in adhesion". J. Adhesion **5**: 39-55.

Wang, W.X., C.L. Bray, D.J. Adams, A.I. Cooper (2008). "Methane Storage in Dry Water Gas Hydrates". Journal of American Chemical Society **130**(35): 11608-11609.

Zajic, L. and G. Buckton (1990). "The use of surface energy values to predict optimum binder selection for granulations". International Journal of Pharmaceutics **59**(2): 155-164.

Zhang, D., J. H. Flory, S.Panmai, U.Batra, M.J.Kaufman (2002). "Wettability of pharmaceutical solids: its measurement and influence on wet granulation". Colloids and Surfaces A: Physicochemical and Engineering Aspects **206**(1-3): 547-554.

3

Granulation of hydrophobic powders

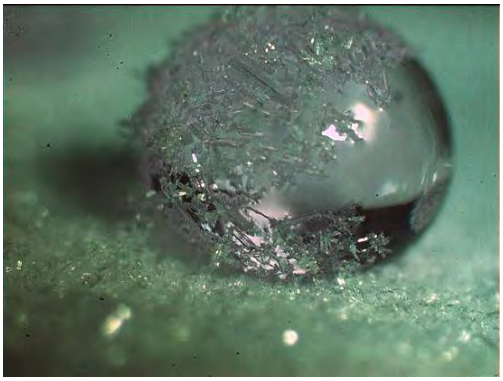

Water marble of salicylic acid

Chapter 3: Granulation of hydrophobic powders

Declaration for Thesis Chapter 3

Declaration by candidate

In the case of Chapter 3, the nature and extent of my contribution to the work was the following:

Nature of contribution	Extent of contribution (%)
Initiation, Key ideas, experimental and analysis work, development	95

The following co-authors contributed to the work. Co-authors who are students at Monash University must also indicate the extent of their contribution in percentage terms:

Name	Nature of contribution	Extent of contribution (%) for student co-authors only
1- Karen P. Hapgood	Supervision, reviewing and editing of the paper, writing up the paper	--

Candidate's Signature		Date

Declaration by co-authors

The undersigned hereby certify that:

(1) the above declaration correctly reflects the nature and extent of the candidate's contribution to this work, and the nature of the contribution of each of the co-authors.

(2) they meet the criteria for authorship in that they have participated in the conception, execution, or interpretation, of at least that part of the publication in their field of expertise;

(3) they take public responsibility for their part of the publication, except for the responsible author who accepts overall responsibility for the publication;

(4) there are no other authors of the publication according to these criteria;

(5)potential conflicts of interest have been disclosed to (a) granting bodies, (b) the editor or publisher of journals or other publications, and (c) the head of the responsible academic unit; and

(6) the original data are stored at the following location(s) and will be held for at least five years from the date indicated below:

Location(s)	Department of Chemical Engineering, Monash University, Clayton Campus

[Please note that the location(s) must be institutional in nature, and should be indicated here as a department, centre or institute, with specific campus identification where relevant.]

Signature 1	--	Date--

Abstract:

Granulation of hydrophobic powders is a growing problem in the pharmaceutical industry. The structural complexity of new drug molecules mean that is increasingly common for entire classes of drug compounds to be highly hydrophobic. This creates considerable difficulty in understanding, controlling and trouble-shooting these industrial granulation processes.

There have been many recent advances in granulation theory. Essential to this theory is wetting and spreading of the fluid through the powder particles which must occur as a prerequisite for good granulation.. The possibility of a fine, hydrophobic powder spreading over the surface of the liquid during nucleation has been identified theoretically based on surface chemistry and as a potential nucleation mechanism. Recently, an investigation confirmed that nucleation can occur by spreading of the sub-micron particles around the template drop. This unique nucleation behavior is called "solid spreading nucleation". The hollow granule structure formed by the solid spreading mechanism suggests the possibility of using the controlled, open granule structure to manufacture "designer pharmaceutical particles" with advantageous properties:

1. Controlled granule size by manipulating the size distribution of the spray drop "templates"

2. Controlled granule structure by exploiting the solid spreading mechanism.

This allows for the potential for designer pharmaceutical particles, with controlled size distribution and excellent ideal flow and handling properties. This paper describes single drop solid-spreading nucleation experiments where single fluid droplets are placed onto loosely packed powder beds of hydrophobic powders and the formation of the powder shell observed via high speed video camera. Experimental results and observations for a model system are presented.

Karen P. Hapgood and Batool Khanmohammadi*, "Granulation of hydrophobic powders", Powder Technology, 2009 (189), 253-262.

Keywords: Hydrophobic powder, Non-wetting, Solid–spreading, Nucleation, Wet granulation, Liquid marble.

3.1. Introduction

Wet granulation is a particle size enlargement process where small particles are agglomerated using a liquid binder to form larger granules. Traditional reasons for granulating a material include improving flow and handling properties, increasing bulk density, reducing dust formation, and reducing segregation of materials [1]. More recently, granulation is motivated by a desire to *design structured agglomerates* for specialty products such as pharmaceuticals, controlled dissolution detergents and "instant" food powders such as sauces [2]. Problems during granulation of specialty products can cause enormous downstream processing problems and product that does not meet regulatory and quality specifications.

Great progress has being made in understanding & controlling granulation mechanisms (e.g. [3-6]) focusing on producing granules with a consistent, reproducible size distribution. This understanding has been applied to many industrial granulation processes, including pharmaceuticals [7], and detergents [8, 5] to improve their performance. However, granulation of poorly wetting powders has not been addressed in the above works but is commonly performed in pharmaceutical, minerals and fertilizer granulation.

Granulation of hydrophobic powders is frequently required in the pharmaceutical industry. The structural complexity of new drug molecules mean that is increasingly common for entire classes of drug compounds to be poorly wetting (contact angles approx 70-90°) or highly hydrophobic (contact angle $\geq 90^{o}$). The poor wetting properties can create considerable difficulty in understanding, controlling and trouble-shooting these industrial granulation processes.

A surfactant is often added to the granulation fluid and/or powders to improve the wetting characteristics of the formulation but this is not possible in some applications such as iron ore granulation or certain pharmaceutical formulations due to either the cost of the surfactant or chemical interactions that may occur. For these industries, the current body of granulation theory is often not applicable, as it is inherently assumed in all current granulation research that the liquid must wet the powder in order for granulation to be successful. We review below the state of knowledge of hydrophobic powder granulation.

3.2. Literature review

3.2.1. Granulation of hydrophobic powders

The contact angle is defined as the internal angle formed by a liquid drop placed on a solid surface at the three phase contact line [9]. Measuring contact angles on powders are generally difficult and the reliable experimental methods have been recently reviewed [10]. In this paper, a hydrophobic powder system is defined as a powder or combination of powders which have a contact angle with the granulating fluid greater than 90°.

The contact angle of the system directly affects the characteristics of the granulated product. Lerk *et al.* [11] measured the contact angles of neat pharmaceutical powders and powder combinations with water using the h-ε method [12]. The calculated contact angles were independent of particle size and cake porosity. For combinations of a hydrophobic drug powder and a hydrophilic excipient, the contact angle depended on the particle sizes. For the large particle size mixtures the hydrophobic material dominated the contact angle but for smaller particle sizes, a linear

relationship was obtained between the cosine of contact angle and proportion of components. Aulton and Banks [13] used water in a fluidized bed to granulate increasing proportions of a hydrophobic powder (salicylic acid with a contact angle of $\theta = 103^o$) with a hydrophilic powder (lactose with contact angle $\theta = 30^o$). The mean granule size decreased linearly as the mixture contact angle increased. One approach to estimating the average contact angle of a powder mixture is to use Cassie and Baxter's approach [9] of an average contact angle θ_{av}:

$$\cos\theta_{av} = f_1 \cos\theta_1 + f_2 \cos\theta_2 \qquad (1)$$

where f_1 is the fraction of the powder mixture with contact angle equal to θ_1, and f_2 is the fraction of the powder mixture with contact angle equal to θ_2. Fig.1 shows how Eq. (1) tends to overestimate the contact angle compared to the measured contact angles for lactose-salicylic acid mixtures [13]. There are a number of limitations with this approach (for example, see [14]) but Eq. (1) gives a result within 15% of more detailed surface analysis which this makes Eq. (1) useful in practical situations.

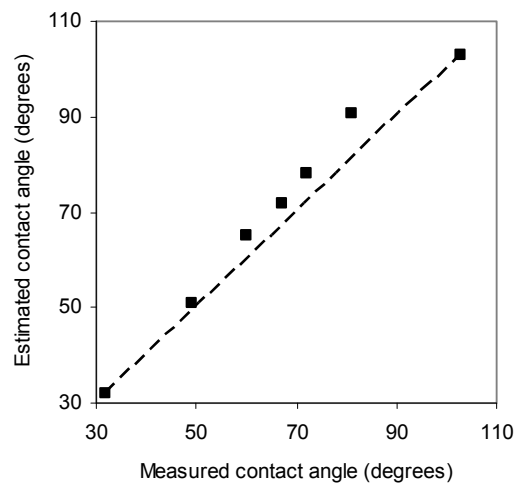

Fig. 1: Comparison of measured contact angles for lactose-salicylic acid combinations [13] versus the values predicted by Eq. (1)

In addition to the demonstrated effect of contact angle on granule size [13], contact angle also directly affects granulation kinetics. Hemati *et al.* [15] granulated sand powders of varying contact angle ($\theta = 38^o$, 58°, 75°, and $>90^o$) with 1% CMC solution in a fluidized bed. As the contact angle increased, the rate of granule growth slowed, until barely any growth was achieved at a contact angle greater than 90°. These granules were observed to grow by coating of the granulating fluid on the particle surface, rather than by coalescence. A plot of the growth rate (based on gradient of each data set) versus adhesion tension was found to be linear [15]. Only one granulating fluid was used in these experiments, and further investigations would be required with several fluids to establish a general relationship between adhesion tension and granule growth kinetics.

Conventional granulation theory assumes that the liquid spreads over the solid particles. However, it is known that hydrophobic powders may spread around the drop during agitation and/or rolling of fluid drops on a hydrophobic powder. Spreading coefficients have been used by the pharmaceutical industry for many years to predict whether adequate wetting of the pharmaceutical powders will occur. The spreading coefficient λ is the difference between the works of adhesion and cohesion [16] and indicates whether spreading (i.e. further replacement of the solid-vapor interface with a solid-liquid interface) is thermodynamically favorable. There are three possibilities in spreading between a solid and a liquid:

a) The liquid may spread over the solid (λ_{LS}) and create a surface film;
b) The solid may spread or adhere to the liquid (λ_{SL}). The latter case will only occur is solid movement is physically possible, such as when the solid is in a powdered form. This is called *solid spreading nucleation* [17].

c) Both the liquid and solid have high works of cohesion, and the solid-liquid interfacial area will be minimized (i.e. no spreading occurs). This final case represents non-wetting.

Granules formed by a fine layer of hydrophobic powder that spreads over the surface of a larger drop undergo "*solid spreading nucleation"* [17].

A few studies of solid-over-liquid spreading (i.e. λ_{SL} driven) have been published but have been investigated on powder compacts [16] or large particles [18] rather than on loose powders of small particle size. Four articles discuss the effect of spreading coefficients on wet granulation [19, 20, 16, 21] but these discuss the case where the drops are smaller than the particles.

Solid spreading nucleation where the powder is fine compared to the size of the liquid drops has been observed [22-24], although the spreading coefficients were not measured to prove that the solid-over-liquid spreading coefficient λ_{SL} was the driving force. Some reports of "beading" of granulation fluid on hydrophobic powders have been published [25] where granulation produced wet patches and lumps. Granulation was improved using a foamed binder addition method [26, 25] with the same granulating fluid, which may exploit pickering stability [9] or other interfacial effects present in foam to initiate contact between the hydrophobic particles, and presents an interesting area for future study.

It is also possible that the observed motion of particles over the surface of the fluid drop is driven by a force unrelated to the spreading coefficient λ_{SL}. Alternative explanations for the observed particle motion include (see Fig. 2):

a) Bulk motion within the drop caused by drop deformation and recoil motion after impact, which drives a corresponding surface flow around the drop entraining particles [27, 28].
b) Particle motion towards low shear zones at the top of the drop to escape a high shear region at the point of maximum drop deformation at impact [29].
c) Lateral capillary forces or other colloidal interfacial effects known to physically stabilize emulsions.

Without detailed characterization of the powder and liquid surface energies, including polar and dispersive components, the spreading coefficient driving force theory cannot be confirmed. This work plus a review of underlying physics of the powder – fluid motion is currently underway.

Fig. 2: Alternate explanations for the movement of particles around the surface of the drop include surface flow as a result of shear flow at the impact point and/or bulk flow within the drop following impact and deformation

3.2.2. Hydrophobic "liquid marbles"

Hydrophobic powder can be used in combination with water to produce stable and structurally strong spherical structures [30, 31] described as "liquid marbles" formed from water droplets covered with hydrophobic lycopodium grains, which roll and bounce like glass marbles but deform and flex like a fluid. The hydrophobic particles sit at the air-water interface due to the high contact angle, and lateral capillary forces (created by deformation of the liquid surface) cause the particles to self assemble into a powder film on the drop surface. The film of particles on the exterior form a powder shell which prevents the liquid from wetting the supporting surface and allows two liquid marbles to collide and rebound without coalescence. Two groups [17, 32] have independently applied the liquid marble approach to produce designer particle assemblies for industrial applications.

Forny *et al.* [32] report "powder encapsulation" of fluid, where a hydrophobic fumed silica powder forms a powder shell encapsulating a water droplet core. They used two different vertical axis mixers – a high shear mixer with knife blades and a triaxe mixer with rotating gyrating paddles. Two alternate methods were used to add water to the silica powder: direct loading of the liquid and powder into the mixer prior to commencing mixer operation; and by atomization over 3-4 minutes. In the lower shear Triaxe mixer, atomization was required to form liquid marbles but they collapsed quickly to form a foam or mousse. The high shear mixer was more successful and liquid marbles formed very quickly (approx 10s). Using the most hydrophobic silica powder and high shear processing conditions, up to 98% w/w water was able to be encapsulated with powder in the high-shear mixer. Formation of stable silica covered drops was most effective at the speeds of 12000 min^{-1} or higher

in a high shear mixer with knife-edged impeller blades. Below this speed, the water formed a puddle at the base of the bowl and could not be successfully dispersed through the powder. Atomization into the high-shear mixer was not attempted. As the hydrophobicity of the silica powder decreased, the system became less stable, requiring lower impeller speed and more powder to encapsulate the same volume of liquid. Less hydrophobic silica powders were also more sensitive to shear conditions and collapse of the liquid marbles into a foam or mousse was reported [32]. The time for collapse reduced as the impeller speed and applied shear increased.

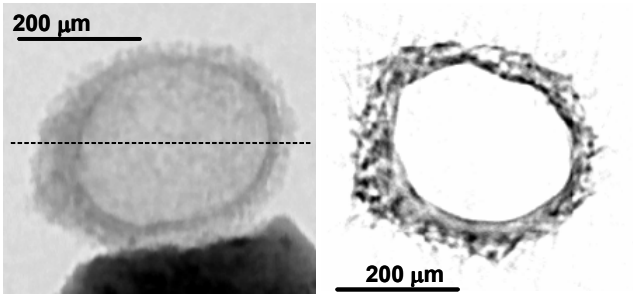

Fig. 3: X-ray transmission image (left) of a dried hollow granule formed from a liquid marble and reconstructed cross-section (right) showing hollow core [17]

Liquid marbles and dry powder encapsulation are examples of particle design where the powder shell is used to protect the fluid interior. Farber *et al.* [17] have extended the "liquid marble" approach by *drying* the liquid marbles to remove the interstitial fluid. The result is a spherical, hollow, granule (see Fig.3) as demonstrated by micro X-ray tomography after drying of the granules. Between 70-78% w/w water was atomized over 7-8 min into a 2L vertical axis high-shear mixer containing 70% w/w of a submicron hydrophobic powder (contact angle >90°). The granules were shown to be robust and survive handling and even milling in a screened comill.

Farber *et al.* [17] is the first to use a high loading of *hydrophobic* drug powder formulated with standard, *hydrophilic* pharmaceutical excipients. The presence of hydrophilic excipients components such as 20% w/w microcrystalline cellulose and 4% hydroxypropyl cellulose binder did not prevent liquid marble formation or self-assembly of the particles at the drop interface. The excipients stabilized the powder shell to allow the hollow structure to be preserved during drying. Even the presence of 1% sodium lauryl sulfate, a surfactant, as a powder did not prevent formation of liquid marbles, since the hydrophobic model drug powder constituted 90% of the batch on a volume basis. The work by [32] and [17] suggests how liquid marbles convert a normally problematic physicochemical property of hydrophobicity into a particle design advantage and show that liquid marbles can be produced using conventional granulation equipment. The work by Farber *et al.* [17] demonstrates that liquid marbles can be exploited as a precursor to hollow granules. This opens the way for a new generation of "designer granules".

Research into formation of hollow granules is an emerging field in melt granulation [33] and hydrophobic granulation [17, 6]. Hollow granules formed by solid spreading nucleation can be used to produce "designer particles" with pre-specified desirable properties, such as:

- Simultaneous control of granule size and structure – granule size is controlled by the drop size under low spray flux conditions and the liquid marble structure is self-assembled during the granulation process.
- Ability to easily handle a high loading of a hydrophobic drug.
- Spherical granules with excellent flow properties.

- Fast, mass-transfer limited drying due to the thin powder shell structure, which eliminates the diffusion-controlled, falling rate drying period.
- Highly porous granules due to hollow interior suggest good particle rearrangement and compression characteristics for tabletting plus reproducible dissolution due to the consistent granule and tablet structure.
- Potential to load one soluble drug in the fluid interior and granulate with a second hydrophobic drug to form the outer shell.

These properties make the design of hollow granules ideal for high-value applications in the pharmaceutical, food and cosmetics industries.

To design a hollow granule design requires a sound understanding of:

1. Controlling mechanisms of liquid marble formation via solid spreading nucleation,
2. Formulating to produce strong stable liquid marbles,
3. Maximizing granule strength and stability to avoid collapse of the structure [17, 32].
4. Granulation mechanism and kinetics linked with the granule growth regime map [3,4].

These main areas of research will ultimately lead to an extension of granulation theory to encompass the granulation of highly hydrophobic powders via solid spreading nucleation. This paper presents the first steps towards this aim, by studying the nucleation behavior of a single drop on a bed of hydrophobic powder.

3.3. Experimental

A loosely packed powder bed was formed by lightly sieving the powder into a petri dish and scraping level to produce a smooth powder surface. A loosely packed bed approximates the powder state in an agitated granulator [34]. A 100μL Hamilton precision syringe with a 22 gauge needle was positioned just above the bed surface. Drops (with 4μL volume) were allowed to detach and gently fall 1-2mm before landing on the bed surface. This distance was selected to minimize drop bouncing and rolling, and is not intended to represent the typical length scale of the granulation process. A Stereo microscope (SMZ Series) with a 3MP camera operating at 30 frames/ second was used to film a single drop impinging on to the powder surface.

3.3.1. Materials

Glass ballotini spheres (Potters Industries Pty. Ltd.) in four size grades (AC, AE, AG, AH) were used. In order to make the glass beads hydrophobic, SIGMACOTE solution (chlorinated organopolysiloxane in heptane, Sigma Aldrich Pty. Ltd.**)** was used. Glass beads are an ideal model powder but other more realistic powders are also required. Two hydrophobic drug powders were used: Salicylic acid (99%ACS Reagent, Sigma Aldrich Pty. Ltd.) with a contact angle of 103° [11] and 2-Ethoxybenzamide (97% Sigma Aldrich Pty. Ltd.) which has been used elsewhere as a model hydrophobic drug [35]. The particle size distribution was analysed by dry laser diffraction using a Malvern Mastersizer 2000, although salicylic acid was measured by sieving. The true density of the particles was measured using Helium pycnometry (Micromeritics Accupyc 1330). Particle properties are summarized in Table 1 and Fig. 4 shows optical microscope images of the needle-shaped salicylic acid and ethoxy-benzamide particles. We note that although the finest particle size specifications is for the AH

ballotini grade, the particle size distributions was essentially identical to the AG grade.

Several different binder fluids were used: distilled water, four grades of poly-ethylene glycol (PEG200, PEG300, PEG400, and PEG600), glycerol and a 1% mass sodium dodecyl sulfate (SDS) solution. A summary of binder properties is given in Table 2.

Table 1: Powder properties summary

Powder Property	Salicylic acid	2-Ethoxy-benzamide (EB)	Hydrophobic Glass Ballotini			
			AC	AE	AG	AH
d_{10}(μm)	69	1.89	139.3	88.65	47.36	47.10
d_{50}(μm)	131.6	4.67	190.86	121.12	65.58	65.22
d_{90}(μm)	501.6	12.74	261.49	165.20	90.44	89.83
Surface mean d_{32}(μm)	Not recorded	3.76	185.25	117.6	63.47	63.11
Volume mean d_{43}(μm)	Not recorded	7.02	196.59	124.64	67.57	67.18
Malvern specific surface area(m^2/kg)	Not recorded	1600	32.4	20.8	94.5	95.1
True Particle Density(g/cm^3)	1.43	1.27	2.48	2.44	2.47	2.46
Molecular Formula	$2^-(HO)C_6H_4CO_2H$	$C_2H_5OC_6H_4CONH_2$	SiO_2	SiO_2	SiO_2	SiO_2

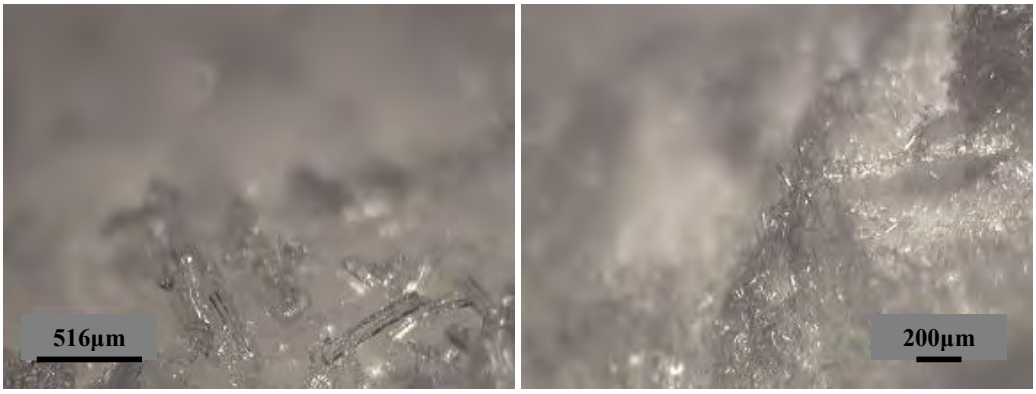

Fig. 4: Optical microscope images of salicylic acid needles (left) and 2-ethoxybenzamide (right)

Table 2: Granulating fluid properties at 20°C

Granulating fluid	Density ρ_L (g/mL)	Surface Tension γ_{LV} (mN/m)	Viscosity μ (mPa.s)	Manufacturer
Distilled Water	1	72.0[a]	1	N/A
1% SDS	~1	35[d]	~1	Sigma-Aldrich
Glycerol	1.25[b]	63.7[a]	950	Fluka
PEG200	1.127[b]	43.7[c]	60[b]	Sigma-Aldrich
PEG300	1.125[b]	43.7[c]	95[b]	Fluka
PEG400	1.126[b]	43.7[c]	120[b]	Sigma-Aldrich
PEG600	1.128[c]	43.7[c]	152.9[c]	Fluka

a – Data from (a) [18] (b) Sigma-Aldrich. (c)[22] and (d) [36].

3.4. Results

Experiments initially focused on screening material combinations to find suitable systems for further study. Table 3 summarizes the experimental observations and some pictures of liquid marbles are shown in Fig. 5. Water was able to form a liquid marble with all the powders tested, and glycerol was able to form liquid marbles with all powders except ethoxybenzamide. The addition of 1%SDS surfactant to the water eliminated liquid marble formation by reducing the contact angle below 90° allowing the drops to penetrate into the powder.

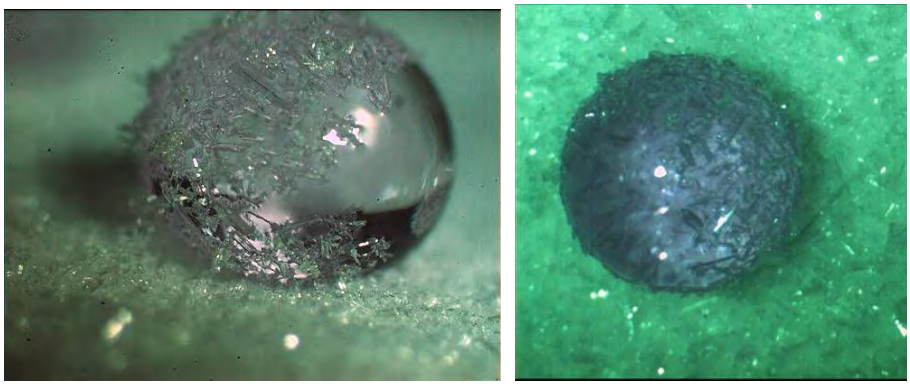

Fig. 5: Example of liquid marbles formed by solid spreading nucleation of salicylic acid powder over a water droplet approximately 2mm diameter

There are some interesting observations noted in Table 3. First, water and glycerol had the two highest surface tensions (of the three fluids that were used) and were able to form liquid marbles with almost all the powders tested. Based on the introduction, we expect that interfacial tension will be an important parameter in liquid marble systems, although with only three data points we cannot draw any conclusion at this stage. Second, there appears to be a viscosity effect, where low viscosity PEG200 was able to form a liquid marble with AG and AH ballotini, but PEG300 and upwards were unsuccessful. However, the most viscous fluid tested so far, glycerol, was able to form liquid marbles which suggests that viscosity is a secondary effect compared to the surface chemistry of the powder –binder system.

Third, there appears to be a particle size effect, where formation of liquid marbles using PEG200 was only successful on the two finest ballotini grades –AG and AH – which had identical particle size distributions as noted earlier. This implies either that the driving force (currently not known) is not strong enough to carry the largest ballotini particles around the drop surface, or that there is a drop to particle size ratio criterion for liquid marble formation.

Finally, it appears to be possible to temporarily form liquid marbles from systems with contact angles less than 90° – a number of combinations in Table 3 were observed to initially form a powder layer on the drop exterior but then penetrate completely into the powder bed. This is shown in Fig. 6 for water on food-grade cinnamon powder. Cinnamon is a naturally-derived material which contains many sub-components. We postulate that a soluble component at the surface of the ground cinnamon particle slowly leaches into the fluid, eventually reducing the contact angle

to below 90 degrees, causing a switch in behavior. However, this explanation does not explain the behavior for several other powder-fluid combinations, such as the ethoxybenzamide powder with PEG and glycerol. Further investigation, including contact angle measurements of the powders, is underway.

Table 3: Summary of liquid marble formation experiments

Powder	Fluid	Liquid marble?	Comments
Salicylic acid	PEG200	No	Drop penetration – no powder shell.
	PEG300	No	Drop penetration – no powder shell
	PEG400	No	Drop penetration – no powder shell
	PEG600	No	Drop penetration – no powder shell
	Distilled Water	Yes	Stable liquid marble formed
	Glycerol	Yes	Stable liquid marble formed
	Water+ 1% SDS	No	Drop penetration– no powder shell
2-Ethoxy-benzamide (E.B.)	PEG200	No	Liquid marble formed and sank simultaneously
	PEG300	No	Liquid marble formed and sank simultaneously
	PEG400	No	Liquid marble formed and sank simultaneously
	PEG600	No	Liquid marble formed and sank simultaneously
	Distilled Water	Yes	Stable liquid marble formed
	Glycerol	No	Liquid marble formed and sank simultaneously
	Water+ 1% SDS	No	Drop penetration – no powder shell
Hydrophobic Glass Ballotini (AC)	PEG200	No	Drop penetration– no powder shell
	PEG300	No	Drop penetration– no powder shell
	PEG400	No	Drop penetration– no powder shell
	PEG600	No	Drop penetration – no powder shell
	Distilled Water	Yes	Stable liquid marble formed
	Glycerol	Yes	Stable liquid marble formed
	Water+ 1% SDS	No	Drop penetration – no powder shell
Hydrophobic Glass Ballotini (AE)	PEG200	No	Drop penetration– no powder shell
	PEG300	No	Drop penetration – no powder shell
	PEG400	No	Drop penetration– no powder shell
	PEG600	No	Drop penetration – no powder shell
	Distilled Water	Yes	Stable liquid marble formed
	Glycerol	Yes	Stable liquid marble formed
	Water+ 1% SDS	No	Drop penetration – no powder shell
Hydrophobic Glass Ballotini (AG)	PEG200	Yes	Stable liquid marble formed
	PEG300	No	Drop penetration – no powder shell
	PEG400	No	Drop penetration– no powder shell
	PEG600	No	Drop penetration – no powder shell
	Distilled Water	Yes	Stable liquid marble formed
	Glycerol	Yes	Stable liquid marble formed
	Water+ 1% SDS	No	Drop penetration – no powder shell
Hydrophobic Glass Ballotini (AH)	PEG200	Yes	Stable liquid marble formed
	PEG300	No	Droplet covered with powder; then sank
	PEG400	No	Droplet covered with powder; then sank
	PEG600	No	Droplet covered with powder; then sank
	Distilled Water	Yes	Stable liquid marble formed
	Glycerol	Yes	Stable liquid marble formed
	Water+ 1% SDS	No	Drop penetration – no powder shell

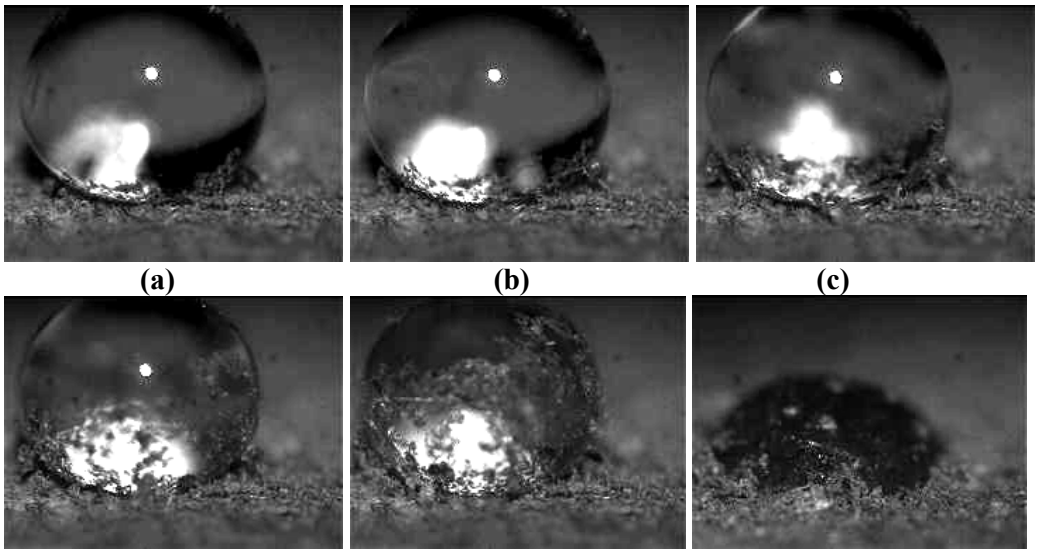

(a) (b) (c)

(d) (e) (f)

Fig. 6: Water droplet (~2mm diameter) on cinnamon powder showing initial stages of liquid marble formation, after (a) impact; (b) 1.4 seconds; (c) 3 seconds; (d) 6 seconds; (e) 10 seconds; followed by penetration into the powder bed (f) after 3 minutes

The experiments in Table 3 were performed by allowing the drop to fall a short distance of approximately 1-2mm. An increased tendency to form a liquid marble was observed when the drop rolled or deformed during impact. A second series of experiments was performed where the drops of water and glycerol were placed extremely gently onto the powder bed to avoid bulk motion within the drop interior due to impact or rolling. Fig. 7 shows that there is no surface coverage when a water drop is carefully placed on several particles, presumably because no bulk motion is created within the droplet to entrain particles in the surface flow. The same behavior was also observed for careful placement of glycerol droplets.

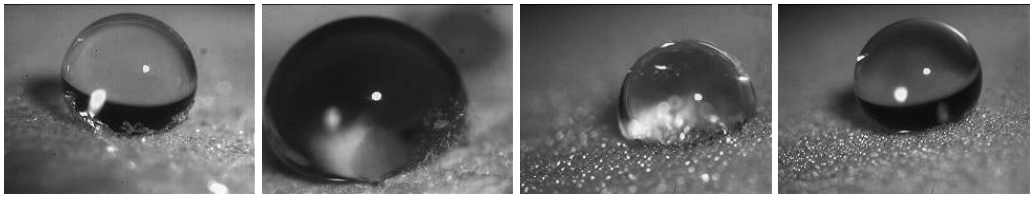

(a) (b) (c) (d)

Fig.7: Careful placement of a water droplet (d_d~2mm) on (a) salicylic acid (b) EB (c) AE glass ballotini (d) AG glass ballotini shows no liquid marble formation

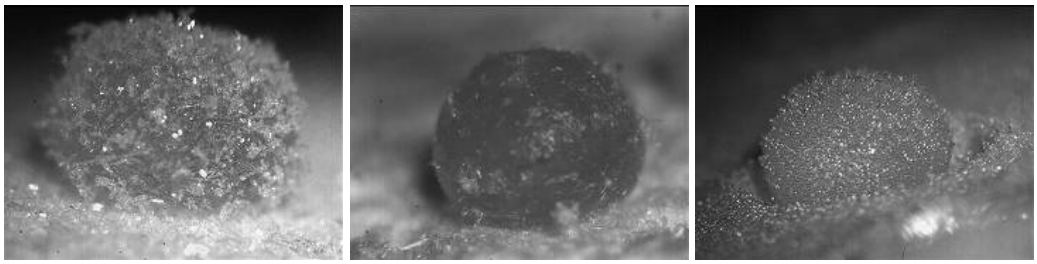

(a) (b) (c)

Fig. 8: Effect of rolling or shaking on surface coverage. (a) water on salicylic acid after shaking (b) water on EB after rolling and (c) glycerol after shaking on AH ballotini (d_d is ~2mm)

Alternatively, the particles can be spread over the uncovered droplet by shaking the petri dish. Fig. 8 shows a much higher level of surface coverage compared to the careful placement experiment shown in Fig. 7. Moreover, if the droplet is allowed to roll on the surface, the droplet will become covered with particles, as described by [30, 31] and shown in Fig. 8 (b).

To test whether bulk motion is responsible for the formation of the powder shell, the drop release height was increased to 15 cm and 30 cm. These heights are more representative of the spray height in a granulation process, although the drop sizes used here are much larger than typically found in an atomized spray. Fig. 9 shows the gradual increase in surface coverage for a water-AC ballotini system as the drop height is increased. The images in Fig. 9 were taken after the system had stabilized and no further powder movement was observed. Since the physiochemical properties of these experiments are constant, the kinetic energy of the drop appears to determine the extent of shell formation. In practical granulation situations, we presume that the drop surface is instantly covered with powder due to the highly agitated powder motion in the fluidized bed or mixer granulator.

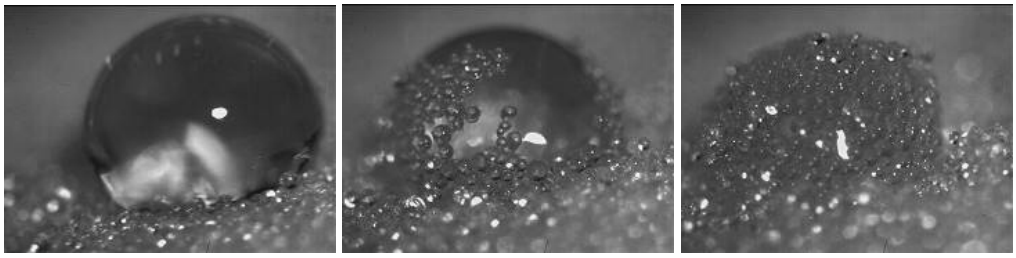

(a) (b) (c)

Fig. 9: Liquid marble formation using water drop (~2mm diameter) and hydrophobic AC ballotini powder from (a) 0cm height (b) 15cm height and (c) higher than 30cm level

When the drop is only partially covered with powder, the powder is not evenly distributed over the powder surface, but instead accumulates to form a sheet powder (refer to Fig. 10). Individual particles move across the drop surface until they aggregate into a film. This phenomenon is caused by attractive lateral capillary immersion forces [32].

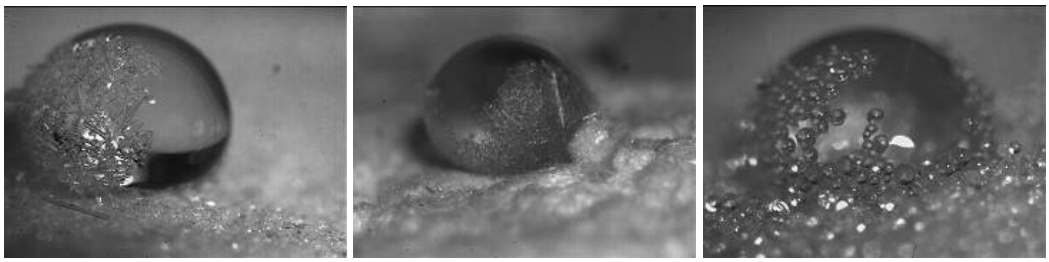

(a) (b) (c)

Fig. 10: Partly formed powder sheets due to lateral capillary forces. Water droplet (d_d ~2mm) on (a) Salicylic acid, (b) EB (c) hydrophobic AC ballotini

3.5. Discussion

The solid-over-liquid spreading coefficient λ_{SL} [16] may provide a quantitative method to predict whether a given formulation will form liquid marbles. However, our results also suggest that bulk motion of the drop, due either to rolling or impact, is required for solid spreading nucleation to occur. It is also possible that solid spreading motion is driven entirely by a physical flow mechanism (refer to Fig. 2), where the

degree of surface coverage is proportional to the size of the bulk flow generated within the drop, and that the spreading coefficients are not applicable to liquid marble formation. Surface energy measurements by inverse gas chromatography are underway to determine whether λ_{SL} can be used as a predictive tool.

All of the hollow granules formed in these studies eventually collapsed into hemispheres (see Fig. 11). Only multi-component formulations can produce inter-particulate bonds to stabilize hollow granules once the template drop has been removed during drying. To date, only one investigation [17] into liquid marbles and solid spreading nucleation has used a multi-component formulation of powders. All other studies have used a single fluid on a neat hydrophobic powder [31, 32]. This is also an area requiring significant further investigation.

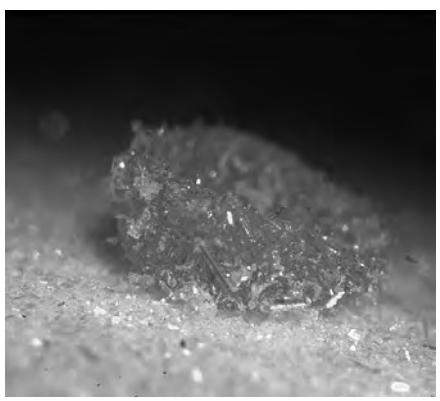

Fig. 11: Water-salicylic acid granule that has collapsed into a hemisphere during air drying. Granule diameter is approximately 2mm

In order for a stable, spherical, liquid marble to form from a single drop via solid spreading nucleation, we outline a series of steps that must occur:

1. A single drop must be formed that is much larger than the size of the powder particles (i.e. $d_d >> d_p$) [37-39] but small enough to form a spherical drop rather than a distorted pool or puddle i.e. Bond number ($B_0=\rho_L g R^2/\gamma_{LV}$) Bo<1[31].

2. The drop must land on the powder and survive the impact without breaking or shattering into smaller droplets i.e. Weber number $We=\rho_L d_d v^2/\gamma_L<1000$ [40] and Ohnesorge number $Oh=\mu/(\rho_L R)^{0.5}\gamma_{LV}>0.05$ [41].
3. The fluid must have a contact angle θ greater than 90° with the powder to prevent penetration of the drop into the powder bed [9, 34].
4. The powder must spread around the air-liquid interface of the drop to form a shell – driven either through impact induced surface flows [27, 28] or by spreading coefficients [16] as discussed earlier.
5. The powder must be able to self-assemble into a sufficiently dense layer to prevent contact of the drop interior with a supporting surface [32].

If any of these conditions are not fulfilled, a liquid marble will not be formed. In addition, in order to maintain small individual drop templates, the dimensionless spray flux must be low [42]. Under low spray flux conditions the granule size would be controlled by the atomized drop size i.e. the drop controlled nucleation regime [43].

Fig. 12 proposes a schematic flow sheet summarizing the formation of stable liquid marbles, incorporating several dimensionless groups identified by previous workers [37, 38, 31, 17] combined with ratios and dimensionless groups that form part of the framework for granulation theory [34, 42].

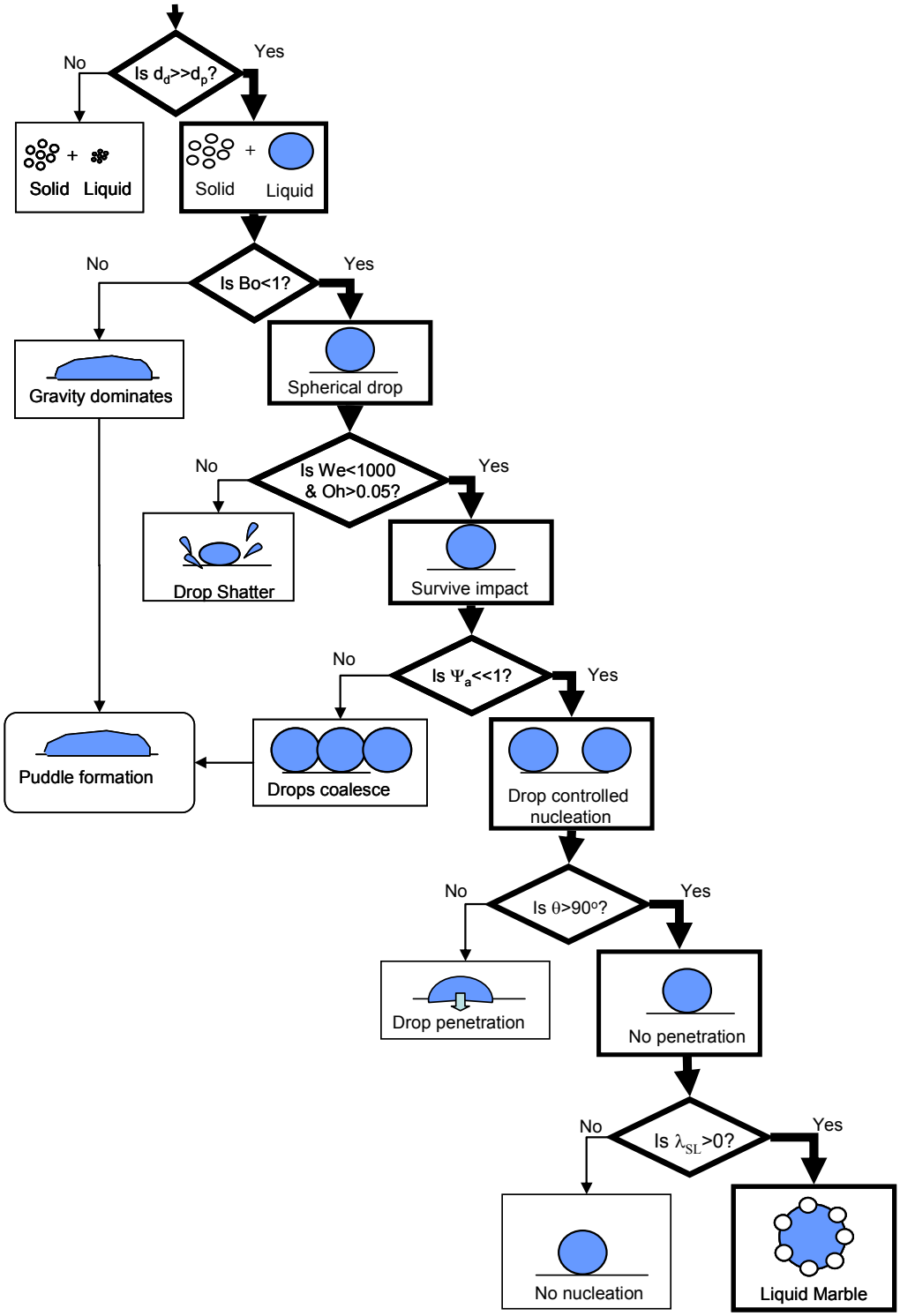

Fig. 12: Schematic flow sheet summarizing the steps and dimensionless groups controlling the formation of liquid marbles during granulation

For a stable, spherical hollow granule to form from a single drop, the following additional steps must occur:

6. In an agitated powder mass, the assembled liquid marble must be sufficiently strong to withstand the stresses experienced within in the agitated bed and subsequent standard powder handling operations.
7. The concentration and distribution of hydrophilic excipients must not negatively affect hollow granule formation, strength or stability.
8. The multi-component powder shell must be sufficiently strong to be self-supporting in order to avoid collapse during drying to form a hollow sphere and subsequent standard powder handling operations.

The controlling groups for these final three steps to form hollow granules are currently unknown but are expected to be complex functions of powder and liquid physiochemical properties and packing arrangements of multi-component particles. This area is the subject of further ongoing research by the authors.

3.6. Conclusion

We report here the first stage of ongoing work studying the granulation of hydrophobic powders by the solid spreading nucleation mechanism [17]. Several combinations of hydrophobic powders and fluids have been shown to exhibit solid spreading nucleation and to form "liquid marbles" [30, 31]. The liquid marble structure seems superficially consistent with the long established spreading coefficients [16], although we also propose an alternate mechanism where bulk motion within the drop creates a corresponding surface flow which entrains particles, creating a shell.

Preliminary experiments suggest that some bulk fluid motion is required for shell formation to occur, and that smaller particle size, lower fluid viscosity and higher kinetic energy during impact all favour the formation of a powder shell. Some unexpected behavior was reported, where a powder shell initially began to form but was not stable and the drop then penetrated into the powder bed. Finally, a framework for liquid marble formation was proposed by outlining the sequential steps and the possible controlling groups for each step. However, the ultimate aim of this ongoing research project is to follow the lead of [17] and dry the liquid marbles to produce hollow granules suitable for pharmaceutical applications.

Acknowledgements

The authors gratefully acknowledge the valuable contributions of Dr. Leslie Yeo, Dept Mechanical Engineering in the early stages of this project. The authors would also like to acknowledge the Monash University Engineering Faculty and Australian Research Council Discovery Projects program (DP0770462) for providing financial support for this work as well as the Monash Graduate Research School for providing scholarship support for B. Khanmohammadi.

Nomenclature

Bo	Bond Number representing dimensionless ratio of gravity forces to surface tension forces acting on a drop ($B0=\rho g R^2/\gamma LV$)
d_d	Diameter of the droplet (m)
d_p	Diameter of the particle (m)
f	Fraction of powder component in Eq. (1) (-)
g	Gravitational acceleration ($9.8 m/s^2$)

Oh	Ohnesorge number representing dimensionless ratio of viscosity and surface tension forces ($Oh = \mu/(\rho_L \gamma_{LV} R)^{0.5}$)
R	Drop radius ($=d_d/2$)
V	Velocity of the fluid drop (m/s)
We	Weber number representing dimensionless ratio of inertia to surface tension ($We=\rho_L d_d v^2/\gamma_{LV}$)
γ_{LV}	Surface or interfacial tension of the fluid in contact with the vapour (mM/m)
λ_{LS}	Spreading coefficient for the liquid over the solid (-)
λ_{SL}	Spreading coefficient for the solid over the liquid (-)
μ	Fluid viscosity (mPa.s)
θ	Contact angle between the solid and liquid phases (degrees)
ρ_L	Density of the liquid phase (kg/m^3)
ρ_S	Density of the solid particles (kg/m^3)
Ψa	Dimensionless spray flux, a measure of spray density and drop overlap in the spray zone (-)

References

[1] J. D. Litster, B. J. Ennis, The science and engineering and granulation processes. Kluwer Academic Publishers, Dordrecht, 2004.

[2] P. C. Knight, Structuring agglomerated products for improved performance, Powder Technology 119(1) (2001)14-25.

[3] S. M. Iveson, J. D. Litster, et al., Nucleation, growth and breakage phenomena in agitated wet granulation processes: a review, Powder Technology 117(1-2) (2001) 3-39.

[4] S. M. Iveson, P. A. L. Wauters, et al., Growth regime map for liquid-bound granules: further development and experimental validation, Powder Technology 117 (2001) 83-97.

[5] P. R. Mort, Scale-up of binder agglomeration processes, Powder Technology 150 (2) (2005) 86-103.

[6] K. P. Hapgood, B. Khanmohammadi, Granulation of Hydrophobic Powders Via Solid Spreading Nucleation, AIChe Annual Meeting, AIChE, San Francisco, 2006.

[7] R. Plank, B. Diehl, et al., Quantifying liquid coverage and powder flux in high-shear granulators, Powder Technology 134(3) (2003) 223-234.

[8] R. Boerefijn, M. J. Hounslow, Studies of fluid bed granulation in an industrial R&D context, Chemical Engineering Science 60(14) (2005) 3879-3890.

[9] D. Myers, Surfaces, interfaces and colloids: principles and applications, VCH Publishers Inc, New York, 1991.

[10] M. Lazghab, K. Saleh, et al., Wettability assessment of finely divided solids Powder Technology 157(1-3) (2005) 79-91.

[11] C. F. Lerk, A. J. M. Schoonen, et al., Contact Angles and Wetting of Pharmaceutical Powders, Journal of Pharmaceutical Sciences 65(6) (1976) 843-847.

[12] P. M. Heertjes, N. W. F. Kossen, Measuring the contact angle of powder-liquid systems, Powder Technology 1(1) (1967) 33-42.

[13] M. E. Aulton, M. Banks, Influence of the hydrophobicity of the powder mix on fluidised bed granulation, Powder Advisory Centre, Basel, Switzerland, 1979.

[14] R. E. J. Johnson, R. H. Dettre, Wettability and Contact Angles, in:E. Matijevic (Ed.), Surface and Colloid Science, Wiley Interscience, 1969, pp. 85-153.

[15] M. Hemati, R. Cherif, et al., Fluidized bed coating and granulation: influence of process-related variables and physicochemical properties on the growth kinetics, Powder Technology 130(1-3) (2003) 18-34.

[16] R. C. Rowe, Binder-substrate interactions in granulation: a theoretical approach based on surface free energy and polarity, International Journal of Pharmaceutics 52(1989) 149-154.

[17] L. Farber, K. Hapgood, et al., Hydrophobic nucleation in particle agglomeration. World Congress of Particle Technology, vol 5, Florida, AIChE, Orlando, April 2006.

[18] L. Zajic, G. Buckton, The use of surface energy values to predict optimum binder selection for granulations, International Journal of Pharmaceutics 59(1990) 155-164.

[19] D. Zhang, J. H. Flory, et al., Wettability of pharmaceutical solids: its measurement and influence on wet granulation, Colloids and Surfaces A: Physicochemical and Engineering Aspects, 206(1-3) (2002) 547-554.

[20] O. Planinsek, , R. Pisek, et al., The utilization of surface free-energy parameters for the selection of a suitable binder in fluidized bed granulation, International Journal of Pharmaceutics, 207(1-2) (2000) 77-88.

[21] I. Krycer, D. G. Pope, An Evaluation of Tablet Binding Agents. Part I. Solution Binders, Powder Technology 34(1983) 39-51.

[22] K. P. Hapgood, Nucleation and Binder Dispersion in Wet Granulation, Department of Chemical Engineering, University of Queensland. Brisbane, Australia, 2000.

[23] K. P. Hapgood, S. M. Iveson, et al., in: A. D. Salman, M. J. Hounslow and J. P. K. Seville (Eds.), Granule Rate Processes, Granulation, Handbook of Powder Technology, vol. 11, Elsevier, London, 2006, p. 11.

[24] S. J. R. Simons, R. J. Fairbrother, Direct observations of liquid binder-particle interactions: the role of wetting behavior in agglomerate growth, Powder Technology 110(2000) 44-58.

[25] R. Flores, C. Keary, et al., Advantages of Foam Granulation and Process Miniaturization for Small Quantities of Micronized Drugs, Annual Meeting of the American Association of Pharmaceutical Scientists, TN, AAPS, Nashville, 2005, November 6-10.

[26] C. M. Keary, P.J. Sheskey, Preliminary report of the discovery of a new pharmaceutical granulation process using foamed aqueous binders, Drug Development and Industrial Pharmacy 30(8) (2004) 831-845.

[27] Mahadevan, L. and Y. Pomeau, Rolling droplets, Physics Fluids 11(1999) 2449-2453.

[28] H. Fujimoto, A. Tong, et al. Numerical and experimental study on oblique collision of water droplet with a solid substrate, Pro. 2005 International Mechanical Engineering Congress and Exposition, IMECE05., 2005.

[29] D. T. Leighton, A. Acrivos, Measurement of Shear-Induced Self-Diffusion in Concentrated Suspensions of Spheres, Journal of Fluid Mechanics, 177 (1987) 109-131.

[30] P. Aussillous, D. Quere, Liquid marbles, Nature 411(6840) (2001) 924-927.

[31] P. Aussillous, D. Quere, Properties of liquid marbles, Proceedings Royal Society A 462(2067) (2006) 973-999.

[32] L. Forny, I. Pezron, et al., Storing water in powder form by self-assembling hydrophobic silica nanoparticles, Powder Technology 171(1) (2007) 15-24.

[33] M. A. Ansari, F. Stepanek, Formation of hollow core granules by fluid bed in situ melt granulation: Modeling and experiments, International Journal of Pharmaceutics 321(1-2) (2006): 108-116.

[34] K. P. Hapgood, J. D. Litster, et al., Drop Penetration into Porous Powder Beds, Journal of Colloid and Interface Science 253(2) (2002): 353-366.

[35] K. Takano, N. Maruyama, et al., Fluidized bed binderless granulation of hydrophobic drugs with fine lactose powder, Advanced Powder Technology 14 (2003) 369-381.

[36] M. S. Kalekar, S. S. Bhagwat, Dynamic behavior of surfactants in solution, Journal of Dispersion Science and Technology 27(7) (2006): 1027-1034.

[37] T. Schæfer, C. Mathiesen, Melt Pelletization in a high shear mixer IX. Effects of binder particle size, International Journal of Pharmaceutics 139(1996) 139-148.

[38] T. Schæfer, C. Mathiesen, Melt Pelletization in a high shear mixer VIII. Effects of binder viscosity, International Journal of Pharmaceutics 139(1996) 125-128.

[39] G. I. Tardos, M. I. Khan, et al., Critical Parameters and limiting conditions in binder granulation of fine powders, Powder Technology 94(1997) 245-258.

[40] S. Agland, S. M. Iveson, The Impact of Liquid Drops on Powder Bed Surfaces, CHEMECA, vol. 99, IEAust/IChemE/RACI, Newcastle, Australia, 1999, September 25-29.

[41] D. Bartolo, C. Josserand, et al., Retraction dynamics of aqueous drops upon impact on non-wetting surfaces, Journal of Fluid Mechanics 545(2005) 329-338.

[42] J. D. Litster, K. P. Hapgood, et al. Liquid distribution in wet granulation: dimensionless spray flux, Powder Technology 114(1-3) (2001): 32-39.

[43] K. P. Hapgood, J. D. Litster, et al., Nucleation Regime Map for Liquid Bound Granules, AIChE Journal 49(2) (2003) 350-361.

4

Liquid marble formation:

Spreading coefficients or kinetic energy?

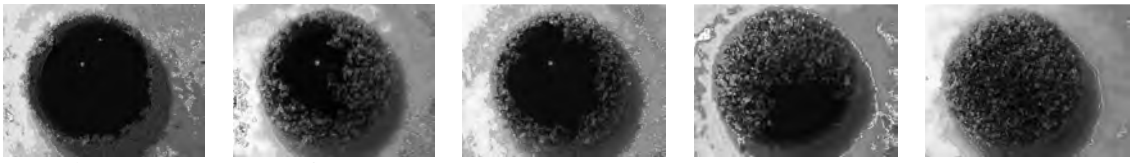

2 cm	4 cm	6 cm	8 cm	10 cm
26% Cov.	60% Cov.	73% Cov.	81% Cov.	91% Cov.

Water marble with PTFE as function of droplet release height

Chapter 4: Liquid marble formation: spreading coefficients or kinetic energy?

Declaration for Thesis Chapter 4

Declaration by candidate

In the case of Chapter 4, the nature and extent of my contribution to the work was the following:

Nature of contribution	Extent of contribution (%)
Initiation, Key ideas, experimental and analysis work, development, writing up the paper	75

The following co-authors contributed to the work. Co-authors who are students at Monash University must also indicate the extent of their contribution in percentage terms:

Name	Nature of contribution	Extent of contribution (%) for student co-authors only
1-Jacques S. Liu	Kinetic energy experiment	15
2-Wei Shen	Initiation, Key ideas, reviewing and editing of the paper	--
3- Karen P. Hapgood	Supervision, reviewing and editing of the paper	--

Candidate's Signature		Date

Declaration by co-authors

The undersigned hereby certify that:

(1) the above declaration correctly reflects the nature and extent of the candidate's contribution to this work, and the nature of the contribution of each of the co-authors.

(2) they meet the criteria for authorship in that they have participated in the conception, execution, or interpretation, of at least that part of the publication in their field of expertise;

(3) they take public responsibility for their part of the publication, except for the responsible author who accepts overall responsibility for the publication;

(4) there are no other authors of the publication according to these criteria;

(5)potential conflicts of interest have been disclosed to (a) granting bodies, (b) the editor or publisher of journals or other publications, and (c) the head of the responsible academic unit; and

(6) the original data are stored at the following location(s) and will be held for at least five years from the date indicated below:

Location(s)	Department of Chemical Engineering, Monash University, Clayton Campus

[Please note that the location(s) must be institutional in nature, and should be indicated here as a department, centre or institute, with specific campus identification where relevant.]

Signature 1	[redacted]	Date
Signature 2	-- [redacted]	--
Signature 3	--	--

Abstract:

A liquid marble is a network of self-assembled hydrophobic powder around a droplet. The mechanism and driving force leading to the formation of liquid marbles have not been investigated. In this study, the solid-liquid spreading coefficient (λ_{SL}) is calculated and the effect of the impact of kinetic energy on liquid marble formation for various fluids and particles is investigated. Single drops of fluid were produced using a syringe and released from different heights onto loosely packed powder bed. The degree of powder coverage over liquid droplet after impact was photographed and analyzed using image analysis. The results show that the spreading coefficients do not predict liquid marble formation, but instead the powder coverage of the drop is exponential to the applied kinetic energy. As the kinetic energy is increased, the percentage of coverage of liquid droplet by powder increases, and as the particle size decreases the percentage of coverage also increases. These results demonstrate that good powder coverage is assisted by increasing the kinetic energy of impact, which increases the size of the initial fluid-powder contact area and causes internal fluid flow within the droplet during impact and rebound, which entrains the particles and forms the powder shell. The knowledge that the level of agitation applied is an important factor in whether liquid marble is successfully produced is expected to facilitate progress in creating liquid marbles as precursors to a wide range of structured powder-liquid products in cosmetics, pharmaceuticals and other advanced materials.

Nicky Eshtiaghi, Jacques S. Liu, Wei Shen, Karen P. Hapgood, "Liquid marble formation: Spreading coefficients or kinetic energy?", Powder Technology, 2009 (196), 126-132.

Keywords: Hydrophobic powder, granulation, nucleation, kinetic energy, liquid marble, powder shell formation, spreading coefficients

4.1. Introduction

Liquid marbles are uniquely structured granules, where a self-assembled network of hydrophobic powder forms a shell around the exterior of a droplet of fluid [1]. Liquid marbles are a novel approach for producing structured fluid-filled particles in the food, cosmetics and pharmaceutical industries [2- 4].

There are now several papers on the formation of liquid marbles, but there are no studies currently published on *why* liquid marbles form. Two different mechanisms have been tentatively proposed to date in the literature:

1. The first suggested mechanism is that liquid marble formation is a surface energy phenomenon, driven by the solid-over-liquid spreading coefficient (λ_{SL}) [2, 4].
2. The second proposed mechanism is that kinetic energy [2,3] is responsible, based on observations of the role of mixing intensity during the manufacture of a large quantity of liquid marbles.

A previous study [2] of liquid marble formation on a loosely packed bed of hydrophobic powder made two critical observations. When a droplet was placed gently onto the powder bed (to avoid fluid flow within the drop interior due to impact or rolling), almost no coverage of the droplet with powder with powder occurred. This implies that the spreading of the powder over the liquid may not be driven by surface tension or spreading coefficients. However, when the drop was released from a height or rolled on the powder surface, an increased tendency to form a complete liquid marble was

observed. These preliminary results [2] suggested that bulk motion of the drop due to the kinetic energy of either rolling or impact, is critical for liquid marble formation. This agreed with other observations of liquid marble formation at pilot scale [3], where the use of higher mixer impeller speed to increase the level of agitation and overall kinetic energy applied during mixing was found to be crucial to effectively encapsulating the water in a shell of hydrophobic powder.

In order to form a stable, spherical, liquid marble from a single drop, a series of steps was proposed [2] as part of a framework. The final step in liquid marble formation was provisionally shown as needing a positive value of the solid-over-liquid spreading coefficient (λ_{SL}).The spreading coefficient is defined as the difference between the works of adhesion and cohesion [5, 6]. Spreading coefficients define that spreading (i.e. further replacement of the liquid-vapor interface with a liquid-solid interface) will occur if it is thermodynamically favorable [6], as indicated by a positive value of the spreading coefficient. Two spreading coefficients are theoretically possible [5] – the liquid may spread over a solid, denoted as λ_{LS}, or the solid may spread over the liquid, denoted as λ_{SL}. For liquid marble formation, we are most interested in how a hydrophobic powder covers a liquid droplet, which is theoretically described by λ_{SL}.

$$\lambda_{SL} = -\Delta G_{SL} = \gamma_{SL} + \gamma_{SV} - \gamma_{LV} \quad (1)$$

A negative value for ΔG_{SL} and a corresponding positive value for λ_{SL} mean that the spreading process occurs spontaneously and the solid will freely spread over liquid. Thus,

if $\lambda_{SL} > 0$ then the solid-liquid interaction is sufficiently strong to promote the spreading of solid over liquid, while if $\lambda_{SL} < 0$ then the solid will not spread over liquid.

Spreading coefficients for phase 1 over phase 2 can be calculated from their dispersive component (indicated by superscript d) and polar component (indicated by superscript p) of the total surface energy (based on Wu's harmonic mean method) [5, 6]:

$$\lambda_{12} = 4\left[\frac{\gamma_1^d \gamma_2^d}{\gamma_1^d + \gamma_2^d} + \frac{\gamma_1^p \gamma_2^p}{\gamma_1^p \gamma_2^p} - \frac{\gamma_1}{2}\right] \tag{2}$$

Eq. (2) can be used to calculate the solid–over-liquid spreading coefficient λ_{SL}, by defining phase 1 as the solid, and phase 2 as the liquid.

Wu's harmonic mean method is an empirical approach where the forces are divided into polar forces and dispersive forces, and has little fundamental basis. It is intended to be applied only to pure fluids, not to solutions aqueous solutions where adsorption of the polymer at the interface has a significant effect on the local surface energy. Despite this the approach has been widely used to predict solid-liquid spreading interactions, including cases of powders spreading over liquids, with apparent success (for example, see [17, 18]). In addition, some of these papers apply the theory to aqueous solutions such as PVP and HPC solutions [17, 18] which is theoretically invalid, although again their experimental results appear to indicate a causal link between spreading coefficients and granule wetting, strength and/or structure.

The solid-liquid spreading coefficient has been proposed as a quantitative method to predict whether a given powder-liquid combination will form a liquid marble [4]. In this paper, we test the hypothesis that the solid-liquid spreading coefficient λ_{SL} predicts liquid marble formation, by calculating the λ_{SL} spreading coefficient using literature values of surface energy and comparing these results to the corresponding experimental observations of liquid marble coverage while holding the kinetic energy as close as possible to zero. The second part of the paper then systematically varies the kinetic energy of the drop at impact and examines the effect on the degree of liquid marble powder coverage, as well as the effect of varying powder size and liquid properties.

4.2. Experimental

4.2.1. Spreading coefficient experiments

For the spreading coefficient experiment, we used 100 μm Polytetrafluoroethylene (PTFE) spheres with droplets of different fluids: distilled water, glycerol (99%, Sigma Aldrich Riedel-de Haen), 6% w/w polyvinylpyrrolidone (PVP(40T), Sigma Aldrich Pty Ltd) and 2% w/w hydroxypropylmethylcellulose (HPMC, Premium LV, E3, The DOW Chemical Company). Each droplet was released from either 0 cm or 10 cm onto a powder bed using 1 cc syringe. PVP and HPMC solution viscosities were measured using a rotational viscometer (Visco Basic Plus, Fungilab, Barcelona).

4.2.2. Kinetic energy experiments

In order to investigate powder motion mechanism, kinetic energy experiments consisted of two phases – firstly using liquids with different viscosities and secondly using powders with different particle size. A loosely packed powder bed of PTFE 100 (Sigma Aldrich

Pty Ltd.) was prepared by sifting the powder through a coarse sieve and collecting the powder in a petri dish. The powder surface was levelled by gently scraping the powder surface with a flat edge. The resulting powder bed was 1.2 cm high (level with the top of the petri dish) and 61% porosity. Droplets were dispensed from a 1cc syringe using an 18g needle with 0.02 mL volume. The syringe needle was oriented horizontally, parallel to the powder bed so that droplet volume would be better controlled. The droplet would have to pool on top of the needle aperture before falling, and so it was possible to pull back on the plunger to prevent multiple droplets being released.

In these experiments 6 mixtures of water and glycerol (99%, Sigma Aldrich Riedel-de Haen) solution - 0%, 20%, 40%, 60%, 80% and 100% glycerol solutions- were chosen (see Table 1 for properties). Droplets of each solution were released from various heights from 2 cm to 25 cm onto a loosely packed powder bed using a 100 μL Hamilton syringe with a 22 gauge needle. In this set of experiments 2 mL of food dye (Queen Fine Foods Pty Ltd) was added to initial 10mL glycerol-water mixture to increase contrast when taking photos. This affected the actual concentration of glycerol. We refer to the fluids by their names before adding the dye (20%, 40%, etc) but the true concentration (including the dye) has been given in the Table 1. The data shown in Table 1 have been interpolated from water - glycerol solution data, assuming that the dye has the same viscosity as water. This is a reasonable method to estimate the solution viscosity. The presence of the food dye reduced the surface tension of the fluids. Table 1 summarizes the surface tensions of the fluids as measured using a dynamic surface tensiometer (Nima

Technology, DST 9005) with platinum DuNouy Ring (ring diameter 20.6 mm and wire diameter 500 µm).

Table 1. Physical properties of fluids (including food dye) at 20 ºC

Fluid	Actual composition including food dye (Glycerol v/v %)	Surface tension (mN/m)	Viscosity (mPa s) [7]
Water	0	71.4	1.0
Glycerol 20%	17	70.6	1.54
Glycerol 40%	33	69.2	2.68
Glycerol 60%	50	66.3	5.26
Glycerol 80%	67	64.6	9.8
Glycerol 100%	83	45.8	509

The kinetic energy of the droplets was calculated from the potential energy of the droplet. By keeping the droplet volume constant at 0.02 mL and accounting for differences in fluid density, the kinetic energy can be varied by changing the release height of the droplet. We assume that the potential energy of the droplets is transformed completely into kinetic energy and this kinetic energy is used upon contact with the powder bed to deform the droplet such that the coverage of the droplet is attained via internal flow of the droplet dragging particles onto it. Kinetic energy losses via powder packing rearrangement, including formation of a crater in the powder bed have not been taken into account.

The effect of powder size was investigated using a similar methodology. Four different size grades of PTFE powder (Sigma Aldrich Pty Ltd) - 100, 35, 12, and 1 μm grades - were used to produce 1.2 cm high loosely packed powder beds with 61%, 75%, 78%, and 87% porosity for 100, 35, 12, and 1 μm particle size, respectively. For these experiments, drops of a water solution (10mL distilled water plus 2 mL dye) were dispensed using the same 100 μL syringe onto the powder beds, and the liquid marble images were analyzed as above.

4.2.3. Image analysis method

After the drop had landed, the fractionally covered liquid marbles were then photographed using a stereo microscope (SMZ series) with a 3MP camera at 1024x768 resolutions using Motic camera imaging software. Two images per droplet were taken from directly overhead: one with the upper surface of the droplet in focus to capture the fine details of the droplet (see Figure 1a) and the other with the outermost circumference of the droplet in focus. This latter image was used to trace the border of the droplet in NIH Image J software (V1.38X) so that the region of interest could be saved and applied to the former image.

After the two images were acquired, the image processing and analysis phase were performed. Firstly, the background was changed to black and foreground to white and the image was then segmented using "*k*-means clustering" (see Fig.1b). Reflections of the fiber optic lighting globes were manually edited out (compare white versus black spots in Fig.1b and c). The image was then converted to a threshold image with a setting of 0-5

(see Fig. 1c) and the percentage coverage in the region of interest was calculated for images including fine details of gaps in the powder sheet (see Fig. 1a versus c).

A fine crack in the powder sheet which we refer to as a "vein" was not a point of interest but affected the percentage coverage results. For this reason, the image processing was continued from the above step to eliminate the veins. The threshold image was converted to a binary image. The resulting image will have the covered region in black and the rest of the image in white (see Fig. 2d). The image was then inverted and dilated twice and eroded once such that the uncovered vein like region diminished. If veins still exist they are either likely to be large enough to be important, or they are cut off from the main uncovered region and only present as small islands which can be omitted by the "particle analysis" tool in Image J. Then, the percentage coverage in binary images was calculated using Image J.

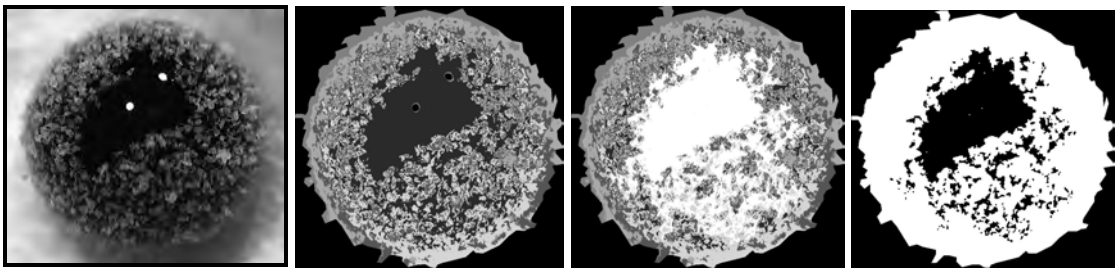

(a) (b) (c) (d)

Fig. 1. Image processing for 20% glycerol-water droplet on PTFE 100 μm from 10 cm height: (a) original photo (b) clustered image after segmentation (c) after threshold and (d) final image after binary processing

Five repetitions of kinetic energy experiment were made for each combination. Fig. 1 shows the process of image J analysis for a mixture of 20% glycerol-water droplet which

was released from 10 cm above a powder bed of PTFE 100 μm. The percentage of coverage for this system varied from 69.7% before deleting veins (Fig.1c) to 81.4% after deleting veins (Fig. 1d).

4.3. Results and discussion

4.3.1. Spreading coefficients theory

According to Rowe [5], the sign of the spreading coefficient λ_{SL} can be used to predict whether the solid powder would spread on the liquid surface or not. The surface energies of all the powders and fluids used in these experiments are summarized in Table 2. Results for the calculated values of λ_{SL} using Eq. (2) are tabulated in Table 3.

Table 2: Summary of dispersive, polar and total surface energies.

Powder or Fluid	Dispersive surface energy (mJ/m^2)	Polar surface energy (mJ/m^2)	Total surface energy (mJ/m^2)	Fluid viscosity (mPa s)
Water	21.8 [8]	51.0 [8]	72.8 [8]	1.0 [7]
Glycerol	37.0 [8]	26.4 [8]	63.4 [8]	509 [7]
6% PVP solution [9]	28.4	25.2	53.6	2.2
2% HPMC solution [9]	18.4	30.0	48.4	3.1
PTFE [10]	18.0	0.0	18.0	--

Rowe [5] proposed that spontaneous spreading of solid powder should occur when λ_{SL} is positive. Table 3 shows that that $\lambda_{SL} > 0$ for pure liquids on PTFE which means that the

spreading of solid powder over liquid should be spontaneous. On the other hand, all combinations of PTFE and pure liquids have $\lambda_{LS} < 0$, which predicts that the spreading of the liquid over the solid should be thermodynamically unfavorable. Predictions of powder behavior based on pure liquids and PTFE are in contradiction with the experimental observations for drops placed gently on the powder bed from a height of 0cm. These drops show no powder coverage (Table 3). Since no consideration of external forces is given in the derivation of equations from (1) and (2), the zero release height experiment simulates the condition where the drop is under no external force. Thus, if liquid marble formation was solely a surface chemistry effect, with positive λ_{SL} it would be expected that a liquid marble would spontaneously form. Therefore, we find that Eq. (2) proposed by Rowe [5] does not predict the spreading of powder over a liquid surface and therefore can not be used to predict liquid marble formation.

Apart from pure fluids, two polymer binder solutions were also studied for their interactions with powders. It is known that for polymer- water solutions the dispersive and polar components cannot be determined using Eq. (2) because of the possible adsorption of polymers on the surfaces of the polymer solutions. The spreading of powder over these polymer surfaces could not be experimentally observed. Literature surface tension data of PVP (6%) and HPMC (2%) solutions [9] show that these polymers quite significantly influence the surface tension of water (Table 2). PVP and HPMC reduce the polar component of water by 50.6% and 41.2%, respectively, and change the dispersion component of water by 30.3% and -15.6%, respectively. Teflon powder shows no tendency of spreading on any of the liquids. The non-spreading

behavior of Teflon power over these polymer solutions further suggests that comparing surface free energy values of the liquid and solid phases (through λ_{SL}) is not a valid predictive indicator for solid powder spreading over liquid surface.

Table 3. Calculated spreading coefficients for several fluid droplets on 100 µm PTFE (15X magnification, and 1200 µm scale bar for all photos)

Fluid	**λ_{SL}**	**λ_{LS}**	**Released from Height = 0 cm**	**Released from Height = 10 cm**
Water	3.44	-106.16	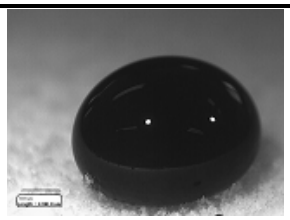	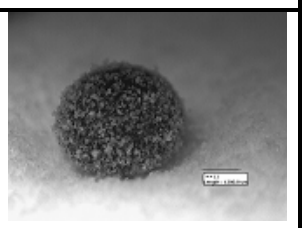
Glycerol	12.44	-78.36	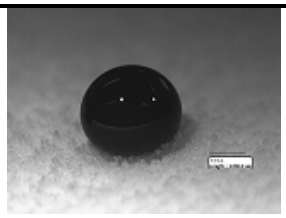	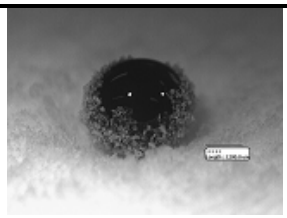
PVP (6%)	-	-	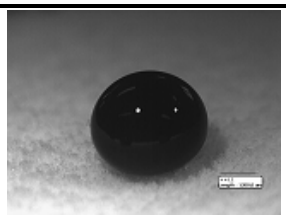	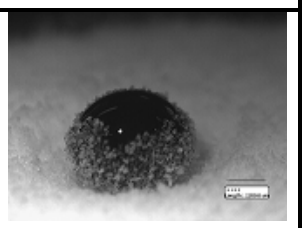
HPMC (2%)	-	-	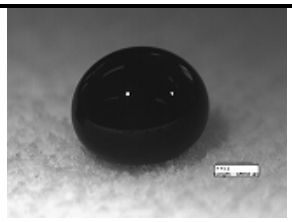	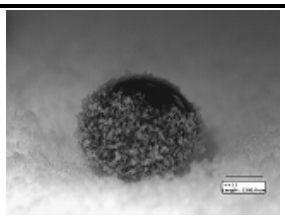

Table 3 also shows variations in the amount of powder coverage when the drops were released from a 10cm height. Although there is some variation in the amount of coverage due to local powder packing, the viewing angle, rolling on landing, etc., the amount of powder coverage appears to decrease as the fluid viscosity (provided in Table 2) increases. The viscosity effect is more systematically investigated in the following Section 3.2.

An obvious reason for the inability of λ_{SL} to predict powder spreading over a liquid surface is that Eq. (2) does not correctly capture the physical process of powder spreading over a liquid surface. When hydrophobic powder spreads over a liquid surface, solid powder particles do not increase their surface area as they spread. Instead, powder aggregates merely disintegrate when they expand their coverage over the liquid surface [20]. In this process, inter-particle attraction forces must be overcome in order for powder particles to spread over a liquid surface. However, the inter-particle attraction forces cannot be equated to the work of cohesion of the solid surface [20]. Therefore λ_{SL}, which is a comparison of liquid-solid adhesion and solid "cohesion", does not reflect the physical process of powder spreading correctly. This is an area of ongoing research effort [20].

4.3.2. Effect of kinetic energy on droplet coverage

An alternative mechanism for liquid marble formation is that powder motion around the shell is driven entirely by kinetic energy [2, 3]. Pilot scale studies of dry water formation showed that increased agitation promoted liquid marble formation [3]. Other studies have shown that an impinging drop undergoes flow circulation in the droplet interior and

consequent surface flow was observed and modeled [11, 12]. We believe that this flow within the droplet is responsible for liquid marble formation [2], and that the driving force is the kinetic energy applied to the system [2, 3].

If the kinetic energy of drop impact on a solid surface is sufficiently high, the drop will first deform and flatten on impact, increasing the maximum radius of the droplet and thus increasing the area of contact between the solid surface and the drop. After the drop has deformed and flattened, the surface tension will cause the drop to recoil back towards a spherical shape. Both the deformation at impact and the recoil after impact create internal flow within the droplet interior, which drives a corresponding surface flow around the drop entraining particles [11, 12]. When a fluid drop lands on a hydrophobic powder surface, it does not penetrate into the powder pores but "sees" an effectively solid powder surface [13]. As soon as the drop touches the powder, a small section of the powder will adhere to the base of the drop. This is the initial step in forming the powder shell of a liquid marble. As the drop deforms and flattens, the contact area between the fluid and powder will increase, and more powder will adhere to the base of the drop. The overall surface area of the drop also increases since the drop is no longer spherical. This process of increasing contact area and increasing powder pickup continues until the maximum drop deformation is reached, and drop recoil commences. During drop recoil, the droplet returns to a spherical shape. The total surface area of the drop decreases back to its original spherical minima, and internal flow is created within the drop as the flattened shape recoils back to spherical. This internal flow creates a corresponding surface flow in the droplet, moving generally from the base of the drop towards the top. The combination

of all of these processes – the increased powder-liquid contact area during deformation, the upward flow of fluid at the drop surface due to the recoils motion, and the temporary increase and then retraction of the drop surface area - all contribute to the formation of a liquid marble.

Since all these processes are enhanced by increasing the kinetic energy of impact, it follows that the degree of liquid marble powder coverage will be exponential to the kinetic energy of the drop as it lands on the hydrophobic powder surface. Although there is some evidence to support this hypothesis from preliminary results [2] and pilot scale studies [3], this hypothesis has not been rigorously tested.

4.3.3. Effect of kinetic energy and fluid viscosity on droplet coverage

The first series of experiments focused on investigating the relationship between the kinetic energy imparted upon droplet and its coverage by powder on a flat loosely packed bed, and the second phase concentrated on particle size effect. Fig. 2 shows the relationship between kinetic energy and percentage coverage for six water-glycerol solutions on 100 μm PTFE powder. The X-scale error bars are representative of the maximum errors in height measurements (±0.5 mm) and the subsequent variation in kinetic energy calculation. The Y-scale error bars represent one standard error of the mean for 5 samples per droplet.

Fig. 2 shows that increasing the kinetic energy causes an exponential increase in the powder coverage for water droplets on 100 μm PTFE powder. Initially, the liquid marble coverage increases rapidly with each increment in the applied kinetic energy. However,

as the coverage gets closer to 100%, the rate of coverage slows and eventually appears to plateau at a maximum value between 85%-95% of complete coverage. Compared with the same data series for water, glycerol liquid marbles have a much lower coverage for a given kinetic energy.

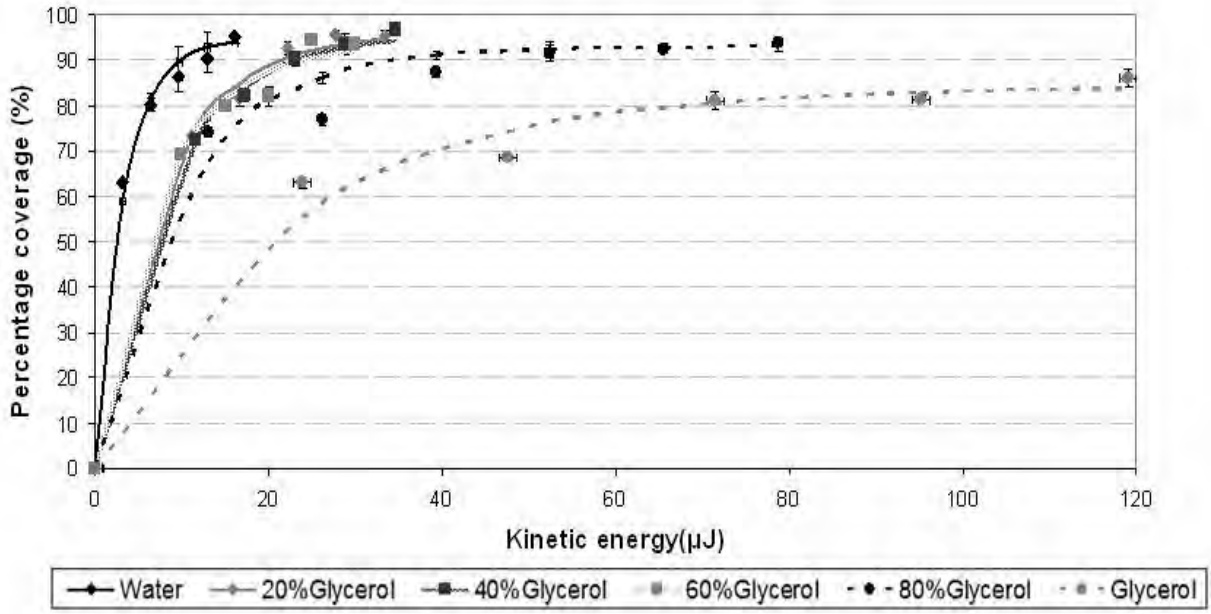

Fig. 2. Kinetic energy and viscosity effects on liquid marble powder coverage for water

For example, powder coverage for a glycerol droplet is around 50% less than for a water droplet the same size released from the same height of 10 cm (see Fig. 3). The strongest glycerol solution used in these experiments had a viscosity 500 times the viscosity of water which significantly impairs the deformation and recoil of the drop upon impact. This consequently gives lower coverage because so much of the kinetic energy is dissipated by viscous forces. In addition, the higher concentration glycerol solutions also have lower surface tensions (refer to Table 1) which reduce the drop recoil forces [14, 15]. Subsequently, higher kinetic energy is needed to expand the drop-powder surface area at contact and also to produce good bulk fluid motion during deformation and recoil

of the viscous drops. Thus, the percentage of coverage for glycerol droplet is much lower than for a water droplet at same given kinetic energy.

. **(a)**

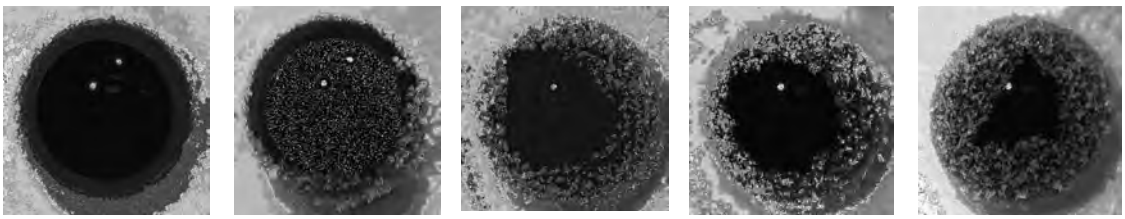

5 cm **10 cm** **15 cm** **20 cm** **25 cm**

26% Cov. **37% Cov.** **62% Cov.** **63% Cov.** **72 % Cov.**

(b)

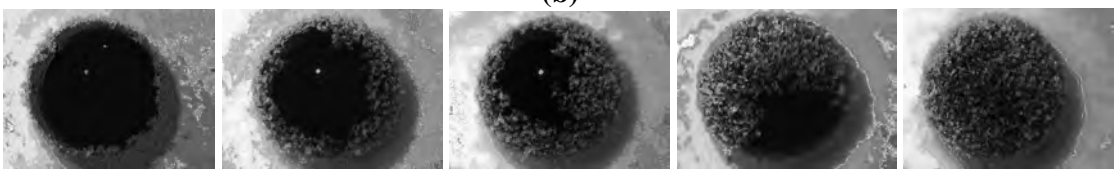

2 cm **4 cm** **6 cm** **8 cm** **10 cm**

26% Cov. **60% Cov.** **73% Cov.** **81% Cov.** **91% Cov.**

Fig. 3. Percent PTFE 100 powder coverage as a function of the drop release height for (a) glycerol droplet, and (b) water droplet.

The liquid marble coverage data shown in Fig.2 are related to kinetic energy using the following empirical equation.

$$Coverage(\%) = A(1 - e^{-bE}) \quad (3)$$

where the A is the maximum extent of liquid marble coverage (%), and the b represents the ease of liquid marble formation (1/μJ) and the E is the kinetic energy of impact (μJ). High values of b means that only a small increment in kinetic energy is required to produce a considerable increase in liquid marble coverage. The values of the parameters

A and *b* were determined by fitting Eq. (3) to each data set shown in Fig. 2 and minimizing the sum square of errors. The results are summarized in Table 4, which shows that the maximum liquid marble coverage *A* is a strong function of the fluid viscosity. Fig. 4 plots that the maximum coverage *A* as a function of the fluid viscosity, and shows the maximum coverage achieved falls sharply as the viscosity increases due to increasing fluid resistance to motion.

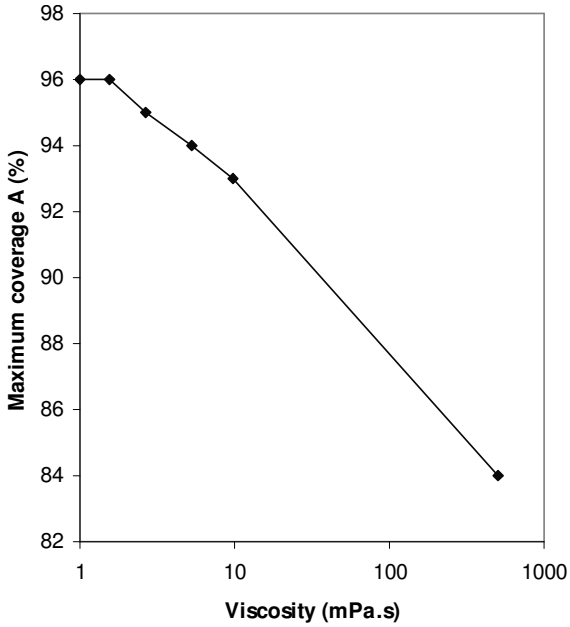

Fig. 4 .The effect of fluid viscosity on maximum extent of coverage for water and glycerol solutions on 100 µm PTFE powder

Fig. 2 and 4 show that the higher the viscosity of the solution, the lower the degree of coverage. Table 4 also shows that the maximum extent of coverage *A* decreases as surface tension decreases due to the loss of driving force for drop recoil. Note that the surface tension of the fluids used varies over a narrow range (see Table 1) compared to the several orders of magnitude variations in fluid viscosity. This again supports the conclusion that surface energy effects are not the main factor in determining the liquid

marble powder coverage, as Fig. 4 shows large differences in coverage where there are differences in viscosity but comparatively small changes in surface tension. The 20%, 40% and 60% glycerol data all overlap because the viscosity differences of these three solutions are relatively small (see Table 1 which shows viscosity varies between 1 and 5 mPa.S). Fluids with higher viscosity and lower surface tension require higher kinetic energy input to produce the same liquid marble coverage.

Table 4. Summary of the ease of formation, *b*, and maximum extent of coverage, *A*, for liquid marbles formed using 100 μm PTFE powder

Fluid	Maximum coverage *A* (%)	Ease of formation *b* (1/μJ)
Water	95	0.3
20% Glycerol	96	0.13
40% Glycerol	96	0.12
60% Glycerol	94	0.13
80% Glycerol	93	0.1
100% Glycerol	84	0.045

The proposed model for liquid marble formation by kinetic energy involves deformation and an increase in surface area of the droplet upon impact followed by recoil which drives fluid flow. Thus we expect that kinetic energy, surface energy and viscosity will all be important factors in determining liquid marble coverage. Plots of the coverage versus various combinations of dimensionless groups relevant to drop deformation and recoil [13, 15, 16], including the modified Weber number, Ohnesorge number, Capillary

number and Bond number did not produce an improved analysis or show a more general trend, and generally looked similar to Fig.2. The reason for the failure of dimensionless analysis in this case is not understood. The conventional analysis of drop impact required high speed dynamic imaging of the drops to determine the maximum spreading diameter, which can then be shown to be related to various functions of We and Re (e.g. [13, 15, 16]). We do not have this data available, and impact on the deformable powder bed creates a "crater" where the drop sinks below the top surface of the bed, which makes capturing the required images much more difficult compared to studying drop impacts on solid, immovable surfaces. Although we expect that the percentage coverage should be a function of the Weber and Reynolds numbers, our data does not support a simple overarching dimensionless relationship between liquid marble powder coverage and dimensionless groups.

4.3.4. Effect of particle size on droplet coverage

The effect of particle size was investigated by repeating the experiments for different particle sizes of PTFE. Fig. 5 shows that the same exponential relationship between kinetic energy and percentage of coverage was found, but the smaller particle sizes exhibit less coverage (see Table 5 and Fig. 5). This is contrary to what is expected – a smaller particle is lighter and should be more easily carried by internal flows of the droplet. We believe that particle agglomeration confounded the effect of particle size. Aside from PTFE 100 μm, all the smaller particle size grades formed agglomerates which were clearly larger than the stated particle size and in some instances formed aggregates even greater than 100 μm. Fig. 6 clearly demonstrates these agglomeration phenomena. These agglomerates hindered liquid marble formation as they resisted movement due to

their higher mass. Thus our results show that the percentage of coverage increases as primary particle size of the powder increases, due to the lower level of agglomeration for the coarser powders tested.

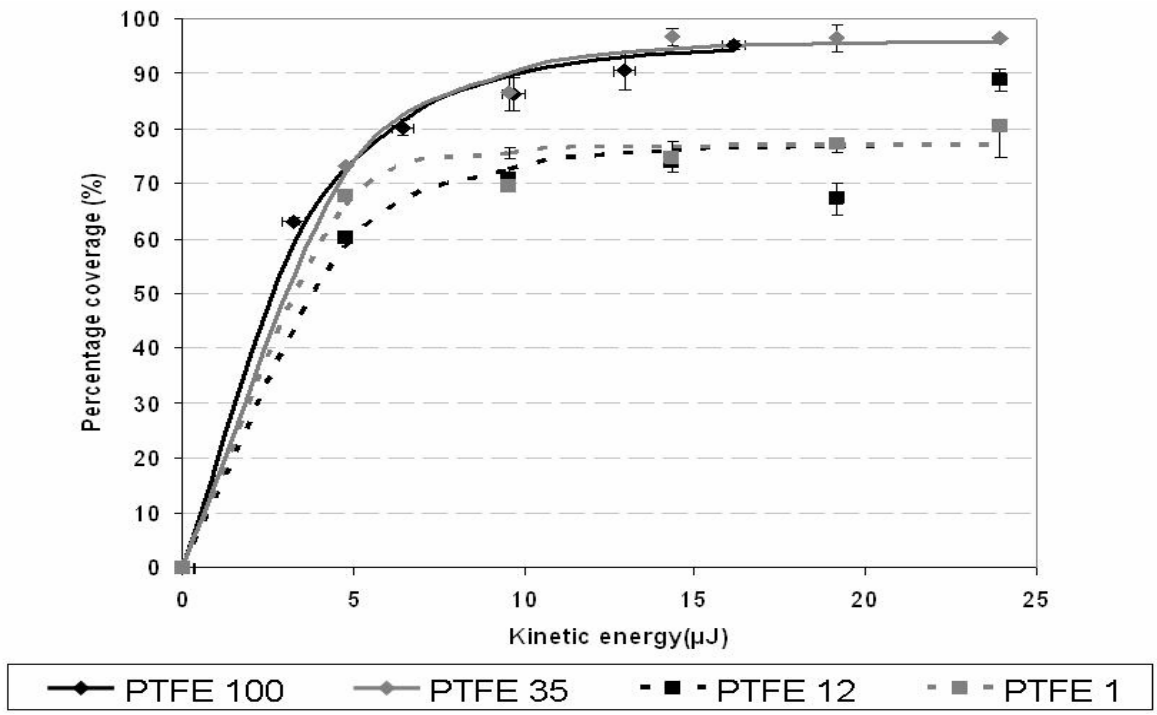

Fig. 5. Particle size effect on liquid marble powder coverage for water droplets on PTFE powders

Table 5. The ease of formation and maximum coverage of water liquid marbles as a function of PTFE particle size.

PTFE Particle size (μm)	Maximum coverage *A* (%)	Ease of formation *b* (1/μJ)
100	95	0.3
35	96	0.3
12	77	0.3
1	77	0.4

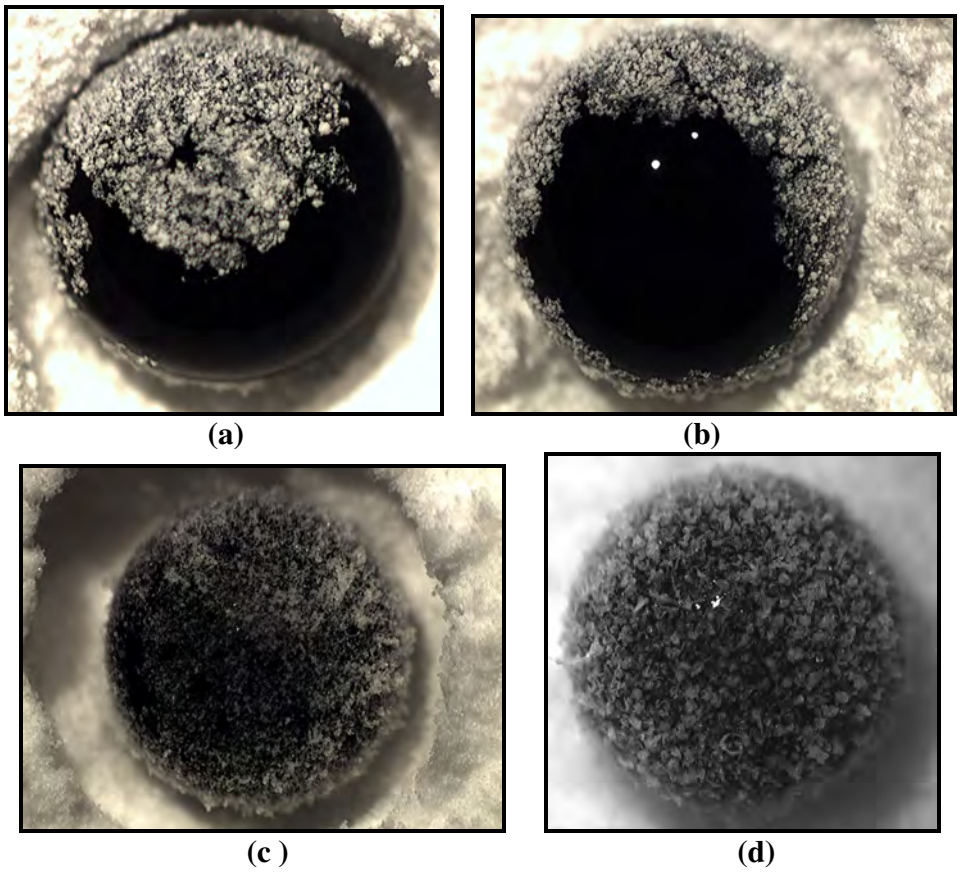

Fig. 6. Water droplet released from 10cm height on (a) 1 µm (b) 12 µm (c) 35 µm (d) 100 µm PTFE powder bed (droplet size and image magnification are constant)

Fig. 6a clearly shows PTFE 1 µm particles containing agglomerates much larger than the theoretical 1 µm particle size. As shown in Fig. 6d for PTFE 100 µm, all of the particles are similar in size and no agglomeration is observed. We expect that the trend of increasing coverage for larger apparent particle size would be reversed for powders where the particles remained well dispersed, although agglomeration of fine particles is well known and extremely common. Kendall (1994) reported that cohesion forces (Vander Waals force) for particle with 1µm size can be up to million times greater than gravity forces depending on the particle size and roughness of the surface in contact [19]. The strong cohesion forces between the finer particles would result in the aggregation of

the powders, as shown in Fig. 6a,b, and may also increase the adhesion between the particles and the bulk of the powder bed. The inter-particle attraction between the particles in the bed would also resist the separation of aggregates and the formation of the powder shell around the liquid marble. More kinetic energy would be required to break the strong cohesion forces between particles as the primary particle size decreases, further retarding the extent of liquid marble coverage.

The results in Fig. 5 appear to show a critical height/kinetic energy where any additional kinetic energy input yields similar coverage. It may be that there is actually 100% coverage but due to minor image analysis bias 100% is not reported. Alternatively it may be that there is a limiting coverage amount of *A* due to the powder properties, including powder packing causing gaps in the self-assembled powder layer, hydrophobic or static repulsion and limitations in the level of droplet deformation that can be achieved.

Differences in particle packing within the petri dish may also have contributed to the unexpected trend in liquid marble coverage as a function of particle size. Often droplets impacting onto the powder bed cause the bed to deform and a "crater" is created. This reduces the overall amount of kinetic energy available for droplet coverage. As particle size decreases, the propensity for crater formation increases, due to the much lower bulk densities of the powder beds, which allow significant bed rearrangement and void collapse. Further investigation into the effects of particle size, aggregate size and powder bed structure is required to determine which is the most important effect.

In addition to the agglomeration issues already noted, the smaller particles were also less opaque compared to the larger 100 μm PTFE powder. If the liquid marbles were only covered in a thin monolayer, the image analysis had more difficulty detecting the opacity (whiteness) of the particles, even if the liquid marble was fully covered. The small focal plane of the camera also aggravated this. Fine uncovered veins in the unfocused regions would be blurred and appear larger than they actually are and these dark areas left exposed would be counted as uncovered regions upon image analysis. This decreases the reported coverage from the true coverage, and this effect may have contributed to the measured maximum coverage and the parameter *A* being consistently less that 100%, even when visual inspection of the liquid marbles appeared to show 100% coverage. An example of this is shown in Fig. 6c, where the side liquid marble can be seen to be well covered by a thin layer of powder, which is more difficult to see compared to the thicker layers on the top of the droplet.

4.4. Conclusions

By calculating solid-liquid and liquid-solid spreading coefficients for several liquid marble formulations confirmed that the spreading coefficient theory [5, 6] is inconsistent with experimental observations of liquid marble formation. An exponential relationship was found between increasing kinetic energy and the percentage of liquid marble coverage. The kinetic energy from impact causes an increase in drop surface area and the drop deformation and recoil create fluid flow which entrains the powder and forms the powder shell. By increasing the drop release height and therefore increasing kinetic energy, the liquid marble powder coverage increases, and the maximum extent of liquid marble coverage falls as viscosity increases and surface tension decreases. As particle

size increased, higher coverage of the droplet was observed but these results were most likely confounded by the effects of agglomeration and/or powder bed rearrangement on impact. The results of this study are the first to study the formation mechanisms of liquid marbles and are an important step in understanding how to create liquid marbles as a precursor to a producing a wide range of structured powder-liquid products and advanced materials.

Acknowledgements

This work was financially supported by the Chemical Engineering Department and Faculty of Engineering at Monash University, and by the Australian Research Council Discovery Projects program (DP0770462). Scholarship support for N. Eshtiaghi was provided by the Monash Graduate Research School. Thanks to Leslie Yeo for initial discussions on kinetic energy effects.

References:

[1] P. Aussillous, D. Quere, Liquid marbles, Nature 411(2001) 924-927.

[2] K. P. Hapgood, B. Khanmohammadi, Granulation of hydrophobic powders, Powder Technology, special issue on granulation, 189 (2009), 253-262.

[3] L. Forny, K. Saleh, I. Pezron, P. Guigon, L. Komunjer, Influence of mixing characteristics for water encapsulation by self-assembling hydrophobic silica nanoparticles Powder Technology, special issue on granulation, 189 (2009), 263-269.

[4] K. P. Hapgood, L. Farber, JN. Michaels, Agglomeration of hydrophobic powders via solid spreading nucleation, Powder Technology, 188 (2009), 248-254.

[5] R. Rowe, Binder-substrate interactions in granulation, a theoretical approach based on surface free energy and polarity. International Journal of Pharmaceutics 52 (1989)149-154.

[6] S.Wu, Polar and non polar interactions in adhesion, Journal of Adhesion 5(1973) 39-55.

[7] D. R. Lide, Ed., CRC Handbook of Chemistry and Physics; CRC Press/Taylor and Francis: Boca Raton, 2008.

[8] P. Luner, M. Sandell, The wetting of cellulose and wood Hemicellulloses, Journal of Polymer Science.: Part C 28 (1969)115-142.

[9] L. Zajic, G. Buckton, The use of surface energy values to predict optimum binder selection for granulations, International Journal of Pharmaceutics 59(1990)155-164.

[10] W. A. Zisman, Influence of constitution on adhesion, Industrial and Engineering Chemistry 55(10)(1963)19–39.

[11] L. Mahadevan, Y. Pomeau, Rolling droplets, Physics of Fluids 11(1999) 2449-2453.

[12] H. Fujimoto, N. J. Hatta, Deformation and rebounding processes of a water droplet impinging on a flat surface above leidenfrost temperature, Journal of Fluid Engineering 118(1996)142-149.

[13] D. Kannangara, H. Zhang, W. Shen, Liquid-paper interactions during liquid drop impact and recoil on paper surfaces, Colloids and Surfaces A: Physicochemical and Engineering Aspects 280(1-3) (2006) 203-215,

[14] S. Middleman, Modeling Axisymmetric Flows, Dynamics of Films, Jets, and Drops. San Diego, Academic Press, Inc., 1995.

[15] T. Mao, D.S. Kuhn, H. Tran, Spread and Rebound of liquid droplets upon impact on flat surfaces, AIChE 43(9) (1997) 2169-2179.

[16] H. Park, W.W. Carr, J. Zhu, J.F. Morris, Single drop impaction on a solid surface, AIChE Journal, 49(10) (2003) 2461-2471.

[17] I. Krycer, D.G. Pope, An Evaluation of Tablet Binding Agents. Part I. Solution Binders. Powder Technology, 1983. 34: p. 39-51.

[18] R.C. Rowe, Binder-substrate interactions in granulation: a theoretical approach based on surface free energy and polarity. International Journal of Pharmaceutics, 1989. 52: p. 149-154.

[19] K. Kendall, Molecules and Mechanics, Science, 263(5154) (1994) 1720-1725.

[20] Nguyen, T.N., N. Eshtiaghi, K.P. Hapgood, W. Shen, An analysis of the thermodynamic conditions for solid powder particles spreading over liquid surface, submitted to Chemical Engineering Science, (2009).

5

An analysis of the thermodynamic conditions for solid powder particles spreading over liquid surface

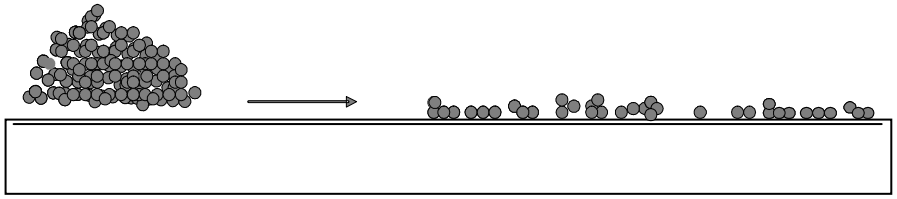

Disintegration of solid powder over a liquid surface

Chapter 5: An analysis of the thermodynamic conditions for solid powder particles spreading over liquid surface

Declaration for Thesis Chapter 5

Declaration by candidate

In the case of Chapter 5, the nature and extent of my contribution to the work was the following:

Nature of contribution	Extent of contribution (%)
Initiation, Key ideas, editing and reviewing the paper	30

The following co-authors contributed to the work. Co-authors who are students at Monash University must also indicate the extent of their contribution in percentage terms:

Name	Nature of contribution	Extent of contribution (%) for student co-authors only
1-Thanh H.Nguyen	Theory development, analysis work, writing up the paper	70
2-Wei Shen	Supervision, reviewing and editing of the paper	--
3- Karen P. Hapgood	Supervision, reviewing and editing of the paper	--

Candidate's Signature		Date

Declaration by co-authors

The undersigned hereby certify that:

(1) the above declaration correctly reflects the nature and extent of the candidate's contribution to this work, and the nature of the contribution of each of the co-authors.

(2) they meet the criteria for authorship in that they have participated in the conception, execution, or interpretation, of at least that part of the publication in their field of expertise;

(3) they take public responsibility for their part of the publication, except for the responsible author who accepts overall responsibility for the publication;

(4) there are no other authors of the publication according to these criteria;

(5)potential conflicts of interest have been disclosed to (a) granting bodies, (b) the editor or publisher of journals or other publications, and (c) the head of the responsible academic unit; and

(6) the original data are stored at the following location(s) and will be held for at least five years from the date indicated below:

Location(s)	Department of Chemical Engineering, Monash University, Clayton Campus

[Please note that the location(s) must be institutional in nature, and should be indicated here as a department, centre or institute, with specific campus identification where relevant.]

Signature 1		Date
Signature 2	-- [redacted]	--
Signature 3	--	--

Abstract:

The spreading of solid powder over a liquid surface is a prevalent phenomenon encountered in many industrial processes such as food and pharmaceutical processes. The driving force for powder spreading over a liquid surface is not clearly understood. The Marangoni effect due to a temperature gradient and the spreading coefficient for solid powder over liquid ($\lambda_{S/L}$) have both been proposed as causes for powder spreading over liquids. The proposed $\lambda_{S/L}$ was based on the same form of the spreading coefficient for a liquid over a solid surface ($\lambda_{L/S}$). Whereas $\lambda_{L/S}$ has a clear thermodynamic definition, the spreading coefficient of solid powder over liquid, $\lambda_{S/L}$, which was defined by simply interchanging the subscripts of the interfacial energy terms, has not been thoroughly analysed. Our experimental results showed that the spreading behaviour of solid powders over liquids cannot be explained or predicted by $\lambda_{S/L}$. In this study we focus on problems associated with the $\lambda_{S/L}$. Through a thermodynamic analysis we conclude that the existing parameter $\lambda_{S/L}$ is unable to predict the spreading behaviour of solid powder on liquid surface, since the interfacial energy approach does not capture the actual physical process of powder spreading over liquid surface. A closer examination of the powder spreading process reveals the fundamental different between liquid spreading over solid surface and solid powder spreading over liquid. This work shows that further research is required to identify and analyse the physical mechanisms which are responsible for powder particles spreading over liquid surfaces.

Thanh H. Nguyen, Nicky Eshtiaghi, Karen P. Hapgood and Wei Shen, Submitted to Powder Technology, under review

Keywords: Liquid marbles, powder spreading over liquid, thermodynamic condition, spreading coefficient, Marangoni effect, liquid surface tension change.

5.1. Introduction

The spreading of liquids over solid surfaces is one of the most widely encountered phenomena in our daily life and also in technology. Its applications in technology range from laundry, lubrication, dyeing/printing to the pharmaceutical and food engineering industries. Thermodynamic predictions of liquid spreading over solid surfaces have been developed for many of those applications [1]. The opposite phenomenon, i.e. solid powder spreading over a liquid surface, is also seen in our daily life and in technology; this phenomenon has important implications in wet granulation [2-4] and food processing [5] and has attracted a number of investigations on the prediction of conditions under which solid powder can spread over a liquid surface.

In many cases when a drop of aqueous liquid is placed on a bed of hydrophobic powder, the powder particles do not spontaneously spread over the drop surface. Instead, the liquid drop must be allowed to roll over the bed and pick up powder particles by contact to gain full powder coverage and to form a liquid marble [6]. McEleney *et al.* [7] showed that hydrophobised fine metal powders do not spread over water sessile drops unless the drops are allowed to roll over the powder bed. The same behaviour is seen for PTFE powders where the powder particles do not spread over water sessile drop (Fig. 1).

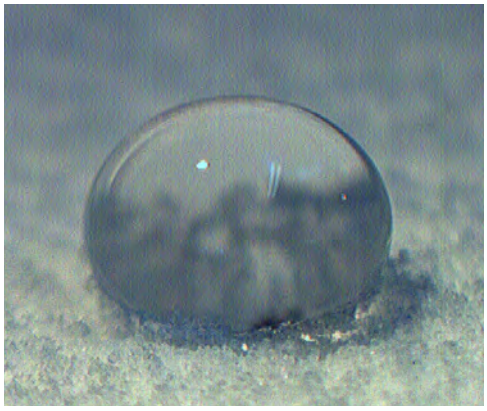

Fig. 1. Non-spreading behaviour of PTFE powder on a gently deposited water droplet

However, there have been observations where hydrophobic powders spread over liquid sessile drops when the drops were placed on the powder bed gently without any rolling movement on the bed. McEleney *et al.* (2009) observed that hydrophobic poly-methylmethacrylate (PMMA) powder spread over the surface of a sessile water drop. In our laboratory, we observed that salicylic acid crystals also can spread over sessile water drops (Fig. 2). The spreading tendency of salicylic acid crystals over water was found to be highly sensitive to minute external disturbance. Slight kinetic energy (0.5 cm impact height) of the water droplet can result in the crystals spreading over the water droplet.

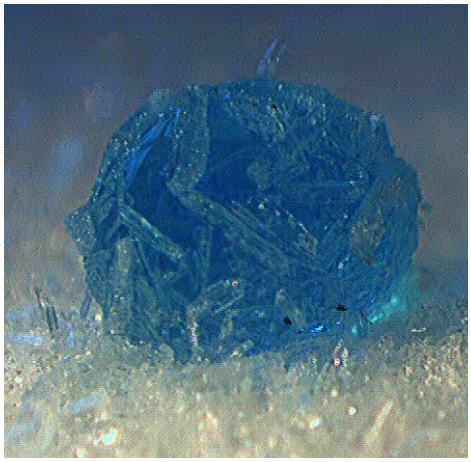

Fig. 2. Surface coverage from a gently placed distilled water droplet (blue dye added as visual aid) on microcrystalline salicylic acid powder bed

Some published work explained the observed "spontaneous" powder spreading behaviour over liquid drops using the concept of favourable thermodynamic spreading coefficients [8]. The spreading coefficient criterion, which is based on the interfacial energetics of the solid-liquid interface, does not offer reliable prediction to the powder behaviours over liquid [9]. While it is obvious that phenomenon of powder spreading over liquid requires more extensive investigations, the purpose of this study is to provide a simple analysis of the spreading coefficient model by Rowe [8] and explain the problems associated with the original development of the model. The proposed spreading coefficient of solid over liquid ($\lambda_{S/L}$) was derived to predict the spreading behaviour of powder over a liquid. The derivation of this model used an analogy of the thermodynamic spreading coefficient for a liquid spreading over a solid surface. The calculation of $\lambda_{S/L}$ further considers the work of adhesion due to the polar and non-polar intermolecular interactions [10] as follows [8]:

$$\lambda_{S/L} = 4\left[\frac{\gamma_S^d \gamma_L^d}{\gamma_S^d + \gamma_L^d} + \frac{\gamma_S^p \gamma_L^p}{\gamma_S^p + \gamma_L^p}\right] - 2\gamma_S \qquad (1)$$

This criterion has been used by other authors to predict powder spreading over liquid [3, 11]. However, the physical validity of the criterion has not been thoroughly analysed in previous research. If the literature surface tension values for PTFE and water are substituted into Eq. (1), a positive value for $\lambda_{S/L}$ is obtained, suggesting that the spreading of PTFE over water would occur, whereas in fact the PTFE powder does not spread over water droplet at all [9]. The predictions made using the $\lambda_{S/L}$ model do not agree with the experimental observations.

The thermodynamic criterion for liquids to spread on solid surfaces has been well studied [1]. The spreading coefficient for liquid spreading over a solid ($\lambda_{L/S}$) provides a thermodynamic prediction of whether such a process can occur spontaneously. The spreading of solid powder over a liquid surface, however, is a very different phenomenon compared to liquid spreading over solid. When a solid powder aggregate expands its apparent coverage over a liquid surface, the behaviour of the molecules in the powder particles is different from the behaviour of molecules of the liquid as they spread over a solid surface. For a hydrophobic powder, solid powder particles do not increase their surface area as they spread. Instead, powder aggregates merely disintegrate as they move towards the free liquid surface. The only change in this process is that a fraction of the solid powder surface becomes a solid/liquid interface. This critical difference between the two spreading processes has not been addressed in sufficient detail previously. The model of solid powder spreading over a liquid surface using $\lambda_{S/L}$ assumes these two spreading processes are similar and can be described by similar physics. It is necessary that the thermodynamics of the process of solid powder aggregate expansion over a liquid surface be studied in detail to allow a clear understanding of the free energy changes of the process and the thermodynamic implications. This analysis will verify the validity of the spreading coefficient $\lambda_{S/L}$ as a criterion for the prediction of powder spreading over a liquid.

To do so we focus on changes in the solid and liquid interface before and after powder spreading over the liquid surface and clarify the correlations between these changes with the free energy changes of the surfaces and interface. Our analysis shows that the existing

spreading coefficient is not valid and unable to predict the spreading of solid powder over liquid. Experiments were also presented to support this view.

5.2. Experimental

To observe the capacity for a powder to spread over a liquid surface, salicylic acid (Sigma-Aldrich, particle size distribution from 90 μm to 2 mm) and polytetrafluoroethylene (PTFE, Sigma-Aldrich, average particle size = 100 μm) were used as the hydrophobic powders for solid spreading. Distilled water was used as the bulk liquid phase. In experiments where powder spreads over liquid surface, Steven's method [5] was employed to observe the behaviour of the powder as it impacts on the liquid surface. In each experiment, approximately 0.15 to 0.25 mL of powder was deposited on a Petri dish of water with the impact height kept constant at 2 cm. The powder disintegration and spreading on the liquid surface was then captured using a digital camera. In experiments where liquid droplets were deposited on powder bed, water droplets were released onto the powder bed from a height of 0.5 cm. The droplet surface coverage by the powders was examined. The degree of droplet surface coverage can be visually and unambiguously assessed when the images of the drops were captured using an optical microscope (Motic 2300 moticam) at a magnification of 11.25 times. The droplet volume was approximately 13 μL.

5.3. Results and discussion

5.3.1. Spreading coefficient and its thermodynamic foundation– liquid spreading over solid substrate

The spreading coefficient for a liquid over a solid or another immiscible liquid surface is used to predict whether or not the spreading of a liquid on either a solid surface or an immiscible liquid surface is spontaneous. The spreading coefficient for a liquid over a solid surface is thermodynamically defined as:

$$\lambda_{L/S} = \gamma_S - \gamma_L - \gamma_{SL} \tag{2}$$

where γ_S, γ_L and γ_{SL} are the interfacial energies of the solid, liquid and solid-liquid interfaces involved. The spreading coefficient in Eq. (2) is also applicable to the spreading of a liquid over another immiscible and denser liquid when the subscripts are properly changed [1]. The spreading coefficient can also be written in the following form:

$$\lambda_{L/S} = W_{A(SL)} - W_{C(L)} \tag{3}$$

W_A and W_C are the work of adhesion between liquid and solid and work of cohesion of the liquid. If W_A is greater than W_C (i.e. $\lambda_{L/S} > 0$), the liquid has a stronger tendency to increase its contact with the solid than to reduce its contact area with the solid; the liquid will therefore spread on the solid surface spontaneously. Conversely, if W_C is greater than W_A (i.e. $\lambda_{L/S} < 0$) the liquid will have a stronger tendency to reduce its contact area with the solid and spontaneous spreading of the liquid over the solid will not occur.

Whilst the thermodynamic definition of liquid spreading over a solid surface is clear, it is still beneficial to carefully observe the physics of the spreading process and understand

the behavior of the liquid molecules in the spreading process. When a liquid phase spreads over a solid or another immiscible and denser liquid, the spreading liquid increases its surface area as well as its interfacial area with the substrate phase. Molecules of the spreading liquid will have to move from the bulk onto the freshly formed surface and interface with the substrate phase. This increase in surface area is against the natural trend of liquids assuming the smallest surface area. The reason for this to occur is that the surface tension of the substrate phase is greater than the sum of the surface tension of the spreading liquid and the interfacial tension of the spreading and substrate phase. Alternatively, from a surface free energy point of view, the work of adhesion between the spreading liquid and the substrate phase is greater than the work of cohesion of the spreading liquid.

The spreading of a liquid over a solid surface bears thermodynamic similarity to the spreading of a liquid over another, but immiscible, liquid. This similarity allows us to appreciate the spreading coefficient through the classic experiment performed by Franklin which clearly demonstrated the behavior of molecules of the spreading liquid. In 1774, Franklin investigated the effect of oil on the tranquillity of the water surface [12]. Upon arriving at a pond on a windy day, Franklin deposited a teaspoon of olive oil onto the water surface in the pond and observed the formation of an oil film that covered approximately half an acre on the pond surface. This oil layer acted as lubricant against the wind, preventing waves being created on the pond surface. The oil film appeared to be very thin and work carried out by Lord Rayleigh showed that the film of the olive oil

on the water was one molecular thick (approximately 25 Å) [12]. A schematic diagram of the oil droplet before and after spreading is shown in Fig. 3.

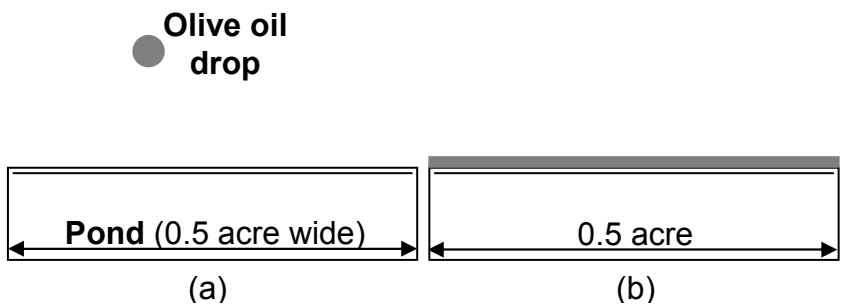

Fig. 3. Schematic diagram of Franklin's experiment of oil spreading on water

The spontaneous increase in the oil/water interface forces the oil surface area to increase. This process brings oil molecules from the bulk of the drop onto the interface and the surface. A thermodynamic derivation taking the initial and final states may be presented as follows:

$$\Delta G = A\gamma_{WO} + A\gamma_O - A\gamma_W - a\gamma_O \tag{4}$$

Where A is the surface area of the pond, a is the surface area of the teaspoonful of oil before it was deposited onto the water surface. Since $A >> a$, this equation can be written as:

$$\frac{\Delta G}{A} = \gamma_{WO} - \gamma_W + \gamma_O = -\lambda_{O/W} \tag{5}$$

This derivation leads to the following equation,

$$\lambda_{O/W} = W_{WO} - W_O \tag{6}$$

Substituting literature values of surface tension of olive oil (32.5 mN/m,) [13] and interfacial tension of olive oil and water (23.6 mN/m) [14] into Eq. (5) leads to a positive

$\lambda_{O/W}$ (15.9 mN/m) which predicts that oil will spread over water. This result agrees with Franklin's experiment.

5.3.2. Spreading coefficient of solid particles over liquid surface

Fig. 4 shows the schematic of a small solid particle aggregate as it disintegrates and expands over liquid surface. We assume that solid particles are inert and do not dissolve in the liquid. The total surface area of the particles in the aggregate is much greater than the apparent outmost surface area defined by volume and the shape of the aggregate (Fig. 4). This situation is very different to the teaspoonful of oil discussed above, where the surface area of the teaspoonful of oil equals exactly to the surface area of the volume that defines it (Fig. 3).

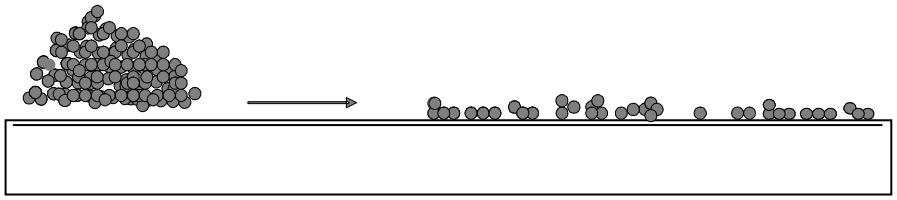

Fig. 4: A schematic of a solid powder aggregate disintegrates and expands over a liquid surface

When powder aggregates disintegrate and expand over the liquid surface, a fraction of the powder surface will be in contact with the liquid, establishing a solid/liquid interface. The other fraction will remain unchanged (Fig. 4). A solid particle will establish a solid/liquid area larger than the liquid area it displaces, depending on the wetting condition of the solid particle by the liquid as schematically shown in the simplified schematic diagram in

Fig. 5. The ratio of the solid/liquid interface area and the liquid surface area it replaces (see Fig. 5) is denoted by β. Under the assumption that solid particles are spherical,

$$\beta = [1 + (h/r)^2] \tag{7}$$

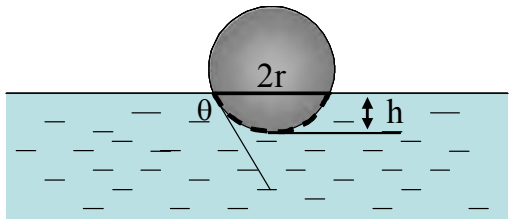

Fig. 5: A non-wettable powder particle contacting a liquid surface. The area of the solid/liquid interface (broken line) and the area of the liquid surface (solid line) the particle replaces as it spreads on the liquid surface; these areas are not the same. The ratio of solid/liquid interface (broken line) to liquid surface (solid line) is represented by β in Eq. (7)

If the solid particle is not wettable by the liquid (i.e. contact angle $\theta > 90^\circ$), β would be in the range between 1 and 2. However, if surface roughness of the particles is considered, β will be larger than 1 but less than 2, due to the Cassie-Baxter effect [15].

As the powder aggregates try to disintegrate, expand and cover the liquid surface, the inter-particle attraction forces must be overcome so that more solid particles can move and establish more particle/liquid interfaces. Since solid powder particles of micron size or larger [7] have very limited intimate contact at the molecular scale between them, the short range attraction forces between the particles due to the Vander Waals interactions are therefore weak [16], but they are responsible for holding the particles in the aggregates together. However, the inter-particle attraction forces bear no quantitative relationship to the solid surface free energy and cannot be described by the solid surface

free energy. It is therefore incorrect to use the surface energy of the solid to define the work of cohesion between solid particles, such as in Eq. (1).

If the powder spreading process over a liquid (Fig. 4) is examined from a thermodynamic viewpoint, the initial and final states need to be defined. With the following assumptions, Fig. 4 provides the initial and final states of the spreading process:

- The solid particles are hydrophobic and will not be fully wetted by the liquid and remain floating on liquid surface.
- The surface area of the particles does not change after contacting water.
- The surface tension of the liquid does not change when exposed to solid powder.

A liquid surface coverage fraction Φ is used to represent the fraction of the liquid surface that becomes covered by the solid powder after the powder spreads over the liquid surface. The total surface free energy of the initial state is ($\gamma_S A_S + \gamma_L A_L$), and the total surface free energy of the final state is ($\gamma_L[1-\Phi]A_L + (1+\beta)\Phi A_L\gamma_{LS} + [A_S-(1+\beta)\Phi A_L]\gamma_S$). The free energy change of the powder spreading process will then be:

$$\Delta G = -A_L \Phi W_{A(LS)} - A_L \beta \Phi(\gamma_S - \gamma_{LS}) \tag{8}$$

$$\frac{\Delta G}{\Phi A_L} = -W_{A(LS)} - \beta(\gamma_S - \gamma_{LS}) \tag{9}$$

where β is defined in Fig. 5. Eq. (8) describes the free energy change between the final and initial states of the solid particle aggregates disintegrate and cover the liquid surface. Eq. (9) further shows that only a fraction (Φ) of the liquid surface replaced by solid/liquid interface was responsible for free energy change. It is not possible for the thermodynamic

relationship of Eq. (1) to be derived from Eq. (8) and (9). This result indicates that the original considerations for the "spreading coefficient of solid over liquid ($\lambda_{S/L}$)" does not capture the physical process of powder spreading over a liquid phase and therefore is an incorrect parameter for predicting powder spreading over liquid surfaces.

5.3.3. Driving forces for solid particles to spread over liquid surface

McEleney *et al.* [7] has recently suggested that the Maragoni effect due to temperature gradient on the liquid drop surface may be a driving force causing the spreading of solid particles over liquid surface. Their suggestion was based on the possible heating effect of the microscope light source on the north pole of the liquid drop under investigation. Under this assumption, the temperature difference between the north and the south poles of the liquid drop could cause circulation the liquid over the drop surface. Whilst the Maragoni effect may be one of the possible driving forces causing powder spreading, it is possible that there may other interfacial forces that are responsible for this phenomenon. More extensive research is required to identify and analyze the physical and physicochemical mechanisms which generate the driving forces and cause powder particles to spread over liquid surfaces.

5.4. Conclusion

This study analyzed and compared the spreading processes of liquid over a solid (or liquid over an immiscible liquid) and to solid particle aggregates over a liquid. These two processes are fundamentally different in their physical nature. Thermodynamic analysis of the two different spreading processes showed that the "spreading coefficient of solid over liquid" proposed previously [8] is invalid, as it does not capture the actual physical

process. Other factors, including the Marangoni effect due to temperature and liquid surface tension gradients, are likely to be the more dominant driving forces which cause the initial movement of solid particles over the liquid surface. Further research efforts are required to identify and analyzer powder spreading driving forces.

Acknowledgements

This project was supported financially by the Australian Research Council Discovery program (DP0770462), and N. Eshtiaghi's scholarship was funded by the Monash Graduate Research School.

References

[1] Adamson, A. W. and A. P. Gast (1967). *Physical chemistry of surfaces*. New York, USA, John Wiley & Sons.

[2] Planinsek, O., R. Pisek, A. Trojak and S. Srcic (2000). "The utilization of surface free-energy parameters for the selection of a suitable binder in fluidized bed granulation". International Journal of Pharmaceutics **207**(1-2): 77-88.

[3] Tuske, Z., G. Regdon Jr., I. Ero, S. Srcic and Pintye-Hodi (2005). "The role of the surface free energy in the selection of a suitable excipient in the course of a wet-granulation method". Powder Technology **155**(2): 139-144.

[4] Zajic, L. and G. Buckton (1990). "The use of surface energy values to predict optimum binder selection for granulations". International Journal of Pharmaceutics **59**(2): 155-164.

[5] Galet, L., T. O. Vu, D. Oulahna and J. Fages (2004). "The wetting behaviour and dispersion rate of cocoa powder in water". *Food and Bioproducts Processing* **82**(4): 298-303.

[6] Aussillous, P. and D. Quere (2001). "Liquid marbles". *Nature* **411**(6840): 924-927.

[7] McEleney, P., G. M. Walker, I. A. Larmour and S. E. J. Bell (2009). "Liquid marble formation using hydrophobic powders". *Chemical Engineering Journal* **147**(2-3): 373-382.

[8] Rowe, R. C. (1989). "Surface free energy and polarity effects in the granulation of a model system." *International Journal of Pharmaceutics* **53**(1): 75-78.

[9] Esshtiaghi, N., J. Liu, W. Shen, K.P. Hapgood." Liquid marble formation: Spreading coefficient or kinetic energy?" Powder Technology, **2009** (196): 126-132.

[10] Wu, S. (1973). "Polar and nonpolar interactions in adhesion". *The Journal of Adhesion* **5**(1): 39 - 55-39 – 55.

[11] He, X., M. R. Barone, P. J. Marsac and D. C. Sperry (2008). "Development of a rapidly dispersing tablet of a poorly wettable compound--formulation doe and mechanistic study of effect of formulation excipients on wetting of celecoxib". *International Journal of Pharmaceutics* **353**(1-2): 176-186.

[12] Erbil, H. Y. (2006). Surface chemistry of solid and liquid interfaces, Wiley-Blackwell.

[13] Liu, H.-S., W.-C. Chiung and Y.-C. Wang (1994). "Effect of lard oil, olive oil and castor oil on oxygen transfer in an agitated fermentor". *Biotechnology Techniques* **8**(1): 17-20.

[14] Fisher, L. R., E. E. Mitchell and N. S. Parker (1985). "Interfacial tensions of commercial vegetable oils with water". *Journal of Food Science* **50**(4): 1201-1202.

[15] Cassie, A.B.D. and S. Baxter, 1944. *Wettability of Porous Surfaces.* Transactions of the Faraday Society, **40**: p. 546-551.

[16] Kendall, K. (2001). *Molecular adhesion and its applications*. New York, Kluwer Academic.

6

Formation of hollow granules from liquid marbles: small scale experiments

Collapsed	Buckled	Perfect
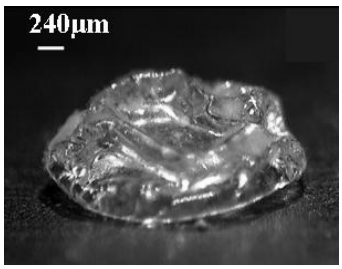	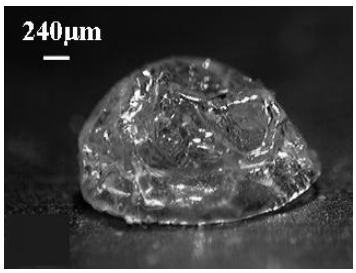	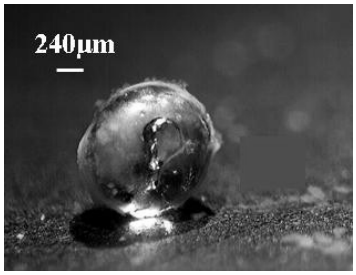
Aerosil & 18% HPC at 100ºC	**Aerosil & 12%HPC at 100ºC**	**Aerosil & 18%PVP at 100ºC**

Water marble coverage with PTFE as function of droplet release height

Chapter 6: Formation of hollow granules from liquid marbles: small scale experiments

Declaration for Thesis Chapter 6

Declaration by candidate

In the case of Chapter 6, the nature and extent of my contribution to the work was the following:

Nature of contribution	Extent of contribution (%)
Initiation, Key ideas, experimental and analysis work, development, writing up the paper	75

The following co-authors contributed to the work. Co-authors who are students at Monash University must also indicate the extent of their contribution in percentage terms:

Name	Nature of contribution	Extent of contribution (%) for student co-authors only
1-Jacques S. Liu	Half of drying experiment	20
2-Karen P. Hapgood	Supervision, reviewing and editing of the paper	--

Candidate's Signature		Date

Declaration by co-authors

The undersigned hereby certify that:

(1) the above declaration correctly reflects the nature and extent of the candidate's contribution to this work, and the nature of the contribution of each of the co-authors.

(2) they meet the criteria for authorship in that they have participated in the conception, execution, or interpretation, of at least that part of the publication in their field of expertise;

(3) they take public responsibility for their part of the publication, except for the responsible author who accepts overall responsibility for the publication;

(4) there are no other authors of the publication according to these criteria;

(5)potential conflicts of interest have been disclosed to (a) granting bodies, (b) the editor or publisher of journals or other publications, and (c) the head of the responsible academic unit; and

(6) the original data are stored at the following location(s) and will be held for at least five years from the date indicated below:

Location(s)	Department of Chemical Engineering, Monash University, Clayton Campus

[Please note that the location(s) must be institutional in nature, and should be indicated here as a department, centre or institute, with specific campus identification where relevant.]

Signature 1	[redacted]	Date
Signature 2	--	--

Abstract:

Research into formation of hollow granules from liquid marbles is an emerging field in hydrophobic granulation. A liquid marble is formed by a network of self-assembled hydrophobic powder around a droplet, and this paper investigates the conditions required for forming hollow granules from a liquid marble precursor.

Single drops of fluid were produced using a syringe and placed onto loosely packed powder beds of hydrophobic powders. Liquid marbles formed from several powder/liquid combinations were dried at several conditions to investigate the drying conditions required for formation of a stable hollow granule.

The formation of stable hollow granules was found to depend on drying temperature and binder concentration. For HPMC and PVP binder, formation of hollow granule is proportional to binder viscosity and for HPC binder, this relationship is constant. Different combinations of powder and binder at both drying temperatures – 60 ºC and 100 ºC - had mixed success rates in forming hollow granules, but generally the success rate was improved by using higher drying temperatures, smaller particles or higher viscosity binder fluids.

Nicky Eshtiaghi, Jacques J.S. Liu, Karen P. Hapgood, " Formation of hollow granules from liquid marbles: Small scale experiments", Powder Technology, 2010 (197), 184-195.

Keywords: Hollow granule, liquid marble, non-wetting, hydrophobic granulation, dry water

6.1. Introduction

Hollow granules can be formed from hydrophobic powders by "solid spreading nucleation" [1] where the powder spreads around a template drop and the interior liquid is subsequently dried to form a hollow granule. The nuclei formed by solid spreading are also known as "liquid marbles" [2, 3] and "dry water" [4], and are used in cosmetic [4] and pharmaceutical formulations [1].

The pre-specified structural properties of hollow granules allow simultaneous control of granule size and structure, excellent flow, good compression for tabletting and fast dissolution rate. These granules are ideal for pharmaceutical products with a high concentration of a hydrophobic drug. Research into formation of hollow granules via either melt granulation [5] or via hydrophobic liquid marbles [1, 6] is an emerging field in hydrophobic granulation.

Solid spreading nucleation can be used to create hollow pharmaceutical granules suitable for compression into tablets [1]. Powder shell formation experiments were performed in a 2L high-shear mixer with 70 mass% of a submicron hydrophobic powder (contact angle $>90^{o}$) and 78% w/w water, which was atomized over 7-8 min into the mixer. In addition, 20% microcrystalline cellulose and 4% hydroxypropyl cellulose binder were added as hydrophilic excipients components plus 1% sodium lauryl sulfate as a surfactant. By drying the liquid marbles to remove internal fluid, stable spherical hollow granules were formed. The presence of excipients and surfactants did not prevent liquid marble formation or self-assembly of the particles at the drop interface since the hydrophobic

model drug powder constituted 90% of the batch on a volume basis. Moreover, the excipients stabilized the powder shell to allow the hollow structure to be preserved during drying [1]. Apart from this one paper, there are no further studies on hollow granule formation from liquid marble precursors.

Bhosale *et al.* [7] studied the strength of liquid marble formed with PTFE (7-12 μm) and 2 types of fumed silica powder, which had been treated with hexamethyldisilazane and dimethyldichlorosilane. Bhosale *et al.* suggested that high surface area nano-particle materials like Aerosil create more uniform powder shells through uniform coverage of the liquid–vapor interface. They found that nano-powder shells form an "elastic" membrane that makes these liquid marbles mechanically robust in comparison with conventional liquid marbles made from larger particles. We expect that liquid marbles formed from nano-particles may be able to withstand higher compressive stresses during drying, and may be more likely to form a hollow granule.

Dandan and Erbil [8] determined the evaporation rate of graphite liquid marble and found that graphite liquid marbles had a much longer lifetime than a pure water droplet of the same size. The presence of graphite retarded the evaporation of water and extended the time required for the liquid to be completely evaporated. Increasing the relative humidity of the medium increases the evaporation resistance. For larger droplets, the lifetime was determined by diffusion controlled evaporation [8]. In comparison to the study of Bhosale *et al.* [7], they found the graphite liquid marble evaporation rate was 7% lower compared to PTFE liquid marbles, which indicated that the liquid marble lifetime is

extended by using large particles (e.g. graphite 10-20 μm) rather than smaller particles (e.g. PTFE 7-12 μm).

Polymeric binder is required to avoid the liquid marble collapsing after drying, as the binder forms solid bridges between the particles during drying which give strength to the powder shell. The physical properties of the binder and the drying temperature are both expected to be important in avoiding granule collapse. Drying of liquid marbles is expected to show some similarities with drying of liquid drops containing solutes. Fundamental studies of the phenomena occurring during the droplet drying process were reported by Charlesworth and Marshall [9]. They developed a technique where an individual droplet was suspended in a controlled air stream, and the weight and temperature were recorded during drying in parallel with visual observations of the appearance and size of the droplet (see Fig. 1). They used an aqueous solution of an inorganic salt droplet in relatively slow rates of evaporation (moderate air temperatures and velocities). The first period of drying was characterized by evaporation from a free liquid surface which is similar for all droplets regardless of the solute or drying conditions. After further drying, crystals formed at the bottom of droplet and gradually formed a crust around the droplet. After completion of the crust formation, drying depended on the solutes and the surrounding air temperature. Charlesworth and Marshall [9] categorized these features into two main sections: air temperature above or below the boiling point of solution. In this study, we are interested in drying a single droplet in air at a temperature below the boiling point of solution. For this case, three different sub-categories were defined [9] (see Fig. 1):

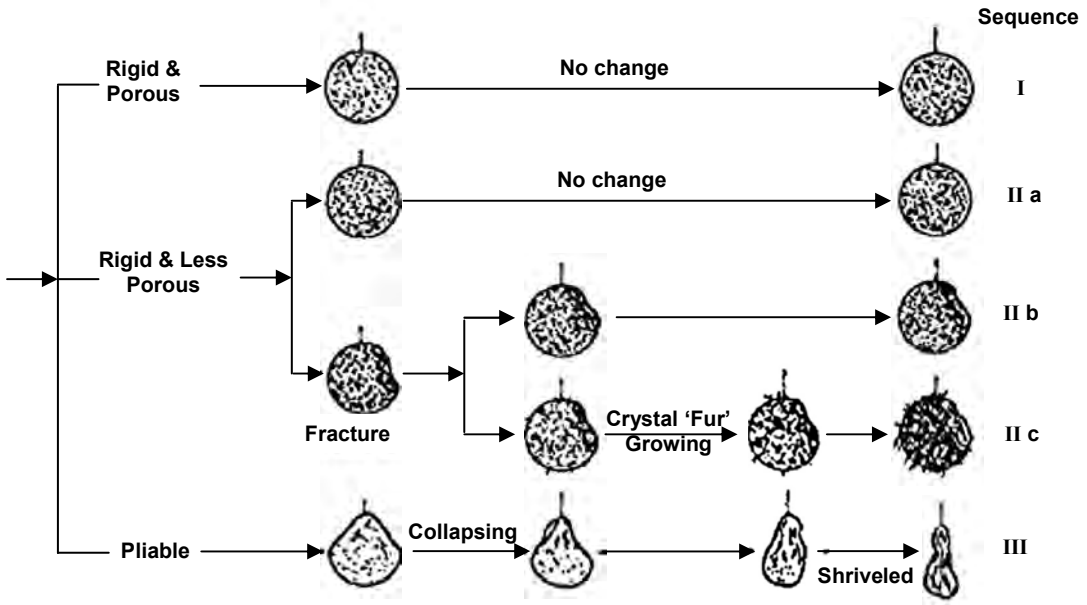

Fig. 1. Selected structures formed after drying of a single droplet below the boiling point of the solution [8]

a) If the crust is rigid and porous, the air-liquid interface retreats between pores and the appearance does not change (I)

b) If the crust is rigid but non-porous, fracture phenomenon occurring on the crust allows air to enter the particle and the air-liquid interface returns to the crust surface under the influence of capillary forces. There are three possible conditions after fracturing:

   I. If fracture remains open, further formation of solid occurs out from particle surface (IIb) or within the crust structure (IIa).

   II. If the fracture closes, the supply of air would be disrupted and the liquid interface once more retreats into the crust interstices. As the amount of liquid decreases, successfully smaller pores are emptied (crystal grows (IIc))

c) Crust is pliable and impervious. Rupture by implosion could eventually occur as the skin thickens and stiffens (III).

Charlesworth and Marshall's [9] study as summarized in Fig.1. is also presumed to be applicable for liquid marble drying, as the outer shell of powder in a liquid marble can be assumed to be similar to the first step of drying from a liquid surface. After further drying and shrinkage, a solid shell-like crust is produced. The permeability of the powder shell and binder matrix will determine whether there are enough pores to allow the interior liquid to be vaporized freely, and thus which of the cases shown in Fig.1. will occur for the drying of liquid marbles.

Walton and Mumford [10] also classified the various types of particle morphology produced at two different temperatures (70 ^{o}C, 200 ^{o}C). They used a single droplet drying technique with a droplet containing dissolved solids under controlled air temperature, humidity and velocity in a simulated spray dryer. Their study demonstrated that both the chemical and physical nature of the material are important in determining particle morphology and the pliable or plastic nature of the skin is related to its chemical and/or physical structures [10]. Polymeric materials tended to form a shriveled thin-walled hollow particle. Particles with a polymeric skin decreased in size without any rupture of the skin surface during initial drying period suggesting that the skin is porous. By increasing the concentration of solute in droplet, the particle diameter tended to stabilize as the particle skin (crust) adopted a more permanent structure, and resulted in a decrease in particle distortion, surface rupture and internal bubble nucleation.

At lower drying temperatures after complete drying, particles tend to shrivel and deform, and some signs of internal bubble nucleation and particle inflation appeared [10]. An increase in drying temperature from 70 ^{o}C to 200 ^{o}C increased the rate of heat and mass transfer experienced by both droplet and particle increased. This resulted in shorter drying times and more violent drying behavior which produced particles with a greater tendency to inflate, shrivel and in some cases explode. At 200 ^{o}C, internal bubble nucleation was rapidly formed and the bubbles expanded to violently distort, and eventually rupture. This caused the particle to collapse, shrive and then re-inflate. This cycle was repeated three or four times until the internal moisture had evaporated (sees Fig.2.).

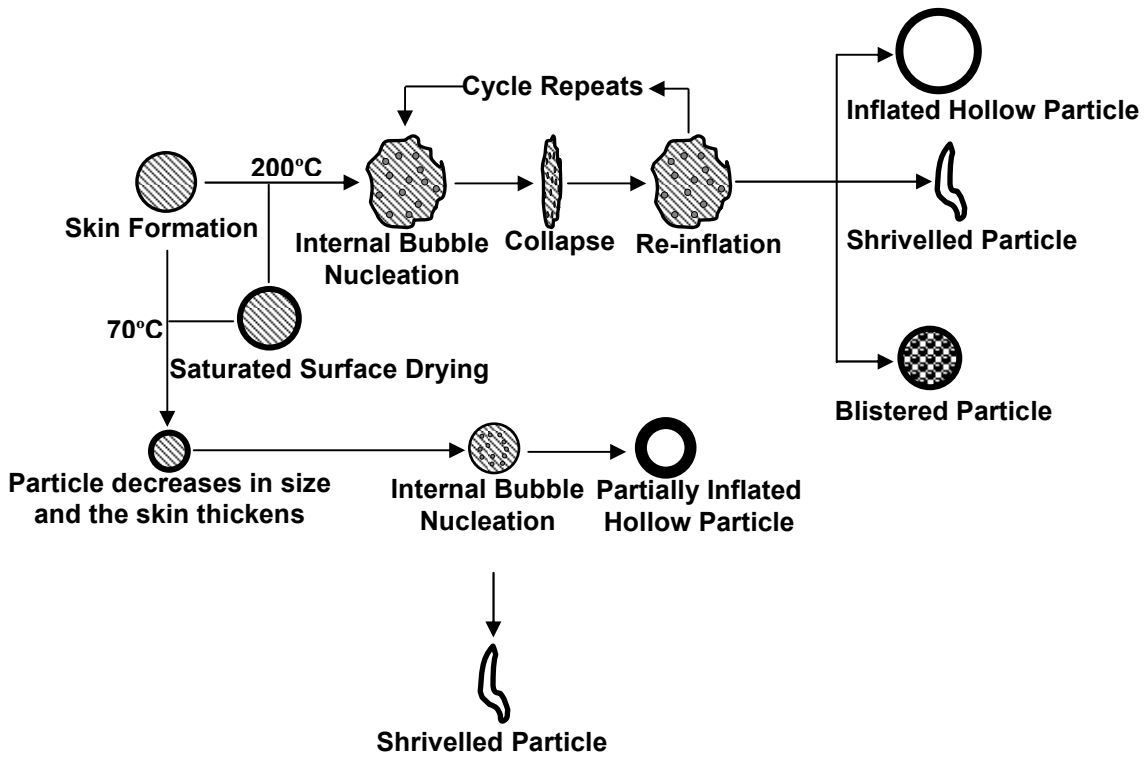

Fig. 2. Selected different particle morphologies formed after drying of a single droplet at 70 °C and 200 °C [10]

In some cases, evaporation of a residual liquid inside partially dried particles caused the liquid to foam and bubble causing internal blistering within the larger parent particle [10]. After drying, the hardened foam gave a blistered appearance to particle. High surface area powders with good gas absorption properties increased the internal porosity of the particles by adsorption of gases during drying. The internal structure of these particles showed much larger vacuoles [10].

This paper will investigate what happens to the liquid marble as the template drop is removed during drying for a variety of powder-fluid combinations and a range of drying conditions. The aim is to identify the right powder-binder combination and the right drying temperature to produce stable hollow granules from liquid marble nuclei.

6.2. Materials and Methods

Glass ballotini spheres (d_{50}=65 μm, AH/AG grade, ρ=2.5 g/cm^3, Potters Industries Pty Ltd.) were used to form liquid marbles. In order to make the glass beads hydrophobic, SIGMACOTE solution (chlorinated organopolysiloxane in heptane, Sigma Aldrich Pty Ltd.) was used. Two additional hydrophobic powders were used: Polytetra fluoroethylene (PTFE) with four different particle size grades (1, 12, 35, and 100 μm, ρ=2.1 g/cm^3, Sigma Aldrich Pty Ltd), and fumed silica Aerosil R974 with primary particle size of 12 nm (Degussa, Germany).

Several different binder solutions were used: PVP (poly-vinyl pyrrolidone (40T), Sigma Aldrich Pty Ltd), HPMC (Hydroxy Propyl Methyl Cellulose, Premium LV, E3, The

DOW Chemical Company), and HPC (Hydroxy Propyl Celloluse, 100,000 Mw, Sigma Aldrich Pty Ltd). Concentrations between 2-18% on a weight basis were used. Fluid viscosities were measured using a rotational viscometer (Visco Basic Plus, Fungilab, Barcelona).

Liquid marbles were prepared by releasing a droplet from a 1mL syringe with an 18 gauge needle approximately 2cm above a loosely packed powder bed. The droplets were then agitated using the syringe needle tip on the surface of the powder bed to form a multilayered liquid marble. At least 10 liquid marbles were dried for each individual combination of temperature, powder and binder. To try to estimate the liquid to solid for each powder-liquid combination, the average weight of 10 liquid marbles was measured using an analytical balance, and compared to the average weight of 10 drops of the fluid. The powder shells were very light, approximately 0.1mg each, and the random variations during weighing were the same or larger than the weight of the powder shell. We were unable to obtain sensible results for the L:S ratio and this data is therefore not reported.

Several drying methods have been used: air drying at 24 ºC and 31% humidity, freeze drying at -50 ºC and 300 mmHg (Bench Top Freeze Dryer, OPERON Co., Ltd.) and oven drying in a fan-forced 60 L laboratory oven (S.E.M.(SA) Pty. Ltd) at 60 ºC, 80 ºC, and 100 ºC and an overall air flow rate of 20 L/min. This gives an air flow rate of 12 cm/min. Based on the inlet air temperature and humidity, the RH in the oven was approximately 3%RH at 60 ºC and less than 1%RH at 80 ºC and 100 ºC. Liquid marbles were dried for at least 12 h to ensure complete drying.

Once dried, the granules were removed from drier and classified visually into categories and counted. To minimize inconsistency, all analysis for each powder/binder combination was performed on the same day. Pictures of the hollow granules were taken with a stereo microscope (SMZ series) with a 3MP Motic camera. The internal structure of selected granules was analyzed using an XUM X-ray microscope.

The effects of changing the drying temperature, powder type and size, binder type and binder concentration were studied to determine the best drying conditions. The matrix of data was first analyzed for each binder solution at different drying temperatures to find the most suitable temperature for drying liquid marbles regardless of binder and powder type. Then, the effects of binder and powder type at two selected drying temperatures (60 ºC and 100 ºC) were examined.

6.3. Results

During experiments we observed that if the liquid droplet was covered with only a thin or mono layer of powder, all the liquid marbles collapsed during drying regardless of temperature, binder and powder type. Survival of hollow granules was generally observed when there was a thick powder layer around the droplet. In practice during granulation in high-shear mixers, it can be assumed that all droplets will have a multi-layer of powder as a result of the frequent collision with powders in the highly agitated powder motion in granulator. Moreover, anecdotal observations suggested that the smaller the droplet size, the higher the chance of hollow granule survival. This is consistent with previous reports of collapsed granules occurring mainly in the larger

granule sizes [1]. Drop sizes in a granulation process are much smaller, typically 100-500 μm, so the liquid marble survival results in this study represent a worst case scenario.

In our analysis we consider two criteria: "survivability" and "quality" of the hollow granules. "Survivability" refers to the propensity of the liquid marbles to form hollow granules, i.e. to avoid collapse during drying. "Quality" of the hollow granules refers to their shape. A variety of different shapes were observed after drying: collapsed granules which often formed an annular blood cell shape; buckled hemispherical granules with one or more depression; and perfect hemispherical granules.

Fig. 3 shows several examples of each type. In a few cases, perfect spherical granules were formed. The success of a given drying condition is a combination of how well the drying condition supports both survivability and quality.

X-ray microscopy was used to confirm that the spherical or hemispherical granules formed after drying were hollow, as shown in Fig. 4, 5, and 6. Fig.6 clearly shows the hollow structure as the absence of particles in the interior of the shell is obvious. X-ray microscopy was conducted only on glass ballotini and Aerosil granules as a confirmation of visual observations. The remaining granules are assumed to be hollow or collapsed based on the shape of the exterior.

A systematic set of experiments was performed with different binder types and powders, at a range of different drying temperatures. Table 1 summarizes the overall results of

these experiments, and indicates the dependency of stability and shape of the hollow granules on the drying temperature, and powder / binder combinations.

a **Collapsed**

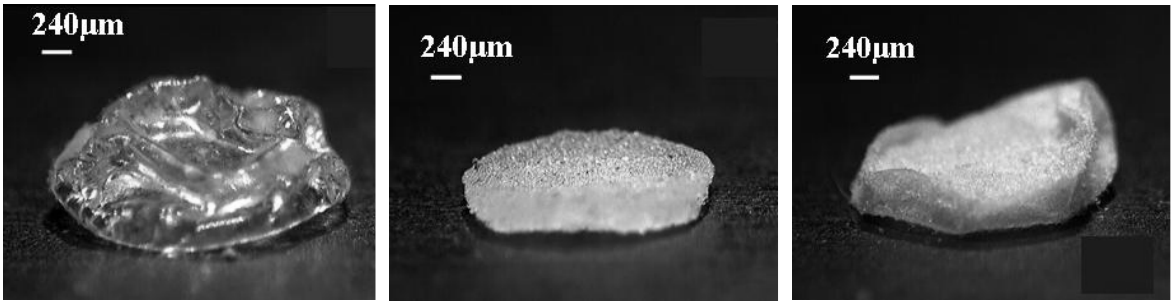

Aerosil & 18% HPC at 100 ºC **Ballotini & 8% PVP at 60 ºC** **PTFE 35 & 5% HPC at 100 ºC**

b **Buckled**

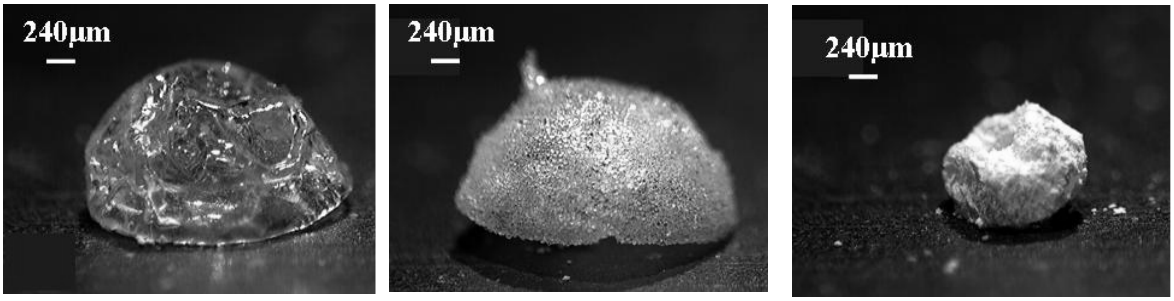

Aerosil & 12%HPC at 100 ºC **Ballotini & 10%HPC at 100 ºC** **PTFE 12 & 8% HPMC at 60 ºC**

c **Perfect**

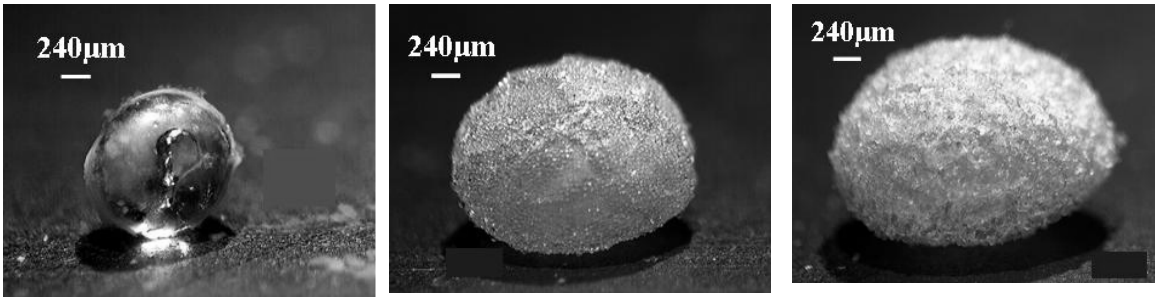

Aerosil & 18%PVP at 100 ºC **Ballotini&12% HPMC at 100 ºC** **PTFE 100&18%HPC at 100 ºC**

Fig. 3. Formed hollow granule structure of Aerosil R974, hydrophobic glass ballotini (AG) and PTFE powder (a) collapsed (b) buckled and (c) perfect

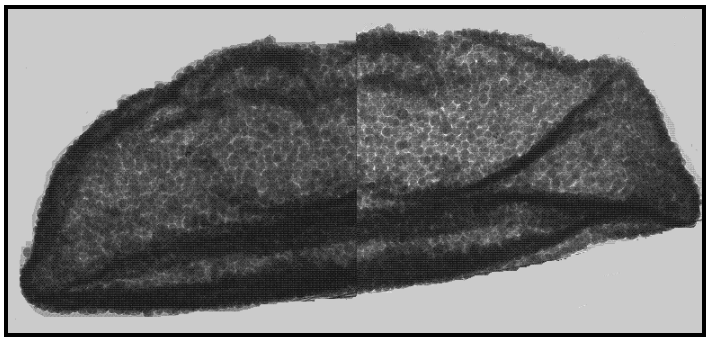

Fig. 4. X-ray microscopy image of a buckled hollow hemisphere granule (3 mm Diameter) made from hydrophobic glass ballotini and 10% HPC dried at 60 ºC

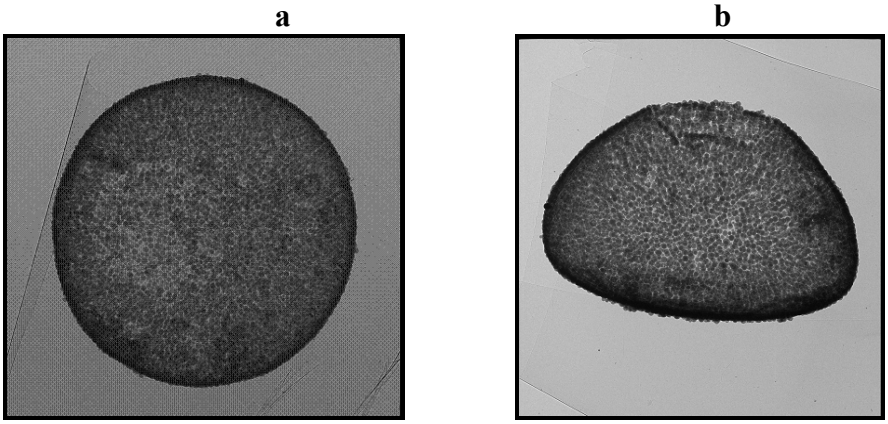

Fig. 5. X-ray microscopy image of hollow spherical granule (2-3 mm Diameter). Hydrophobic glass ballotini and 10% HPC dried at 100ºC (a) top view, and (b) side view

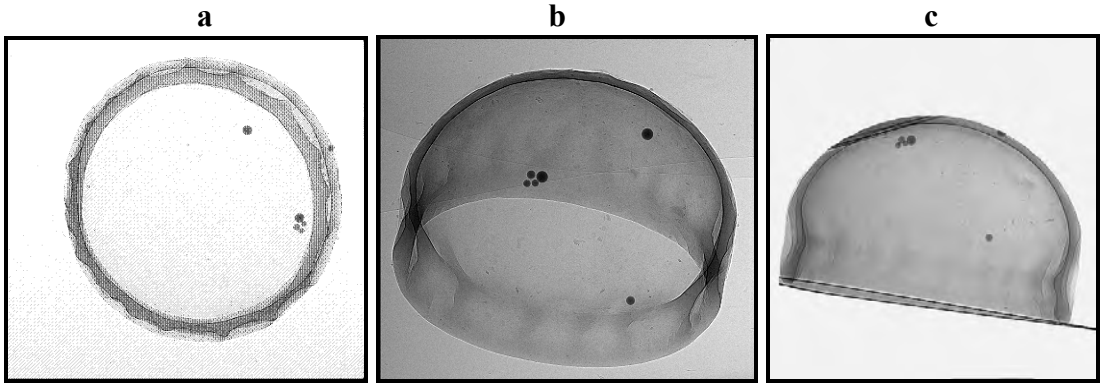

Fig. 6. X-ray microscopy image of hollow hemispherical granule (2-3mm Diameter) of Aerosil R974 and 8% HPC from, (a) top view, (b) bottom view, (c) side view

Table 1. Preliminary Drying studies for hydrophobic glass ballotini & Aerosil R 974

Powder and Binder		Freeze drying (at -50 ºC, 300mm Hg)	Air drying (at 24 ºC, 31%H)	60 ºC	80 ºC	100 ºC
Hydrophobic glass ballotini	5% PVP	Collapsed	Collapsed	Collapsed	Collapsed	Collapsed
	5% HPMC	Collapsed	Collapsed	Collapsed	Collapsed	Buckled hemisphere
	5%HPC	Collapsed	Collapsed	Collapsed	Perfect and buckled hemisphere	Perfect hemisphere
Aerosil R974	5% PVP	Collapsed	Collapsed	Perfect hemisphere	Perfect hemisphere	Perfect hemisphere
	5% HPMC	Collapsed	Collapsed	Perfect hemisphere	Perfect hemisphere	Perfect hemisphere
	5%HPC	Collapsed	Collapsed	Perfect hemisphere	Perfect hemisphere	Perfect hemisphere

From Table 1, PVP polymer was not able to stabilize glass ballotini liquid marbles at any tested drying temperatures, but HPMC polymer was successful at 100 ºC and HPC above 80ºC. Maintaining a hollow granule throughout the drying process appears to be aided by higher drying temperatures. All the tested binders were able to make hollow granules with Aerosil at drying temperatures above 60 ºC. The results in Table 1 imply that the ability to form hollow granules after drying depends on both binder type and drying temperature.

The stability of the hollow granule appears to depend on the powder used as indicated by Walton and Mumford [10], as different drying temperatures are required for each powder to ensure hollow granule survival. For example, glass ballotini hollow granules survive above 80 ºC while Aerosil granules survive as long as the drying temperature is above 60 ºC. Moreover, by increasing the temperature from 60 ºC to 100 ºC the shape of hollow granule gradually improves until a perfect hemisphere is reached (see Table 1). This result shows that the final quality of the hollow granules depends on the drying temperature. At higher drying temperatures, quick removal of the interior liquid improves the stability of hollow structure. The receding surface of the drying droplet does not generate as much capillary stress on the particle shell. It may also form a rigid porous shell at higher drying temperatures (as per case Ia in Fig.1.) and form a pliable shell (see case III in Fig.1.) at lower drying temperatures [9].

To find a general trend for drying liquid marbles it is necessary to examine a matrix of data for different binder/powder combinations at two selected temperatures- 60 ºC and

100 ºC - which had shown reasonable hollow granule formation after drying in the preliminary drying studies in Table 1. Each binder - HPMC, PVP, and HPC - is discussed individually below before analyzing the overall trends observed during the experiments.

6.3.1. HPMC binder

As the HPMC binder concentration increased, the survivability of the liquid marbles improved as well as the quality of the hollow granules. As shown in Fig.7, by increasing HPMC concentration from 5% to 18% the proportion of perfect hollow granules increased from 19% to 72% and the percentage collapsed was reduced from 58% with 5% HPMC to 0% with 18% HPMC. This result is consistent with the previous study reported by Walton and Mumford [10] as they reported that by increasing the concentration the particle distortion and surface rupture decreased. The formation rate for buckled granules was unaffected over the concentration tested. Data in Fig.7 is a combination of result for all powders- Aerosil, glass beads and PTFE - at both drying temperatures – 60 ºC and 100 ºC.

Fig. 8 illustrates how increasing the concentration of HPMC affected the quality of hollow granules formed from Aerosil. The 12% HPMC granule (left) is almost a hemisphere and has a hole in the base. In contrast, the granule formed from 18% HPMC (right) is noticeably more spherical and has no hole in the base. Some of the produced hollow granules produced with 18% HPMC had odd striped patterns on their surface (see Fig. 9). The striated surface may be the first step toward buckling. As the overall shape of these hollow granules was still hemispherical, these hollow granules were classed as hemispherical rather than buckled.

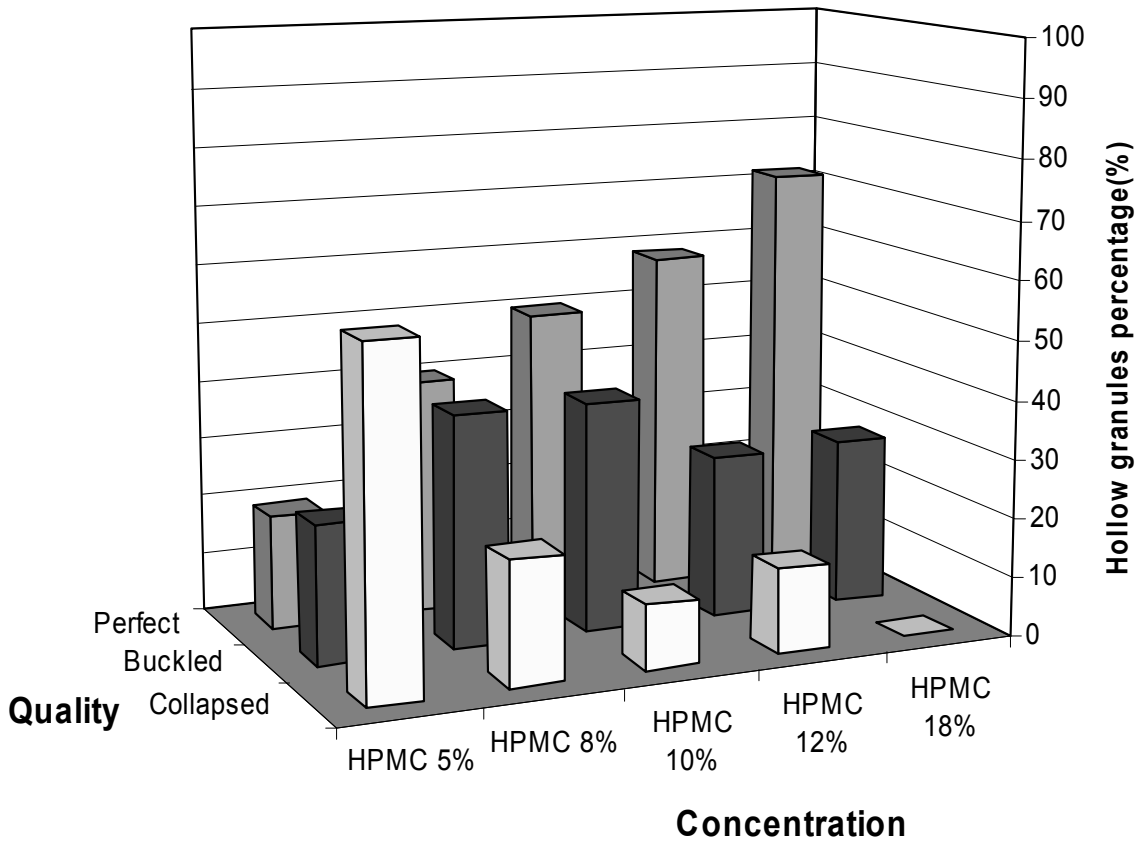

Fig.7. Effect of increasing HPMC binder concentration. Graph combines data for all powders and both drying temperatures

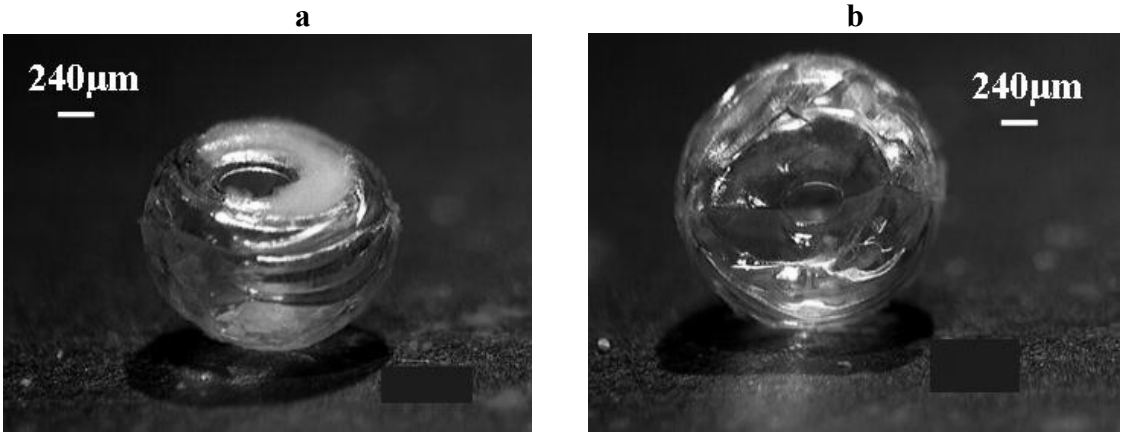

Fig. 8. Hollow granules formed at 100 ºC from Aerosil R974 and (a) 12% HPMC, and (b) 18% HPMC

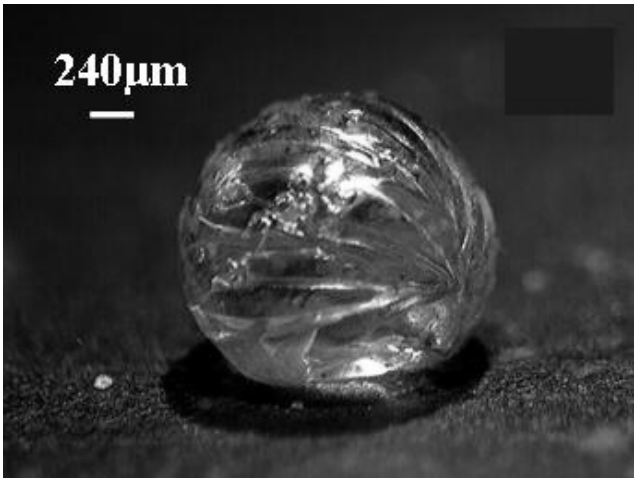

Fig. 9. Hollow granule formed with Aerosil R974 and 18% HPMC dried at 100 ºC showing striated surface

Increasing the drying temperature from 60 ºC to 100 ºC improved the success rate for hollow granule formation using HPMC binder across all powders (Fig. 10). For example, 8% HPMC dried at 100 ºC exhibited less collapsing compared to drying at 60 ºC. It appears that increasing the drying temperature does not significantly affect the proportion of buckled granules. Fig. 10 shows a steady amount of buckled hollow granules across HPMC 8% to 18%, while the amount of collapsed granules decreases and the number of perfect granules increases. Thus, increasing the drying temperature considerably improves both the survivability and quality of hollow granules formed with HPMC as a binder.

Increasing the drying temperature at higher HPMC concentrations (12 &18%) had little effect on the quality or survivability (see Fig. 10.). When the desired hollow granule is achieved at a lower temperature, there is no advantage in increasing the drying temperature further.

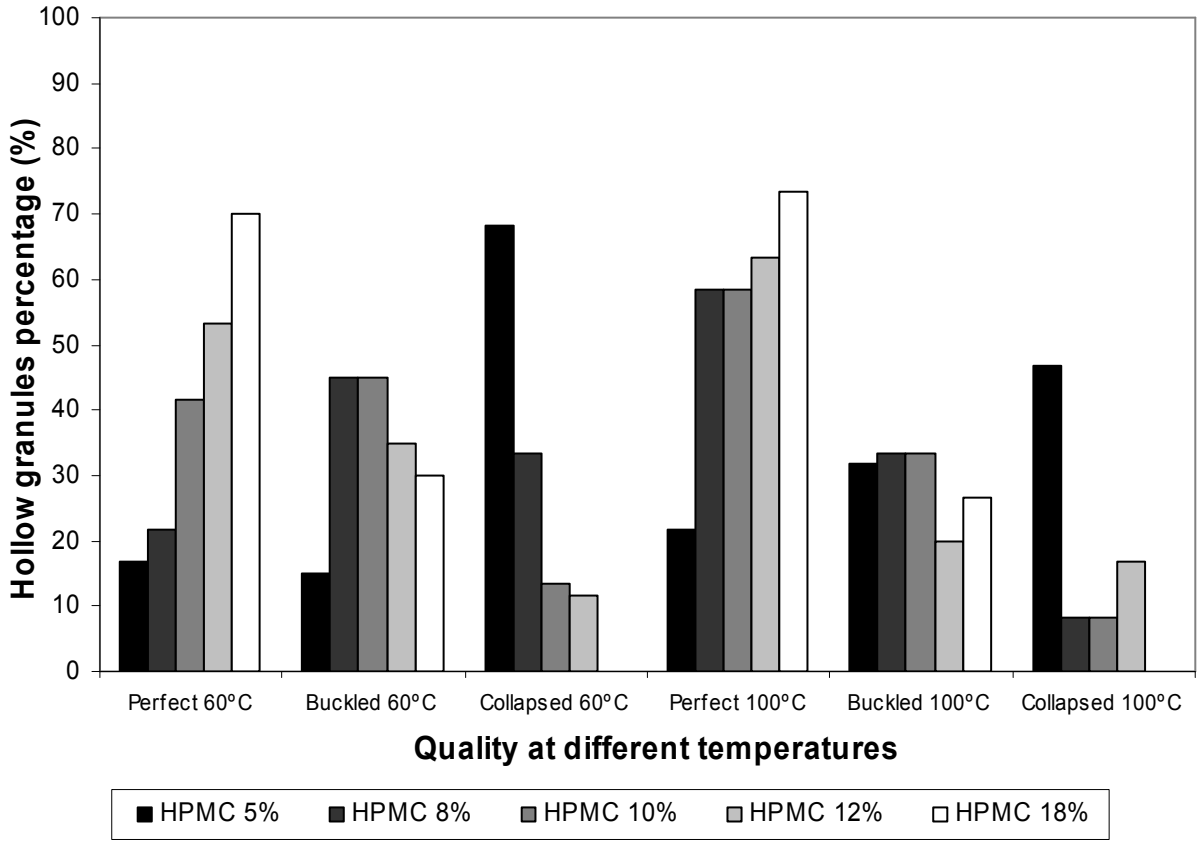

Fig. 10. Effect of HPMC concentration and drying temperature on survivability and quality of hollow granules (graph includes data for all used powders)

Fig.11 shows the survivability and quality of HPMC granules as a function of the powder used. Data for all HPMC concentrations and both drying temperatures have been combined to show the overall trend in Fig. 11.

Overall, Aerosil is clearly most successful powder in terms of survivability as well as the quality of formed hollow granule. The loosely aggregate floc-like structure of the nano-sized silica particles creates a highly porous shell and consequently increases the chance of survival (see case I in Fig. 1.). These resilient Aerosil liquid marbles are consistent with reports by Bhosale *et al.* [7] that nano-sized Aerosil forms stronger liquid marbles compared to larger size particles. This is demonstrated in Fig.11, where Aerosil is

produces a very high proportion of perfect hemispherical hollow granules compared to PTFE and glass beads as these liquid marbles will withstand higher compressive stresses and tensile loads [7], as experienced during drying.

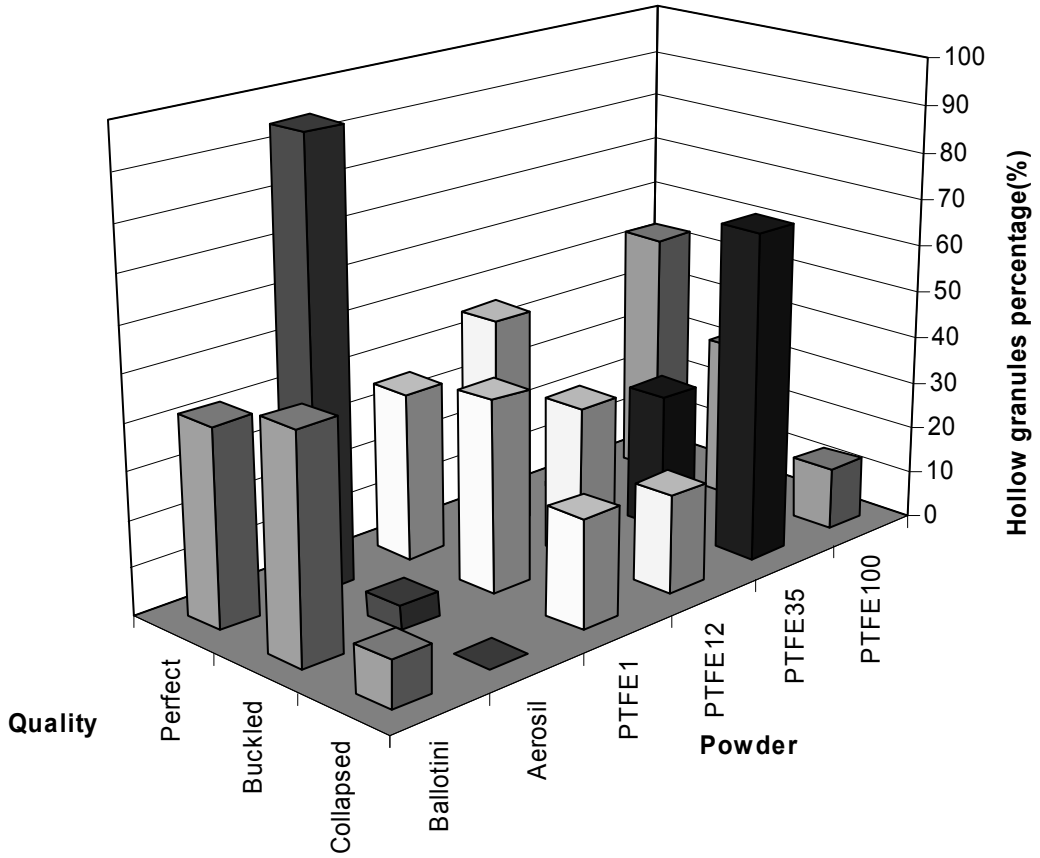

Fig.11. Effect of powder type on hollow granule survivability and quality. Data for all HPMC concentrations and drying temperatures have been combined

It was expected that as particle size decreased, the chance of survival would increase as small particles are subjected to less gravity force due to the reduced weight of the small particles. However, for PTFE powder, the largest PTFE 100 μm powder was the most successful, then the 12 μm and 1 μm size grades, and finally the 35 μm size grade which was the least successful. The 12 & 1 μm size grades of PTFE may form better multilayered powder shells due to their cohesiveness and this would improve the

survivability. The PTFE 100 may also provide good coverage as each particle was large and the particles were observed to pack fairly densely in the powder shell, leaving relatively only small regions of the droplet surface uncovered. The chance of survival of the liquid marbles will be high as powder creates a uniform particle layer in the liquid-vapor interface [7]. These factors would explain the apparent superiority of 100, 12, and 1 μm PTFE powders over the 35 μm size grade, which was neither large nor cohesive and could not achieve good liquid coverage.

6.3.2. PVP binder

Increasing the PVP binder concentration also increased the success rate for hollow granule formation. As shown in Fig.12, increasing the concentration of PVP from 5% to 18% improved survivability. Increasing the binder concentration had only a slight effect on the quality of the granules formed, as there is no significant change in the number of perfect hollow granule across 5 to 18% PVP concentration.

Increasing the drying temperature from 60 ºC to 100 ºC improved PVP hollow granule survival by decreasing the number of collapsed granules and increasing number of buckled granules across all PVP concentrations (Fig.13).

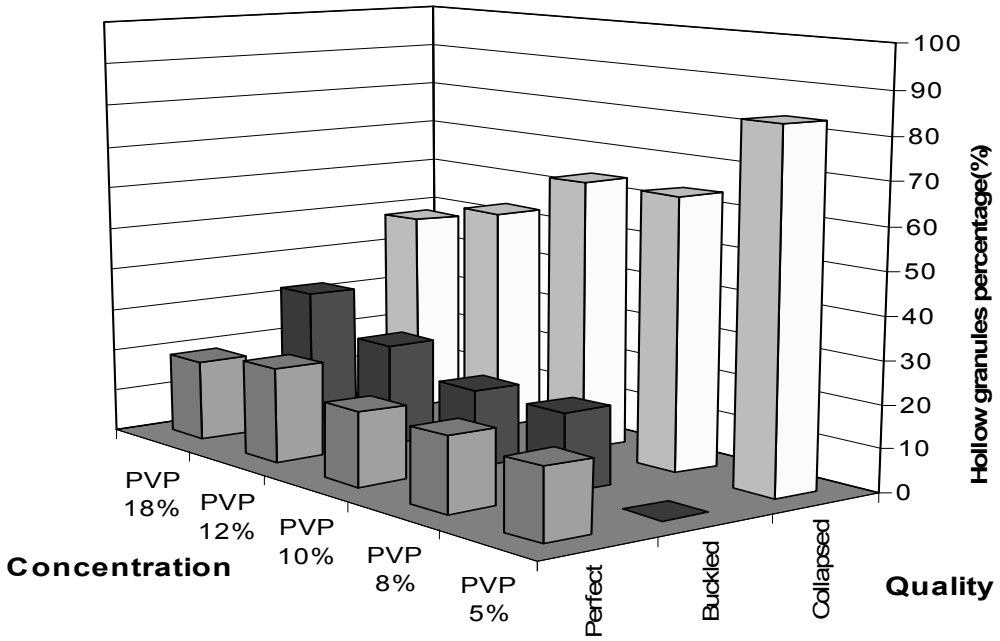

Fig.12. Effect of increasing PVP binder concentration on survivability of hollow granule (graph includes data for all used powders and both drying temperature: 60 ºC and 100 ºC)

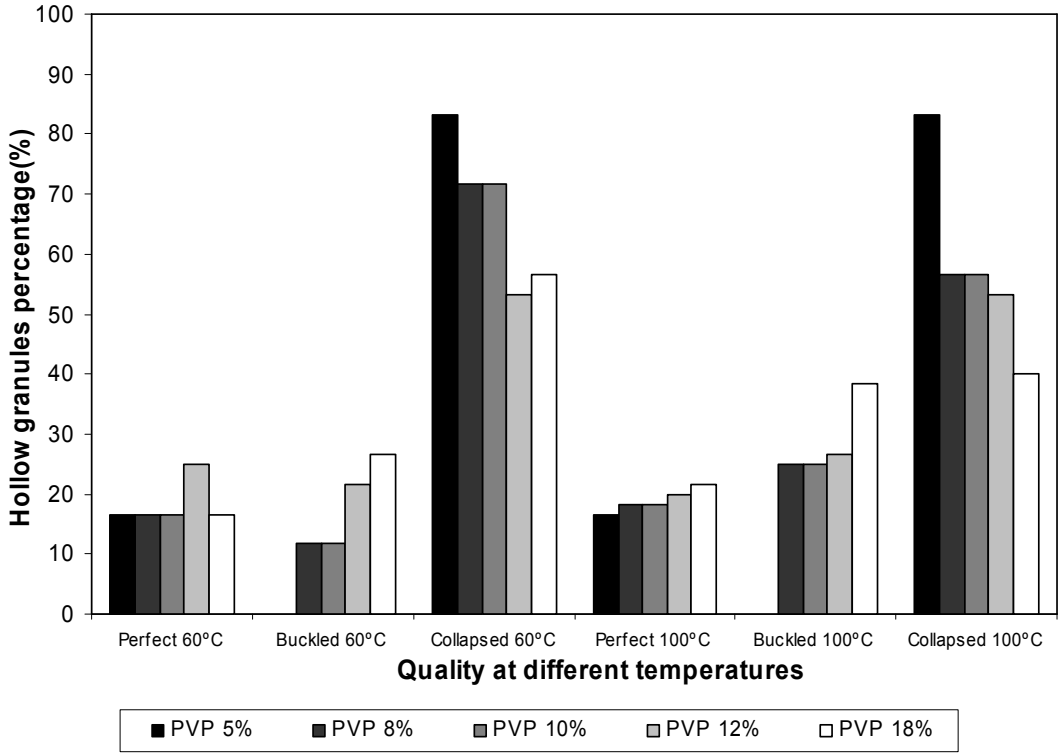

Fig.13. Effect of increasing drying temperature on survival of hollow granules using PVP binder

From Fig. 14, Aerosil was the most successful powder (see lowest left image in Fig. 3.) with PVP binder, and glass ballotini was the least successful. Hollow PVP granules are most likely to survive if the particle size is small – the nano-sized Aerosil R974 produced 100% perfect granules and the 1μm and 12 μm grades of PTFE had high survival rates close to 50%. For glass ballotini neither increasing binder concentration nor increasing drying temperature could produce any form of hollow granule. The complete collapse under all conditions implies that some property of the glass powder – perhaps the higher density - is incompatible with PVP binder which corresponds with Walton and Mumford [10] study that the final morphology of particles depends on the chemical and physical natures of the skin material. In summary, the survival of PVP hollow granules improves as the particle size decreases, the drying temperature increases and the concentration of PVP increases.

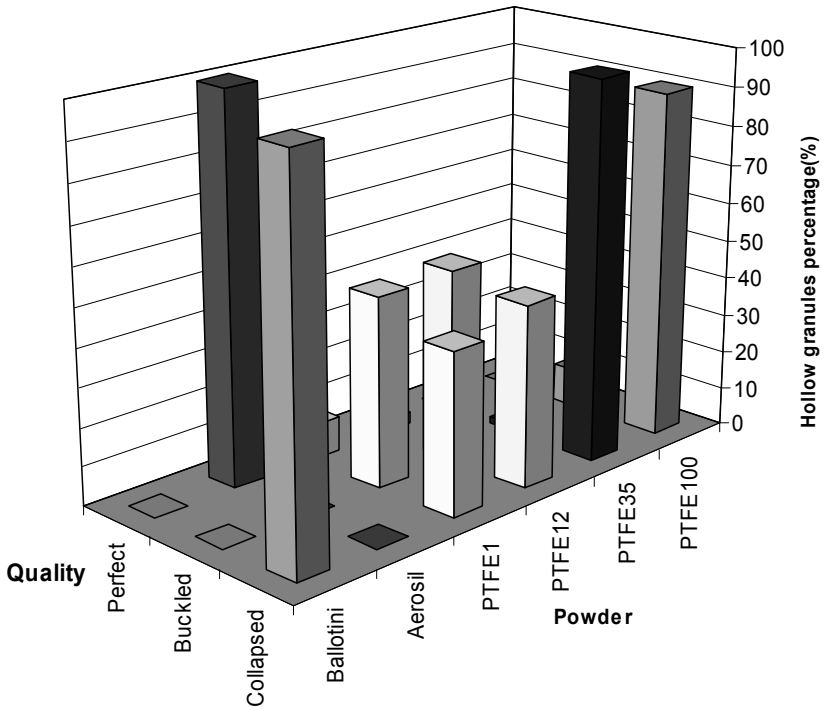

Fig. 14. Effect of powder type on survivability of hollow granule. Data from all PVP concentrations and both drying temperatures have been combined

6.3.3. HPC binder

Fig. 15 summarizes whether a hollow granule survived during drying process as a function of HPC binder concentration across all used powders and drying temperatures. As the HPC concentration increases from 5% to 18%, the number of collapsed granules remains almost constant but the quality improves as shown by the decreasing number of buckled granules and increasing number of perfect hollow granules. Above 10% HPC concentration, it seems that the quality of the formed granules decreases while the number of collapsed granules remains constant. In other words, increasing HPC concentration above 10% causes previously perfect hollow granules to start buckling. This implies that there is a limit in increasing the concentration of binder (see Fig. 15) and that there is an optimum binder viscosity and/or surface tension which occur at 8-10% HPC.

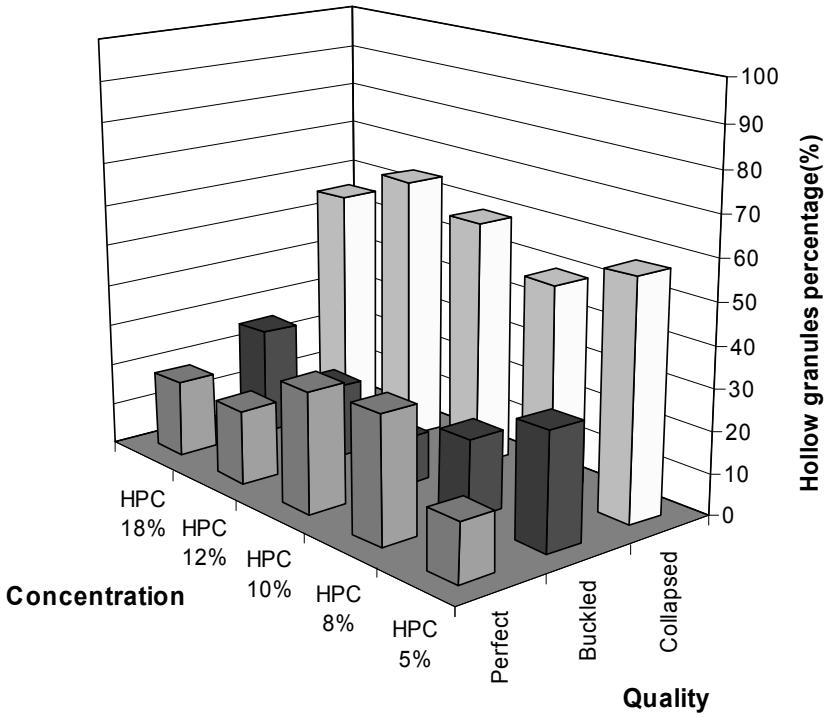

Fig. 15. Effect of HPC concentration on the hollow granule quality (graph combines data for all powders and both drying temperatures)

Fig. 16 and Fig. 17 summarize hollow granule survivability during drying, as a function of HPC concentration and temperature for ballotini and Aerosil. Higher HPC concentrations are expected to produce stronger hollow granules due to a stronger and denser network of solid bridges which form during the drying process. The lowest HPC concentration of 2% was not able to properly assemble particles together to prevent collapsing the liquid marble during drying, even at the highest drying temperatures (100 ºC) with Aerosil (see Fig. 16). These figures show that there is a minimum concentration of HPC required to avoid granule collapse, and that the minimum HPC concentration varies for each different powder. For example, 5% HPC could stabilize hollow granules of Aerosil R974 (Fig. 16) at 60 ºC, but a higher concentration of HPC (10%) was needed to maintain the hollow structure for glass ballotini (Fig. 17) at the same temperature. The reason for this phenomenon may be related to the particle size and density, as larger and denser glass particles would need higher binder concentration to provide enough inter-particulate bonds to withstand the gravitational forces.

Increasing the concentration of HPC binder also affects the hollow granule shape. As can be seen in Fig. 17, by increasing the concentration of HPC binder, more "perfect" granules – including a full "base" are formed from glass ballotini. For instance, by increasing the HPC concentration from 8% to 10%, just over 50% of the hollow granules formed from glass ballotini had a full base at 100ºC. By further increasing the HPC concentration to 18%, all of the formed granules had a base (see Fig. 17). The reason why no bases were formed for Aerosil granules despite a wide range of HPC concentrations is not clear.

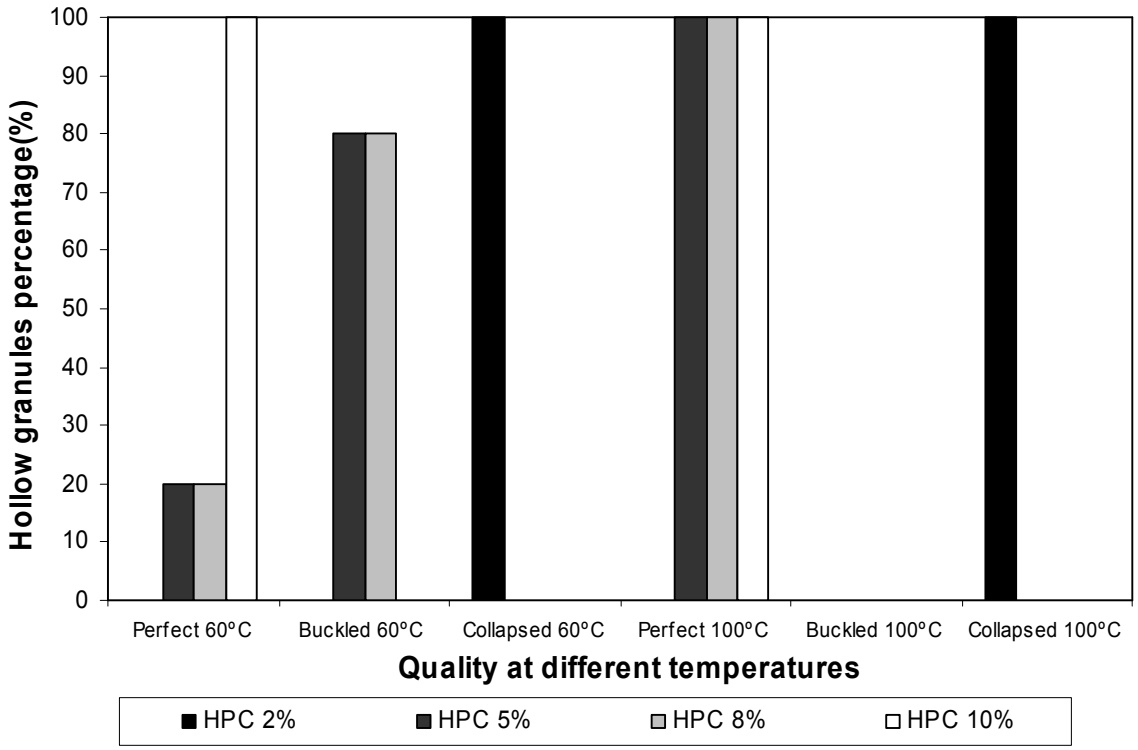

Fig. 16. Effect of HPC concentration on quality of Aerosil R974 hollow granule (graphs combines data for both drying temperatures)

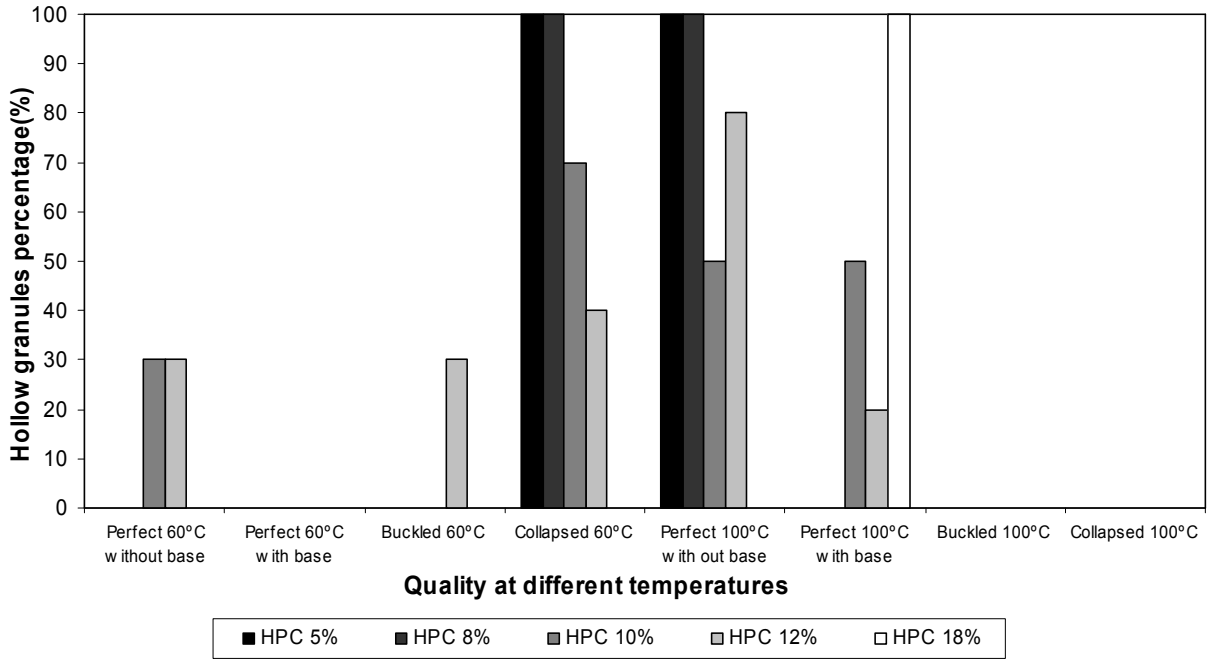

Fig. 17. Effect of HPC concentration on quality of glass ballotini hollow granules (graph combines data for both drying temperatures)

The survivability of hollow granule dried at lower temperatures can be increased if the HPC concentration is increased. From Fig. 17 for glass ballotini and up to 8% HPC in binder, all glass ballotini liquid marbles dried at 60ºC collapsed. By increasing the binder concentration from 8% to 10% and 12%, the hollow granule survival rate after drying at 60°C increased 30% and 60%, respectively.

Fig. 16 and 17 show that the survivability and quality of the hollow granules are different for each powder. PTFE 100 μm powder performed the best with HPC binder in terms of survivability and the proportion of perfect hemispherical shaped granules, compared to the smaller PTFE grades (see Fig. 18). Fig. 18 also shows that Aerosil performs better than other powders, perhaps due to its nano-particle size or the low density of the fractal particle aggregates. Although hydrophobic glass ballotini particles are smaller (65 μm) than PTFE 100 μm and lighter, hollow granule formation was less successful with glass ballotini which indicates the significance of careful powder selection.

In summary, Aerosil R974 was the most successful powder with HPC, and increasing HPC concentration improved the hollow granule quality. The effect of increasing the drying temperature was mixed.

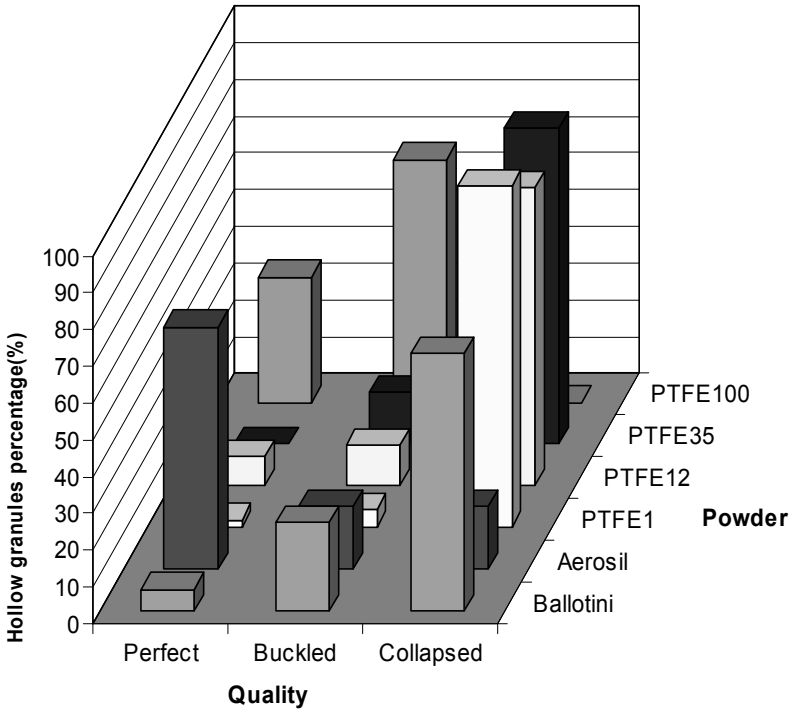

Fig. 18. Effect of powder type on survivability of hollow granules for HPC binder. Data from all HPC concentrations and both drying temperatures have been combined

6.4. Discussion

6.4.1. Comparing all three binders: HPMC, PVP and HPC

HPMC appeared to be the best binder as it worked well across the various powders and temperatures (see Fig. 19). HPC and PVP seemed to both perform poorly in comparison. However they seemed to complement each other in their response to different conditions: HPC performed well with the glass ballotini while PVP didn't, and vice versa with respect to the PTFE 1 and PTFE 12 powders.

In general, increasing temperature increases survivability in all cases (see Fig. 10 and Fig.13) and improves significantly the quality of granules formed with HPMC (see Fig. 10). Temperature had no significant effect on the quality of hollow granules formed with

PVP (see Fig.13) and HPC (data not shown). There may be a viscosity effect involved, as the PVP was much less viscous than HPC and HPMC (see Table 2). For comparison, Fig. 20 shows the survivability of hollow granules as a function of viscosity for different concentrations of HPMC, PVP and HPC binders. As shown in Fig. 20, for PVP and HPMC there is a consistent proportional relationship between binder fluid viscosity and the proportion of formed hollow granule. In order for a liquid marble to collapse, the drop must deform which requires internal fluid flow. We propose that a higher viscosiy binder fluid resist this flow and therefore enhances liquid marble stability during drying.

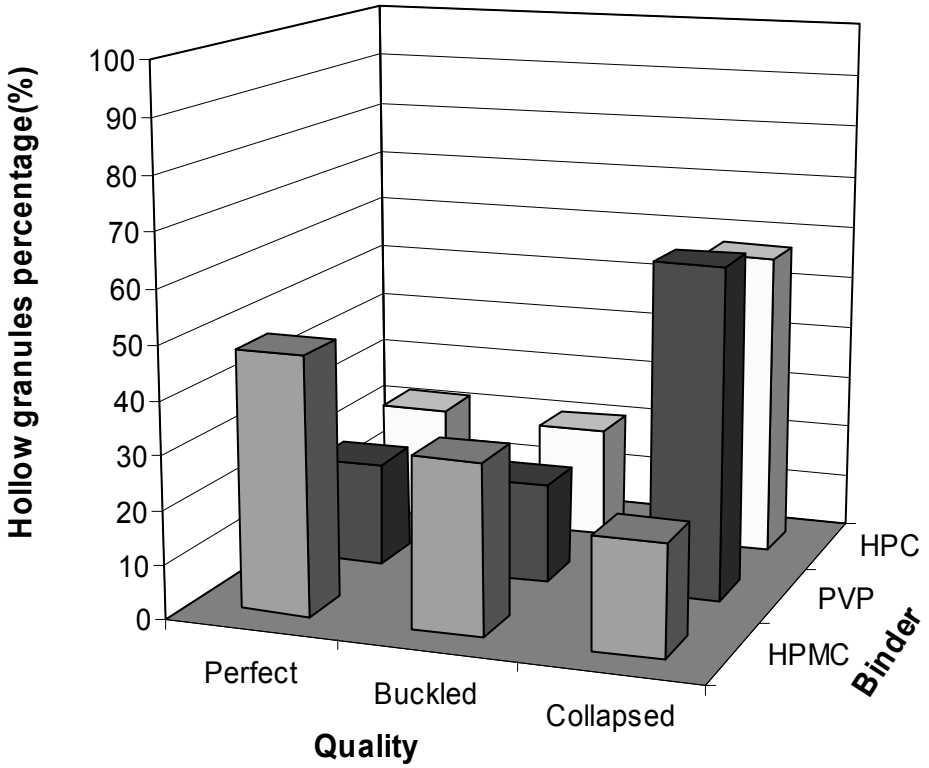

Fig. 19. Effect of changing binder on hollow granule formation. Graph includes data for all used powders and both drying temperatures (60 ºC and 100 ºC)

However, for HPC, the average survival rate remains relatively constant between 40 and 50% regardless of the HPC concentration or viscosity. This may be related to the precipitation of HPC and decreasing solubility of polymer in water at higher temperature.

HPC is freely soluble in water below 38 ºC, forming a smooth, clear, colloidal solution and changes to a swollen floc at a temperature between 40 and 45 ºC [12]. HPC precipitates out when the temperature increases above the cloud point, where the hydrogen bonds between water and the polymer chains become less favorable. .The solubility of the HPC in water then decreases and a polymer-rich phase precipitates [11] which affects the uniformity of the polymeric bridges formed during drying. For example, the cloud point of a 250 ppm HPC solution is 43.5 ºC [11] well below even the lowest drying temperature of 60 ºC. As the polymer concentration decreases, the cloud point increases [11]. This may at least partly explain why increasing HPC concentration caused previously perfect hollow granules to start buckling, as the lower cloud point caused earlier precipitation of the HPC which adversely affected the survival rate.

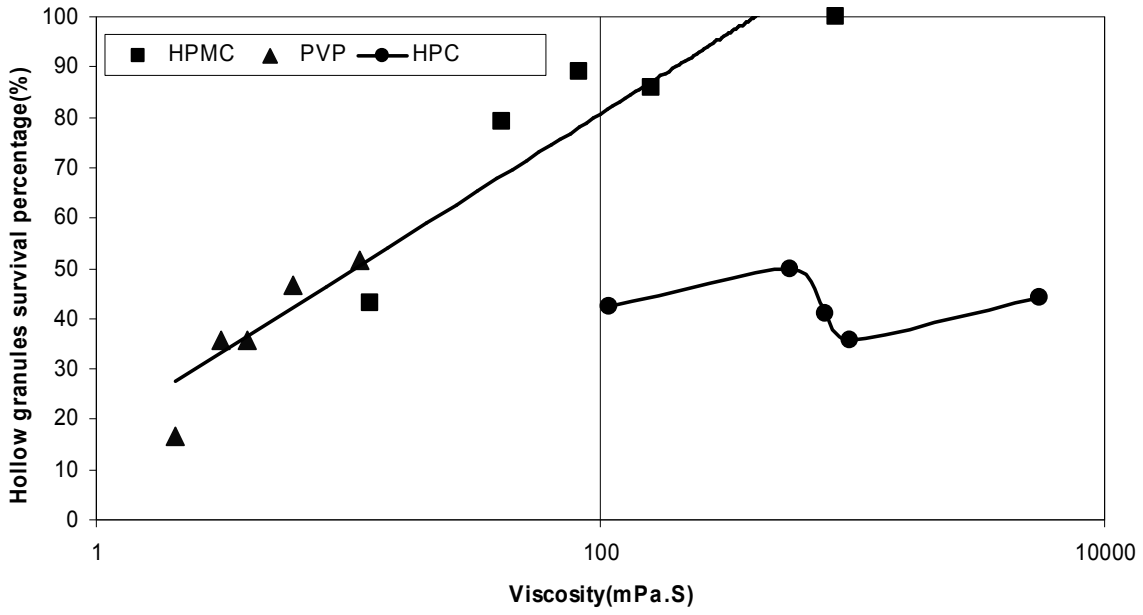

Fig. 20. Effect of binder viscosity on survivability of hollow granules

Table 2. Survivability of hollow granules for different concentrations of HPMC, HPC, and PVP binders

Binder Type	Binder Concentration (wt %)	Binder Viscosity (mPa.s)	Survivability (%)
HPMC	5	12	43
	8	41	79
	10	83	89
	12	158	86
	18	855	100
PVP	5	2.1	17
	8	3.1	36
	10	4.0	36
	12	6.0	47
	18	11.1	52
HPC	5	108	45
	8	566	50
	10	785	41
	12	970	36
	18	5504	44

Aerosil was the most successful powder for forming perfect hollow granules with all the binders tested (see Fig. 21). However, there were some exceptions at higher binder concentration (18% HPC and 18% HPMC) and at the highest drying temperature at 100ºC. The most successful combination was 12% HPMC binder using Aerosil R974

dried at 100 ^{o}C. The results for glass ballotini had mixed success. It was highly unsuccessful with PVP, and moderately successful with the HPMC/HPC and did better at higher temperatures. PTFE powders had mixed success again but at least some of the grades worked with all binders.

Fig. 22 shows the effect of PTFE particle size on the hollow granule survival rate for the three tested binder fluids. For PVP, there is a critical particle size somewhere between 12 μm and 35 μm where only hollow granules formed from particles smaller than this size can survive. HPMC also shows a sharp drop in survival rate for PTFE 35, although the survival rate then rebounds for the large PTFE 100 particles. In contrast, HPC shows a high success rate only for the largest PTFE particles.

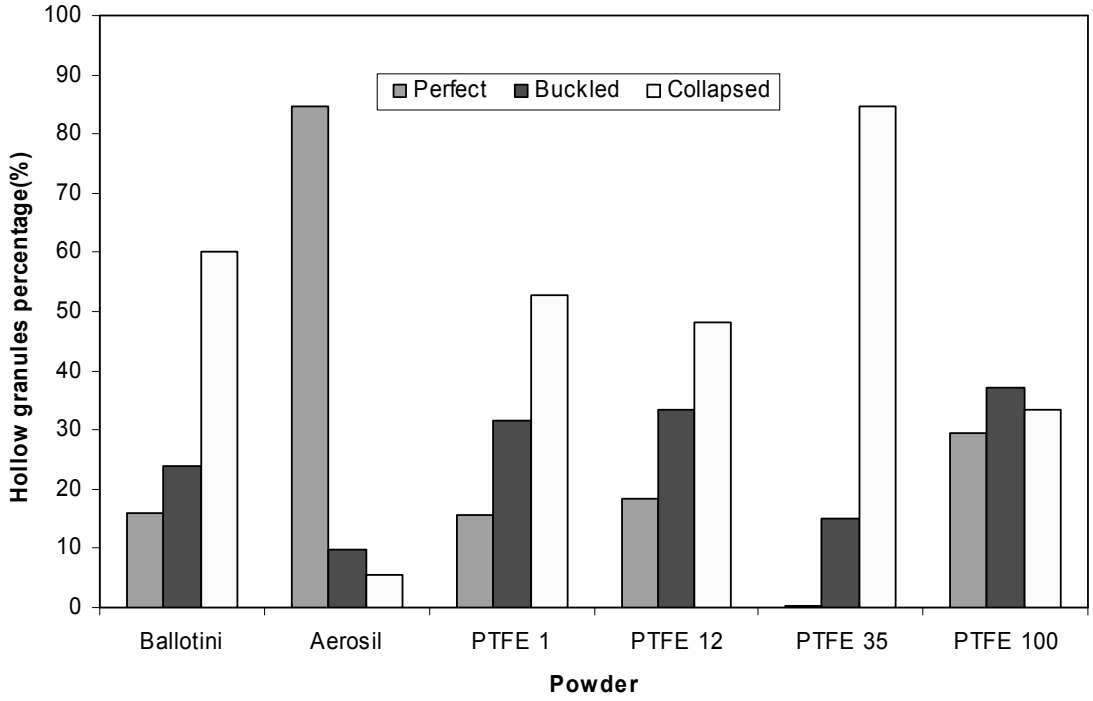

Fig. 21. Survivability and quality of all powder hollow granules. Data from all binders and both drying temperatures have been combined

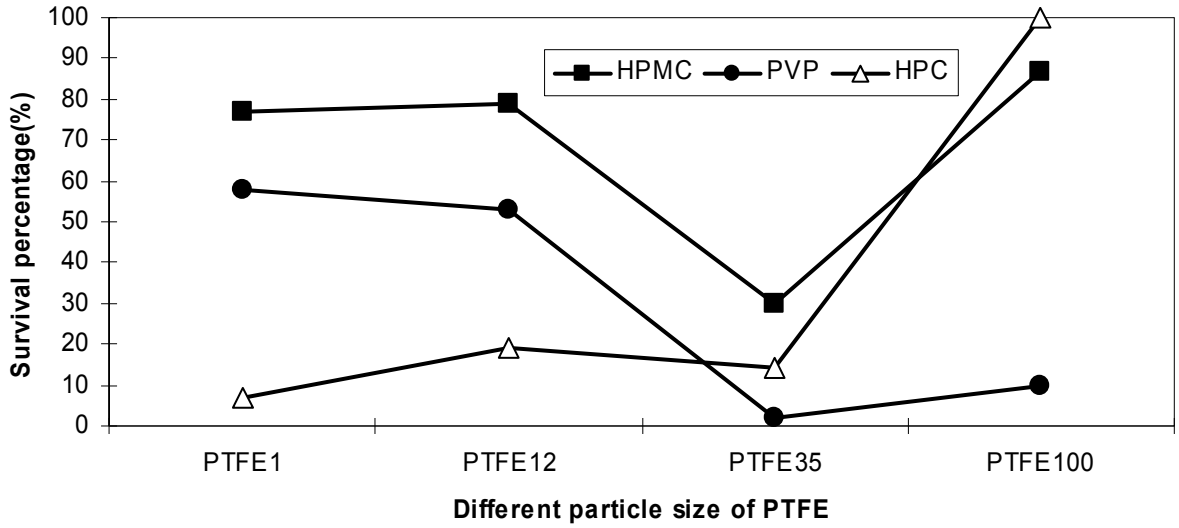

Fig. 22. Effect of PTFE particle size on hollow granule survivability

When drying marbles formed with high binder concentrations, in some instances a higher drying temperature induced collapsing or buckling. At higher binder concentrations, the fluid viscosity could be quite high which causes the droplets to be slightly larger and thus more prone to deformation during the drying process. When dried at 60 ºC, more shrinkage of the liquid marbles occurred (see Fig. 23) and this may have increased survivability, as opposed to 100ºC where shrinkage would occur less. Thus, the beneficial effects of drying at a lower temperature when using high concentrations of binder may be due to the enhanced shrinkage and strengthening of the liquid marble during drying. These points at least partly explain the unexpected lack of success at high binder concentrations and higher drying temperatures for both HPMC and HPC binders.

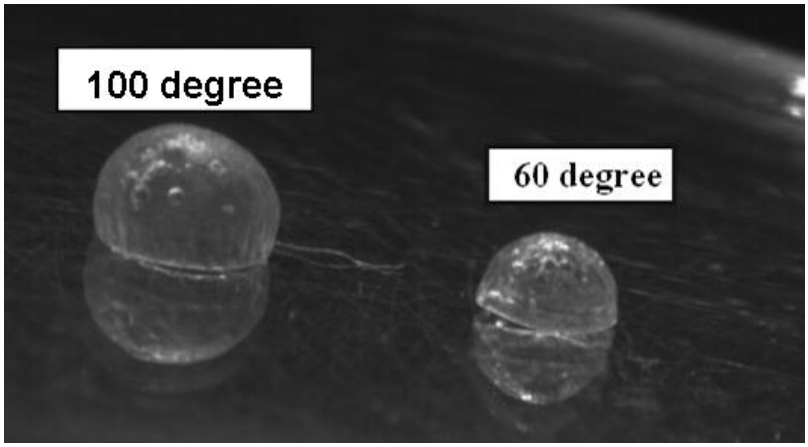

Fig. 23. Comparison of two perfect hollow hemisphere granules of Aerosil with 8% HPC, dried at 60 ºC (1.5 mm diameter), and 100 ºC (3 mm diameter). Spots on the granule surface are caused by trapped air bubbles.

6.4.2. Particle size effect

As drying continues the particles pack closely enough that inter-particle repulsions resist further shrinkage [13]. The binder, however, continues to vaporize through the holes between the particles [8]. The decrease in binder volume causes the receding of the drying surface into the droplet. Buckling of liquid marble can then occur because decreasing droplet pressure exerts a compressive capillary stress on the particle shell. When this stress becomes large enough to overcome the repulsive forces between the particles the outer shell undergoes buckling and wrinkling. It is clear inter-particle forces play an important role in determining droplet buckling, and any other ingredients in the particle shell can affect these forces and the buckling behavior of liquid marble. Polymers are an example of material that can significantly change the interaction between solid particles [13].

Aerosil was the most successful powder with all of binders, presumably because the inter-particle forces between the nano-particles are high and able to resist the capillary stress. This is in agreement with the previous study by Bhosale *et al.* [7] who indicated that the loosely aggregate floc-like structure of the nano-sized silica particles creates a highly porous shell and consequently increases the chance of survival. This hypothesis also agrees with case I in Fig.1. by Charlesworth and Marshall [9].

6.4.3. Shrinkage of liquid marble during drying

During drying of the liquid marbles, the droplet shrinks and the final granule size is smaller than the original droplet. The level of shrinkage depends on the drying temperature. Fig. 23 shows two granules of Aerosil with 8% HPC dried at 60 ^{o}C and 100°C. Although their initial primary droplet size was the same, it is clearly seen that the granule dried at 60 ºC is smaller than granule size at 100 ºC. The higher drying temperature creates a granule size more comparable with primary droplet size. This can be seen as an additional variable requiring control, or as an additional variable which can be used to manipulate the granule size. We expect that the granules shown in Fig. 23 would also have different granule strengths, due to both the physical size and the film thickness, although we have not performed any experiments to test this to date.

6.4.4. Implications of liquid marble drying behavior

We have previously postulated a series of steps for liquid marble formation and for hollow granule formation [1]. The final step was that "the multi-component powder shell must be sufficiently strong to be self-supporting in order to avoid collapse during drying to form a hollow sphere and subsequent standard powder handling operations" [1].

Qualitatively, the drying behavior of liquid marbles is in agreement with the types of drying behaviors observed by Charlesworth and Marshall [9] and shown in Fig. 1. All crust structures except IIC were observed during this study. We conclude that the optimal drying conditions for liquid marbles are driven by similar mechanisms for drying of solute drops, except that liquid marbles begin the drying process with a powder shell "crust" already in place. This observation should be of practical use during formulation and product development of cosmetic and pharmaceutical products based on liquid marbles and hollow granules.

6.5. Conclusion

The optimal condition for stabilizing liquid marbles during drying and formation of hollow granules were investigated for several types of powder and binder at different drying temperatures. Higher drying temperature, smaller or nano-size particles and higher binder concentration tend to promote the formation of perfect hollow granules. It was found that the survival rate was directly proportional to binder viscosity for HPMC and PVP. However, for HPC binder the survival rate was essentially constant regardless of HPC concentration. Different combinations of drying temperature, binder type, binder concentration, and powder type/grade could result in quite large changes in survival rate indicating the importance of careful formulation during hollow granule process development.

Acknowledgements

This project is financially supported by the Australian Research Council under Discovery Projects DP0770462. Scholarship support for N. Eshtiaghi was provided by the Monash

Graduate Research School. We express our grateful thanks to Sherry Mayo for taking X-ray microscopy photo of our samples in Manufacturing and Material Technology Group of CSIRO lab.

References

[1] K. P. Hapgood, L. Farber, JN. Michaels, Agglomeration of hydrophobic powders via solid spreading nucleation, Powder Technology, 188 (2009) 248-254.

[2] P. Aussillous, D. Quere, Liquid marbles, Nature, 411 (2001) 924-927.

[3] P. Aussillous, D. Quere, Properties of liquid marbles, Proceedings of Royal Socierty A, 462 (2006) 973-999.

[4] L. Forny, K. Saleh, I. Pezron, P. Guigon, L. Komunjer, Influence of mixing characteristics for water encapsulation by self-assembling hydrophobic silica nanoparticles Powder Technology, special issue on granulation, 189 (2009) 263-269.

[5] M. A. Ansari, F.Stepanek, Formation of hollow core granules by fluid bed in-situ melt granulation: Modelling and experiments, International Journal of Pharmaceutics, 321 (2006) 108-118.

[6] K. P. Hapgood, B. Khanmohammadi, Granulation of hydrophobic powders, Powder Technology, 188 (2009) 248-254.

[7] P. S. Bhosale, M. V. Panchgnula, H. A. Stretz, Mechanically robust nanoparticle stabilized transparent liquid marbles, Applied Physics Letters, 93 (2008) 034109/1-034109/3.

[8] M. Dandan, H.Y. Erbil, Evaporation rate of graphite liquid marbles: comparison with water droplets, Langmuir (2009), DOI: 10/1021/la900729d.

[9] D. H. Charlesworth, W. R. J. Marshall, Evaporation from drops containing dissolved solids, AIChE Journal, 6 (1960) 9-23.

[10] D.E. Walton, C.J. Mumford, The morphology of spray-dried particles: the effect of process variables upon the morphology of spray-dried particles, Chemical Engineering Research & Design ,77 (1999) 442-460.

[11] F. M. Winnik, Effect of temperature on aqueous solutions of pyrene-labled (Hydroxypropyl) cellulose, Macromolecules, 20 (1987) 2745-2750.

[12] R.J. Harwood, "Hydroxypropyl Cellulose", in Handbook of Pharmaceutical Excipients, 5th edition, R.C. Rowe, P.J. Sheskey and S.C. Owen (eds), Pharmaceutical Press, London, 2006.

[13] Y. Sugiyama, R.J. Larsen, J. Kim, D. A. Weitz, Buckling and crumpling of drying droplets of colloid-polymer suspensions, Langmuir, 22 (2006) 6024-6030.

7

Producing Hollow Granules from Hydrophobic Powders in High-Shear Mixer Granulators

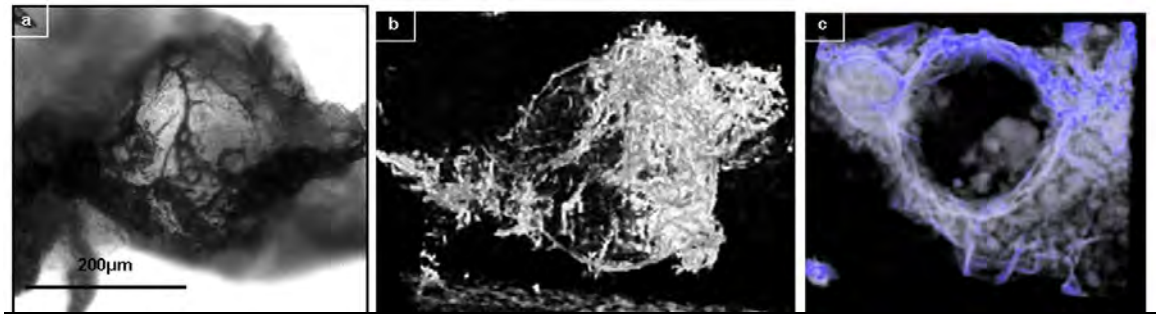

Hollow granule of Aerosil R202 with 5%HPC

Chapter 7: Producing hollow granules from hydrophobic powders in high-shear mixer granulators

Declaration for Thesis Chapter 7

Declaration by candidate

In the case of Chapter 7, the nature and extent of my contribution to the work was the following:

Nature of contribution	Extent of contribution (%)
Initiation, Key ideas, experimental and analysis work, development, writing up the paper	85

The following co-authors contributed to the work. Co-authors who are students at Monash University must also indicate the extent of their contribution in percentage terms:

Name	Nature of contribution	Extent of contribution (%) for student co-authors only
1. Benedicta Arhatari	XRT experiment	10
2. Karen P. Hapgood	Supervision, reviewing and editing of the paper	--

Candidate's Signature		Date

Declaration by co-authors

The undersigned hereby certify that:

(1) the above declaration correctly reflects the nature and extent of the candidate's contribution to this work, and the nature of the contribution of each of the co-authors.

(2) they meet the criteria for authorship in that they have participated in the conception, execution, or interpretation, of at least that part of the publication in their field of expertise;

(3) they take public responsibility for their part of the publication, except for the responsible author who accepts overall responsibility for the publication;

(4) there are no other authors of the publication according to these criteria;

(5)potential conflicts of interest have been disclosed to (a) granting bodies, (b) the editor or publisher of journals or other publications, and (c) the head of the responsible academic unit; and

(6) the original data are stored at the following location(s) and will be held for at least five years from the date indicated below:

Location(s)	Department of Chemical Engineering, Monash University, Clayton Campus

[Please note that the location(s) must be institutional in nature, and should be indicated here as a department, centre or institute, with specific campus identification where relevant.]

Signature 1	[redacted]	Date
Signature 2	--	--

Abstract:

The formation of hollow granules from hydrophobic powders in a high-shear mixer granulator has been investigated by changing the binder/powder mass ratio and studying its effects on granule size and structure. In this study, a mixer granulator was filled with 100 g of hydrophobic fumed silica and then varying quantities of 5% Hydroxy Propyl Celuolose solution was slowly sprayed into granulator. A range of liquid to solid mass ratios between from 0.5:1 to 15:1 was used. Granules were then dried at 60 ºC in a fan forced oven. This paper compares the particle size distributions, scanning electron microscopy (SEM) images and X-ray tomography (XRT) images of hollow granules as a function of the liquid to solid mass ratio. The granule mean size increased and the fraction of un-granulated (fine) particles decreased as the liquid to solid mass ratio increased. Simultaneously, the morphology and structure of the hollow granules changed from a spherical to a deformed structure which indicates the importance of choosing the optimal liquid to solid mass ratio. The optimal liquid to solid mass ratio for Aerosil R202 powder in this study was found to be between 3:1 and 6:1. The final granule shape and size distribution are dependent on the liquid to solid ratio if the liquid marble nucleation process starts with a preformed droplet template.

Nicky Eshtiaghi, Benedicta Arhatari, Karen P. Hapgood, "Producing hollow granules from hydrophobic powders in high-shear mixer granulators", Advanced Powder Technology, 2009 (20), 558-566.

Keywords: Hollow granule, Liquid marbles, Dry water, Hydrophobic, Granulation, Agglomeration, XRT

7.1. Introduction

A tablet with good characteristics such as good flow and compressibility, uniform concentration of active ingredients and excipients, and few fine particles is not made on a tablet press; it is made in granulation process [1]. Wet granulation is the process of collecting particles together by creating bonds between them using a binding agent. The granulation process combines one or more powders and forms granules that will allow the tabletting process to be predictable. Wet granulation is one of the most common ways to granulate. The granulation process can be very simple or very complex depending on the characteristics of the powders. If the active ingredient represents a high percentage of the blended material and is also hydrophobic like many drugs in the pharmaceutical industry, problems may then begin. In many processes, a surfactant is added to overcome the problematic characteristics of hydrophobic powders, but in some cases the surfactant is either not compatible or too expensive to be used [2].

Hollow granule formation is a new way to solve the problematic granulating behavior of hydrophobic powders. The dissolution rate of tablets made from hollow granules is rapid and the drying is fast due to the thin shell thickness [3]. These granules also show good compressibility characteristics during the tabletting process [3].

Hollow granules can form from hydrophobic powders by "solid spreading nucleation" [2, 3] where the powder spreads around a template drop in the nucleation process and the interior liquid is subsequently dried to form a hollow granule. The nuclei formed by solid spreading are also known as "liquid marbles" [4, 5] and "dry water" [6], and are used in

cosmetic and pharmaceutical formulations. Liquid marbles and dry powder encapsulation are examples of particle design.

There are now several studies on producing liquid marbles and hollow granules at laboratory scale. McEleney *et al.* [7] studied the effect of powder density and particle size on the stability of the liquid marbles and reported the formation of a hollow granule shell after drying poly-methylmethacralate (PMMA) liquid marbles. In another study, Eshtiaghi *et al.* [8] reported three different granule shapes - perfect, buckled and collapsed - after drying liquid marbles in small scale experiments. The formation of perfect hollow granules was generally improved by increasing the binder viscosity, increasing the drying temperature and decreasing the particle size of the powder. In a laboratory scale study, Bhosale *et al.* [9] investigated the strength of liquid marbles formed with PTFE (7-12 μm) and two types of treated fumed silica powder. High surface area nanoparticle powders (e.g. Aerosil) created more uniform powder shells through uniform coverage of the liquid–vapor interface. They found that nano-powder shells form an "elastic" membrane that makes these liquid marbles mechanically robust in comparison with conventional liquid marbles made from larger particles, and that these liquid marbles formed from nano-particles are able to withstand higher compressive stresses during drying, and may be more likely to form hollow granules [9]. These studies did not investigate or attempt the production of hollow granules on a larger scale.

Although there are now several published papers on the production of liquid marbles and hollow granules via laboratory techniques [7, 8, 9], only two methods of mass producing of hollow granules are reported in the literature [2, 5, 10].

The first method for mass production of hollow granules is melt granulation [10] where a single granule is formed from a binder particle by sequential deposition of hydrophilic primary particles on its molten surface. If the first layer of particles forms a stable arch and does not collapse as the binder liquid from the core is drawn by capillary force to the shell region, a hollow core granule is formed.

The second method is via solid spreading nucleation in a high-shear mixer [2, 6] and there are two related studies in this area. In one study, "Dry water" was produced by encapsulation of water with various grades of hydrophobic silica [6]. In this study, they found that by decreasing the hydrophobicity of powder, powder shell formation became more sensitive to intense mixing conditions. The liquid marbles became less stable and required lower impeller speed and more powder to encapsulate the same volume of liquid. Atomization into the high-shear mixer was not performed. In this study, the liquid marbles were the desired end product.

Stable hollow granules [3] were successfully produced by drying liquid marbles which were formed via solid spreading nucleation. The granules were produced in a 2 L granulator using a formulation of 70 wt% hydrophobic drug powder, 20% microcrystalline cellulose and 4% hydroxypropyl cellulose binder as hydrophilic

excipients and 1% sodium lauryl sulfate surfactant. The hollow granules were strong enough to withstand the downstream milling process as the excipients stabilized the powder shell to allow the hollow structure to be preserved during drying. Hapgood *et al*. [3] studied the effect of wet massing time on granule structure for two different liquid ratios and found that the granules tended to deform and elongate as the amount of fluid and/or wet massing time increased. There are no further studies on the effect of changing the binder liquid ratio on the morphology of the hollow granules. More investigation in this area is required.

The objective of this present work is to perform a systematic study of the effect of the binder fluid to powder mass ratio on the size distribution and internal microstructure of granules formed by a high-shear mixer granulation process.

7.2. Materials and methods

Aerosil R202 (Degussa Co. Germany) is the commercial name for highly hydrophobic fumed silica which has been silanised to turn the surface hydrophobic. The original powder is very fluffy and somewhat dusty with a reported primary particle size of around 16 nm and a high 300 m^2/g BET surface area. However, it tends to self-agglomerate to form large and loose flocculated networks with a much larger particle size between 1and 30 μm. Fig. 1 shows a SEM image of Aerosil particle aggregates and Fig. 2 shows the particle size distribution as measured by laser diffraction. HPC (Hydroxy Propyl Cellulose, 100,000 Mw, Sigma Aldrich Pty Ltd.) with 5% concentration was used as a

binder solution. The viscosity of the 5% HPC solution was measured using a rotational viscometer (Visco Basic Plus, Fungilab, Barcelona) and found to be 108 mPa.s.

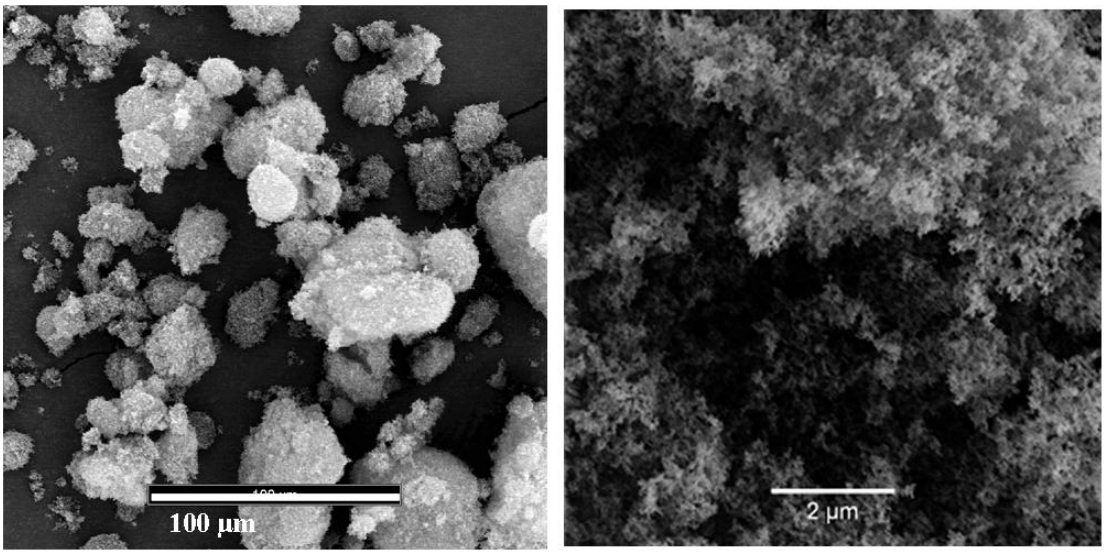

Fig. 1. SEM micrograph of un-granulated Aerosil R202

Granules were prepared in a high shear KG-5 (Series IV) laboratory scale granulator from the fumed silica and 5 mass% HPC. The metal mixing bowl was 20 cm in diameter and 13 cm height. A three bladed impeller was mounted at the base of the bowl, and the fluid was added through a nozzle port in the perspex lid. The ratio of binder fluid to powder mass (L:S) was varied between 0.5:1 and 15:1. The granulator bowl was loaded with 100g of fumed silica and mixing was performed at constant impeller speed of 155 rpm. At this impeller speed, the powder exhibited roping flow. The silica was dry mixed for 2 min in order to break down any weak, loose aggregates of primary particles.

The 5% HPC binder solution was then sprayed into the granulator using Unijet nozzle (400017) at 5.6 bar pressure and 90 g/min flow rate. The distance from the nozzle tip to

the powder surface was approximately 3 cm and the spray width at this point was almost 1 cm. The droplet size distribution 3 cm below the nozzle was measured using a Malvern Spraytec with a 300 mm lens, which measures up to a nominal drop size range of 0.5-900 μm. The d_{50} drop size was 442 μm, with a broad distribution of (d_{10} = 145 μm, d_{90} = 763 μm). The total spray time varied with the liquid ratio. To reach a liquid ratio of 6:1 took 6.67 min of spraying while a liquid ratio of 15:1 was reached after 16.75 min of spraying. At the completion of the granulation step, approximately one third of the wet granulated powder was tray-dried in a forced-fan oven at 60 ^{o}C.

Particle size distributions were analyzed by laser diffraction using a Malvern Mastersizer 2000 with detectable particle size between 0.2 and 2000 μm. Analysis was performed in dry mode using 3 bar pneumatic transportation for un-granulated Aerosil powder and at 0.5 bar for analyzing the hollow granules. The vibrating feeder was set to 100% to obtain an obscuration between 1 and 6 %. These conditions were chosen based on titration of the pneumatic transport pressure and vibrating feeder settings, to ensure reproducible data. The Aerosil R202 was quite difficult to measure reproducibly due to its aggregated initial state and sensitivity to electrostatic forces. A pneumatic pressure of 3 bar was found to be the optimum pressure for dispersing the un-granulated Aerosil. Below 3 bar, significant large aggregates of primary particles were found while increasing the pressure above 3 bar caused the Aerosil particles to re-aggregate. The pneumatic transport pressure used for analyzing the granules was 0.5 bar, which was again found to be the optimum which was able to disperse the particles in the laser beam without significant breakage of the granules.

Laser diffraction uses an assumption of constant density across the entire size range when reconstructing the particle size distribution of the sample. There are many cases where this assumption is questionable, including when analyzing "normal" granule size distributions where there is a mixture of porous granules and non-porous particles from the raw powder. In these experiments, the "un-granulated" fine Aerosil particles are also low-density, fractal aggregates of nano-particles with >90% void space. Thus, any density differences between the hollow granules and the raw aggregated powder is expected to be far less than would occur in a "normal" granulation experiment.

Granules were sieved into size fractions (1000, 500, 250, 125, 63 μm) and the microstructure of each sieve fraction was characterized scanning electron microscopy (SEM) and X-ray tomography (XRT). Representative granule samples were imaged using either JEOL 840A SEM equipment (back scattering at 20 kV acceleration voltage, 3e-10 probe current or at 15 kV and 1e-9 probe current), or JEOL 6300 FEG SEM equipment at 5 kV acceleration voltage. Back scattering and/or low acceleration voltages were required to overcome granule charging problems which occurred while taking some images.

Three dimensional X-ray images of granules were obtained using X-ray micro computed tomography machine (Xradia Inc. USA) with approximately 2 μm resolution. The X-ray sources operated at 40 kV. Each granule was scanned by acquiring 361 or 721 projections taken at 0.5º or 0.25º rotational increments. The distance between the source and sample was 80-125 mm, and the sample detector distance was fixed at 20-25 mm. Different

exposure times and magnifications were used for scanning different mesh size granules to acquire sufficiently detailed images. After collecting a set of phase contrast projections (where each projection shows mainly the edge enhancement of the sample), these projections were processed with tomography reconstruction software to produce three dimensional phase contrast data.

The phase contrast projection data-set from some samples were then selected to apply a phase retrieval step. Phase retrieval is applied to each phase contrast projection image to obtain a phase map of the object in each projection. The resulting phase images are then tomographically reconstructed to produce a 3D phase map of the sample. Phase retrieval represents a considerable advance over phase contrast images in terms of obtaining a quantitative measure of the object reflective index, whereas phase contrast can obtain only qualitatively the object structure that can be seen typically in the edge enhancement This is a useful technique for imaging a transparent material (e.g. Aerosil) as transparent materials produce poor absorption contrast, and require an intermediate step of phase retrieval to acquire more detailed images.

7.3. Results

The effect of liquid–solid ratios ranging from 0.5:1 up to 15:1 on granule morphology and size distribution was investigated. The liquid ratio of 15:1 was the upper limit of liquid to solid ratio. After adding 1.5 kg of solution to 100 g of powder, the granulated mass showed behavior similar to a soft solid, where vibrating the powder bed would cause the bed to wobble like jelly due to attaching liquid marbles to each other. This was

also the upper limit that could be handled in the 4 L mixer bowl as the bed swelled so dramatically that the granule flow was visibly constricted by the granulator lid.

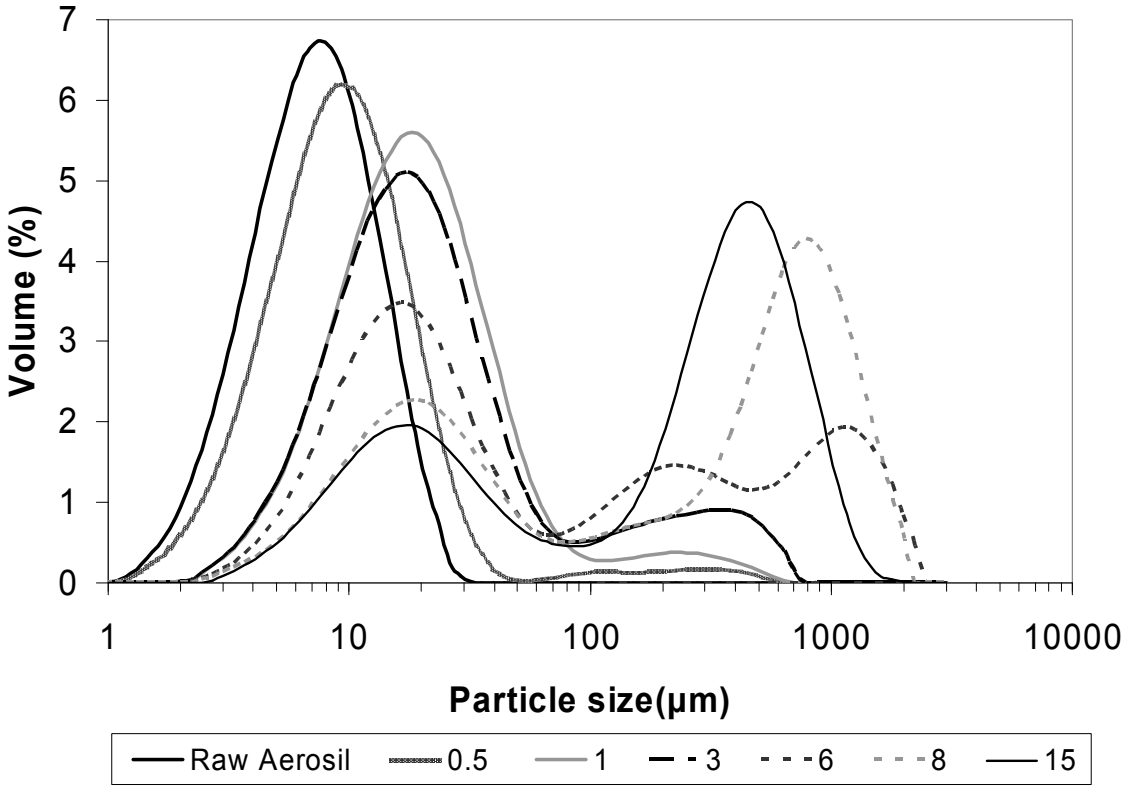

Fig. 2. Particle size distributions for un-granulated and granulated Aerosil with different HPC binder mass ratio in high shear mixer granulator

Fig. 2 shows particle size distribution (PSD) for the granulated Aerosil as a function of liquid ratio. The particle size distribution of the un-granulated Aerosil R202 is shown for comparison. Prior to granulation, the raw Aerosil powder is aggregated between 1 and 30 µm. After 50 g of water has been added (i.e. L:S ratio of 0.5:1) the main ungranulated powder peak is mostly unchanged, but a small proportion of newly formed granules appear as a second peak between approximately 80 and 600 µm. The location of this main granule peak seems to coincide with median drop size of the spray, suggesting that these granules are being formed directly from the drop templates in the spray. Adding a

further 50 g of liquid to reach a 1:1 liquid ratio shifts the un-granulated peak slightly to the right and the proportion of granules formed increases. The shift in the un-granulated peak suggests that the finest particles in the feed powder are being granulated first.

As the liquid to powder ratio increases to 6:1 the amount of un-granulated powder decreases sharply and two peaks are seen in the granule distribution – the first at approximately 200 μm and the second at approximately 1mm. At 8:1 liquid ratio, the batch is more than half granulated and the main granule peak has shifted upwards to approximately 1 mm. Further liquid addition to the limit of 15:1 appears to show some breakage of the granules as relatively few granules larger than 1 mm remain. Overall, Fig. 2 shows that as the liquid to solid mass ratio increases, the proportion of granules (approx 100 μm- 2 mm) steadily increases with a major granule peak around the mean droplet size (440 μm) while the amount of un-granulated Aerosil (<100 μm) steadily decreases. Table 1 summarizes the particle size distribution statistics as a function of liquid level.

Fig. 3 presents SEM images of the granules and Fig. 4 presents X-ray tomography (XRT) images as a function of both granule size and liquid ratio. The particle size distribution results in Fig. 2 are consistent with observations from the SEM images (Fig. 3). The sieve cut of 63-125 μm contains a mixture of un-granulated and granulated powder. As the binder: solid ratio increases from 0.5:1 to 15:1 (see Fig. 3a, d, g, j, n and s) the amount of un-granulated powder in the 63-125 μm SEM images also visibly decreases, which is consistent with the size data in Fig. 2. For L:S ratios between 0.5:1 and 6:1, a second

peak representing small granules appeared in Fig. 2. XRT images shown in Fig. 4a-c confirm that these small granules are indeed hollow.

We also observed that as the L:S ratio increased, the liquid marbles tended to attach to each other and produce larger, irregularly shaped granules, which are not desirable (compare Fig. 3p with Fig. 3c). The granules gradually become elongated and deformed as the liquid level and average granule size increases, as observed in another liquid marble system [3]. Many of the granules shown appear to be partially collapsed or buckled in shape. This kind of structure is not seen in conventional granulation, but has been observed previously in solid spreading nucleation systems [2, 8].

Fig. 3 shows the gradual evolution in granule size up to a maximum of approximately 500 μm. Although the laser diffraction results in Fig. 2 show that there are granules above 1 mm in size, these samples generally broke during the SEM or XRT sample preparation procedure, which indicates that they are loose aggregate of particles. Only at the two highest liquid ratios tested – 8:1 and 15:1 – could images of the largest granules be taken. An XRT image of a 1 mm loose aggregate formed at 8:1 liquid ratio is shown in Fig. 4s. The structure of this fragile granule is clearly different to all the other granules shown and the granule was not hollow.

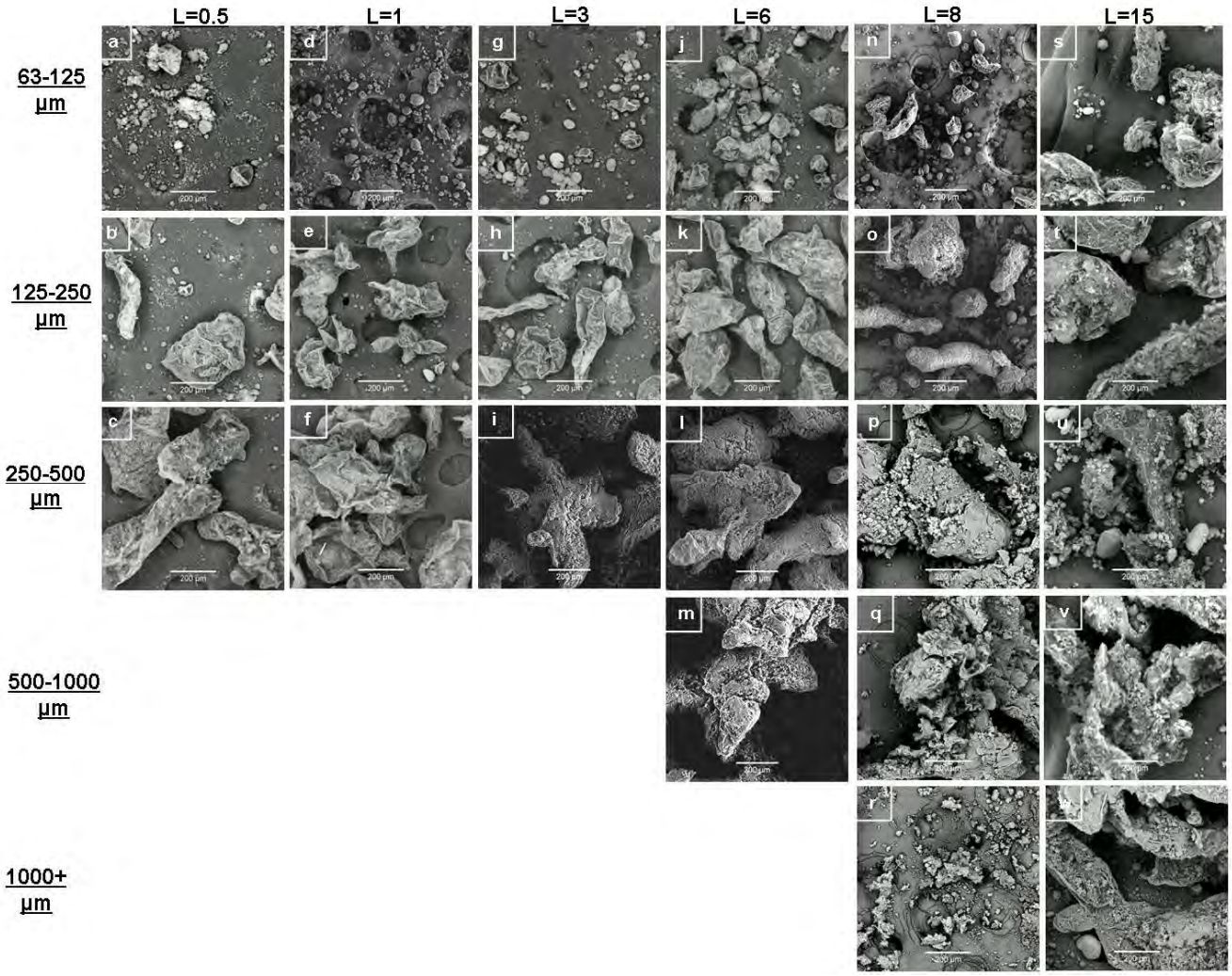

Fig. 3. SEM micrograph for 63-1000µm mesh cut of granulated Aerosil with different HPC binder mass ratio in high shear mixer granulator (scale bar is 200 µm)

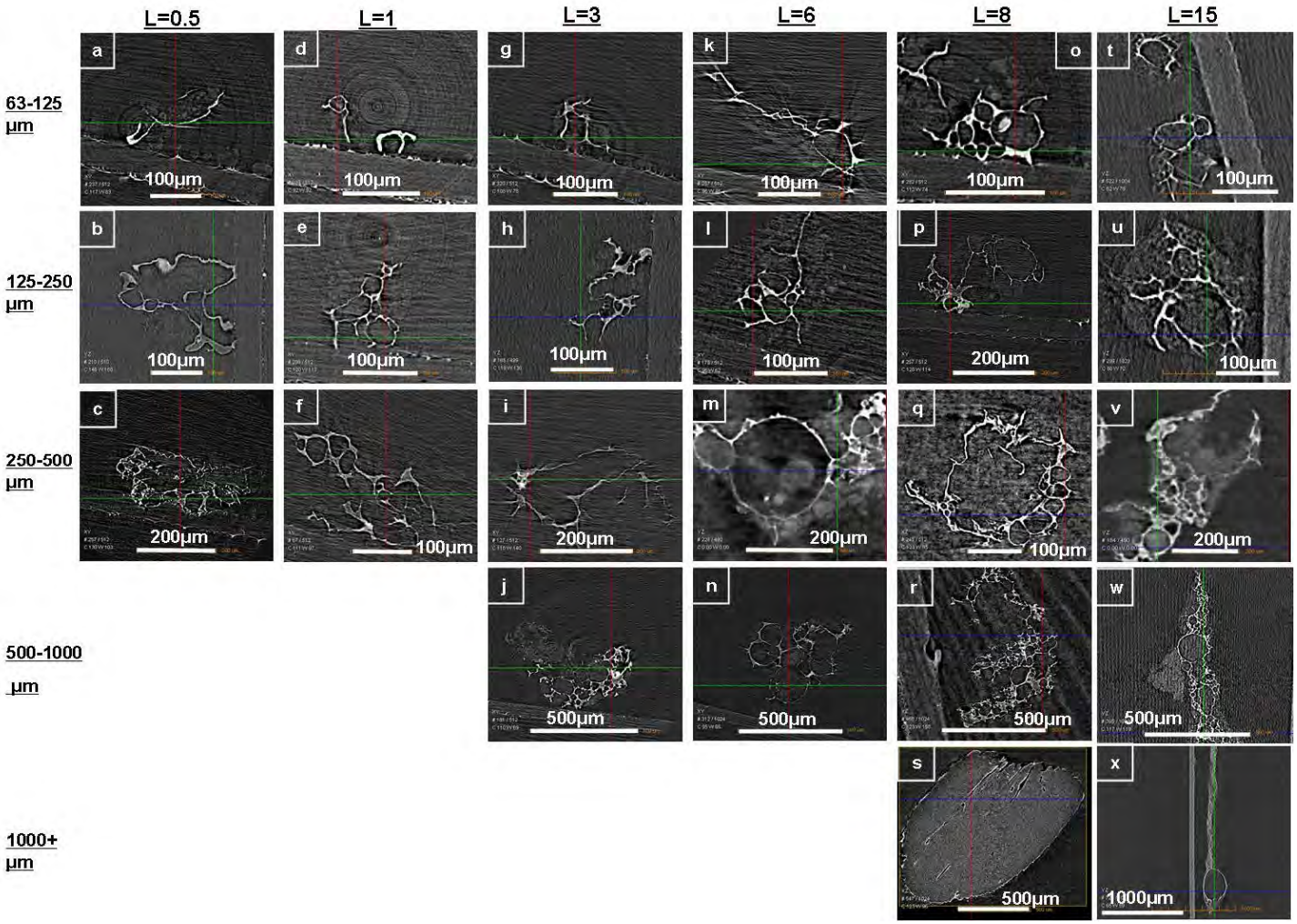

Fig. 4. X-ray tomography of the granule internal structure as a function of liquid binder mass ratio and granule size

The XRT images in Fig. 4 demonstrate that most of the hollow granules formed across all L:S ratios have a complex and almost foam-like internal shape structure. As the L:S ratio increases, this structure stretches and finally produces a filament-shaped granule. These stretched granules are clearly seen in SEM images (see Fig. 3b, e, h, k, o and t) and XRT images (for example see Fig. 4w and x). Only a few spherical hollow granules containing only one hollow cavity were found and an example is shown in Fig. 7. These granules were mostly in the 63-125 μm sieve cut and can be seen as small round granules in the top row of Fig. 3, although the example shown in Fig. 7 is a larger 250-500 μm example. This is in contrast to previous work on hollow granules [3], where single cavity spherical granules were commonly found and even the larger granules only contained 2-4 hollow cavities rather than the complex foam structure observed here. The reasons for the differences in structure are unknown and could be related to the formulation, the processing conditions, or both.

The maximum granule size at the highest L:S ratio of 15:1 decreases from 1000 μm to around 500 μm (see Fig. 2) which is indication of granule breakage. We expected to see loose aggregate granules above 1 mm but the X-ray image of this mesh cut (Fig. 4x) at 15:1 liquid:solid ratio indicates the existence of hollow granules. The corresponding SEM image for this mesh cut (Fig. 3w) also reveals large granules, and is quite different in appearance to Fig. 3r which shows the same sieve cut at a lower liquid ratio of 8:1. The appearance of at least some hollow granules greater than 1 mm at the highest L:S ratio of 15:1 may be related to the availability of enough binder fluid to granulate all the particles. However, none of these examples of granules greater than 1mm are suitable for drug

delivery as they are either loose aggregate of the primary particles or flattened and stretched filament of hollow granules (see Fig. 4s and x, respectively).

As granulation proceeds, we see increased coalescence of the granules as the L:S ratio is increased. The granules tended to coalescence in layers or sheets to form large granules (typically 500 μm and larger) with a foam-like internal structure. Fig. 5 and 6 show XRT cross sectional images of foam sheet for 500 μm mesh cut of 3:1 and 15:1 L:S mass ratio, respectively. We expect these granules will have different strengths as their shell thicknesses are quite different. The foam formation is most likely caused by compression and squeezing of the liquid marbles during processing, perhaps even in the highly turbulent spray zone. The Aerosil R202 powder has an extremely low bulk density and the roping flow pattern in the granulator was significantly disrupted as it passed beneath the overhead nozzle. Preliminary experiments with smaller batches showed that it was possible for the force of the spray to blast the powder out of the way and land directly on the metal base of the bowl. Forny *et al.* [11] have shown that there is a threshold energy per unit mass, above which a phase inversion to form a "mousse" can occur. In our experiments, no bulk phase inversion of the batch occurred, and the patches of foam-like structure could either be coalescence of liquid marbles or localized areas of phase inversion to form a mousse. Alternatively, the foam structure may be related to foaming and bubbling during drying which can occur due to the evaporation of a residual liquid inside partially dried particles [12]. Walton and Mumford [12] reported high surface area powders with strong gas absorption properties had higher internal porosity after drying due to adsorption of absorbed gases.

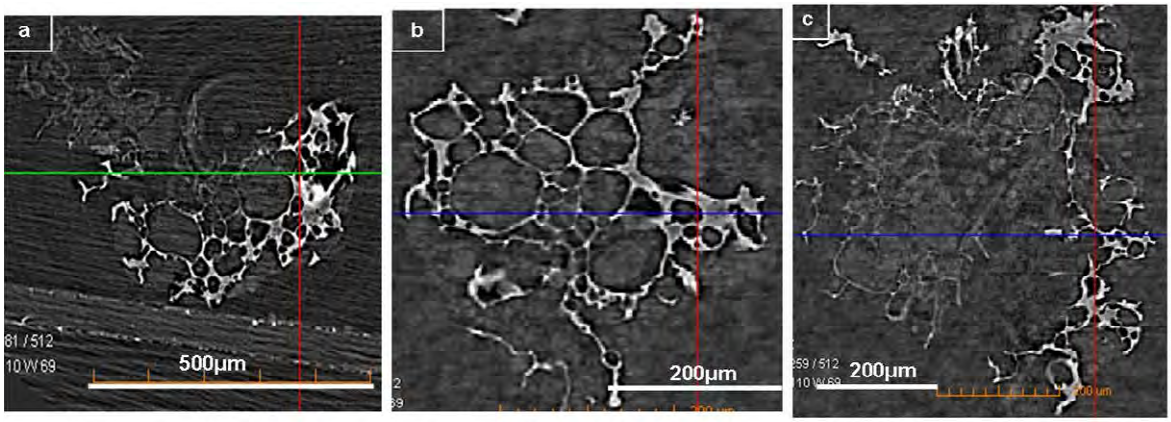

Fig. 5 (a)X-ray tomography of 3:1 binder: powder granules, (b) bottom cross sectional area of image a, (c) top cross sectional area of image a

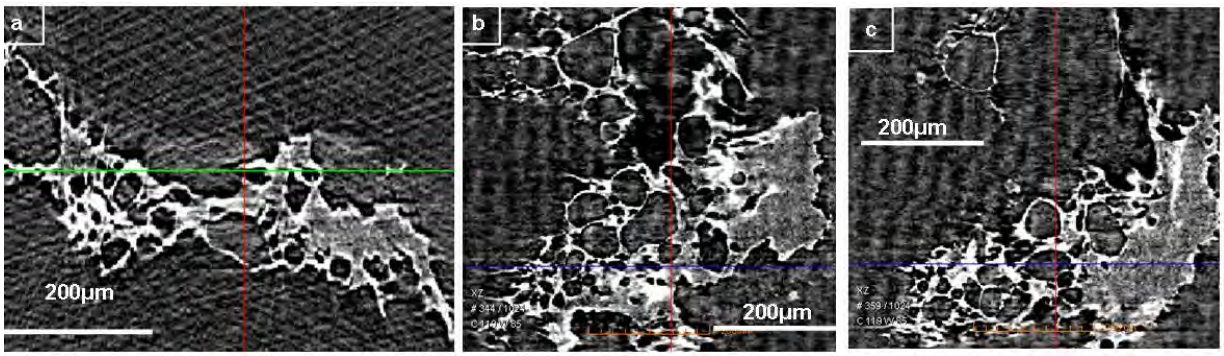

Fig. 6 (a)X-ray tomography of 15:1 liquid: powder granules (b) bottom cross sectional area of image a, (c) top cross sectional area of image a

To maximize the number of spherical, single cavity granules and minimize the formation of foam sheets, choosing the optimal L:S ratio is important. For the process examined in this paper, the optimum L:S ratio appears to be between 3:1 and 6:1. The size distribution data in Fig. 2 shows a reasonable conversion of dry powder to hollow granules, while the granules morphology shown in Figs. 3 and 4 show minimal occurrences of all undesirable effects such as foam sheet formation, stretched filament granule, and also considerable amount of un-granulated fine particles are less illustrated in this range.

There are some interesting features hidden in X-ray tomography images when they are reanalyzed as phase retrieval images instead of phase contrast images. All images in Fig. 4 are phase contrast images except Fig. 4m and v. Fig. 7 demonstrates phase retrieval image of L:S mass ratio of 6:1 for 250-500 μm mesh cut. A spherical hollow granule is shown, which appears to be filled with smaller spherical powder aggregates. The internal aggregates may be formed during granulation, or perhaps are related to erosion of the interior of the granule shell during drying, transportation, sampling, or sample characterization, or can be related to internal blistering occurred during drying [12]. This internal blistering produces small particles or blisters within the larger parent particle. The bright outlines surrounding the circumference of the spherical granule in Fig. 7d-f (and the small foam sheet around the granule in Fig. 7e) indicate a denser wall structure formed from Aerosil and HPC binder, while the faded white color within the granule is consistent with lower density un-granulated Aerosil.

The phase retrieval images also help to interpret some features observed in the SEM images. Many of the granules shown in the SEM micrograph images in Fig. 3 have multiple small, spherical attachments on the surface. For example, see Fig. 3p and u. From the SEM images, it is not clear whether these attachments were small hollow granules or small aggregates of the primary particles. By comparing SEM and X-ray images (see Fig. 8) the low-density circles on the outside of the granule outline are clearly not hollow. We conclude that these small exterior attachments are mostly aggregate of un-granulated Aerosil particles.

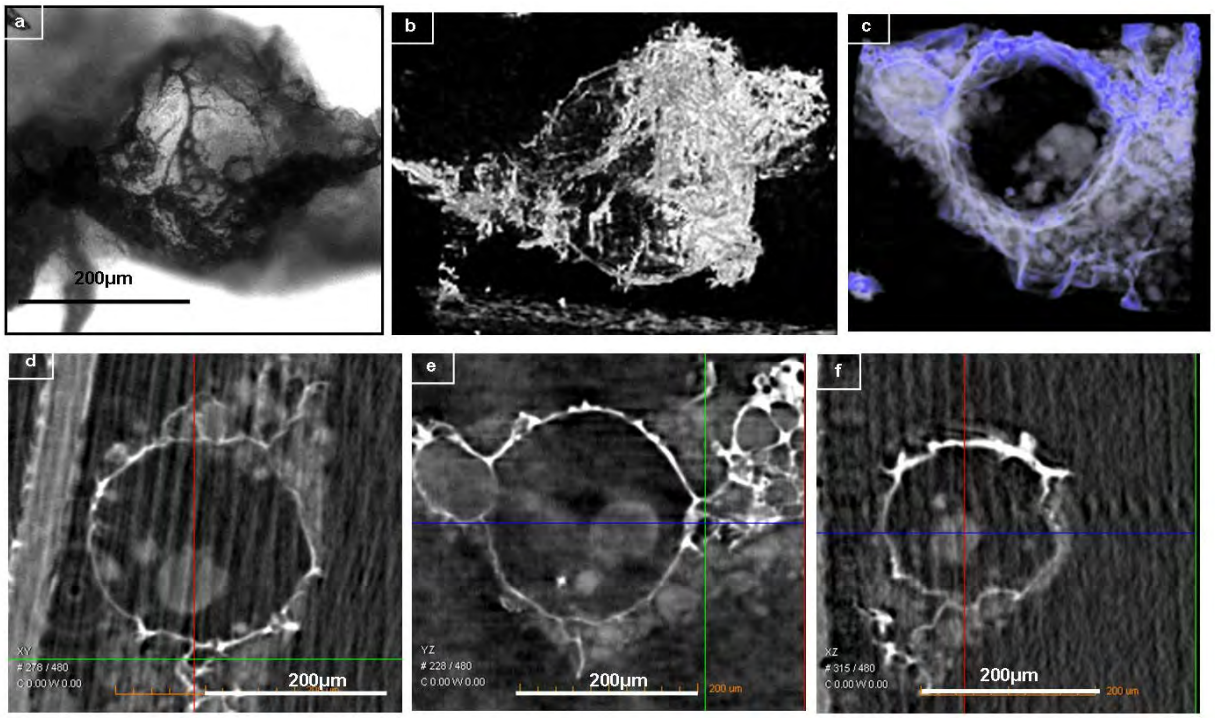

Fig. 7 XRT image of 6:1 L: S ratio (a) Three dimensional microscope image, (b) Three dimensional X-ray tomography phase contrast image, (c) Three dimensional x-ray tomography phase retrieval image, (d) XY cross sectional area, (e) YZ cross sectional area, (f) XZ cross sectional area

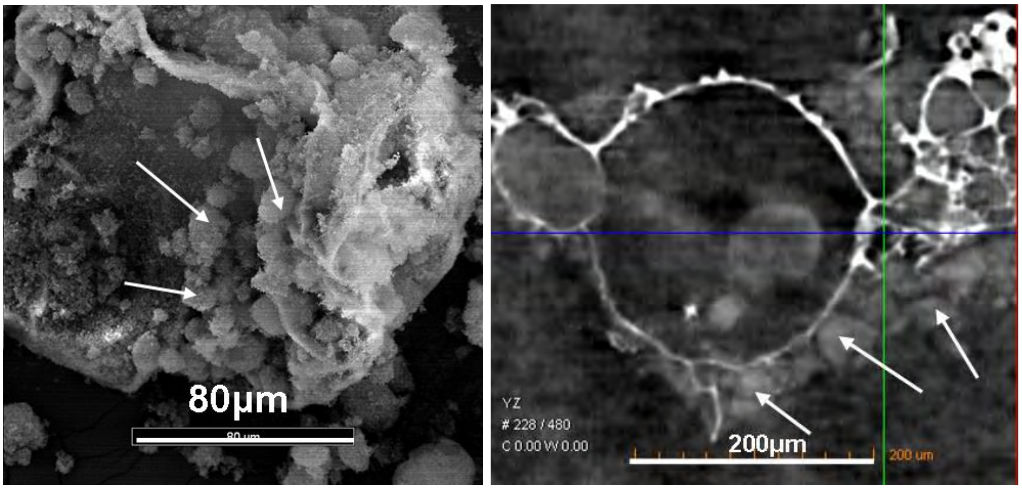

(a) (b)

Fig. 8 Images of 6:1 binder ratio (a) SEM micrograph image (b) X-ray tomography image

7.4. Discussion

The work presented here has shown that stable hollow granules can be produced from liquid marbles formed from hydrophobic Aerosil R202 and 5% HPC binder in a high-shear mixer granulator. The formulation used here is far simpler than the formulation reported previously [3] although the granule structure is far more irregular and complex than the earlier reports. This may be due to the extremely high liquid ratios used; differences in the formulation used, or due to the processing conditions including the high-shear mixer design. In comparison, the maximum liquid to solid ratio in the previous report of hollow granule formation from liquid marbles was only 0.78:1 [3]. The smaller liquid ratio may have made their system simpler to control, as even the larger granules contained a single hollow cavity [3] rather than the complex foam structure found in this work. In addition, the formulation used in the previous study contained several different components with different functionality, including a surfactant and water absorbing cellulose [3]. This more complex formulation changes the interactions between the solid and liquid and may have contributed to producing spherical, single cavity granules. The dramatic differences in granule structures indicate the importance of performing X-ray tomography experiments during hollow granule formulation design.

Our experimental results show Aerosil R202 powder, which is the most hydrophobic commercial pharmaceutical grade, can encapsulate up to 15 times of its own weight of 5% HPC solution, which is extraordinary. Previous studies on a similar system of Aerosil R202/ R812S and pure water in a high-shear mixer granulator were able to encapsulate 24 times the powder weight [6]. This was not attempted in this study due to the volume

restriction of used granulator. Forny *et al.* [6] reported that the formation of liquid marble becomes less sensitive to mixing conditions as the hydrophobicity of the Aerosil powder increases, and that liquid marbles can be produced using any impeller design at the correct speed. We were able to encapsulate fluid 15 times of powder weight without producing a bulk mousse. We note that the mixing conditions and rotational speeds used in this study were different from previous study [6]. This demonstrates that liquid marbles can be formed in any equipment using highly hydrophobic Aerosil as long as the mixing condition remains in roping regime [13]. The roping regime ensures good mixing from top to bottom of the powder in the granulator. If powder mixing is poor, the binder will accumulate in bottom of granulator and fewer liquid marbles will form. Poor mixing can occur if the powder flow is in the bumping flow regime [13] or if the powder circles the exterior wall of the granulator due to low mass and high centrifugal forces (e.g. high Froude number). We found that centrifugal flow is easy to induce when using a low-density, highly aerated powder like Aerosil.

Forny *et al.* [6] reported that changing the liquid to solid ratio does not affect on the shape or size distribution of the formed granules. In contrast, our study showed that the shape and the size distribution of granules were influenced by L:S ratio. The discrepancy between our observations and previous work may be related to liquid addition method, as we atomized the liquid into the high-shear mixer but in previous work the bulk of water was added into mixer. By spraying liquid, the granulation process starts with a preformed droplet, but by adding bulk of liquid then mixing, the process of nucleation starts in mechanical dispersion regime [14]. These two methods of adding liquid indicates two

different nucleation mechanisms for forming the drop templates for the liquid marble. These different methods in turn cause changes in the granule shape and particle size distribution in response to changes in the operating variables.

In the melt granulation method for producing hollow granules, Ansari and Stepanek [10] reported that the un-granulated fine particle fraction dropped as L:S ratio increased, but the granule size was only affected slightly. We also found that the proportion of un-granulated particles decreases as the L:S ratio increases, in contrast to Forny *et al.* [6] who used an almost identical formulation. This may imply that nucleation of liquid marbles from a preformed droplet template determines how the granulation process will proceed, regardless whether solid spreading nucleation [3] or melt granulation [10] is being used.

Although, the mechanism of hollow granule formation in our study and Ansari's study [10] was different, the "solid spreading" nucleation stage of both processes starts with a preformed droplet template. Both studies found that the granule morphology was affected by the L:S ratio. This was not seen in Forny's study [6] even though also had a "solid spreading" nucleation process.

The SEM and XRT data showed that as the hollow granule size increases, they tend to become buckled, which has also been reported previously [2, 7-9]. As reported in our previous study [8] using a similar formulation, 80% of Aerosil (R974) and 5% HPC granules buckled at 60 ºC drying temperature and only 20% of granules had perfect

hemispherical shape. In this study, we also see the same buckled and spherical shaped hollow granules, but had expected to see more spherical granules due to the smaller droplet size of the binder (less than 500 μm). The previous work used much larger, 3 mm diameter single droplets and liquid marble quality was improved as droplet size decreased [8]. Also, the Aerosil R202 used in this study had higher surface area compared to Aerosil R974 [6] which may produce a more uniform shell and more robust liquid marbles during drying [9]. The probability of buckling during drying appears to increase as more liquid marbles attach to each other due to longer residence times in the mixer, or perhaps during sample handling while wet. These larger granules will experience more compressive stresses during drying [9]. This may be because the irregular shape and higher mass of the large granules creates stresses that break the wet bridges between particles during drying. Symmetric spherical granules are inherently more mechanically robust because the spherical shape is a somewhat self-supporting. Irregularly shaped granules would require much more concentrated binders to support the same mass of powder.

The intention of this study was to determine the optimum conditions for producing perfect spherical hollow granules but as can be seen from Fig. 3 most of the granules are buckled with many depressions and twists on the exterior surface. The appearance of a buckled surface was also seen in small scale experiments during drying of liquid marbles [7-9]. For PVP and HPMC solutions, success rate of hollow granule formation was proportional to the binder fluid viscosity [8]. However, for HPC solutions, the average survival rate remained relatively constant regardless of the HPC concentration/viscosity

[8]. This may imply that the shear experienced by granules during the longer residence time in the granulator is important in determining the extent of granule buckling and deformation in granulator. Specifically, higher liquid ratios and longer spray times mean that the total shear experienced by the granules is also higher. Consequently, the proportion of deformed or buckled hollow granules as well as filament and foam-like granule increases. These large scale experiments had less success in producing high quality hollow granules compared to small scale experiments [8] even though we used a higher surface area Aerosil and smaller droplet size. Both of these were expected to produce more robust spherical hollow granules. Choosing the optimal L:S ratio is very important in terms of maximizing the chance of survival of spherical hollow granules and minimizing the portion of un-granulated fine material. In addition, shorter residence times may be better for producing spherical hollow granules, although further experiments with different types of powders are required to test this. In all cases, the existence (or not) of hollow granules should be confirmed with XRT.

7.5. Conclusion

The effect of liquid to solid mass ratio on hollow granule formation in high-shear mixer granulator has been studied. The final granule size was found to be increasing as the liquid to solid mass ratio increased. As the liquid to solid ratio increased, the amount of un-granulated fine particles decreased but the proportion of flattened and stretched filament granules increased which indicates the importance of choosing an optimal liquid to solid ratio. The optimal L:S ratio for Aerosil R202 in this study was found to be between 3:1 and 6:1. In this L:S range, more of the raw fine particles were granulated and

fewer flattened hollow granules were produced. The final granule shape and size distribution were dependent on liquid to solid ratio when the liquid marble nucleation process began with a preformed droplet template from an atomized spray. When there is no droplet template at the start of process (e.g. mechanical dispersion of a large bulk of fluid, [6]), the final shape and size of granules is independent of liquid to solid ratio and formation of liquid marbles occurs in a mechanical dispersion regime.

Acknowledgements

This project is financially supported by Australian Research Council under Discovery Projects DP0770462. Scholarship support for N. Eshtiaghi was provided by Monash Graduate Research School.

References

[1] M. D.Tousey, The granulation process 101, basic technologies for tablet making, Pharmaceutical Technology Journal, Tableting & Granulation Yearbook (2002) 8.

[2] K. P. Hapgood, B. Khanmohammadi, Granulation of hydrophobic powders, Powder Technology 188 (2009) 248-254.

[3] K. P. Hapgood, L. Farber, JN. Michaels, Agglomeration of hydrophobic powders via solid spreading nucleation, Powder Technology 188 (2009) 248-254.

[4] P. Aussillous, D. Quere, Liquid marbles, Nature 411 (2001) 924-927.

[5] P. Aussillous, D. Quere, Properties of liquid marbles, Proceedings of Mathematical, physical, and engineering sciences 462 (2006) 973-999.

[6] L. Forny, K. Saleh, I. Pezron, P. Guigon, L. Komunjer, Influence of mixing characteristics for water encapsulation by self-assembling hydrophobic silica nanoparticles Powder Technology, special issue on granulation 189 (2009) 263-269.

[7] P.McEleney, G. M.Walker, I. A.Larmour, S. E. J. Bell, Liquid marble formation using hydrophobic powders., Chemical Engineering Journal 147 (2009) 373-382.

[8] N.Eshtiaghi, S. Liu, K. P.Hapgood,, Formation of Hollow Granules from Liquid Marbles: Small scale experiments, (2009), Powder Technology, Accepted, DOI:

[9] P. S. Bhosale, M. V. Panchgnula, H. A. Stretz, Mechanically robust nanoparticle stabilized transparent liquid marbles, Applied Physics Letters 93 (2008) 034109/1-034109/3.

[10] M. A. Ansari, F.Stepanek, Formation of hollow core granules by fluid bed in-situ melt granulation: Modelling and experiments, International Journal of Pharmaceutics 321 (2006) 108-118.

[11] L.Forny, I. Pezron, Kh. Saleh. Dry water: From physico-chemical aspects to process related parameters, 9th International symposium on agglomeration and 4th international granulation workshop, Sheffield, UK (2009).

[12] D.E.Walton, C.J. Mumford, The morphology of spray-dried particles: the effect of process variables upon the morphology of spray-dried particles, Transactions of the

Institution of Chemical Engineers. Part A, Chemical Engineering Research & Design **77** (1999**)** 442-460.

[13] J.D. Litster, K.P. Hapgood, J.N. Michaels, A. Sims, M. Roberts and S.K. Kameneni, Scale-up of mixer granulators for effective liquid distribution, Powder Technology 124 (2002) 272–280.

[14] Hapgood, K. P., S. M. Iveson, *et al.* (2008). Granule Rate Processes, in: Granulation, Handbook of Powder Technology. A. Salman, M. Hounslow and J. P. K. Seville (eds). Elsevier Science, London, 2007, P. 11.

8

Framework for formation of liquid marbles and hollow granules

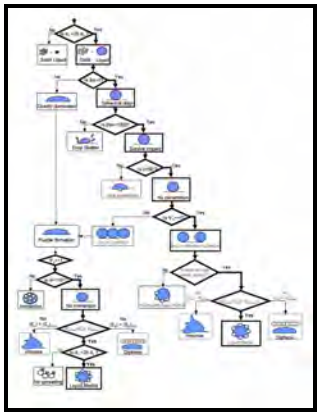

Framework for liquid marble formation

Chapter 8: Framework for formation of liquid marbles and hollow granules

Based on the initial literature review and preliminary experiments, a framework for liquid marble formation was proposed in Chapter 3 (see Figure 12 in Chapter 3 or Figure 8.1 below) for the formation of a stable, spherical, liquid marble from a single drop via solid spreading nucleation. The aim of this chapter is to validate the proposed framework for liquid marble formation and extend it to cover the additional required steps for the formation of hollow granules, based on the experimental work explained in Chapters 4 to 7.

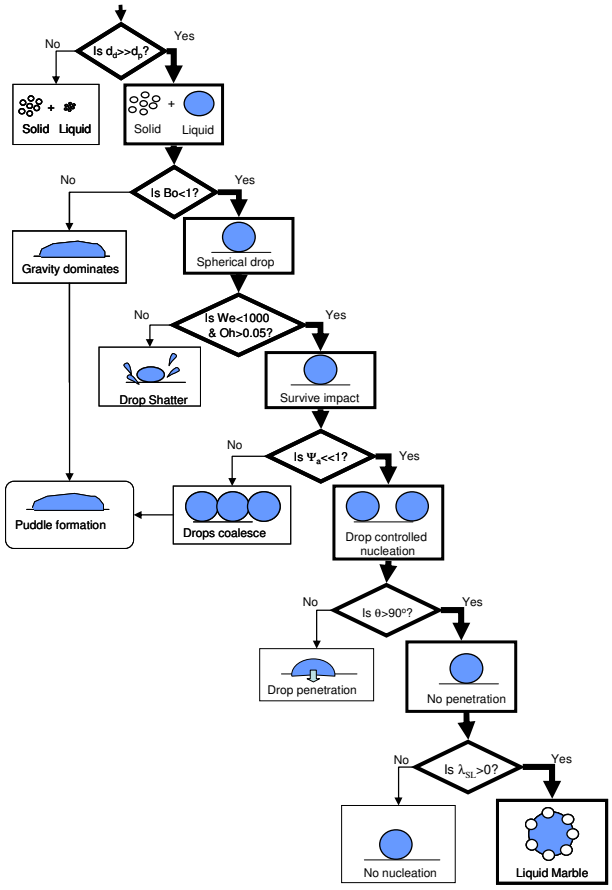

Figure 8.1: Schematic flow sheet summarizing the steps and dimensionless groups controlling the formation of liquid marbles during granulation (Figure 12 in Chapter 3)

8.1 Droplet and particle size

As explained in the discussion of Chapter 3, each drop must be much larger than the size of the primary powder particles (i.e. $d_d >> d_p$) in order for the particle to spread around the droplet template. The question is: to what extent must the droplet size be larger than the particle size? Experimental data and literature data were reviewed to find the quantitative correlation between droplet size and particle size. Table 8.1 summarizes the actual droplet and particle sizes that were used in Chapter 3, 4, and 7 as well as literature studies of liquid marble formation. Table 8.1 shows that for a wide range of powder and liquid combinations, a liquid marble forms if the droplet diameter is at least 25 times of the particle diameter. Therefore, the first step of the proposed flow chart was modified to include the precise ratio of droplet diameter to particle diameter, $d_d > 25\ d_p$, as presented in Figure 8.2.

Figure 8.2 also shows all the other modifications to the framework which will be discussed in this chapter. Note that Figure 8.2 applies only to droplet-template controlled liquid marble formation. Formation in the mechanical dispersion regime will be discussed later.

Note that the particle size presented in Table 8.1 is the reported primary particle size. In practice, several of these powders were aggregated. For example, the reported manufactured particle size for Aerosil used in this study is 16 nm, but this powder is tend to self-agglomerate to form large and loose networks with a much larger particle size between 1 to 30 μm (Chapter 7). Dandan and Erbil (2009) also reported graphite had a

primary particle size of 2 to 30 μm but 60% of the graphite was aggregated in clusters between 10 and 20 μm. PTFE 1, PTFE 12, and PTFE 35 with reported particle size of 1, 12 and 35 μm, respectively, were also noted to agglomerate but the agglomerate particle size was not measured.

Table 8.1: Droplet and particle size value for liquid marble formation

Powder	Fluid	Particle diameter (d_p, μm)	Droplet diameter (d_d, μm)	Droplet diameter /Particle diameter (d_d/d_p)	Liquid marble?
Small scale experiment					
Aerosil PTFE 1 PTFE 12 PTFE 35 PTFE 100 Hydrophobic glass bead (AG/AH)	Water or Glycerol	1-30 1 12 35 100 65	3400	113-3400 3400 283 97 34 52	Yes
PTFE 1 PTFE 12 PTFE 35 PTFE 100	PEG 200	1 12 35 100	2580	2580 215 74 26	Yes
Hydrophobic glass bead (AH)	PEG 200	65	2580	40	Yes
Hydrophobic glass bead (AE)	PEG 200	121	2580	21	No
Hydrophobic glass bead (AC)	PEG 200	191	2580	14	No
Large scale experiment					
Aerosil	5%HPC	0.02	442	22000	Yes
Literature data					
PTFE (Bhosale *et al.* 2008)	Water or Glycerol	7-12	1200	100-170	Yes
Aerosil (Bhosale *et al.* 2008)	Water or Glycerol	0.2-0.5	1200	2400-6000	Yes
Lycopodium (Aussillous and Quere, 2001)	Water	20	2000	100	Yes
Graphite micro powder (Dandan and Erbil, 2009)	Water	2-30	2000, 4000	67-2000	Yes
Aerosil (Bink and Murakami, 2006)	Water	0.02-0.03	50- 400	2500-20000	Yes
PTFE (Gao and McCarthy, 2007)	Water & Ionic liquid	35	1280	37	Yes
OTFE (Gao and McCarthy, 2007)	Water & Ionic liquid	35	1280	37	Yes
Hydrophobic copper powder (McEleney *et al.*, 2009)	Water	9 15	2000	220 130	Yes
		320	2000	6	No*
Poly-methylmethacralate (PMMA; McEleney *et al.*, 2009)	Water	42	2000	48	Yes
Aerosil (Forny *et al.*, 2009b)	Water	0.016	80	5000	Yes

* Maximum coverage of liquid marble was 60-70%.

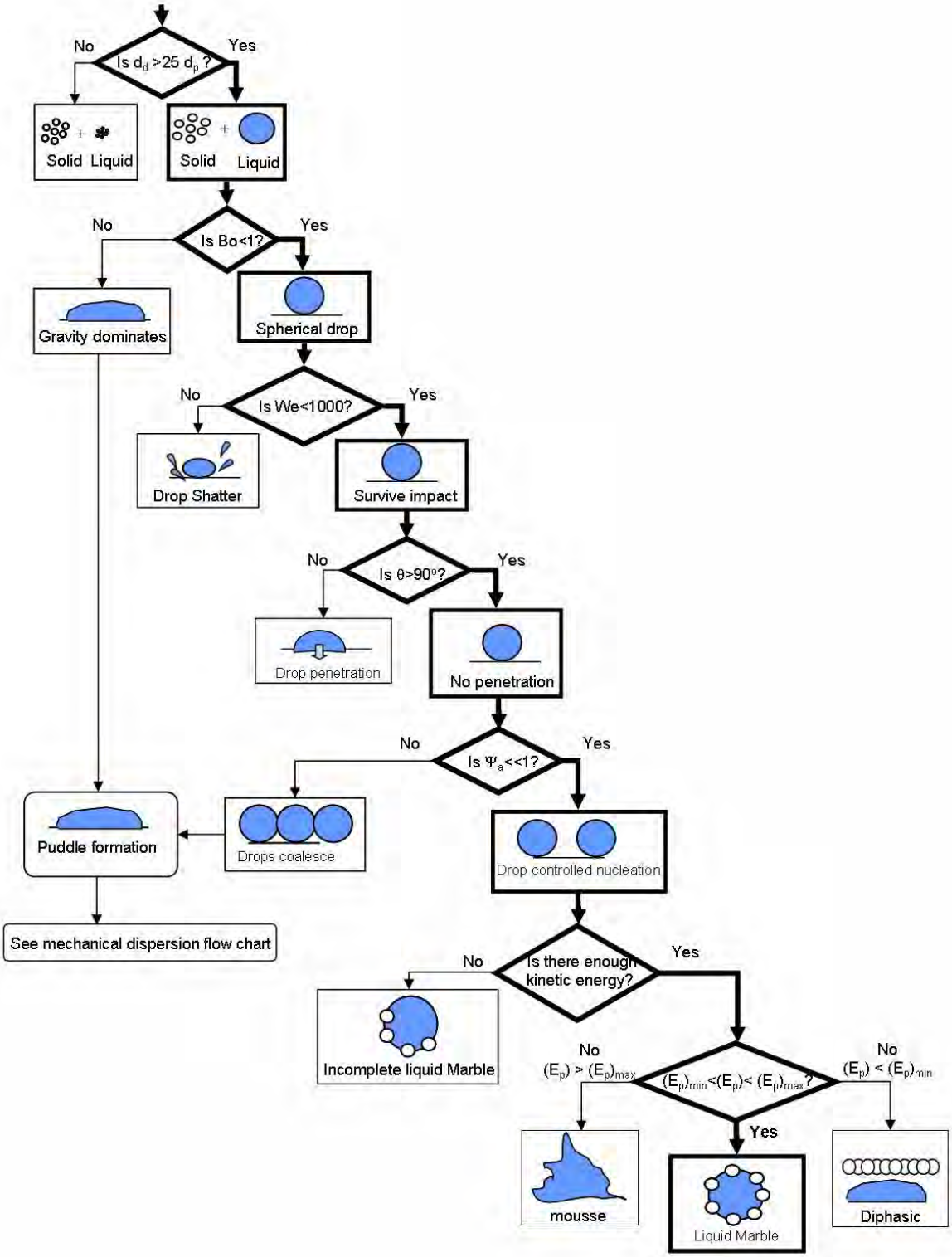

Figure 8.2: Modified schematic flow sheet for formation of liquid marble through droplet template regime

8.2 Dimensionless groups for drop impact

In addition to the requirement that the droplet size be at least 25 times the particle size, the droplet size must also be small enough to form a spherical drop on powder bed rather than a distorted pool or puddle. For this reason, the next step of liquid marble formation flow chart is Bond number (Eq. 8.1).

$$Bo = \frac{\rho g R^2}{\gamma} \tag{8.1}$$

If the Bond number is above one, the droplet forms a puddle shape on a powder bed surface after impinging (Aussillous and Quere, 2006). Figure 8.3 shows puddle shape of PEG200 droplet on hydrophobic glass bead for a Bond number equal to 1.14. If the Bond number is below one, the droplet forms a spherical shape on powder bed (Figure 8.4).

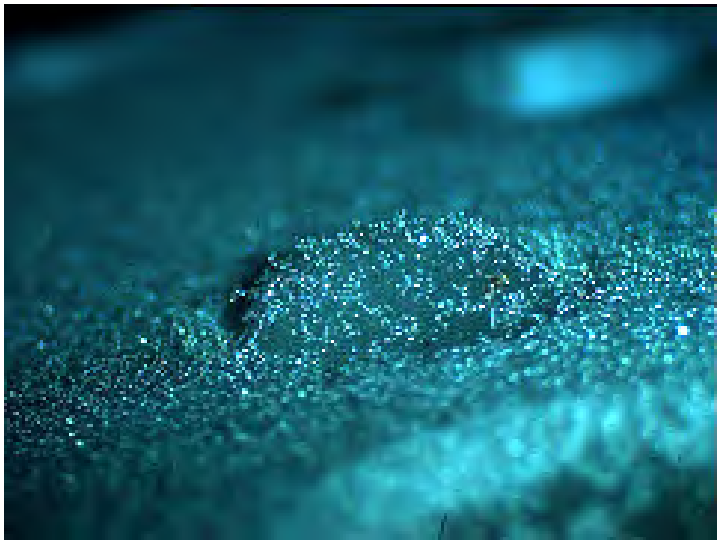

Figure 8.3 : Puddle form of 4 mm PEG200 droplet on hydrophobic glass beads (AG), Bo=1.14

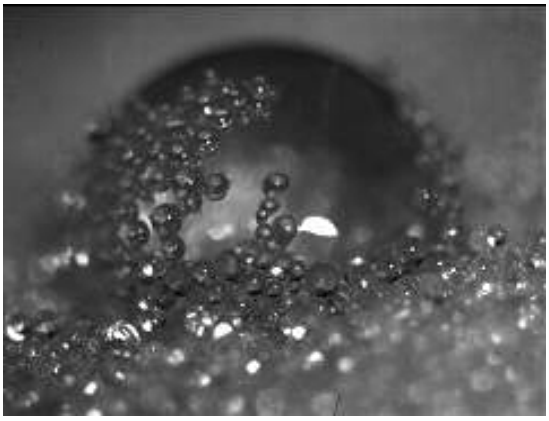

Figure 8.4: Spherical cap of 3 mm water droplet onto hydrophobic glass bead (AG) (15 cm release height, Bo=0.3, We= 300, *Oh*= 0.08)

Droplet impact phenomena were reviewed in section 2.6. Ideally, the drop should land on the powder and survive the impact without breaking or shattering into smaller droplets. Section 2.6 in Chapter 2 found that the critical criteria were We<1000 and $Oh \geq 0.05$ (Hapgood and Khanmohammadi, 2009; Agland and Iveson, 1999; Bartolo *et al.*, 2005). Table 8.2 presents the calculated value of We (Eq. 8.2), *Oh* (Eq. 8.3) and Bond number for the experiments conducted in Chapter 4 and shows whether the drop landed intact or shattered. Generally, the table supports the We<1000 criteria.

$$We = \frac{\rho_L d_d v^2}{\gamma_{LV}} \tag{8.2}$$

$$Oh = \frac{\mu}{(\rho_L \gamma_{LV} R)^{0.5}} \tag{8.3}$$

Table 8.2: Calculated value of We, *Oh* and Bond number

Fluid	Powder	Height (cm)	Fluid diameter (mm)	We #	*Oh* #	Bond #	Shattered?
Water	Hydrophobic glass bead (AG)	15	3	~300	0.08	0.3	No
Water	Hydrophobic glass bead (AG)	80	3	~3000	0.08	0.3	Yes
Water & dye	PTFE 1, 12, 35	2.5	3.4	28	0.003	0.48	No
		5		56			
		7.5		85			
		10		113			
		12.5		141			
Water & dye	PTFE 100	2	3.4	15	0.002	0.48	No
		4		31			
		6		46			
		8		61			
		10		76			
		92		1050			Yes
	Hydrophobic glass bead (AH)	92	3.4	1050	0.002	0.48	Yes
20% Glycerol & dye	PTFE 100	5	3.4	53	0.003	0.5	No
		7.5		80			
		10		106			
		12.5		133			
		15		159			
40% Glycerol & dye	PTFE 100	5	3.4	56	0.005	0.54	No
		7.5		84			
		10		112			
		12.5		140			
		15		169			
60% Glycerol & dye	PTFE 100	5	3.4	51	0.009	0.58	No
		7.5		76			
		10		101			
		12.5		127			
		15		152			
80% Glycerol & dye	PTFE 100	5	3.4	68	0.02	0.6	No
		10		137			
		15		205			
		20		273			
		25		342			
		30		411			
	Hydrophobic glass bead (AH)	75		1094			Yes
100% Glycerol & dye	PTFE 100	5	3.4	175	1.08	0.88	No
		10		35			
		15		525			
		20		701			
		25		876			

Figure 8.5 and 8.6 show some examples of the survived droplets after impact which was mentioned in Table 8.2. Figure 8.7 shows the shattered droplet of 80% glycerol and water droplet on glass beads.

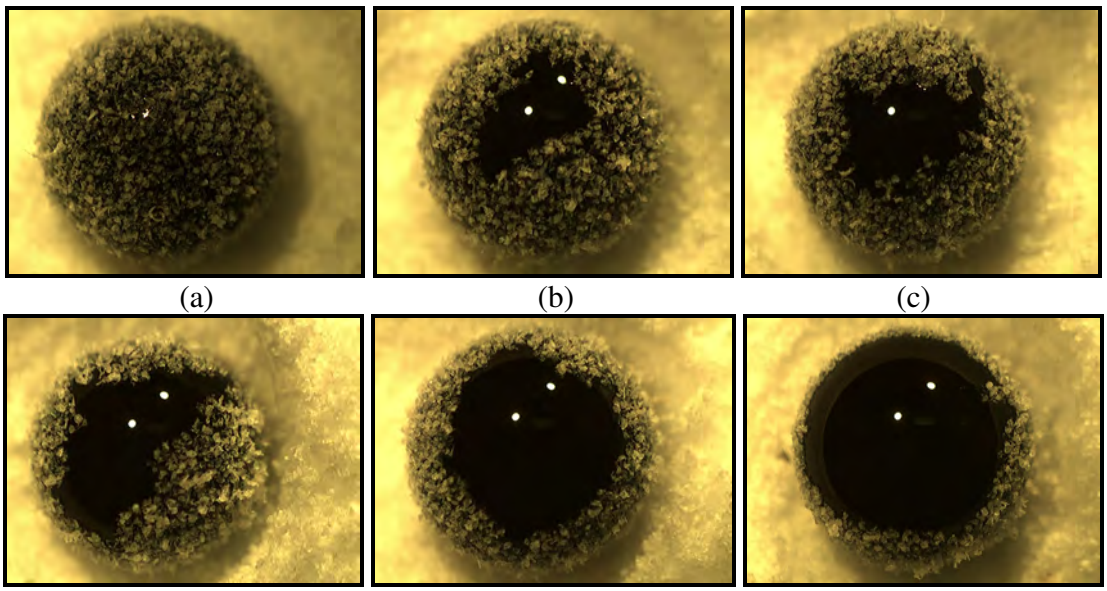

(a) (b) (c)

(d) (e) (f)

Figure 8.5: Survived and spherical 3.4 mm (a) water (Bo=0.48, We= 76, *Oh*= 0.002) (b) 20% glycerol (Bo=0.5, We= 106, *Oh*= 0.003) (c) 40% glycerol (Bo=0.54, We= 112, *Oh*= 0.005) (d) 60% glycerol (Bo=0.58, We= 101, *Oh*= 0.009) (e) 80% glycerol (Bo=0.6, We= 137, *Oh*= 0.02) (f) 100% glycerol (Bo=0.88, We= 35, *Oh*= 1.08) droplet released from 10 cm height on PTFE 100 powder bed

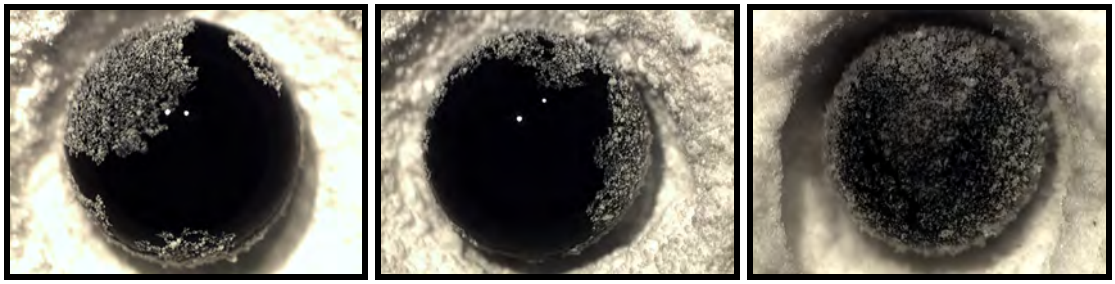

(a) (b) (c)

Figure 8.6: Survived and spherical 3.4 mm water droplet released from 10 cm height on (a) PTFE 1 (b) PTFE 12 (c) PTFE 35, Bo=0.48, We= 113, *Oh*= 0.003

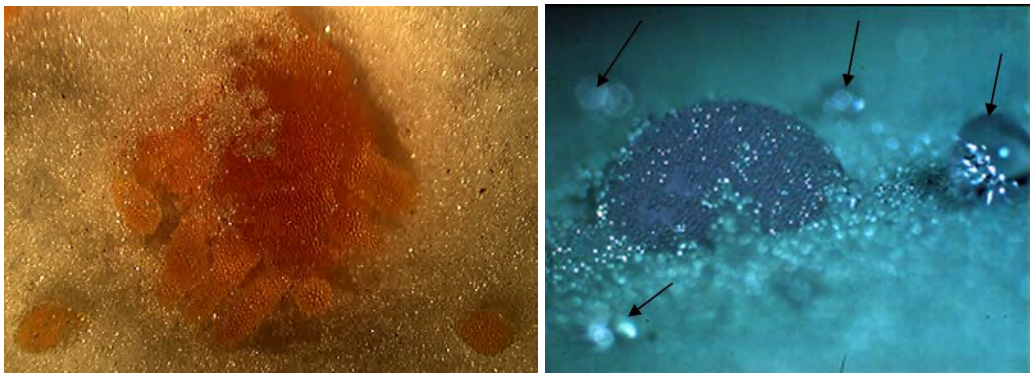

(a) (b)

Figure 8.7: Shattered (a) 3.4 mm 80% glycerol droplet released from 75 cm (Bo=0.6, We= 1094, *Oh*= 0.02) and (b) 3 mm water droplet released from 80 cm release height (Bo=0.3, We= 3000, *Oh*= 0.08) onto hydrophobic glass bead (AG). Arrows indicate the produced drops from shattering the original droplet

Line 2 in Table 8.2 shows one example of 3 mm water droplet released from 80 cm onto hydrophobic glass beads. In this case, *Oh* is greater than 0.05, but shattering still occurred (See Figure 8.7b) because the Weber number was We=3000, much greater than criteria for landing droplet on powder bed without shattering (We<1000).

There are also several examples in Table 8.2 where *Oh* was below 0.05, but the droplet did not break up because the Weber number was below 1000. For example, 3.4 mm 20% glycerol released on PTFE100 from 15 cm (We=159 and *Oh*=0.003). Table 8.2 also contains data with We>1000 and *Oh* >0.05 but where the droplet shattered (e.g. Shattered 3 mm water droplet on glass beads (AG) surface with We=3000 and *Oh*=0.08). Data in Table 8.2 was summarized as a plot in Figure 8.8 which plots *Oh* versus We and indicates where shattering occurred. These results shown in Figure 8.8 show that the We number is critical in determining whether a drop will shatter after impact. In contrast, *Oh* does not predict shattering. Thus, the *Oh* number was deleted from the new framework (Figure

8.2). The revised framework recommends We<1000 which is in agreement with the earlier conclusions by Agland and Iveson (1999).

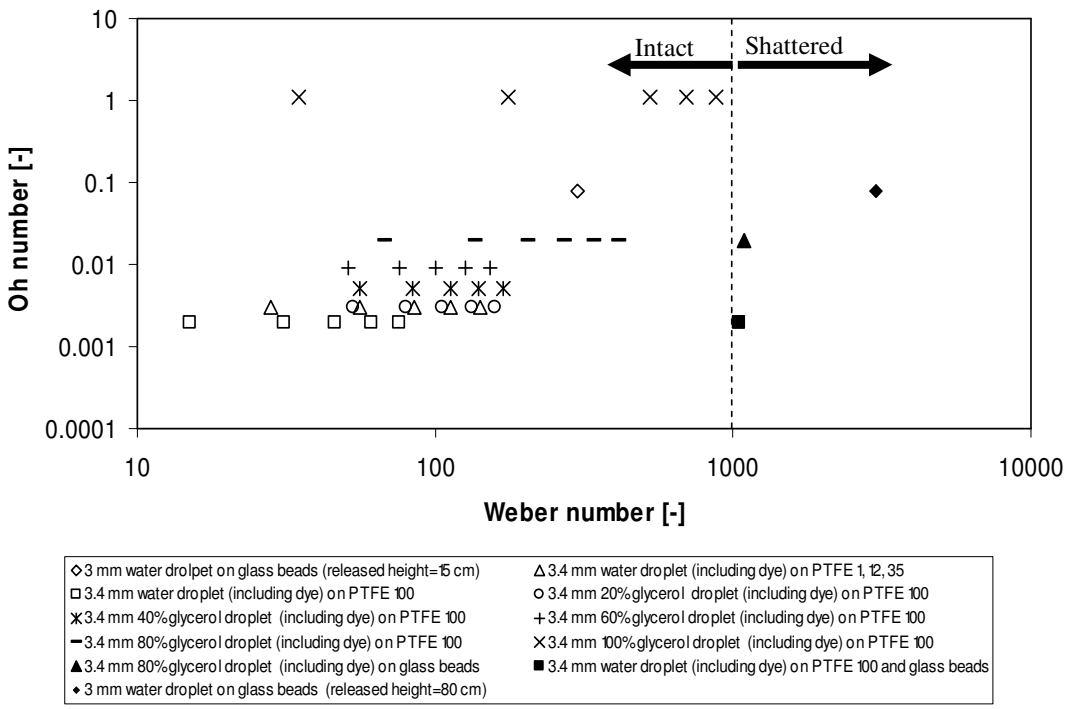

Figure 8.8: Shattered and intact liquid droplet as a function of We and Oh

8.3 Contact angle

The fluid must have a contact angle θ greater than 90° with the powder to prevent penetration of the drop into the powder bed. Table 8.3 presents the contact angle value of various powders based on the values reported in the literature. Direct data for Aerosil R202 is not available. However, Forny *et al.* (2009b) reported the following ranking for different grades of fumed silica in increasing order of hydrophobicity:

R711 < R972 < R812S < R202

The contact angle for R812S is 113º (Forny *et al.* 2009a). In this study, Aerosil R202 was used, which is the most hydrophobic powder and is assumed to have a contact angle above 113º. Table 8.3 shows that all reviewed studies of liquid marble formation have used a powder and liquid with a contact angle above 90º.

Table 8.3: Contact angle value for different powder with water

Powder	Contact angle	Reference
PTFE	140	Zismman (1963)
OTFE	177	Gao and McCarthy (2007)
Aerosil R972	103	Forny et al. (2009a)
Aerosil R812S	113	Forny et al. (2009a)
Aerosil R202	> 113	Forny et al. (2009a)
Hydrophobic copper powder	157	McEleney et al. (2009)
Poly-methylmethacralate (PMMA)	120	McEleney et al. (2009)
Lycopodium powder	>150	Aussillous and Quere (2001)
Graphite micro powder	145-160	Dandan and Erbil (2009)

8.4 Spray flux

In order to maintain small individual drop templates, the dimensionless spray flux must be low (Litster *et al.*, 2001). Under low spray flux conditions (Ψ_a<0.1) the granule size would be controlled by the atomized drop size, i.e. the drop controlled nucleation regime (Hapgood *et al.*, 2003). The originally proposed framework required Ψ_a<0.1 and assumed that nucleation of liquid marbles occurred only in the drop controlled regime (see Figure 8.1). However, the work in Chapter 7 and Forny *et al.* (2009b) have shown that the production of liquid marbles via mechanical dispersion (Ψ_a>1) is also possible. In this study, the calculated value of dimensionless spray flux for the system examined in Chapter 7 was in fact greater than one (Ψ_a=1.4). Although the spray flux was above 1, no obvious puddle formation or adverse affect on liquid marble formation phenomena was

observed. However, deformed and stretched hollow granules were formed around the mean droplet size instead of individual spherical hollow granules. This may imply that there is possibility of forming liquid marbles via mechanical dispersion of the fluid, although single cavity hollow spheres are still are expected to be promoted by low spray flux conditions. This needs to be demonstrated by further research.

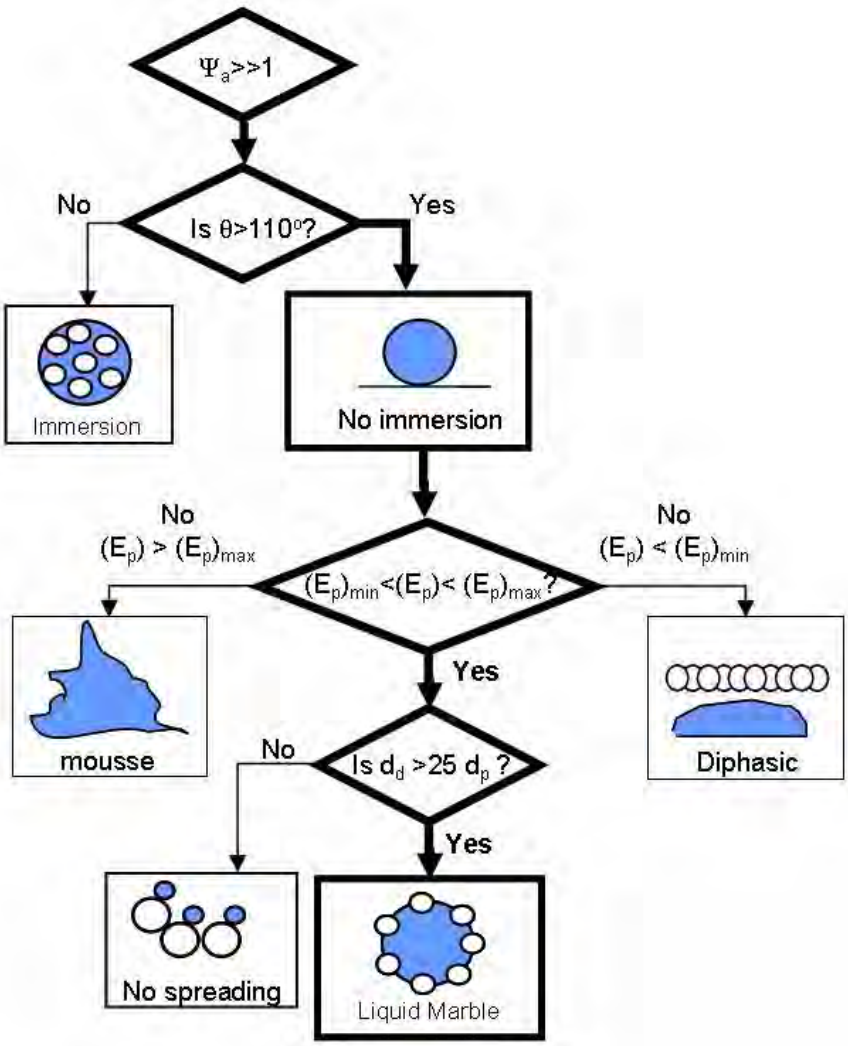

Figure 8.9: Schematic flow sheet for formation of liquid marble through mechanical dispersion regime

In the mechanical dispersion regime, Ψ_a>1 (see Figure 8.9), the fluid must have a contact angle θ greater than 110° (Forny *et al.*, 2009a) because highly energetic conditions during mechanical dispersion can generate strong hydrodynamic liquid flow that could lead to immersion of moderately hydrophobic particles into the liquid phase (Forny *et al.*, 2009a). In the system studied in Chapter 7 with spray flux above 1, the liquid marble formation process was successful and no immersion was observed because Aerosil R202 had a contact angle greater than 113º.

Forny *et al.*, (2009a) also reported that there is a threshold energy per unit mass, above which a phase inversion to form a "mousse" can occur. For this reason, Forny *et al.* (2007) reported that atomization was required to form liquid marbles in the "lower shear" Triaxe mixer for moderately hydrophobic particles. Although the Triaxe mixer is classified as a "low" energetic mixer, when the rotational speed of the Triaxe was set to high (> 100 min^{-1}) in order to disperse the bulk of the liquid, a white mousse was formed (Forny *et al.,* 2007). Although in this study no bulk phase inversion was observed for the process investigated in Chapter 7, patches of foam-like structure were observed. These could be either related to localized areas of phase inversion to form a mousse or due to coalescence of liquid marbles.

Forny *et al.*, (2009a) also reported that if the energetic contribution of mixer (E_p) is less than minimum threshold energy, the hydrophobic particles and the fluid will form separate phases. Forny *et al.* (2007) reported separate phase formation for high

hydrophobic Aerosil R812S in lower shear Triaxe mixer, as energy produced by this mixer was lower than minimum threshold requirement for liquid marble formation.

Figure 8.9 summarizes the steps required for formation of liquid marbles in the mechanical dispersion regime. The contact angle needs to be above 110º and E_p must be within upper and lower threshold energy limits. The final step is that under high shear conditions and turbulent liquid flow, the bulk liquid is divided in stable droplets. Once again, the droplet size must be 25 times larger than particle size; otherwise, no spreading of particles around the droplet can occur.

8.5 Role of kinetic energy in liquid marble formation

Originally, the final step of the proposed framework for liquid marble formation (Figure 8.1) was provisionally shown as needing a positive value of the solid-over-liquid spreading coefficient λ_{SL} (see Chapter 3). The hypothesis of whether the solid-liquid spreading coefficient λ_{SL} predicts liquid marble formation was tested in Chapter 4 by calculating the solid-liquid spreading coefficient λ_{SL} and comparing with the experimental results. The calculated solid-liquid and liquid-solid spreading coefficients for several liquid marble formulations demonstrated that the spreading coefficient theory is inconsistent with experimental observations of liquid marble formation. Chapter 4 also investigated the effect of the kinetic energy of the droplet impact on the degree of liquid marble powder coverage. An exponential relationship was found between increasing kinetic energy and the percentage of liquid marble coverage. The kinetic energy from impact causes an increase in drop surface area due to the drop deformation. The

subsequent drop recoil creates fluid flow which entrains the powder and forms the powder shell (see references [11] and [12] in Chapter 4). Increasing the drop release height (and therefore increasing the kinetic energy of impact) increases the liquid marble powder coverage. The maximum extent of liquid marble coverage also decreases as the fluid viscosity increases and/ or surface tension decreases.

McEleney *et al.* (2009) also reported that the attainable surface coverage decreases with increasing particle size. They reported that by shaking and rolling of water droplet on 320 μm hydrophobic copper powder, the maximum attainable powder–water surface coverage was between 60 to 70%. This implies that shaking or rolling of water droplet did not produce enough kinetic energy in order for large particles entrain on liquid surface. For this situation, more vigorous agitation such as mixing in a granulator would be required for complete surface coverage.

Based on the experimental data and discussion presented in the Section 4.3.3 of Chapter 4, the solid-liquid spreading coefficient was removed from the original framework. The final step of formation was modified to include the effect of kinetic energy as presented in Figure 8.2. In practice during granulation in high shear mixers, it can be assumed that all droplets will receive enough kinetic energy as a result of the frequent collision with powders in the highly agitated powder motion in granulator.

Although there may be enough kinetic energy in granulator for liquid marble formation, it is also important to consider the energetic contribution of the process. Forny *et al.*

(2009a) introduced a state diagram for the quality of the final product in liquid marble formation process. The final product of a hydrophobic powder-liquid system can be liquid marbles or a mousse, or a diphasic mixture (i.e. a separate phases of liquid and solid). If energetic contribution of system per unit mass (E_p) is below the minimum threshold energy requirements $(E_p)_{min}$, there is no granulation and hydrophobic-liquid system forms a diphasic state. On the other hand, if energetic contribution of system per unit mass E_P is above the maximum requirement of $(E_p)_{max}$, a phase inversion occurs to form a mousse (Forny *et al.*, 2009a). Therefore, it is required to add another step to the liquid marble formation flow chart to meet the optimum requirement of threshold energy per unit mass. The final step is that $(E_p)_{min} < (E_p) < (E_p)_{max}$, this is shown in Figure 8.2.

Figure 8.10 summarizes the entire revised framework for liquid marble formation, including formation via drop-template controlled and via mechanical dispersion. This framework will aid future research and development into mass production of liquid marbles.

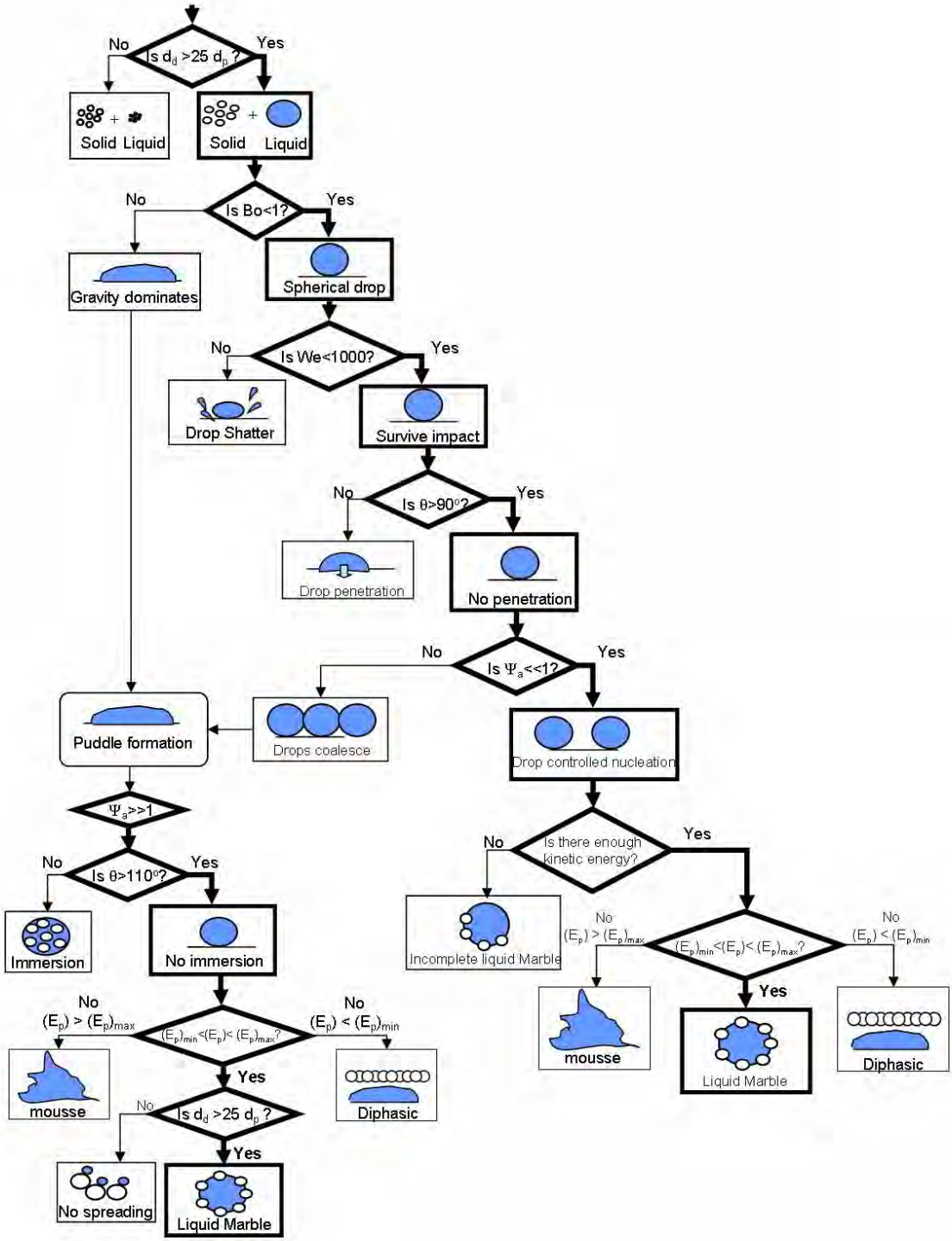

Figure 8.10: Schematic flow sheet for formation of liquid marble through droplet template and mechanical dispersion regime

8.6 Hollow granule formation

As previously mentioned in Chapter 3 in order to form a hollow granule, the powder shell must be sufficiently strong and self supporting in order to avoid collapse during the drying process and subsequent standard powder handling operations. Figure 8.11 outlines a series of steps required for hollow granule formation from a liquid marble.

As mentioned in Chapter 6, a polymeric binder is required to avoid the liquid marble collapsing after drying, as the binder forms solid bridges between the particles during drying which give strength to the powder shell. The work by Walton and Mumford (1999) also demonstrated that polymeric materials tended to form a porous skin that can help the formation of hollow granule during drying period without any rupture. Experimental results showed that all of the hollow granules formed without polymeric binder in the formulation collapsed, as expected. Thus, the first step in hollow granule formation is the existence of a polymeric binder in formulation.

The next step in the successful formation of hollow granules is controlled by compatibility of the polymeric binder with the chemical and physical properties of the powder. For example in Chapter 6 (Section 6.3.2.), the experimental results showed the complete collapse of all hollow granules formed with PVP binder and glass beads at all the drying temperatures tested. On the other hand, HPC performed well with the glass ballotini. This may imply that some property of the glass powder – perhaps due to the higher powder weight due to the density of the glass - is incompatible with PVP binder. Walton and Mumford (1999) study also indicated that the final morphology of a spray

dried hollow sphere depends on chemical and physical nature of the skin material. Chapter 6 (Section 6.4.1), showed that HPMC was the most compatible polymeric binder with all the powders used in this work.

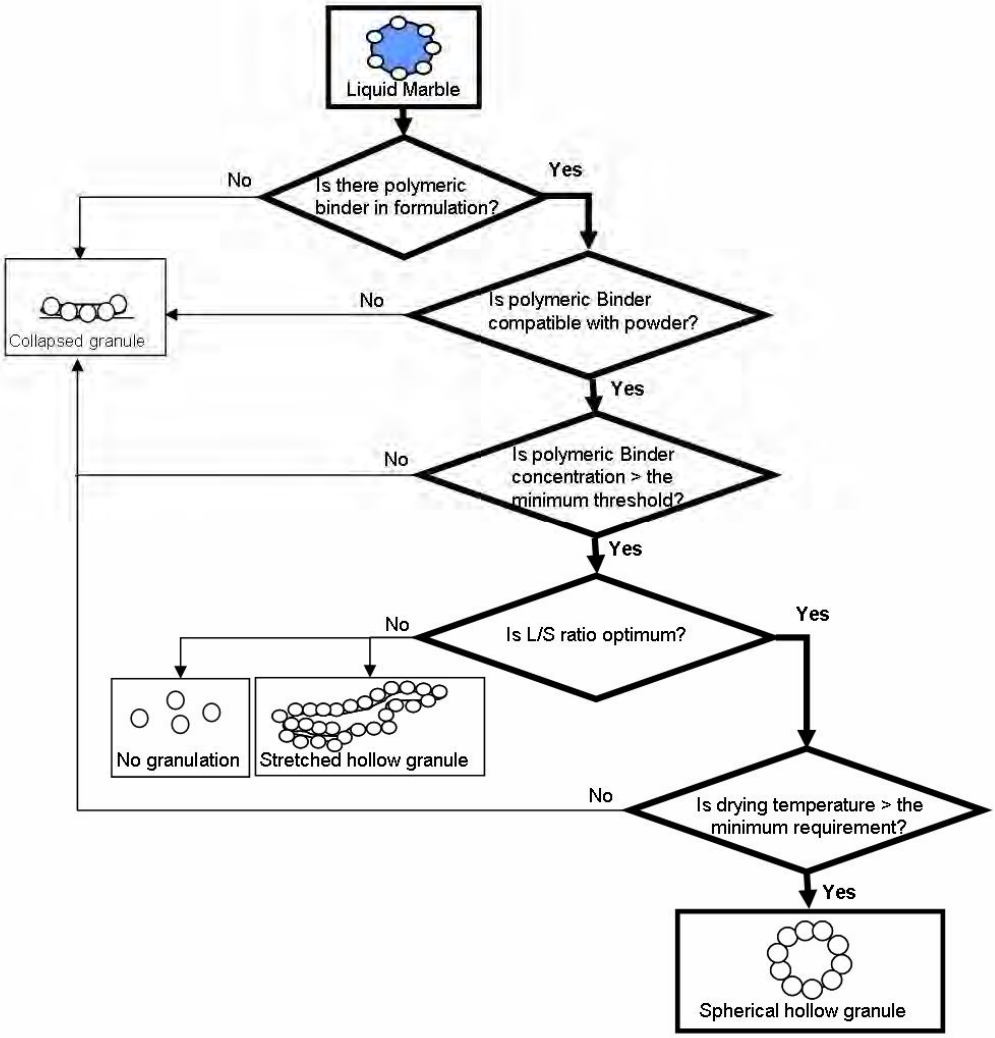

Figure 8.11: schematic flow sheet for formation of hollow granules from liquid marbles

There is also a minimum polymeric binder concentration needed in the formulation (Section 6.3.3 in Chapter 6). For example, the lowest HPC concentration of 2% was not able to properly assemble glass particles together to prevent collapsing the liquid marble during drying (Section 6.3.3). Walton and Mumford (1999) also reported that by

increasing the concentration of polymeric binder, the particle distortion and surface rupture decreased. Experimental results showed that for HPMC and PVP, there is a consistent proportional relationship between binder fluid viscosity (which is related to concentration of binder) and the proportion of hollow granules formed (see Section 6.4.1). However for HPC binder, the survival rate remained constant regardless of the HPC concentration, presumably due to precipitation of HPC above the cloud point (Winnik, 1987).

The next step in the hollow granule formation flow chart (Figure 8.11) is selecting the optimum liquid to solid ratio during granulation. To maximize the number of spherical, single cavity granules and minimize the formation of foam sheets, choosing the optimal L:S ratio is important. At optimum L:S ratio, more of the raw fine particles will be granulated and fewer flattened hollow granules be produced (Section 7.3 in Chapter 7). The optimal liquid to solid ratio of granulation processes cannot be predicted in advance and must be determined by trial and error. However, the L:S ratio will be far higher than conventional granulation, and generally will lie between approximately 1:1 to 6:1 (see Table 8.4). Conventional granulation typically uses liquid to solid ratios around 0.3 to 0.5:1.

Table 8.4: Optimum L:S ratio in different studies of hollow granule formations

Investigated range of L:S ratio	Optimum L:S	Reference
0.7-0.78:1	0.74:1	Hapgood *et al.* (2009)
0.5-15:1	3:1 - 6:1	This study
33:1	Not reported	Forny *et al.* (2009b)

The liquid to solid ratio data from small scale single drop studies has been omitted, as this data can be difficult to measure and it has not been shown to extrapolate to full scale. We do not know whether the powder shell structure and thickness is the same or different for liquid marbles formed from a single drop, compared to liquid marbles formed in bulk via a spray.

The final criteria established for formation of hollow granules is the drying temperature. The drying temperature is as important as the polymeric binder concentration. As an example, glass bead hollow granules survived if the drying temperature was above 80 ºC while Aerosil granules survived as long as the drying temperature was above 60 ºC (Section 6.3 in Chapter 6). This implies that there is a different minimum temperature requirement for various powders in order to form a hollow granule. In general, increasing temperature increases the survivability and improves the quality of hollow granules except for HPC binder if the drying temperature exceeds the cloud point of binder (45ºC).

8.7 Conclusion

In this chapter, the proposed flow chart for liquid marble formation via solid spreading coefficient (presented in Chapter 3) was validated based on the experimental work explained in Chapter 4 to 7 and other literature studies of liquid marble formation. A revised flow chart for formation of liquid marble through droplet template regime was presented. In this revised framework, the first step was replaced with a precise ratio of droplet diameter to particle diameter. In addition, the requirement for a positive value of the solid-over-liquid spreading coefficient λ_{SL} and $Oh > 0.05$ was also deleted from

preliminary framework. Instead, criteria for the kinetic energy of the impact and the optimum threshold energy per unit mass were added.

This work and Forny *et al.* (2009b) work revealed the possibility of the formation of liquid marble via mechanical dispersion regime. A new flow sheet for formation of liquid marble via mechanical dispersion regime was developed. The main difference between droplet template regime and mechanical dispersion regime is the contact angle and spray flux requirement. When spray flux becomes greater than one, granulation switches from droplet template regime to mechanical dispersion regime. Liquid marble can form successfully in mechanical dispersion regime if the contact angle is above 110º. This is higher than the angle proposed for the drop template framework, as the particles must be more hydrophobic in the mechanical dispersion regime in order to resist immersion into the fluid, destroying the liquid marbles.

In addition, a framework for formation of hollow granules was proposed based on experimental work explained in Chapter 6 and 7. In this framework, the importance of the presence of a compatible polymeric binder with optimum concentration was emphasized. Then, in the final step of the flow chart, the consequences of not choosing optimum L:S ratio and drying temperature was presented.

These frameworks give a better understanding of the controlling mechanisms in the granulation of hydrophobic particles and provide guidance on how to mass produce liquid marbles and hollow granules. However, further work needs to be done in following areas:

- Currently, the energetic contribution of system per unit mass E_p range in the state diagram of liquid marble formation (Forny *et al.,* 2009) is unknown. Further work using powders with different degrees of hydrophobicity in the granulator should be performed to quantify the energetic contribution of granulation process for both the state diagram by Forny *et al.* (2009), and for the frameworks produced in this thesis. This might be helpful for predicting an optimum impeller speed without performing experimental work, although this is currently a challenging task in all granulation processes.
- The experimental work in Chapter 7 with Aerosil should be repeated but under drop controlled regime conditions (Ψ_a~0.1) to determine whether the foam-like structure of granules can be eliminated by more controlled spray conditions. If not, the foam granules are most likely to have formed due to the high energetic contribution of process E_p, causing a local phase inversion to form a mousse.

8.8 References

Agland, S. and S. M. Iveson (1999). "The Impact of Liquid Drops on Powder Bed Surfaces". CHEMECA, Newcastle, Australia, IEAust/IChemE/RACI.

Aussillous, P. and D. Quere (2001). "Liquid marbles". Nature **411**(6840): 924-927.

Aussillous, P. and D. Quere (2006). "Properties of liquid marbles". Proceedings. Mathematical, physical, and engineering sciences **462**(2067): 973-999.

Bartolo, D., C. Josserand, D.Bonn (2005). "Retraction dynamics of aqueous drops upon impact on non-wetting surfaces." J.Fluid Mech. **545**: 329-338.

Bhosale, P. S., M. V. Panchgnula, H. A. Stretz (2008). "Mechanically robust nanoparticle stabilized transparent liquid marbles". Applied Physics Letters **93**: 034109/1- 034109/3.

Binks, B., R. Murakami (2006). "Phase inversion of particle-stabilized materials from foams to dry water". Nature Materials Letters **5**:865-869.

Dandan, M., and H.Y. Erbil (2009). "Evaporation rate of graphite liquid marbles: comparison with water droplets". Langmuir, DOI: 10/1021/la900729d.

Forny, L., I. Pezron, Kh. Saleh (2009a). "Dry water: From physico-chemical aspects to process related parameters". 9th International symposium on agglomeration and 4th international granulation workshop, Sheffield, UK, 22-26 June.

Forny, L., K. Saleh, I. Pezron, P. Guigon, L. Komunjer (2009b). "Influence of mixing characteristics for water encapsulation by self-assembling hydrophobic silica nanoparticles". Powder Technology, special issue on granulation **189**: 263-269.

Forny, L., I. Pezron, K. Saleh, P. Guigon, L. Komunjer (2007). "Storing water in powder form by self-assembling hydrophobic silica nanoparticles." Powder Technology **171**(1): 15-24.

Gao, L., T.J. McCarthy (2007)." Ionic Liquid Marbles". Langmuir **23**:10445-10447.

Hapgood, K. P., B. Khanmohammadi (2009). "Granulation of hydrophobic powders". Powder Technology, special issue on granulation **189** : 253-262.

Hapgood, K. P., L. Farber, JN. Michaels (2009). "Agglomeration of hydrophobic powders via solid spreading nucleation". Powder Technology **188**: 248-254.

Hapgood, K. P., J. D. Litster, R.,Smith (2003). "Nucleation Regime Map for Liquid Bound Granules". AIChE **49**(2): 350-361.

Litster, J. D., K. P. Hapgood, et al. (2001) "Liquid distribution in wet granulation: dimensionless spray flux". Powder Technology **114**(1-3): 32-39.

McEleney, P.G., M. Walker, I. A.Larmour, S. E. J. Bell (2009). "Liquid marble formation using hydrophobic powders". Chemical Engineering **147**: 373-382.

Walton, D.E., and C.J. Mumford (1999). "The morphology of spray-dried particles: the effect of process variables upon the morphology of spray-dried particles". Chemical Engineering Research & Design **77**: 442-460

Winnik, F. M. (1987). "Effect of temperature on aqueous solutions of pyrene-labled (Hydroxypropyl) cellulose". Macromolecules **20**: 2745-2750.

Zisman, W. A. (1963). "Influence of constitution on adhesion". Industrial and Engineering Chemistry **55** (10): 18-38.

9

Conclusions and recommendations for future work

Chapter 9: Conclusions and recommendations for future work

This thesis investigated fundamentals and mechanisms on granulation of hydrophobic powders. This thesis proposed a unique approach to address the wetting problem of hydrophobic powders with an entirely new philosophy – solid spreading nucleation – which transformed the normally problematic hydrophobicity into a powerful tool for creating "designer pharmaceutical granules". The knowledge gained in this thesis can provide a practical insight during formulation and product development of cosmetic and pharmaceutical products based on using liquid marble as a precursor and drying to produce a hollow granule. The intention of this chapter is to summarize the major outcomes achieved in this thesis and initiate ideas for future work.

9.1 Conclusions

The key findings attained from this research included:

- For the first time, a framework for liquid marble formation via solid spreading nucleation (droplet template) and mechanical dispersion was proposed by outlining the sequential steps and possible controlling groups for each step. The first step of the framework via droplet template starts with $d_d > 25\ d_p$ then it follows with Bo<1 and We<1000 in order to produce a spherical drop without shattering on powder bed. The next step requirement is that the contact angle of the liquid on the powder must be above 90º. If spray flux is low enough ($\Psi_a << 1$) and there is enough kinetic energy, an individual spherical liquid marble will be formed, providing that the energetic contribution E_p of system is within the acceptable range. The main difference between droplet template and mechanical

dispersion frameworks are contact angle and spray flux requirement. When spray flux becomes greater than one (Ψ_a>1), granulation switches from droplet template regime to mechanical dispersion regime. Liquid marble can form successfully in mechanical dispersion regime if the contact angle is above 110 º (Chapter 8).

- A framework for hollow granule formation from liquid marbles was developed for the first time in this study. In this framework, the importance of presence of compatible polymeric binder at the optimum concentration was emphasized as the first requirement for hollow granule formation. The optimum L:S ratio and drying temperature are additional criteria for a successful formation of single cavity hollow granule (Chapter 8).

- This study is the first study on the mechanism and driving force for liquid marble formation. Significant insight gained in this thesis enhances the knowledge of how to create liquid marbles as a precursor for producing a wide range of structured powder-liquid products. Based on experimental results, a proportional relationship was found between increasing the kinetic energy and the percentage of liquid marble coverage. The kinetic energy from impact causes an increase in drop surface area and the drop deformation and recoil creates fluid flow which entrains the powder and forms the powder shell. By increasing the drop release height and therefore increasing kinetic energy, the liquid marble powder coverage increases. The maximum extent of liquid marble coverage falls as viscosity increases and surface tension decreases. As particle size increases, a higher coverage of the droplet was observed but these results were most likely

confounded by the effects of agglomeration and/ or powder bed rearrangement on impact (Chapter 4).

- For the first time a rigorous thermodynamic analysis on the existing solid–liquid spreading coefficient has been performed, pointing out the flaws in the assumptions used by Rowe (1989) for the derivation of solid-liquid spreading coefficient. By calculating the spreading coefficient, this study proved that the existing solid-liquid spreading coefficient is not a predictive method for liquid marble formation. Also, it revealed that why the solid-liquid spreading coefficient is not reliable method to predict the interaction between the liquid binder and solid particles. The original liquid-solid spreading coefficient derived by Wu (1973) describes the thermodynamic condition of liquid spreading over a solid substrate, but a simple interchanging the subscripts of the interfacial energy in spreading coefficient equation does not describe the thermodynamic conditions taken place in spreading solid over liquid. This is due to expansion and disintegration of powder aggregates over liquid surface is different to the expansion of the liquid phase on solid substrate. When powder aggregates expand over a liquid surface, a fraction of the powder surface establishes a solid/liquid interface and the other fraction remains unchanged. Moreover, a solid particle establishes a solid/liquid area larger than the liquid area it displaces, depending on the wetting property of the solid particle. The Marangoni surface tension effect was introduced as a possible driving force for spreading solid particles on a flat liquid surface (Chapter 5).

- A systematic set of experiments employing different types of binders and powders at a range of different drying temperatures was performed for the first time to find the optimum drying condition for formation of hollow granules from liquid marbles. A higher drying temperature, smaller or nano-size particles and higher binder concentration tend to promote the formation of perfect hollow granules. It was found that the survival rate was directly proportional to binder viscosity for HPMC and PVP. However for HPC binder, the survival rate was essentially constant regardless of HPC concentration due to precipitation of HPC binder above the cloud point. Different combinations of drying temperature, binder type, binder concentration, and powder type/grade could result in quite large changes in survival rate indicating the importance of careful formulation during hollow granule process development (Chapter 6).

- This study revealed the importance of performing X-ray tomography during hollow granule formulation design, and also considering phase retrieval tomography instead of phase contrast tomography for imaging a transparent material due to their poor absorption contrast (Chapter 7).

- Studying the effect of different liquid to solid ratio on the mass production of hollow granules via solid spreading nucleation in high shear granulator revealed the importance of choosing the optimum L:S ratio. At the optimum L:S ratio, more of the raw fine particles are granulated and fewer flattened and stretched hollow granules were produced as these granules are not suitable for drug delivery. Also, this study highlighted the importance of material formulation as well as the importance of starting the process with preformed droplet template in

order to control final granule size with L:S ratio. In this study, it was found that the final granule size increases as L:S ratio increases and at the same time the amount of un-granulated fine particles decreases if nucleation starts with a preformed droplet template. Despite the fact that a simple formulation for hollow granule formation was used, complex foam-like hollow structures were formed. This may imply that different formulations and processing conditions may produce different hollow granule structures, including single cavity liquid marbles or foam-like porous granules (Chapter 7).

9.2 Recommendation for future work

The focus of this thesis was on the formation of liquid marbles and hollow granules from hydrophobic powders. For the first time, the mechanism and framework for liquid marble and hollow granule formation was proposed. Further investigation is recommended in the following areas:

- The spray time used in the granulation experiments in Chapter 7 was quite long (up to 16 minutes). Further studies to produce hollow granules in the granulator with different powders is required to investigate whether a shorter spray time, which reduces the length of time that the wet liquid marbles are exposed to the forces in the granulator, is better for producing spherical hollow granules, or whether longer spray times in order to reduce the spray flux would be more successful.
- Currently, the energetic contribution of system per unit mass E_p range in the state diagram of liquid marble formation (Forny *et al.,* 2009) is unknown. Further work using powders with different degrees of hydrophobicity in the granulator should

be performed to quantify the energetic contribution of granulation process for both the state diagram by Forny *et al.* (2009), and for the frameworks produced in this thesis. This might be helpful for predicting an optimum impeller speed without performing experimental work, although this is currently a challenging task in all granulation processes.

- The experimental work in Chapter 7 with Aerosil should be repeated but under drop controlled regime conditions (Ψ_a~0.1) to determine whether the foam-like structure of granules can be eliminated by more controlled spray conditions. If not, the foam granules are most likely to have formed due to the high energetic contribution of process E_p, causing a local phase inversion to form a mousse.
- Detailed characterization of the hollow granule wall thickness and granule strength should be conducted on granules produced at small scale and large scale, and dried at different temperatures, to find whether the powder shell structure and shell thickness is the same or different for hollow granules formed from a single drop, compared to hollow granules formed from much smaller atomized drops in the granulator.

The framework relies in part on other researchers' work, including work in research areas which were not in the scope of this thesis. Further investigation on the following areas which is less directly related to the thesis scope is also recommended:

- Studying a single liquid marble with different powders and liquids under confocal microscopy may give a better understanding of liquid marble strength and stability. The outcome of this part may help to formulate more stable liquid marbles in granulator in order to prevent merging them.

- Studying the drying behavior of a single liquid marble with different powder sizes and different binders under different controlled drying conditions (such as temperature, humidity and constant air flow rate) is required to obtain a better understanding of different morphologies- collapsed, buckled, perfect sphere- form during drying and to find out the effect of the powder size and chemistry effect. Determining a quantitative time frame for collapsing and buckling of liquid marbles would be useful.
- Investigating the shrinkage of liquid marbles during drying at different drying temperatures and finding the relationship with the original droplet size for different formulations is useful to predict the possible granule size forms after drying.
- Studying the inter-particle forces between a few selected hydrophobic powders and binder particles using AFM (atomic force microscopy) technique might be helpful to explain why some powders are not compatible with some binders, and why the success rate of hollow granule formation is higher for some powders.

A

SEM images

L/S: 15/1, 63-125 µm

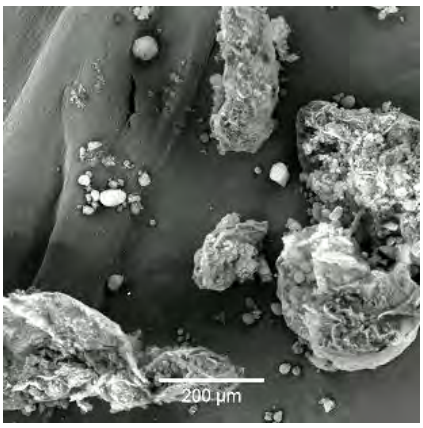

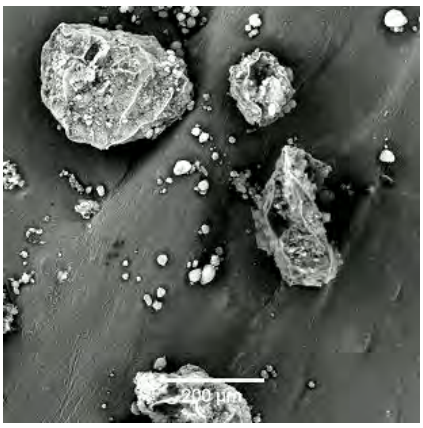

L/S: 15/1, 125- 250 µm

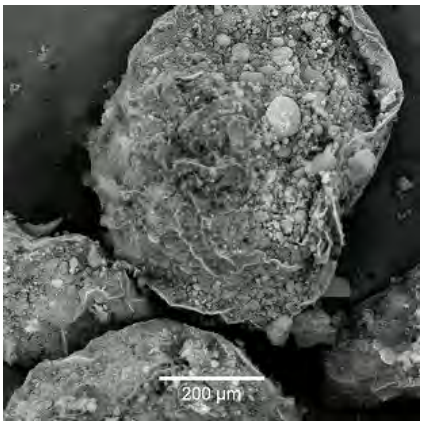

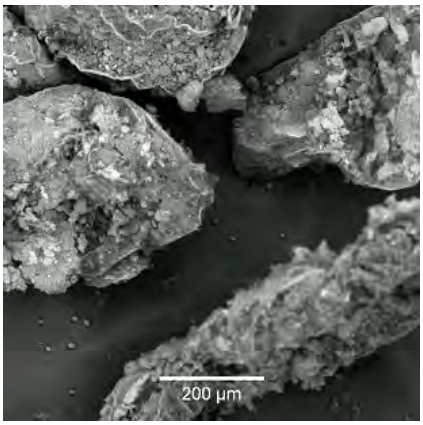

L/S: 15/1, 250- 500 µm

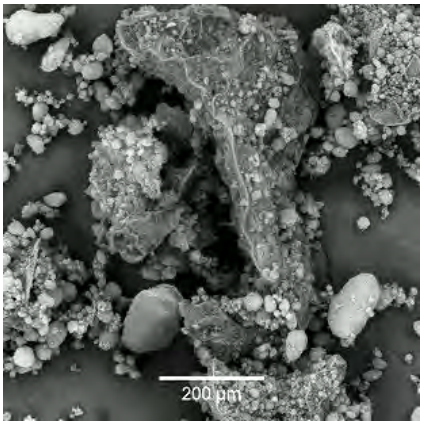

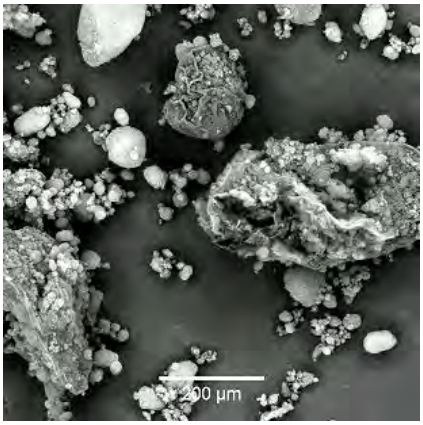

L/S: 15/1, 500- 1000 µm

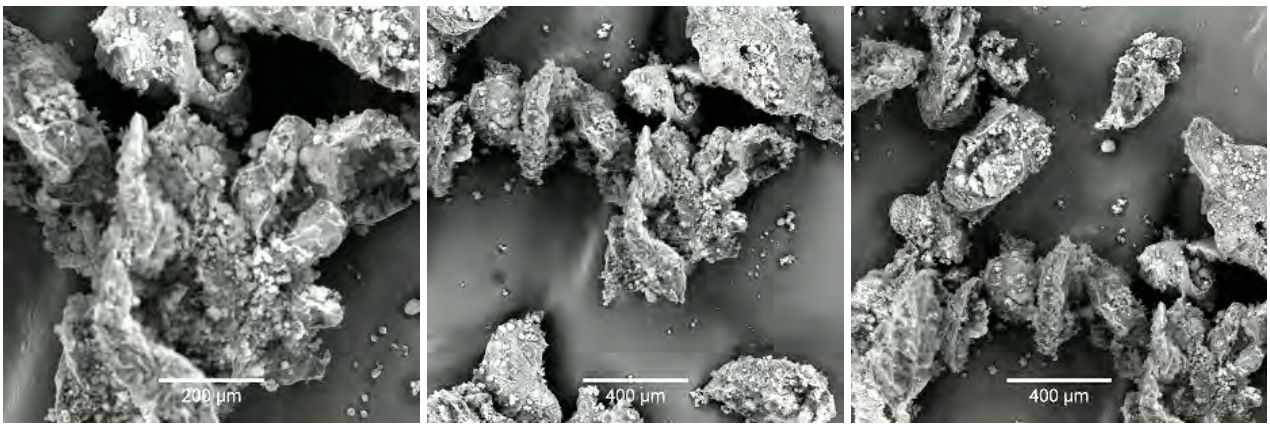

L/S: 15/1, 1000 µm+

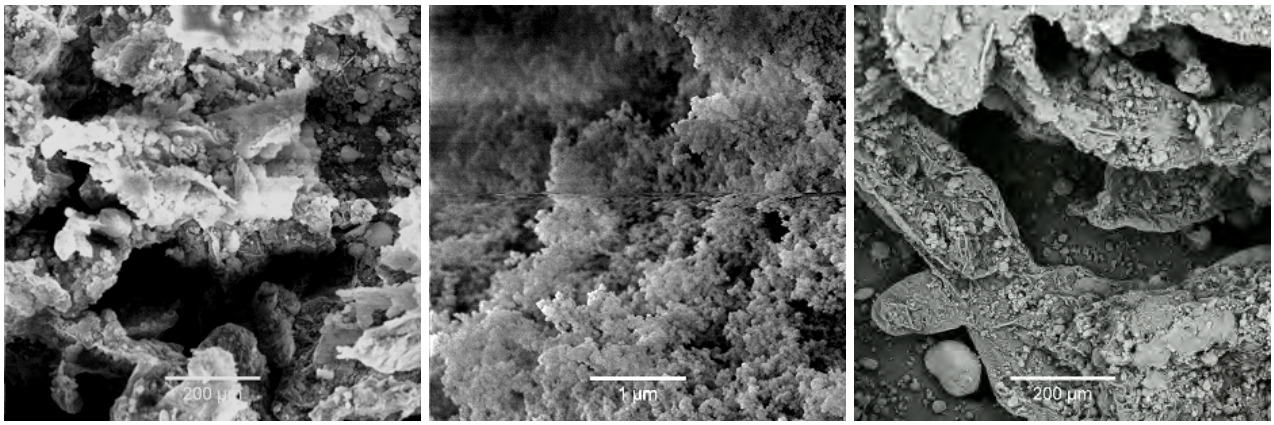

L/S: 8/1, 63-125 µm

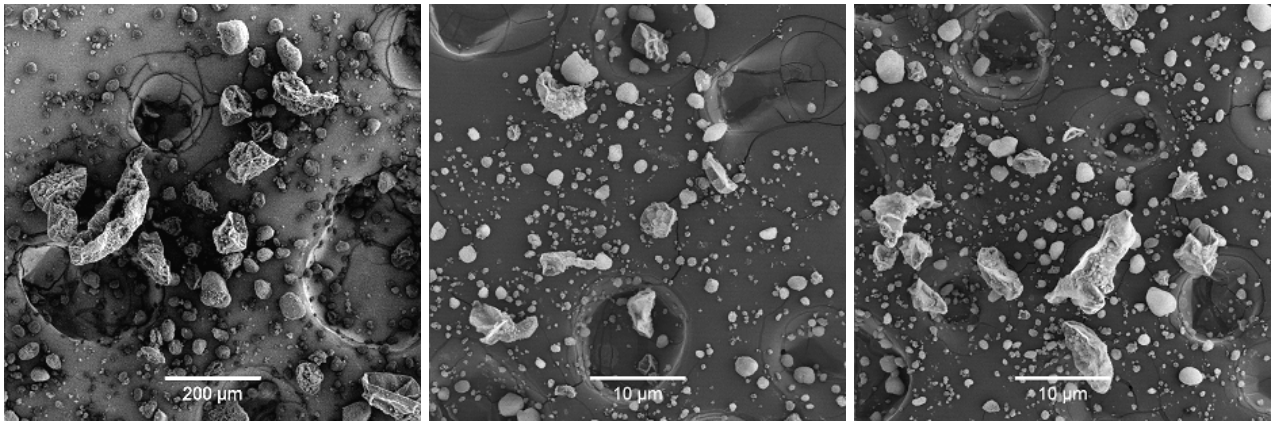

L/S: 8/1, 125-250µm

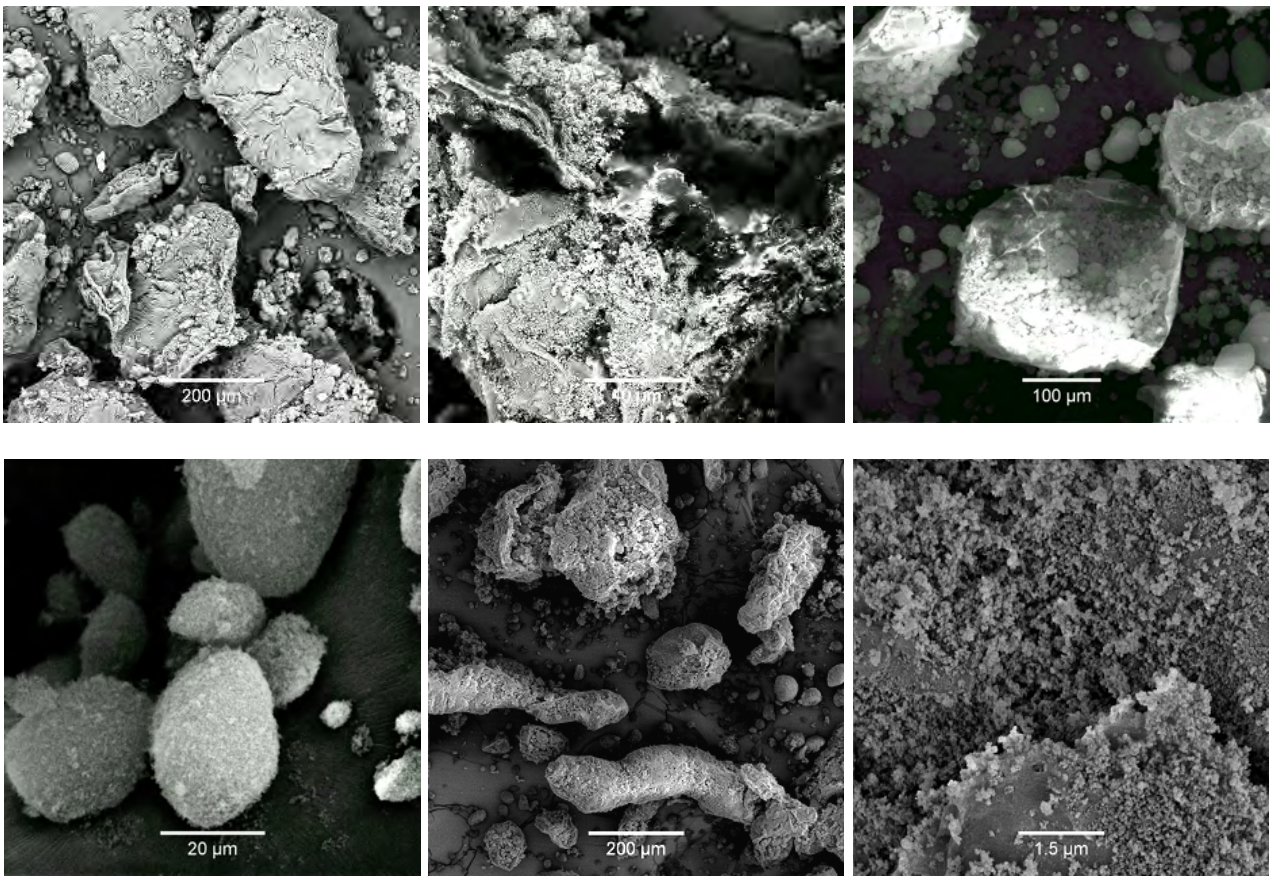

L/S: 8/1, 250-500µm

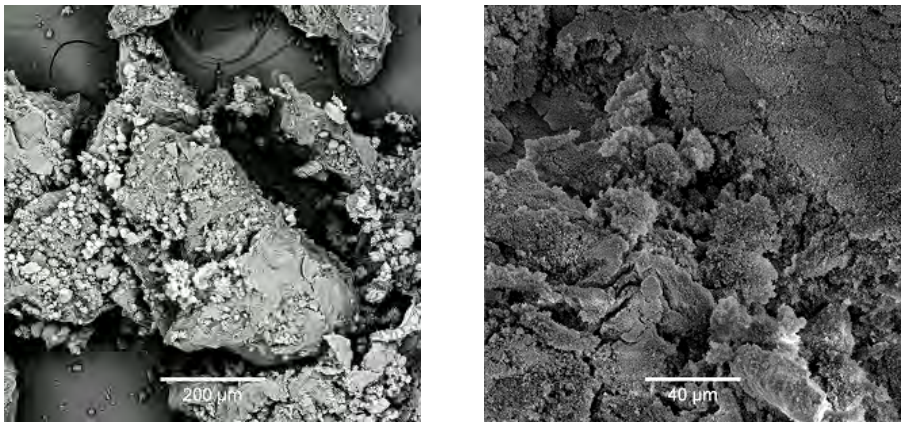

L/S: 8/1, 500- 1000 µm

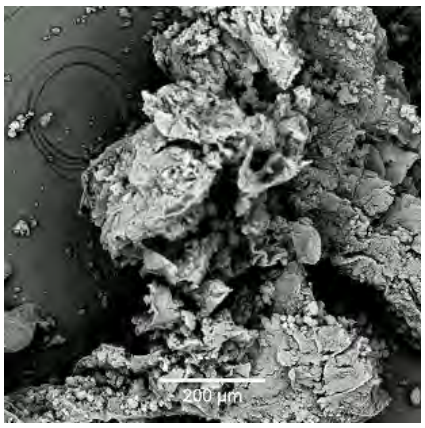

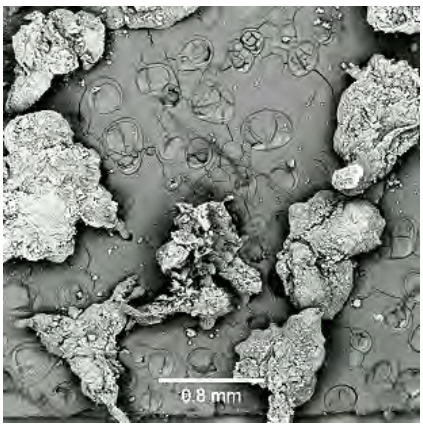

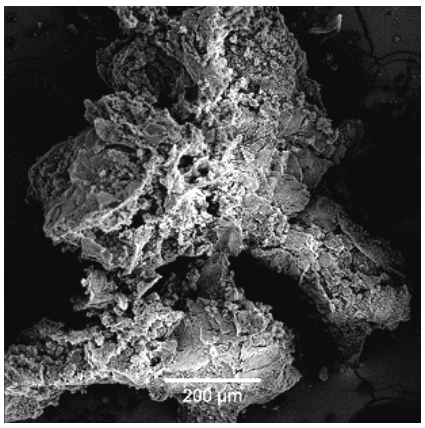

L/S: 8/1, 1000 µm+

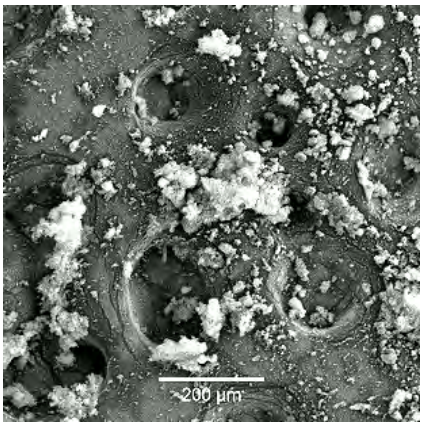

L/S: 6/1, 63-125 µm

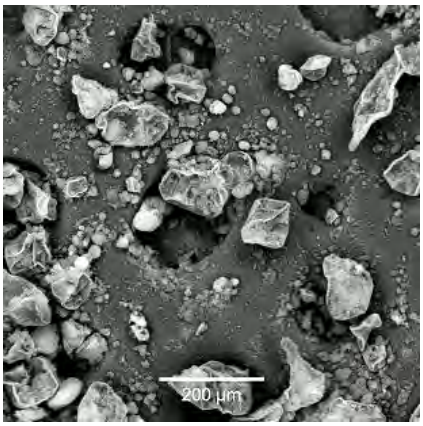

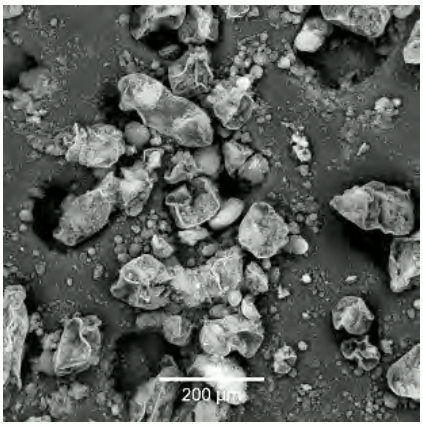

L/S: 6/1, 125-250 µm

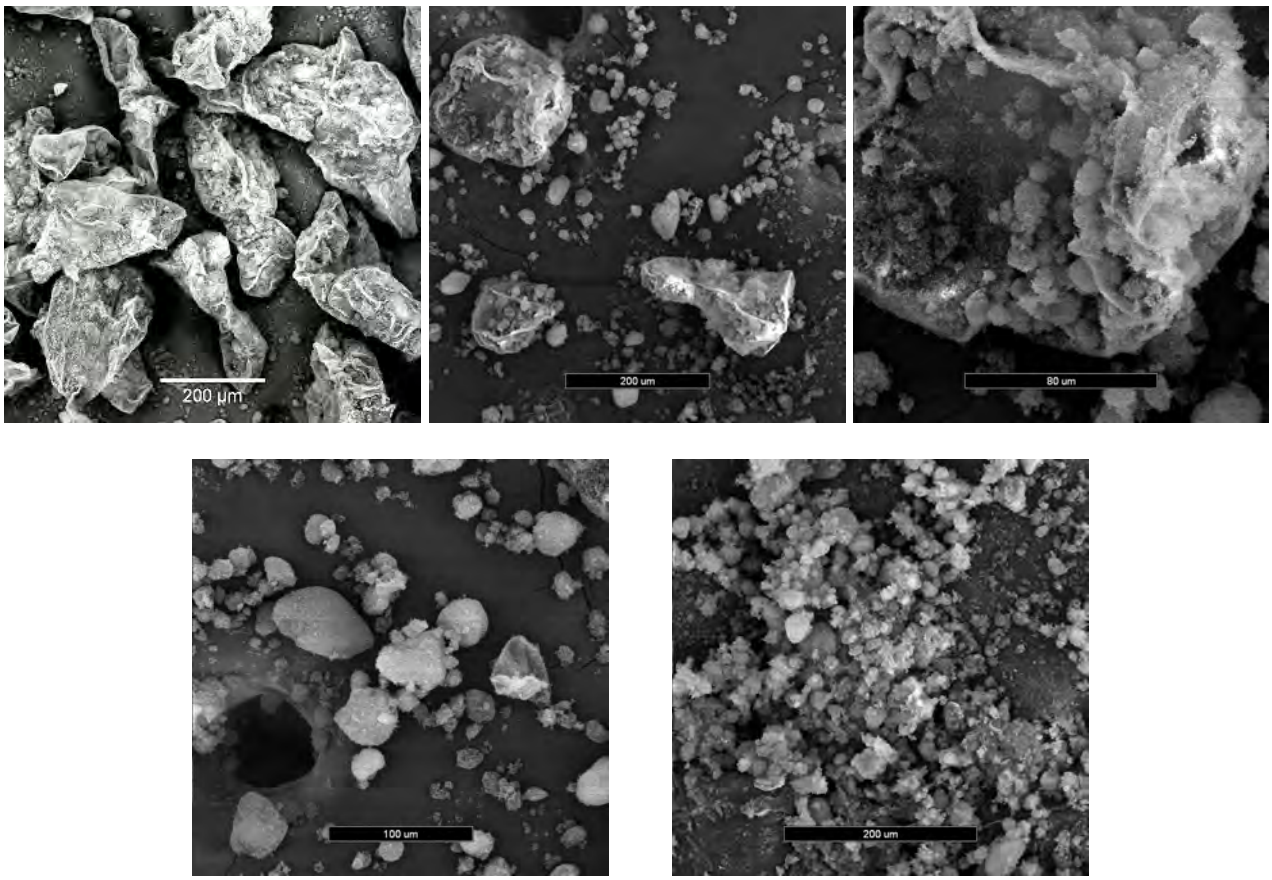

L/S: 6/1, 250-500 µm

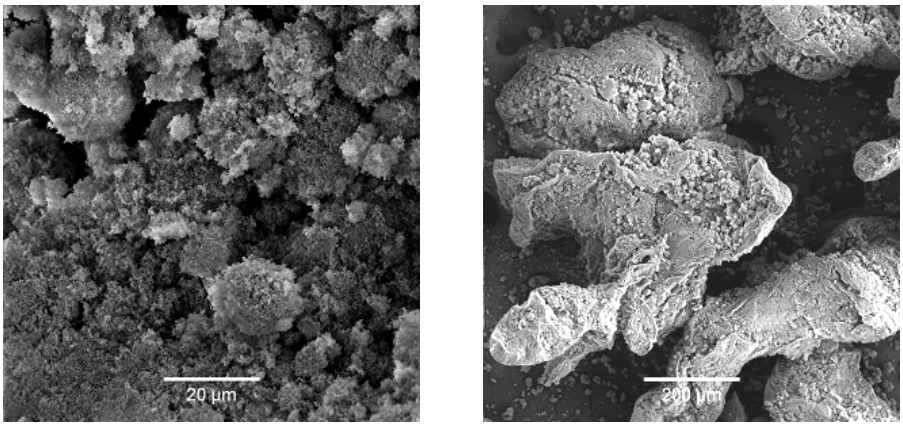

L/S: 6/1, 500-1000 µm

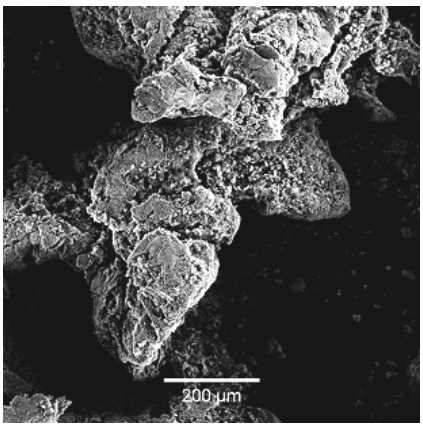

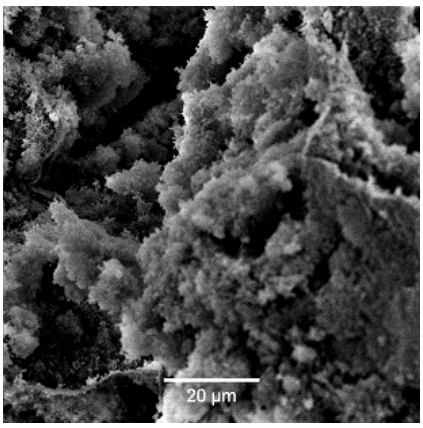

L/S: 3/1, 63-125 µm

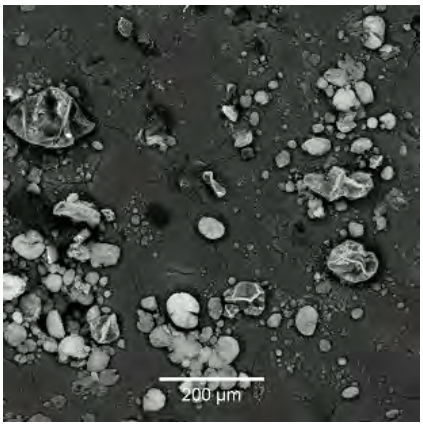

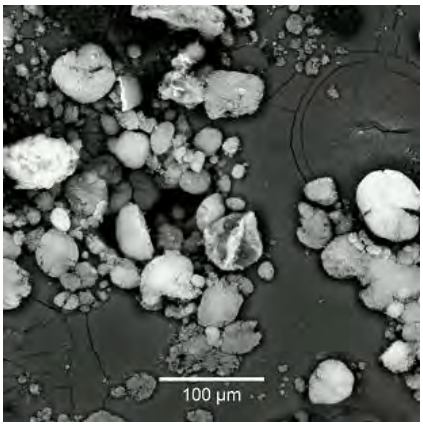

L/S: 3/1, 125-250 µm

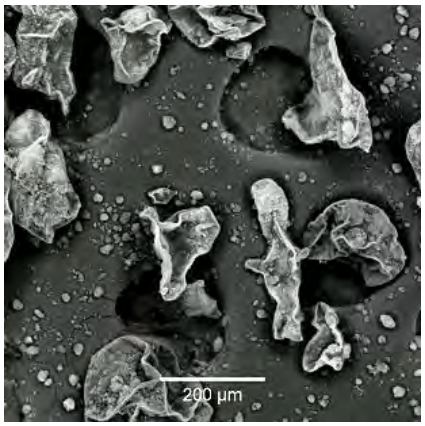

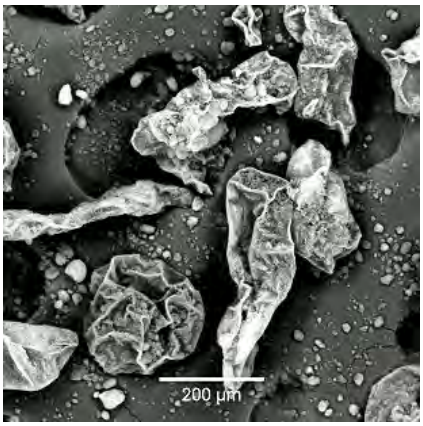

L/S: 3/1, 250-500 µm

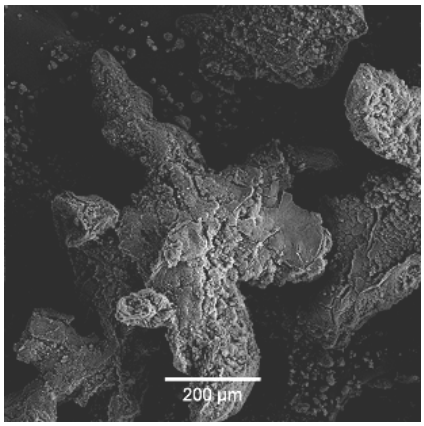

L/S: 1/1, 63-125 µm

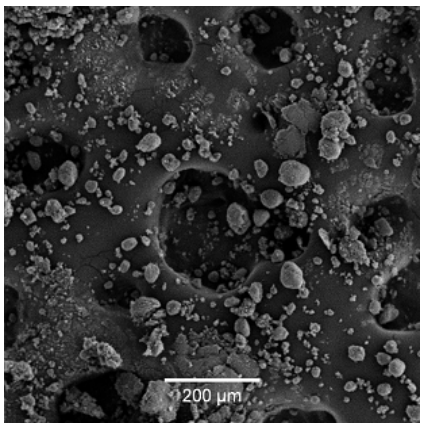

L/S: 1/1, 125-250 µm

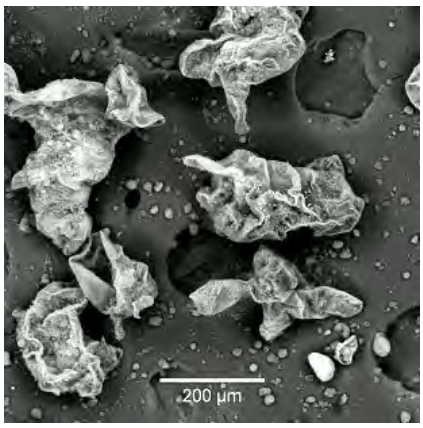

L/S: 1/1, 250-500 µm

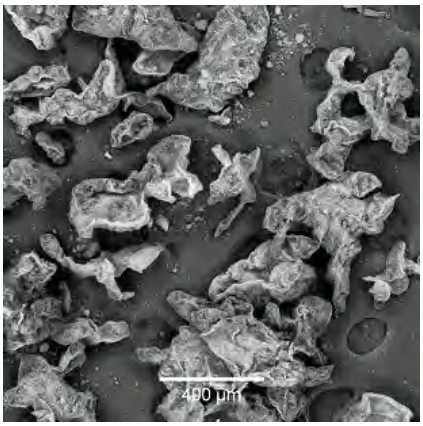

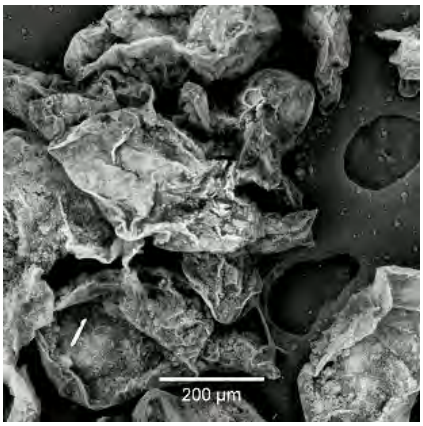

L/S: 0.5/1, 63-125 µm

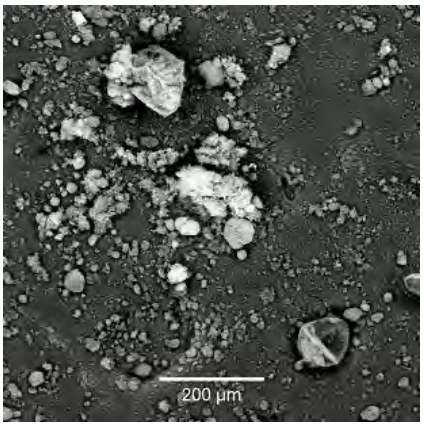

L/S: 0.5/1, 125-250 µm

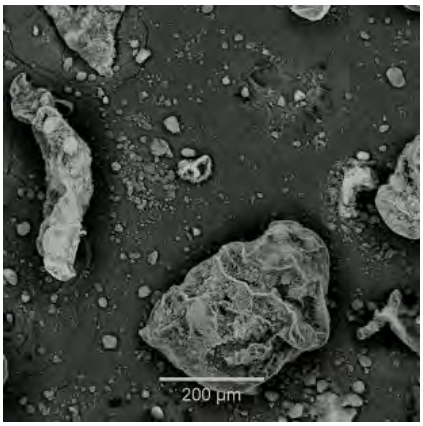

L/S: 0.5/1, 250-500 µm

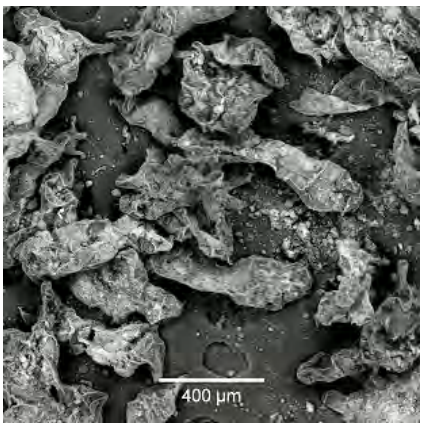

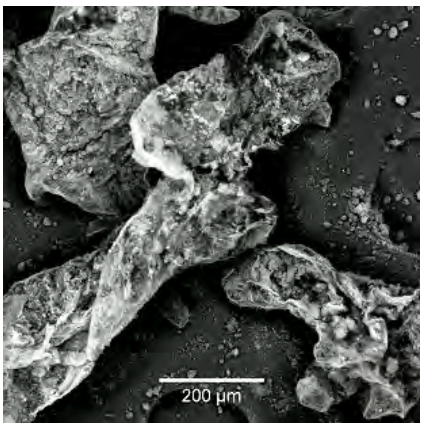

B

X-ray tomography images

Following X-ray tomography images shows three coordinates (YZ, XZ, XY) cross section of granules. Then, some of the images follow by horizontal cross section images of the first image.

L/S: 15/1, 63-125 µm (scale bar: 100 µm)

(a) YZ cross section (b) XZ cross section (c) XY cross section

Another example: L/S: 15/1, 63-125 µm (scale bar: 100 µm)

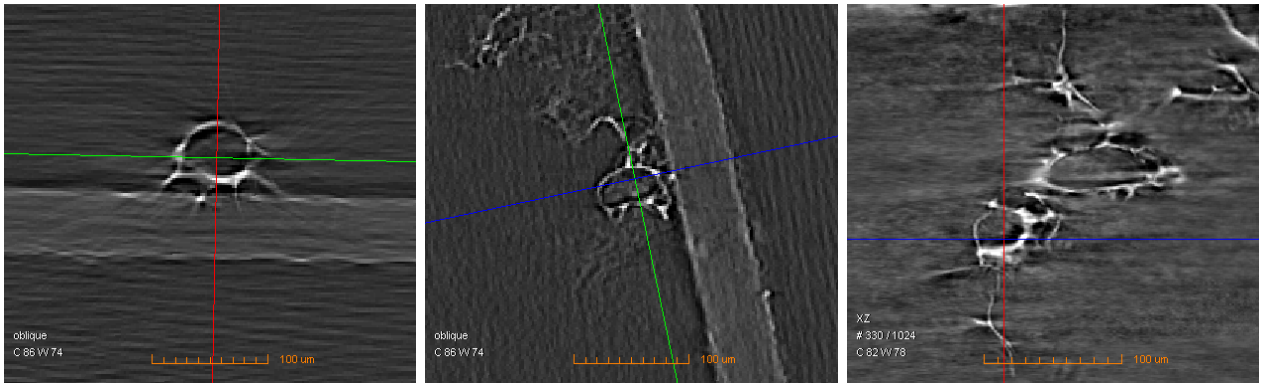

(a) XY cross section (b) YZ cross section (c) XZ cross section

L/S: 15/1, 125-250 µm(scale bar: 100 µm)

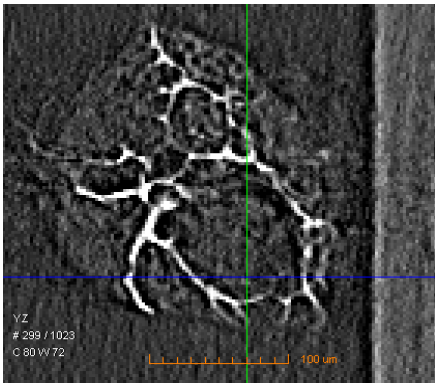

(a) YZ cross section

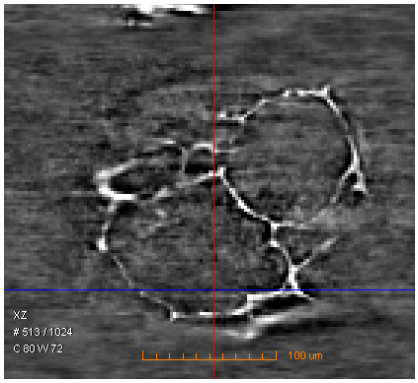

(b) XZ cross section

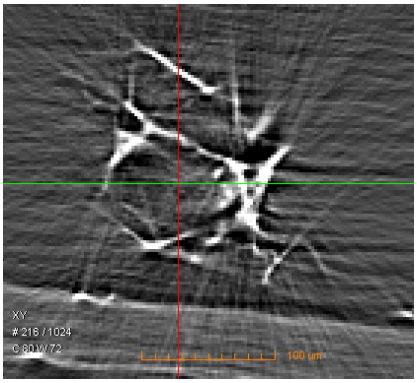

(c) XY cross section

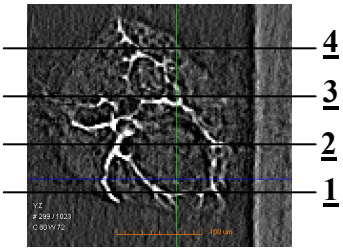

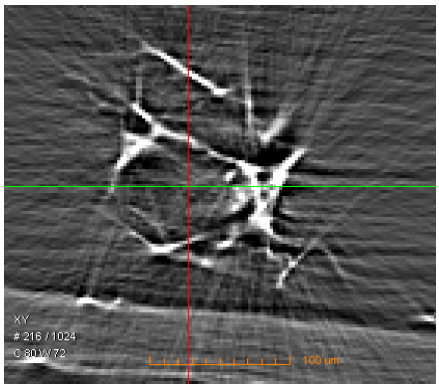

(a) XY cross section-1

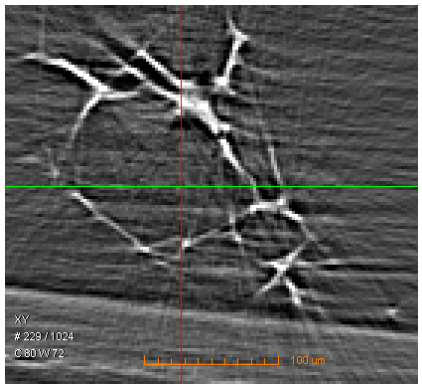

(b) XY cross section-2

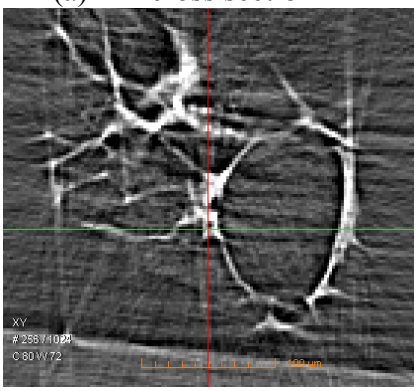

(c) XY cross section-3

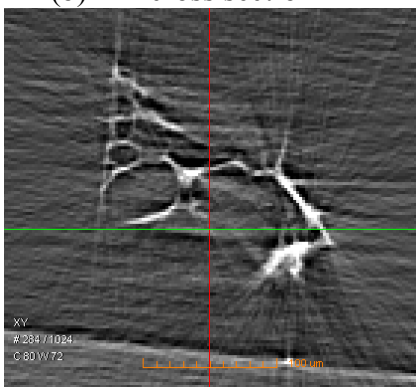

(d) XY cross section-4

L/S: 15/1, 250-500 µm (scale bar: 200 µm)

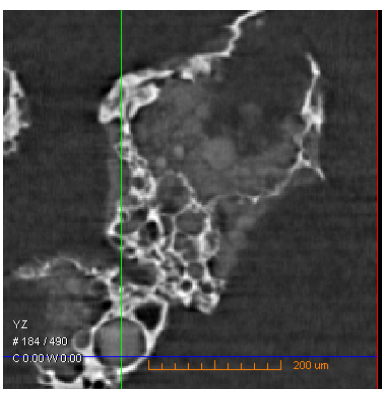

(a) YZ cross section

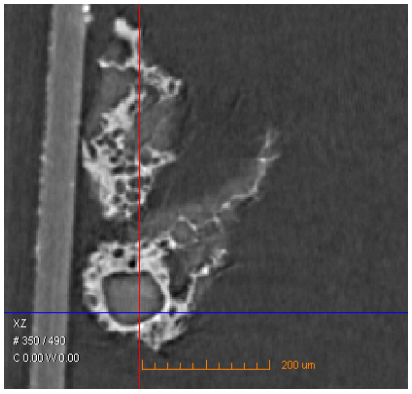

(b) XZ cross section

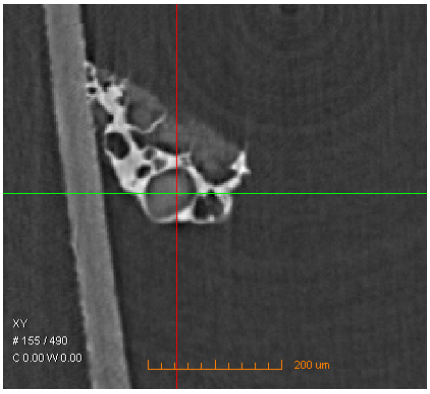

(c) XY cross section

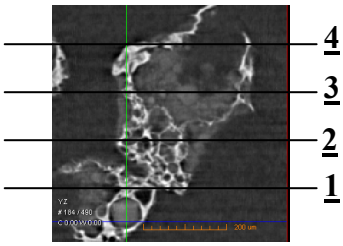

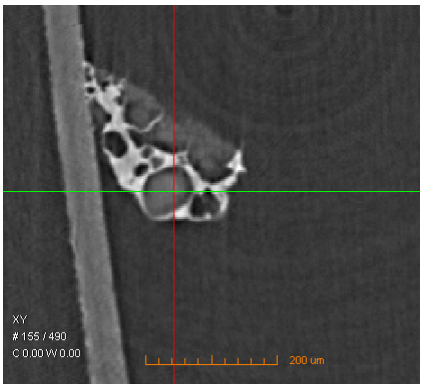

(a) XY cross section-1

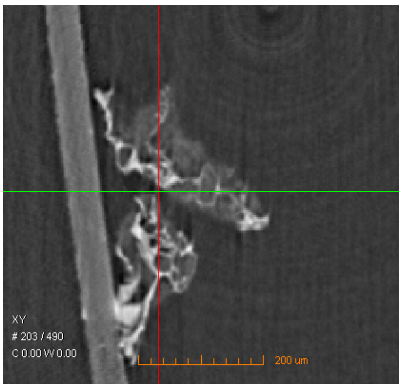

(b) XY cross section-2

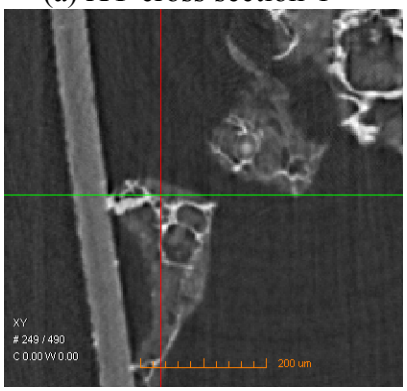

(c) XY cross section-3

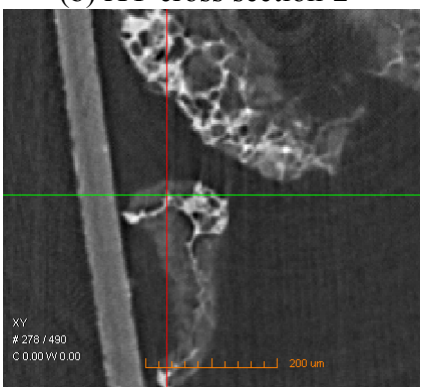

(d) XY cross section-4

Another example L/S: 15/1, 250-500 µm (scale bar: 200 µm)

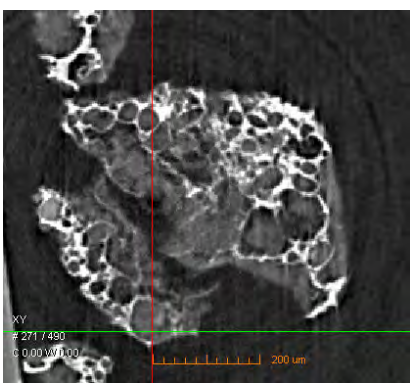

(a) XY cross section

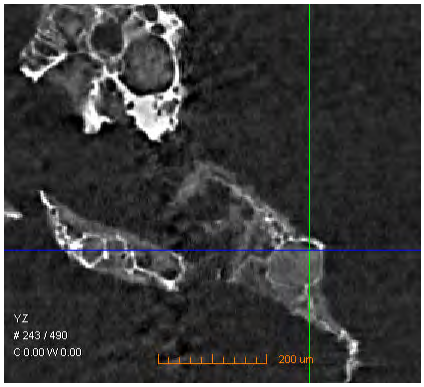

(b) YZ cross section

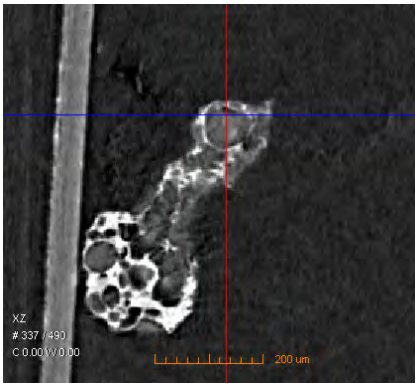

(c) XZ cross section

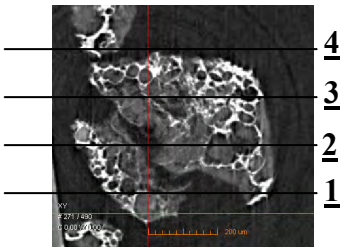

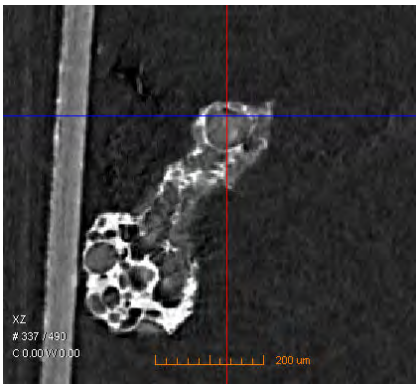

(a) XZ cross section-1

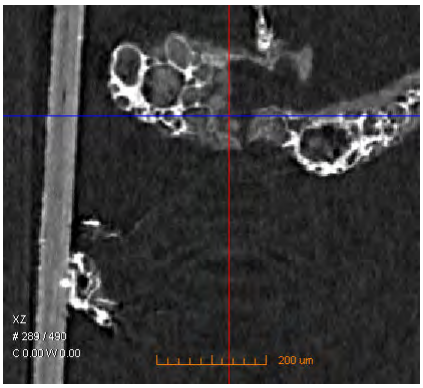

(b) XZ cross section-2

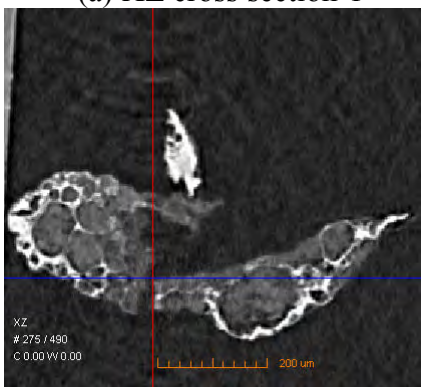

(c) XZ cross section-3

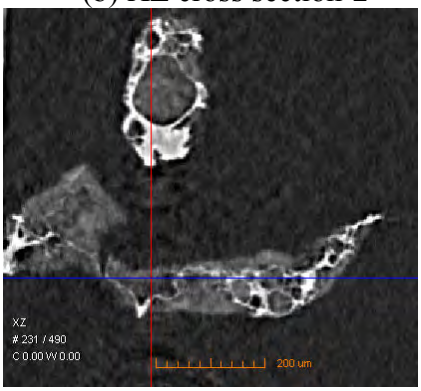

(d) XZ cross section-4

L/S: 15/1, 500-1000 µm (scale bar: 500 µm)

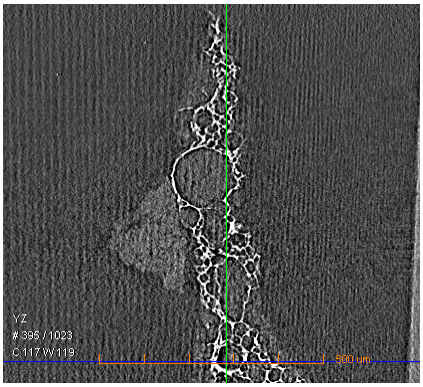

(a) YZ cross section

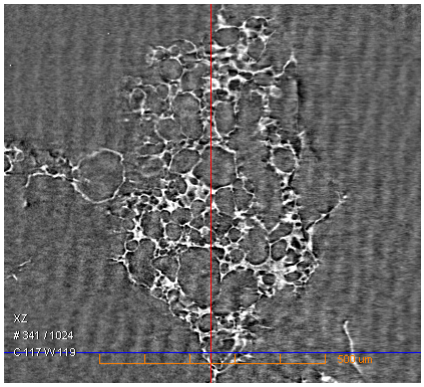

(b) XZ cross section

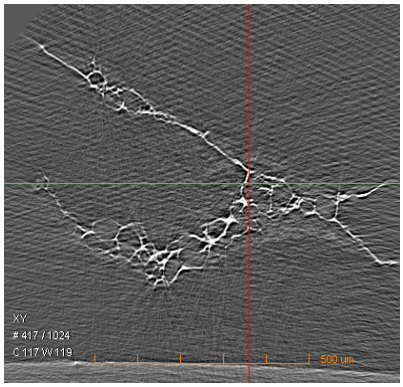

(c) XY cross section

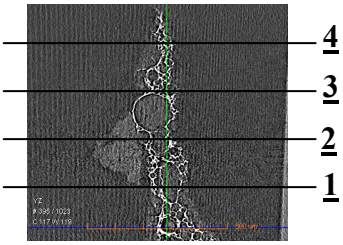

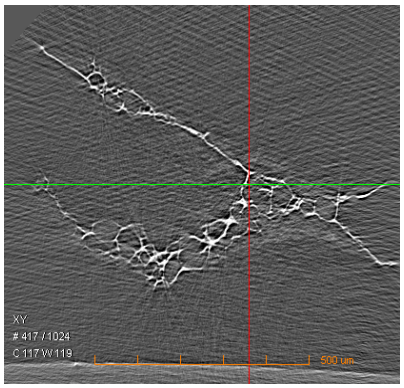

(a) XY cross section-1

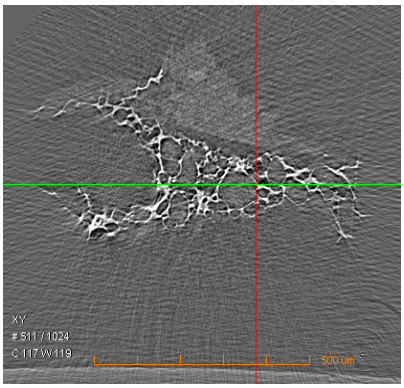

(b) XY cross section-2

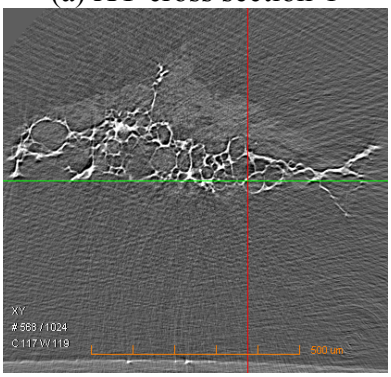

(c) XY cross section-3

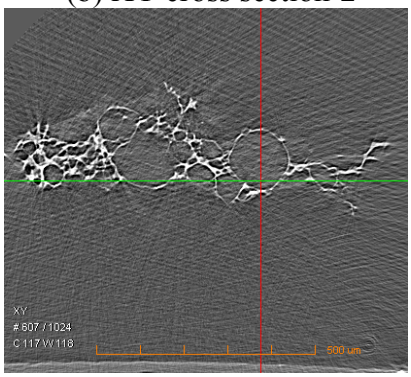

(d) XY cross section-4

Another example L/S: 15/1, 500-1000 µm (scale bar: 500 µm)

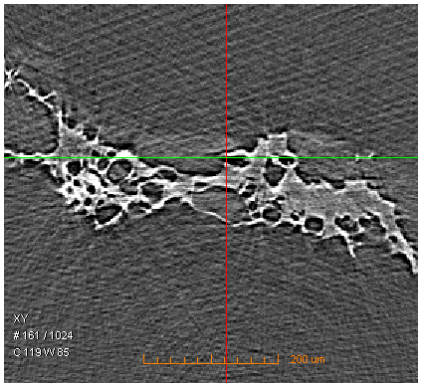

(a) XY cross section

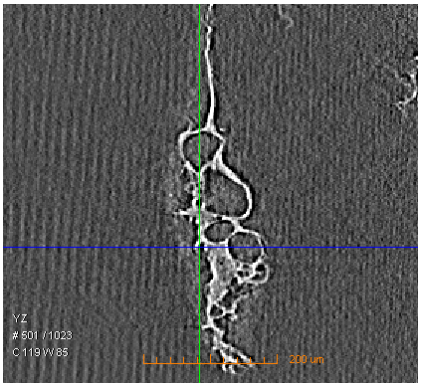

(b) XZ cross section

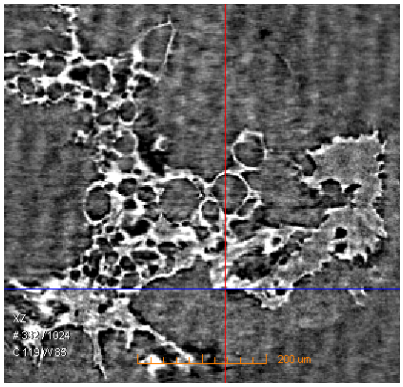

(c) XZ cross section

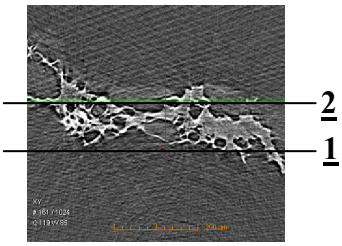

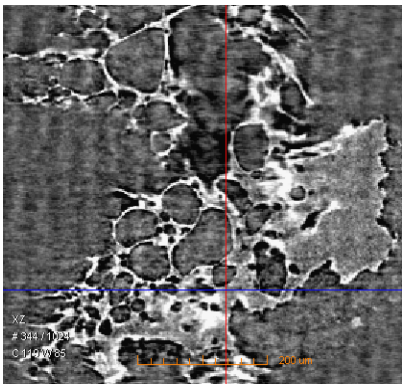

(a) XZ cross section-1

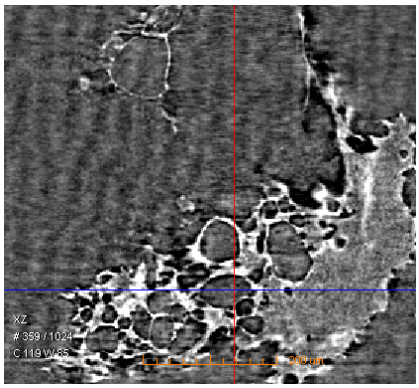

(b) XZ cross section-2

L/S: 15/1, 1000 + µm (scale bar: 1000 µm)

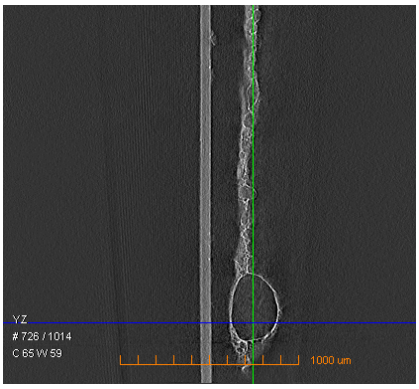

(a) YZ cross section

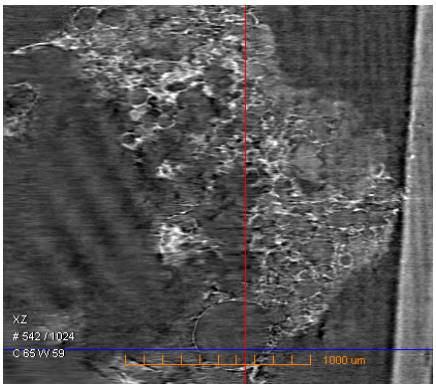

(b) XZ cross section

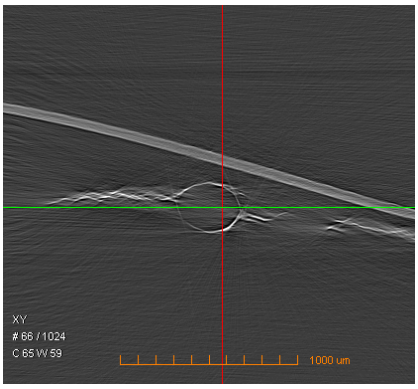

(c) XY cross section

L/S: 8/1, 63-125 µm (scale bar: 100 µm)

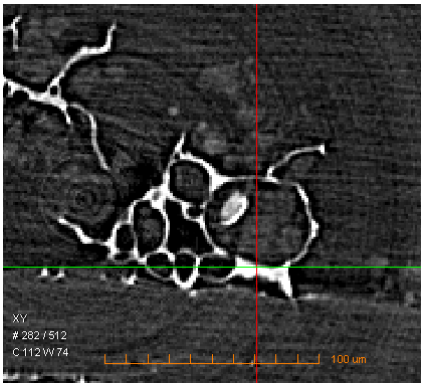

(a) XY cross section

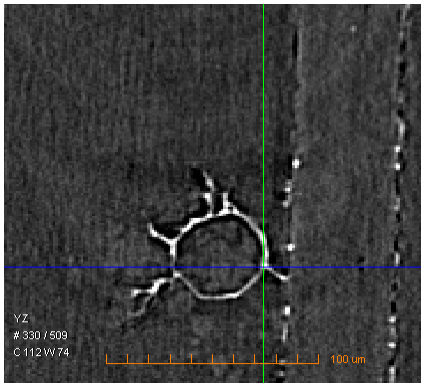

(b) YZ cross section

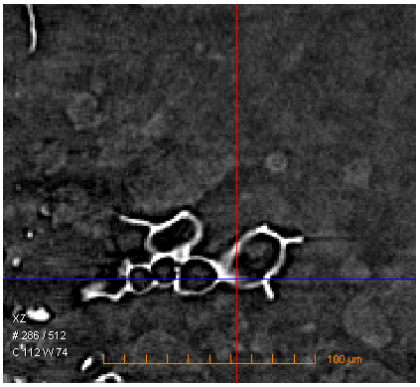

(c) XZ cross section

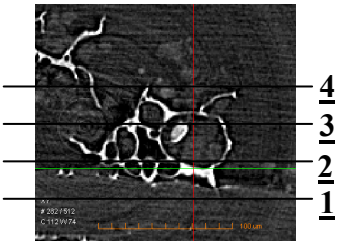

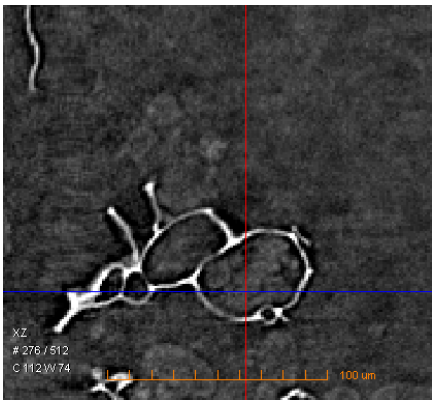

(a) XZ cross section-1

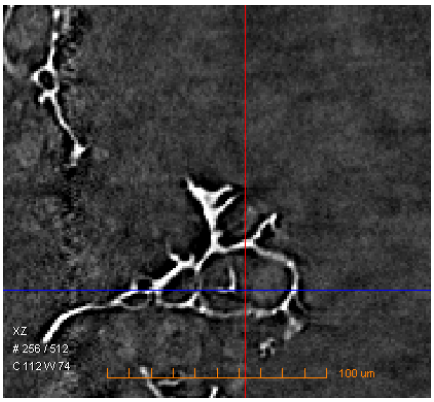

(b) XZ cross section-2

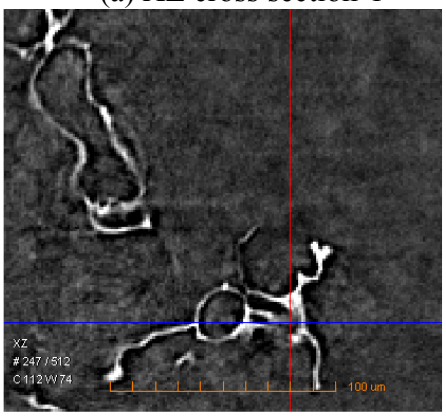

(c) XZ cross section-3

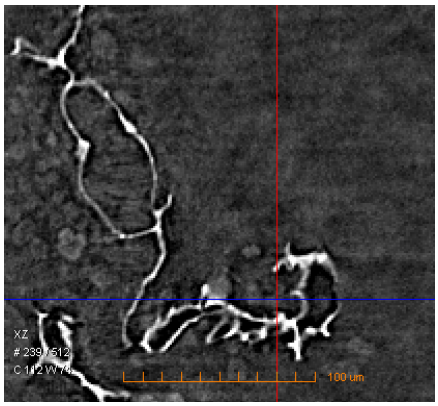

(d) XZ cross section-4

Another example: L/S: 8/1, 63-125 µm (scale bar: 100 µm)

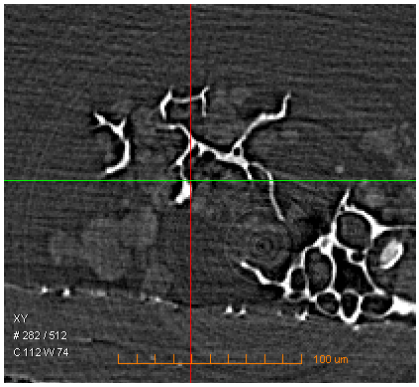

(a) XY cross section

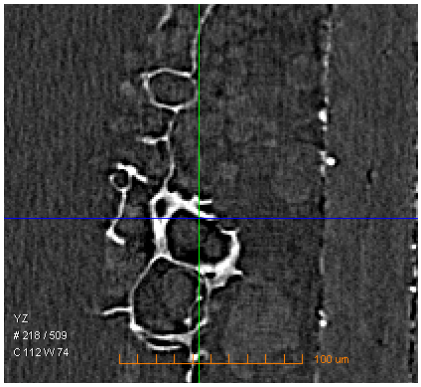

(b) YZ cross section

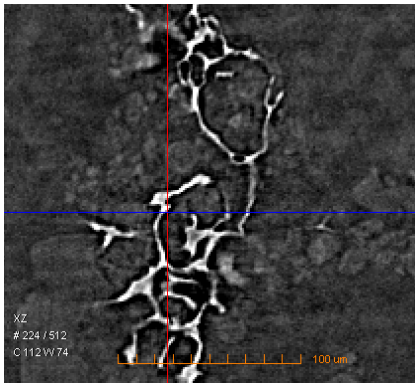

(c) XZ cross section

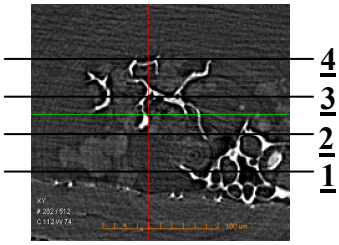

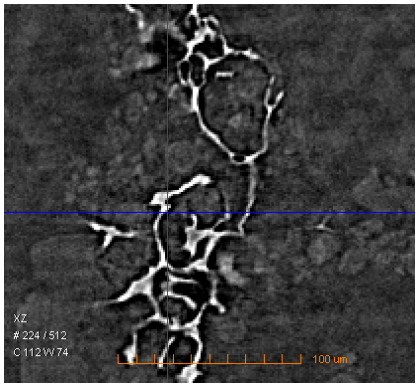

(a) XZ cross section-1

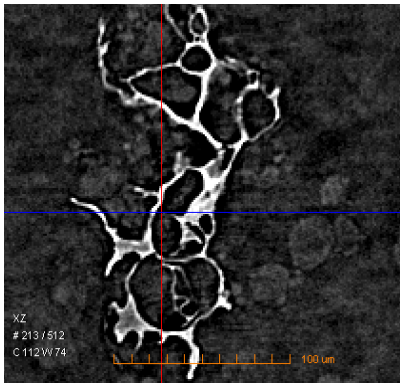

(b) XZ cross section-2

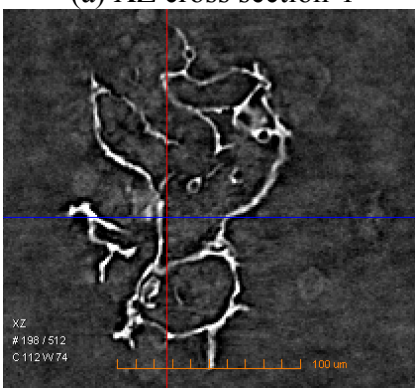

(c) XZ cross section-3

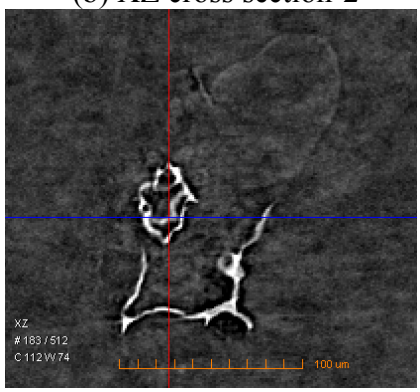

(d) XZ cross section-4

L/S: 8/1, 125-250 µm (scale bar: 200 µm)

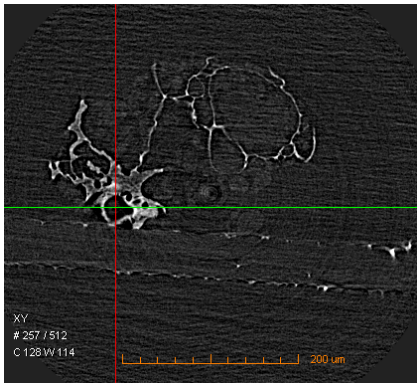

(a) XY cross section

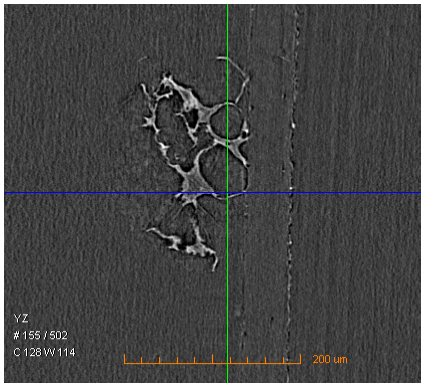

(b) YZ cross section

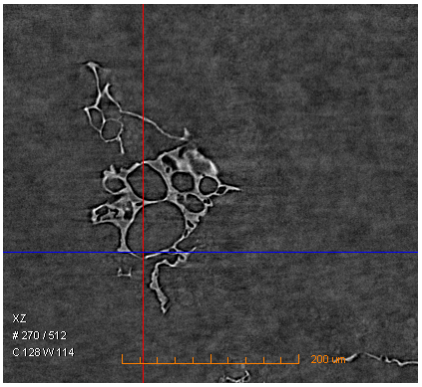

(c) XZ cross section

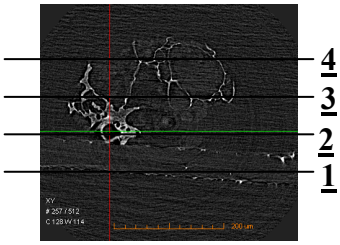

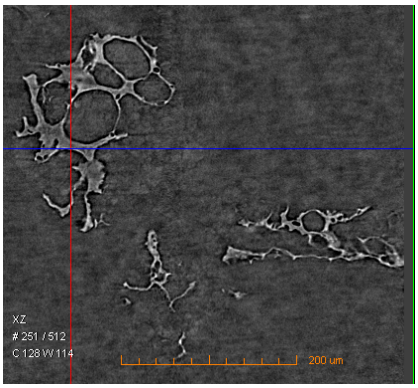

(a) XZ cross section-1

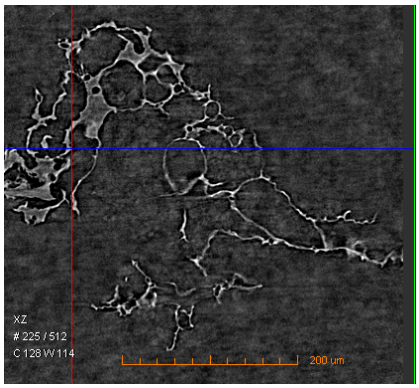

(b) XZ cross section-2

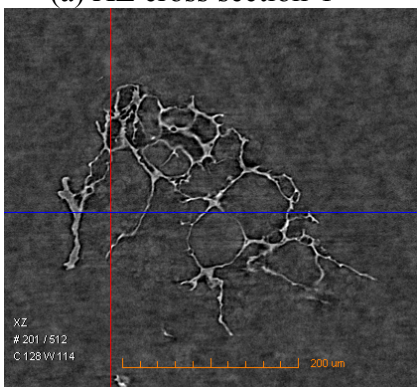

(c) XZ cross section-3

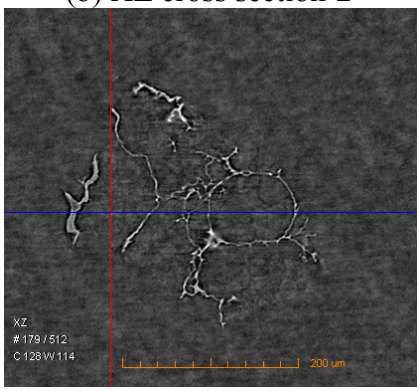

XZ cross section-4

L/S: 8/1, 250-500 µm (scale bar: 200 µm)

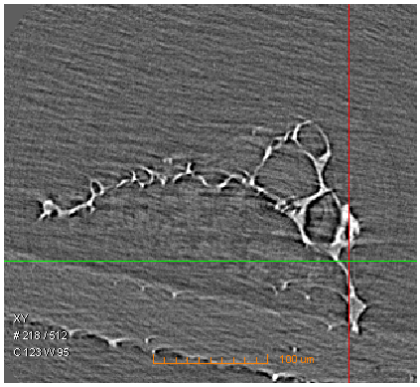

(a) XY cross section

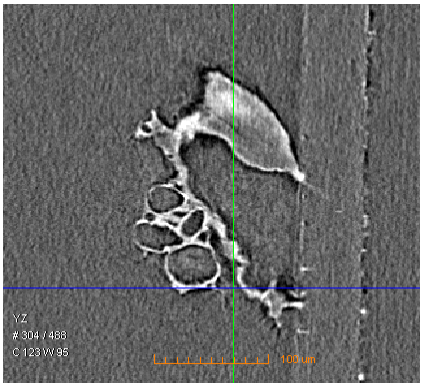

(b) YZ cross section

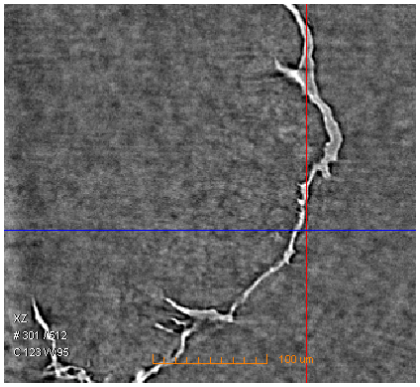

(c) XZ cross section

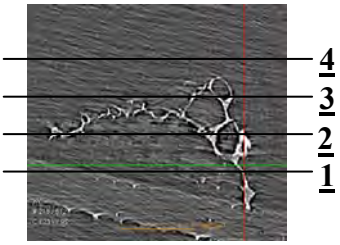

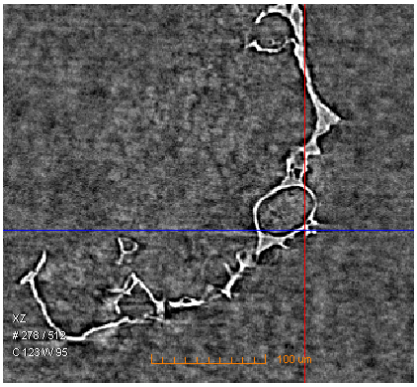

(a) XZ cross section-1

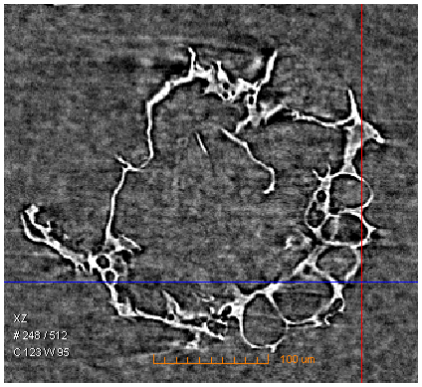

(b) XZ cross section-2

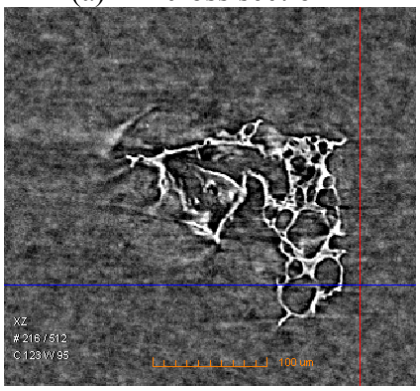

(c) XZ cross section-3

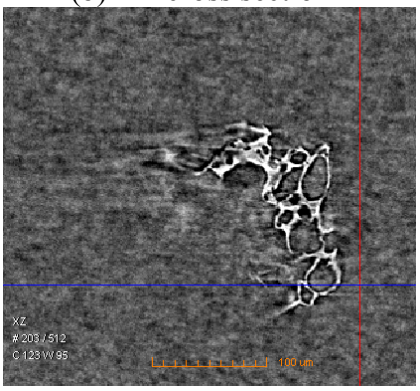

(d) XZ cross section-4

L/S: 8/1, 500-1000 µm (scale bar: 500 µm)

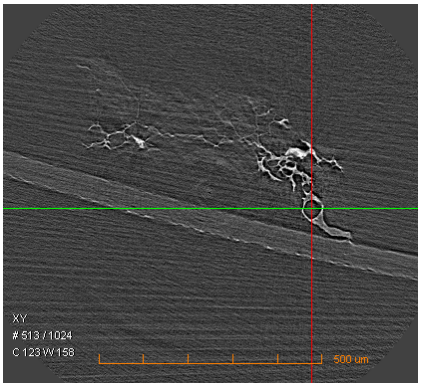

(a) XY cross section

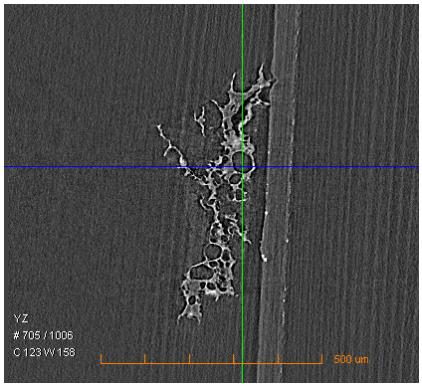

(b) YZ cross section

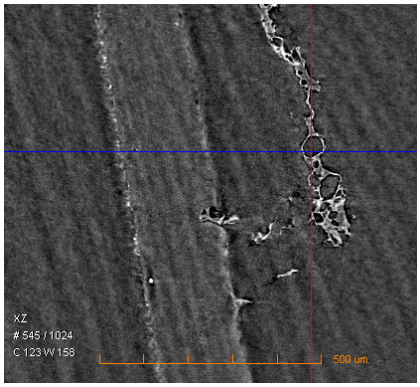

(c) XZ cross section

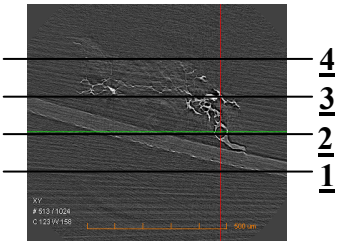

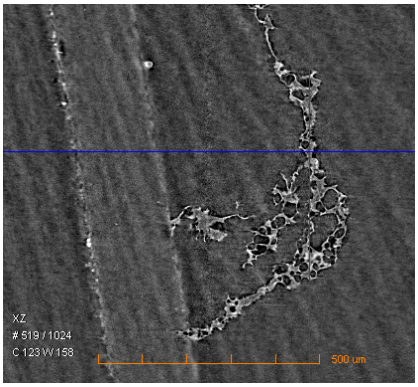

(a) XZ cross section-1

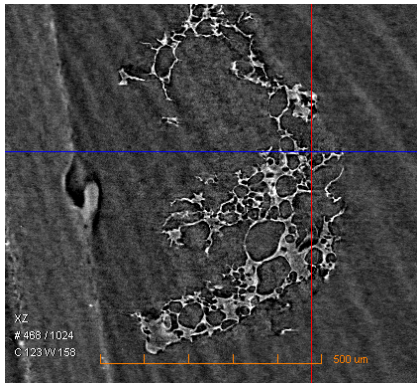

(b) XZ cross section-2

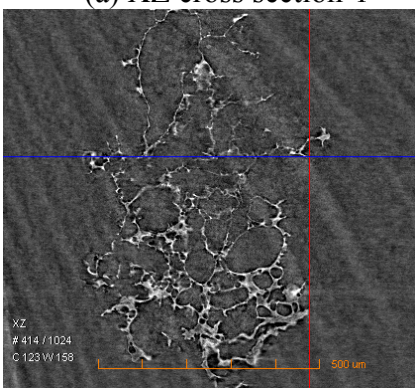

(c) XZ cross section-3

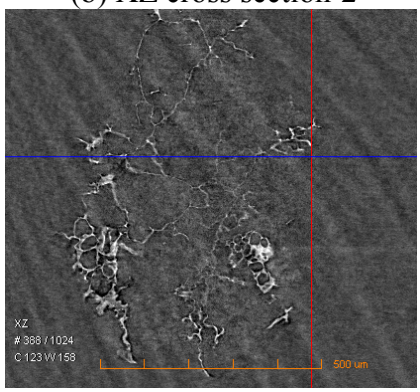

(d) XZ cross section-4

L/S: 8/1, 1000 + µm (scale bar: 1000 µm)

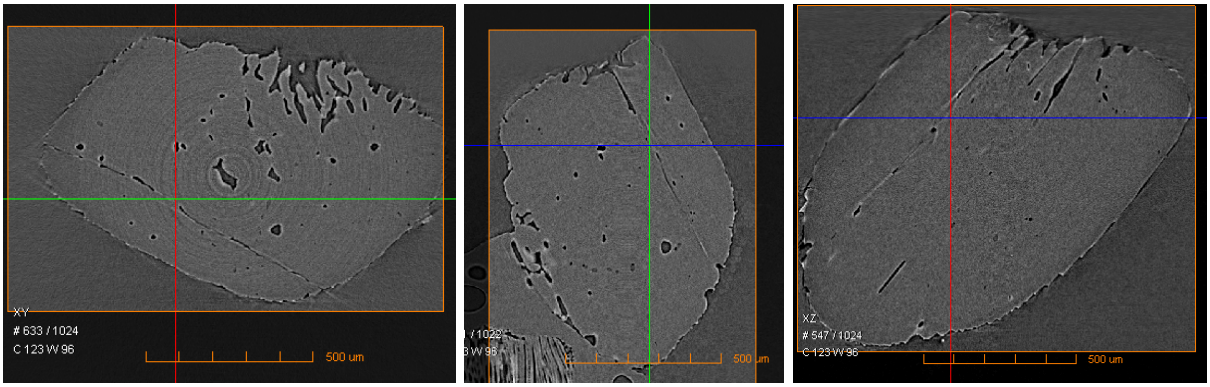

(a) XY cross section (b) YZ cross section (c) XZ cross section

L/S: 6/1, 63-125 µm (scale bar: 100 µm)

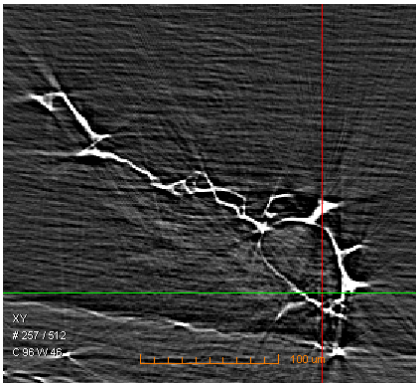

(a) XY cross section

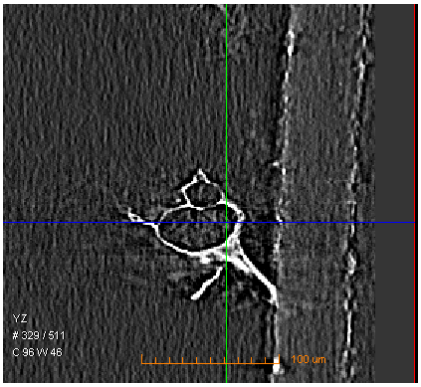

(b) YZ cross section

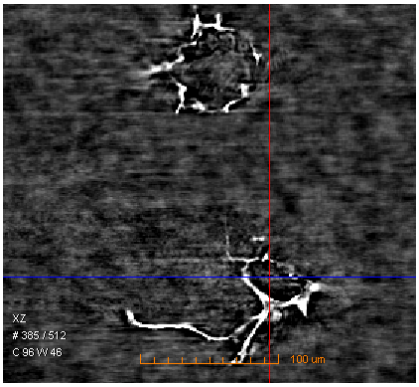

(c) XZ cross section

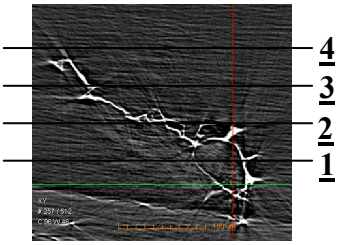

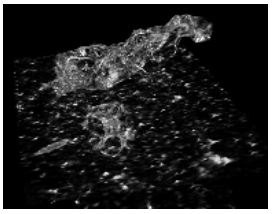

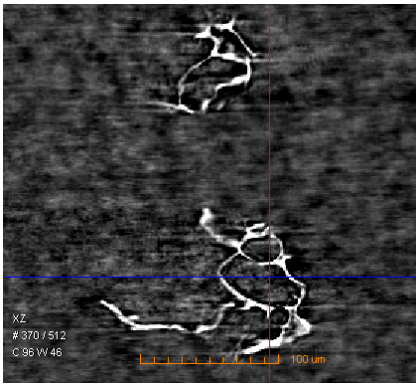

(a) XZ cross section-1

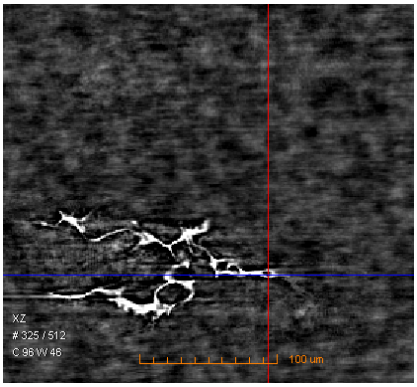

(b) XZ cross section-2

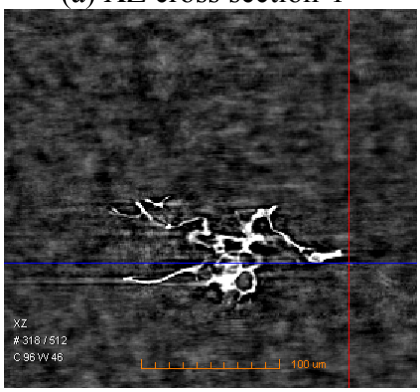

(c) XZ cross section-3

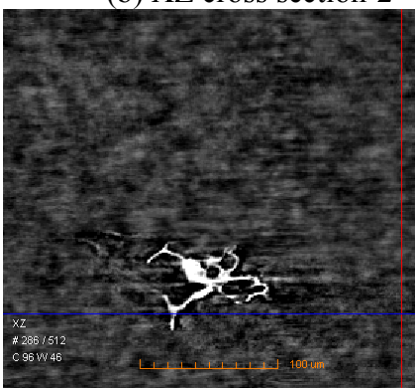

(d) XZ cross section-4

L/S: 6/1,125-250 µm (scale bar: 100 µm)

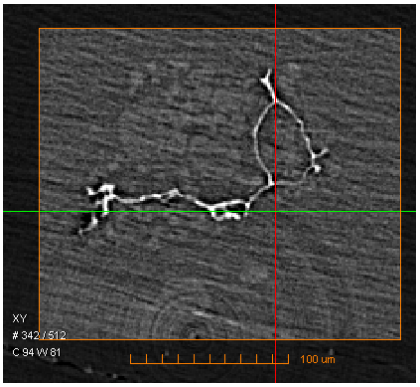

(a) XY cross section

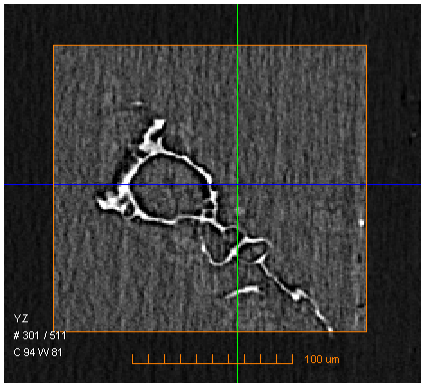

(b) YZ cross section

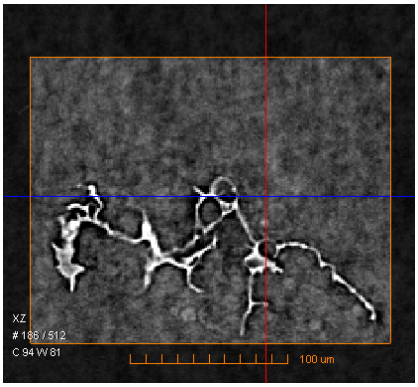

(c) XZ cross section

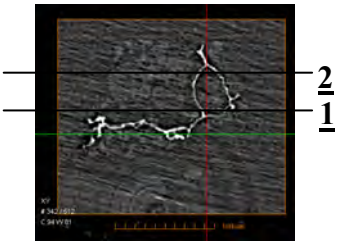

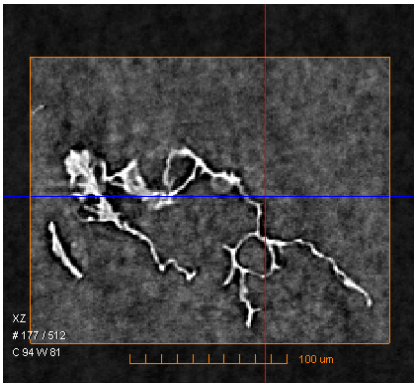

(a) XZ cross section-1

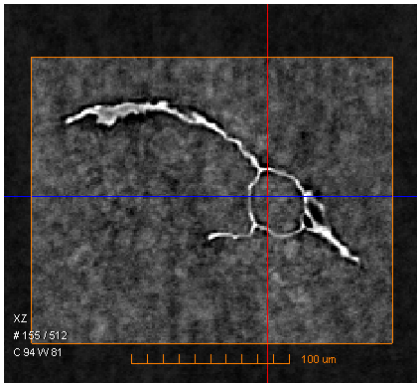

(b) XZ cross section-2

Another example: L/S: 6/1,125-250 µm (scale bar: 100 µm)

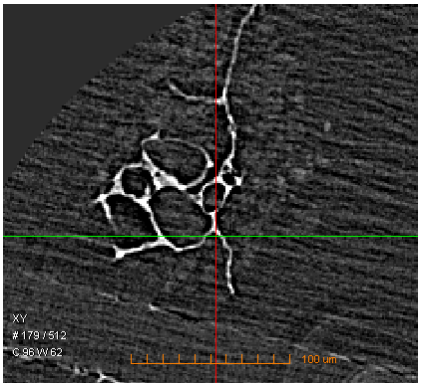

(a) XY cross section

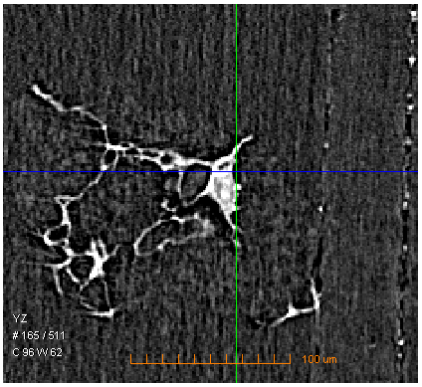

(b) YZ cross section

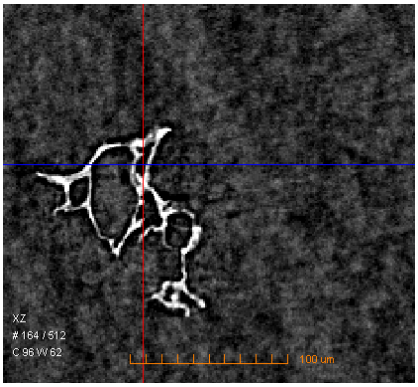

(c) XZ cross section

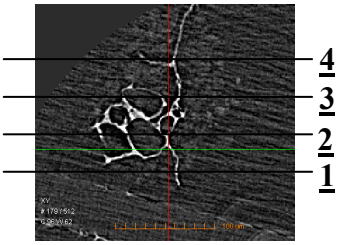

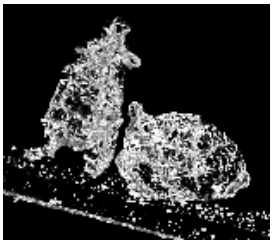

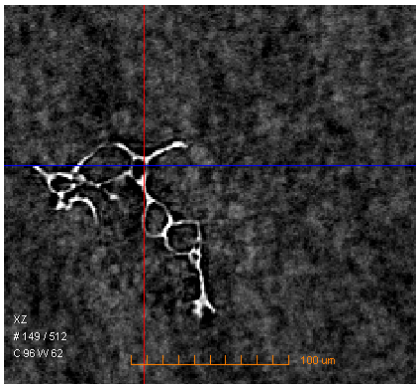

(a) XZ cross section-1

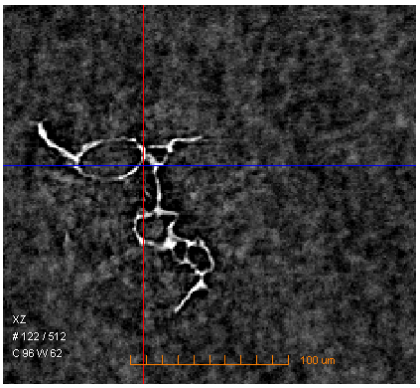

(b) XZ cross section-2

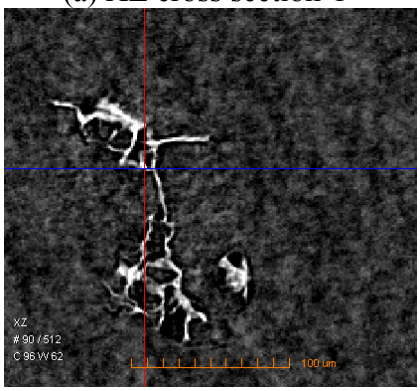

(c) XZ cross section-3

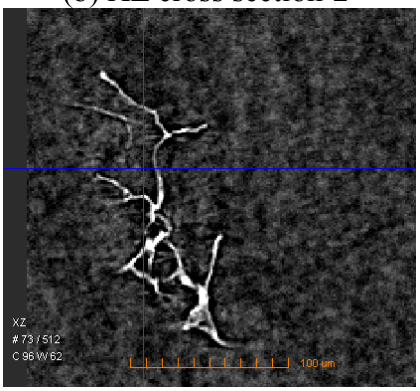

(d) XZ cross section-4

L/S: 6/1, 250-500 µm (scale bar: 200 µm)

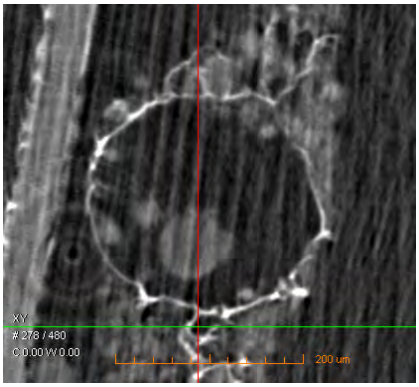

(a) XY cross section

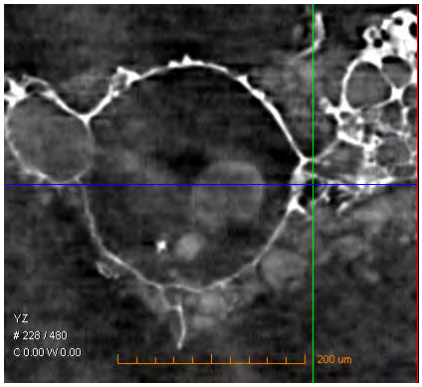

(b) YZ cross section

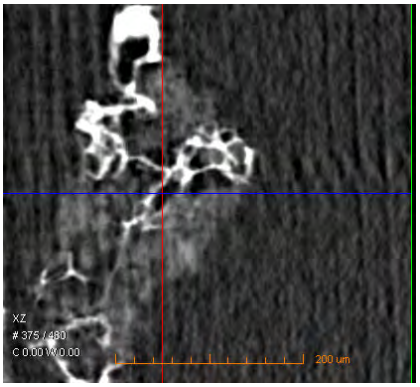

(c) XZ cross section

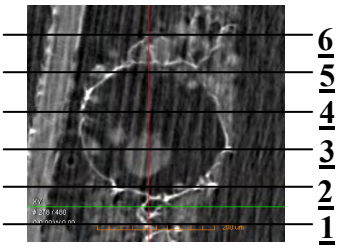

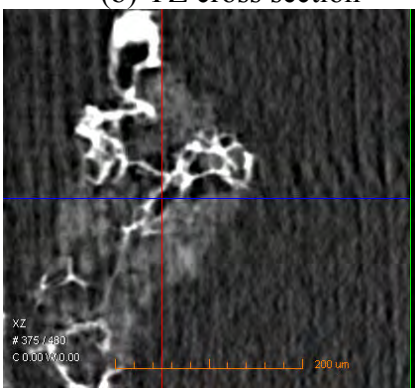

(a) XZ cross section-1

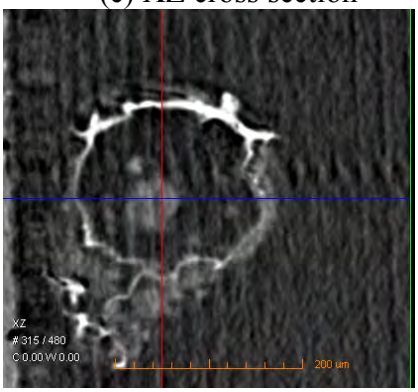

(b) XZ cross section-2

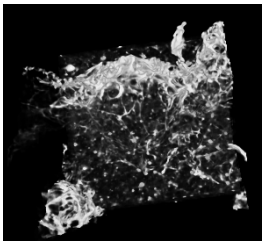

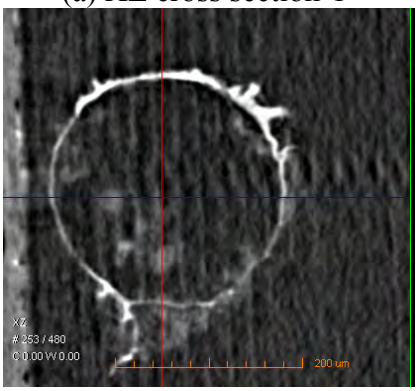

(c)XZ cross section-3

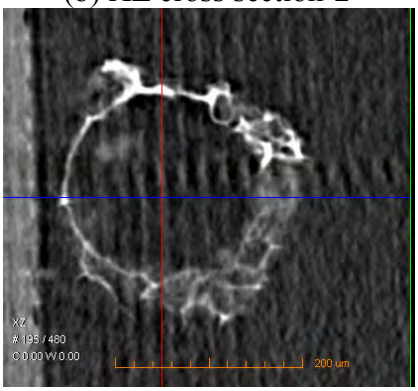

(d) XZ cross section-4

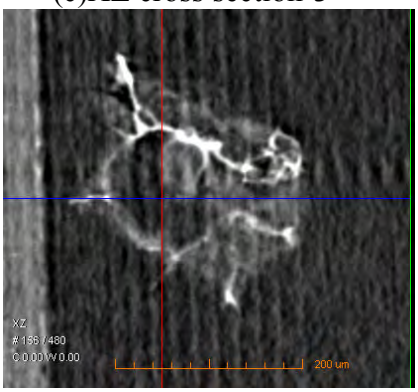

(e) XZ cross section-5

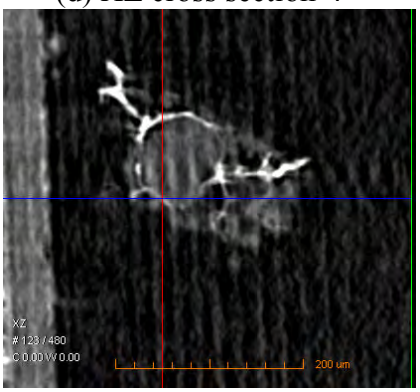

(f) XZ cross section-6

Another example: L/S: 6/1, 250-500 µm (scale bar: 200 µm)

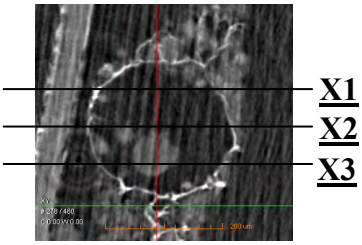

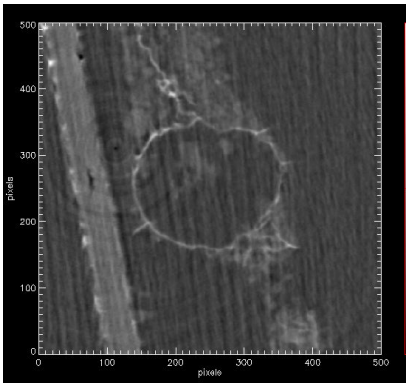

X1: Top cross section

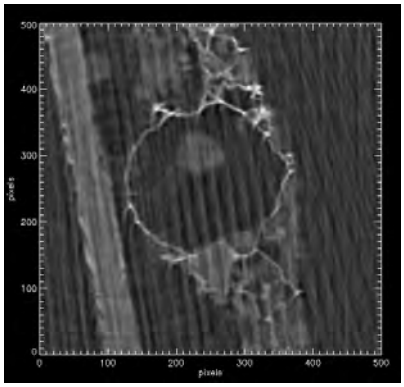

X2: Middle cross section

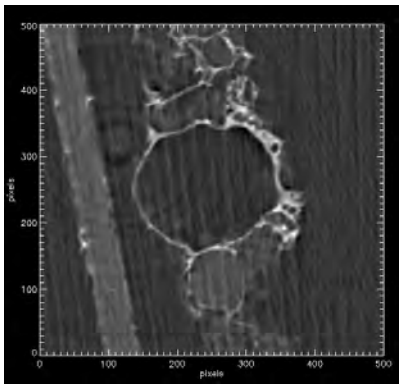

X3: Bottom cross section

L/S: 6/1, 500-1000 µm (scale bar: 500 µm)

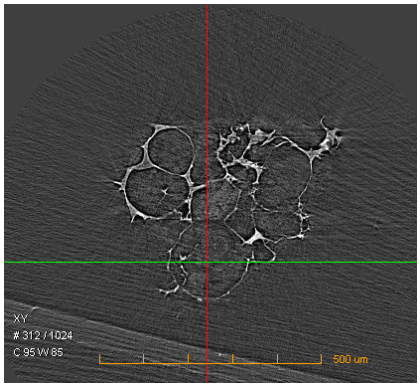

(a) XY cross section

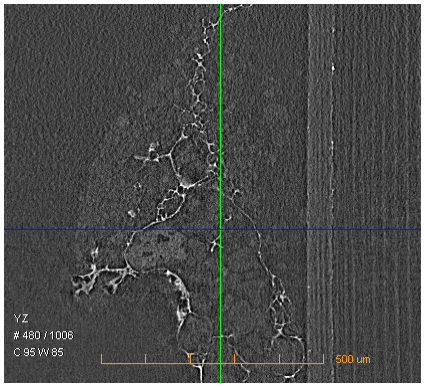

(b) YZ cross section

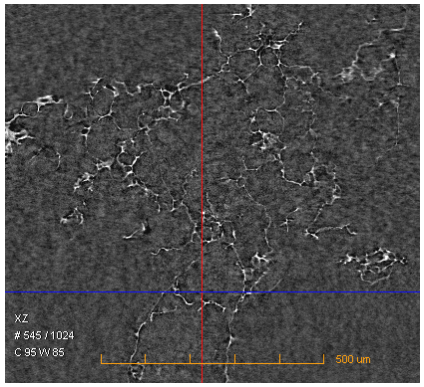

(c) XZ cross section

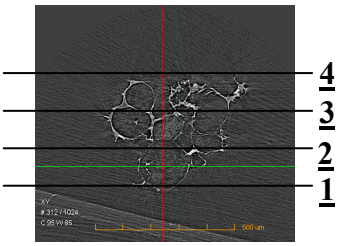

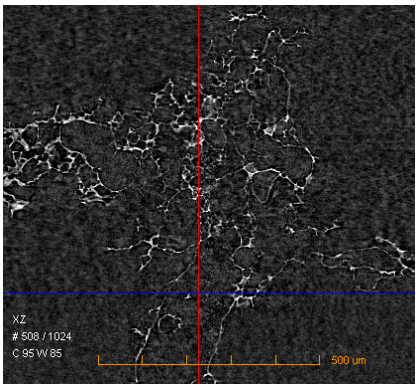

(a) XZ cross section-1

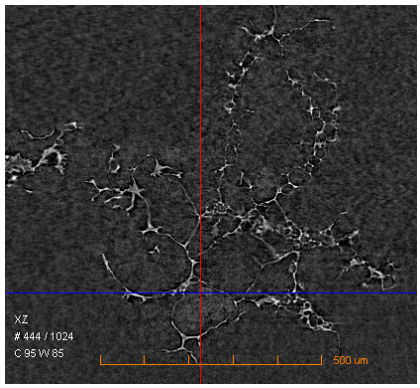

(b) XZ cross section-2

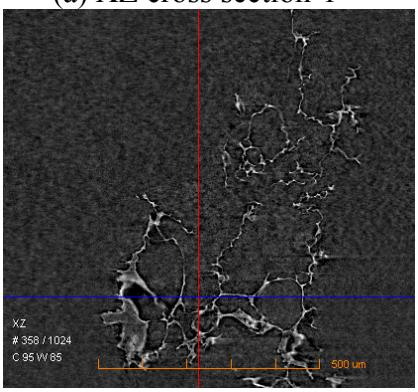

(c) XZ cross section-3

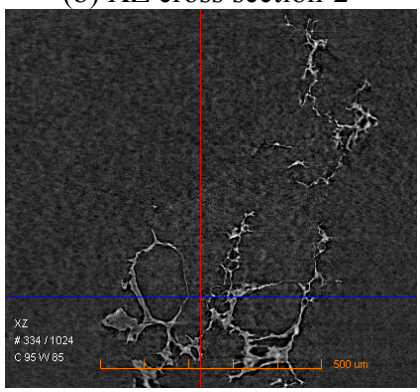

(d) XZ cross section-4

L/S: 3/1, 63-125 µm (scale bar: 100 µm)

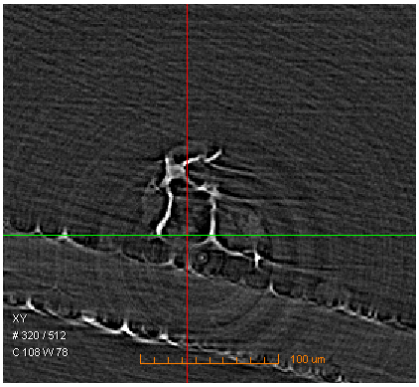

(a) XY cross section

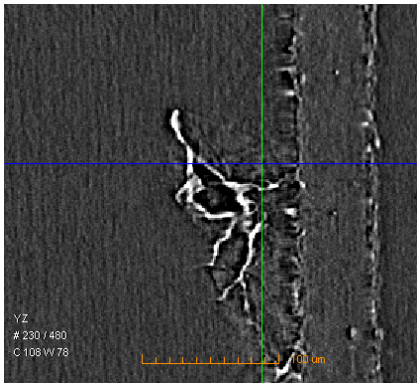

(b) YZ cross section

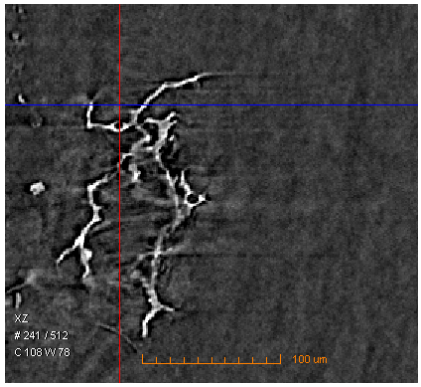

(c) XZ cross section

L/S: 3/1, 125-250 µm (scale bar: 100 µm)

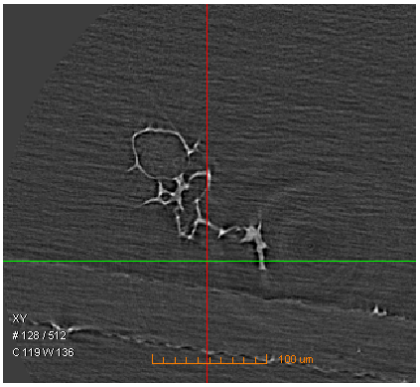

(a) XY cross section

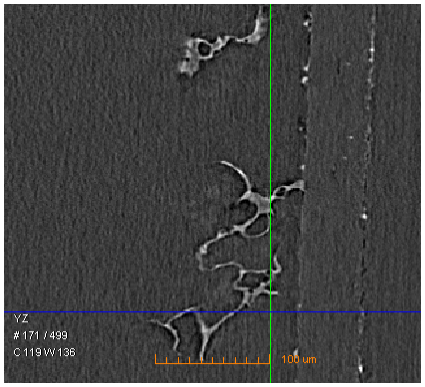

(b) YZ cross section

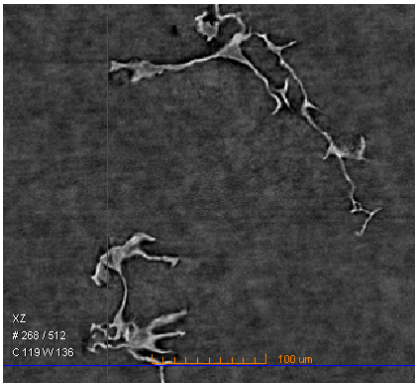

(c) XZ cross section-1

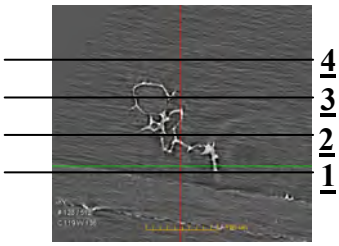

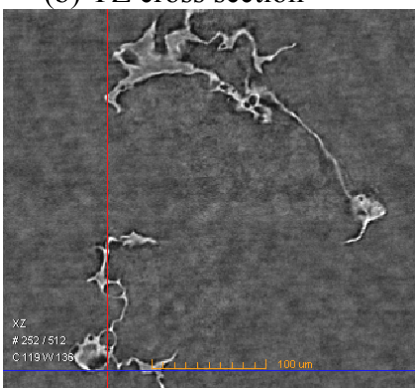

(a) XZ cross section-1

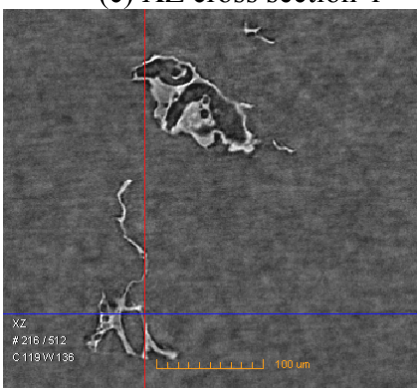

(b) XZ cross section-2

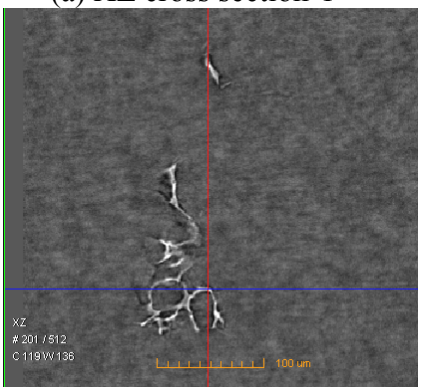

(c) XZ cross section-3

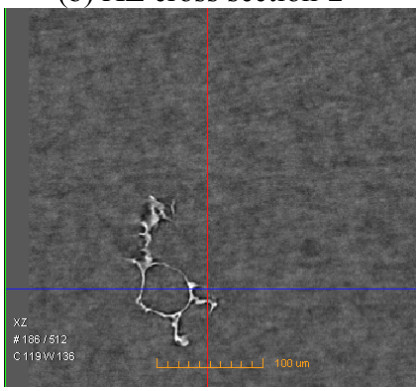

(d) XZ cross section-4

L/S: 3/1, 250-500 µm (scale bar: 200 µm)

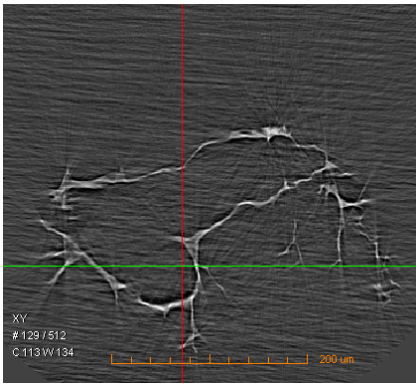

(a) XY cross section

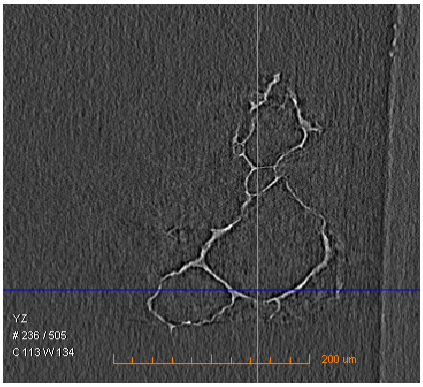

(b) YZ cross section

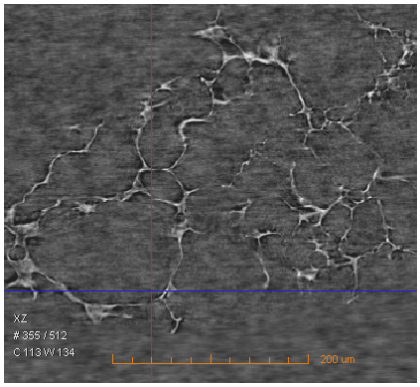

(c) XZ cross section

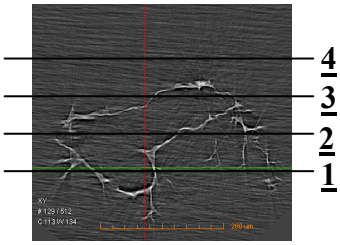

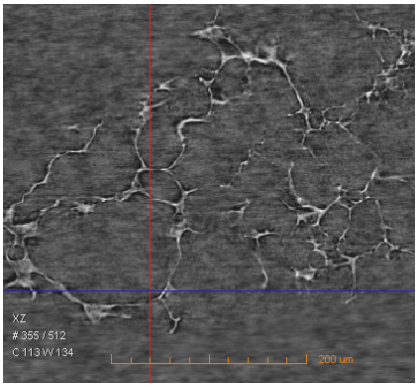

(a) XZ cross section-1

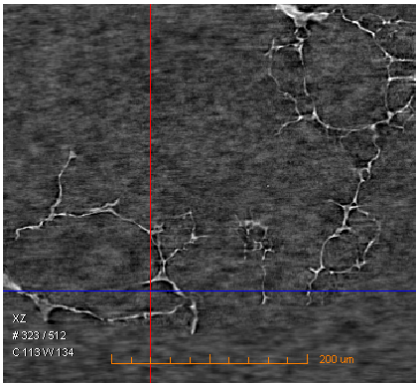

(b) XZ cross section-2

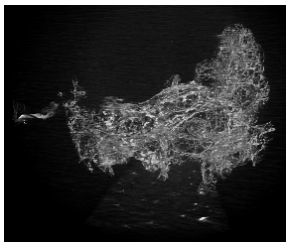

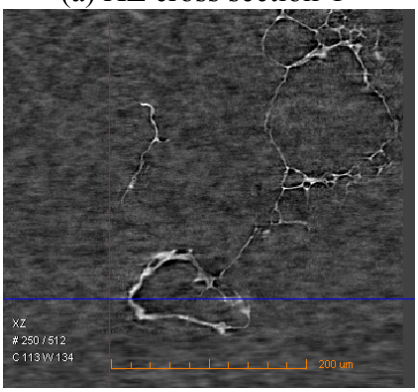

(c) XZ cross section-3

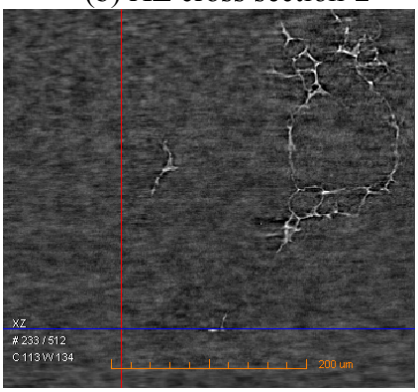

(d) XZ cross section-4

L/S: 3/1, 500-1000 µm (scale bar: 500 µm)

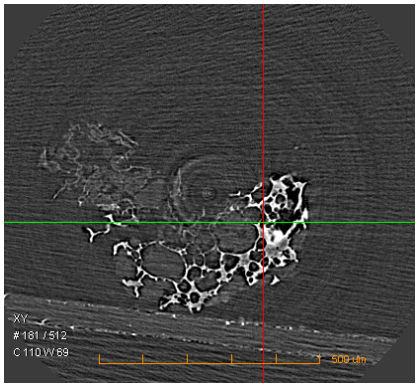

(a) XY cross section

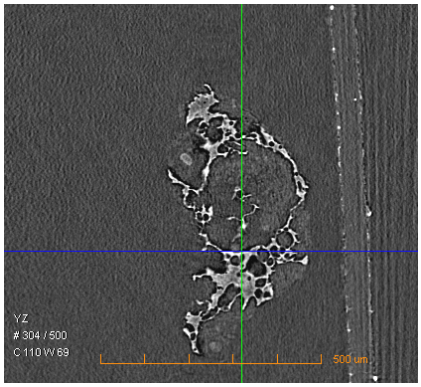

(b) YZ cross section

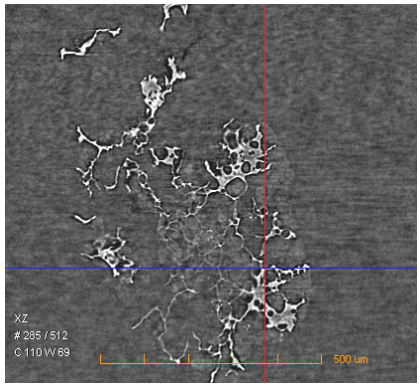

(c) XZ cross section

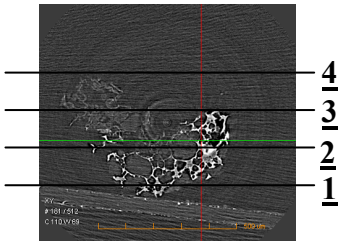

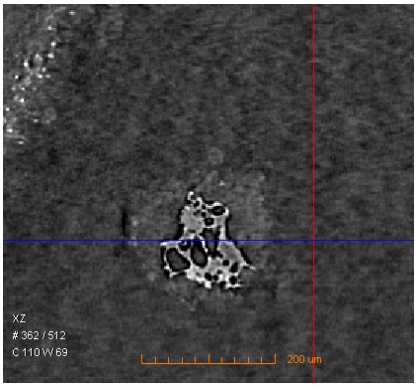

(a) XZ cross section-1

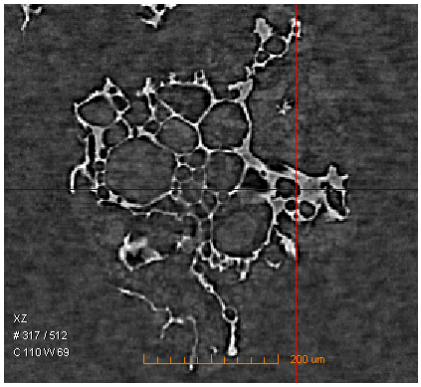

(b) XZ cross section-2

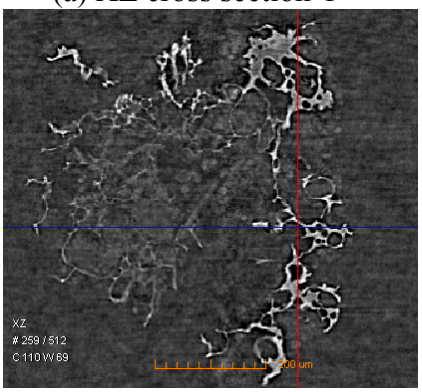

(c) XZ cross section-3

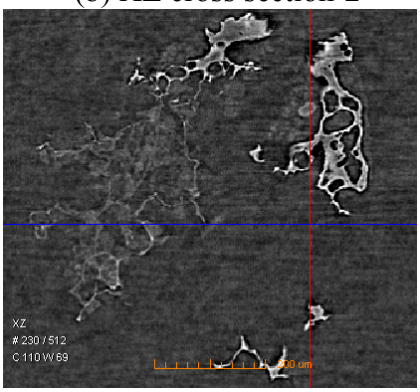

(d) XZ cross section-4

L/S: 1/1, 63-125 µm (scale bar: 100 µm)

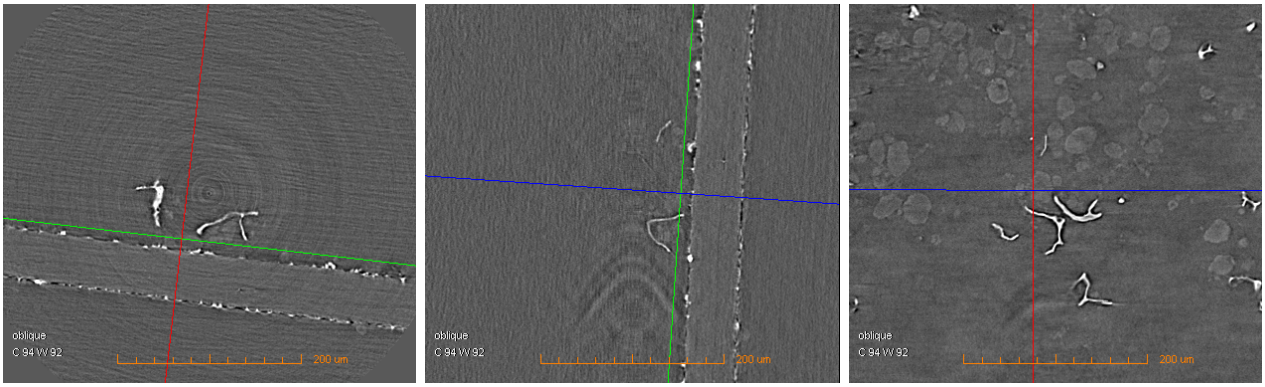

(a) XY cross section (b) YZ cross section (c) XZ cross section

Another example: L/S: 1/1, 63-125 µm (scale bar: 100 µm)

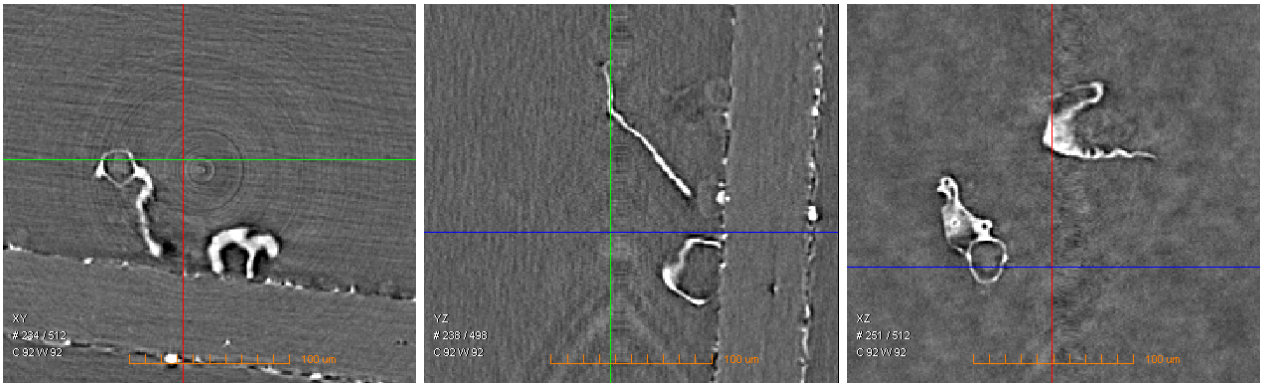

(a) XY cross section (b) YZ cross section (c) XZ cross section

L/S: 1/1, 125-250 µm (scale bar: 100 µm)

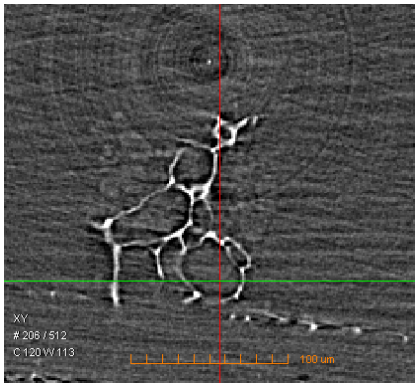

(a) XY cross section

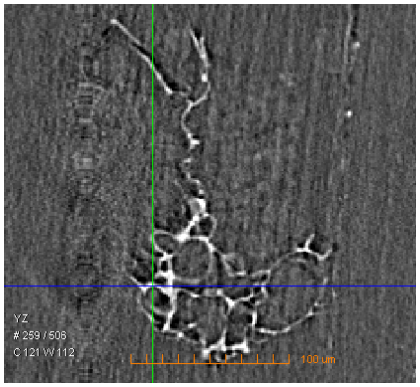

(b) YZ cross section

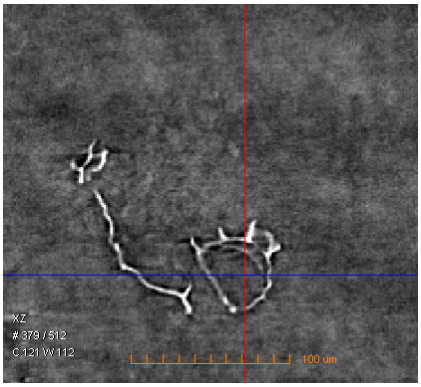

(c) XZ cross section

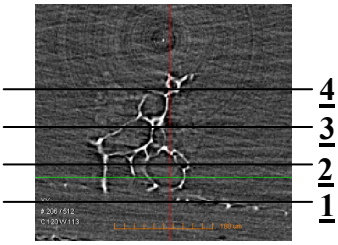

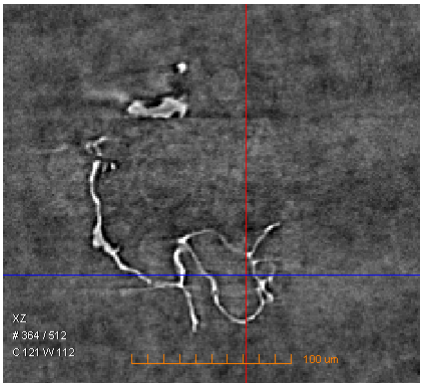

(a) XZ cross section-1

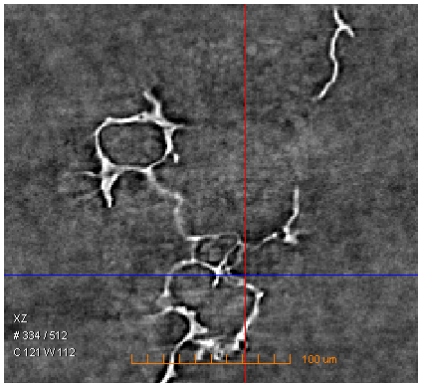

(b) XZ cross section-2

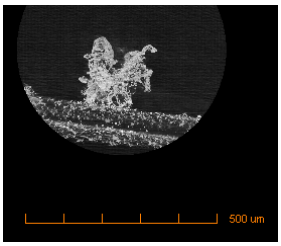

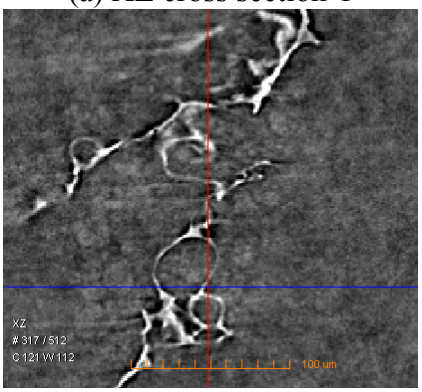

(c) XZ cross section-3

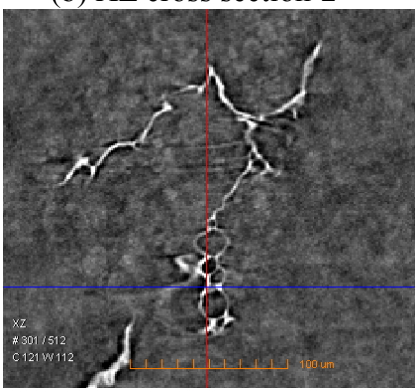

(d) XZ cross section-4

L/S: 1/1, 250-500 µm (scale bar: 200 µm)

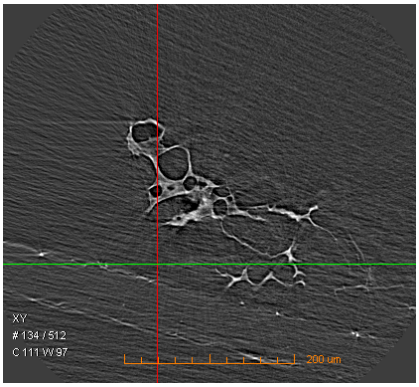

(a) XY cross section

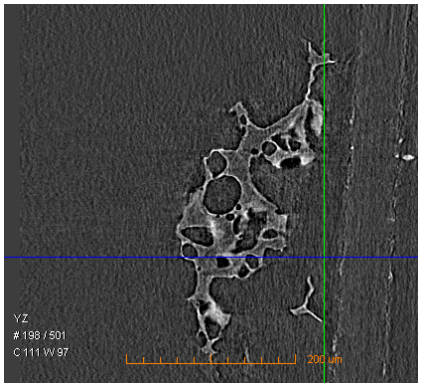

(b) YZ cross section

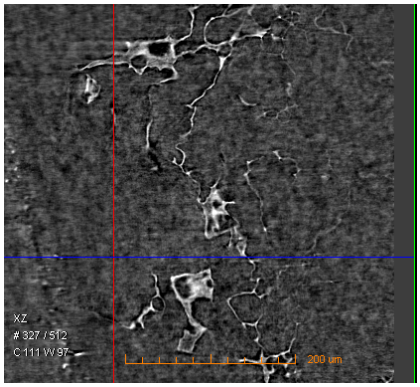

(c) XZ cross section

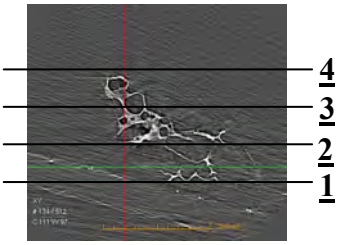

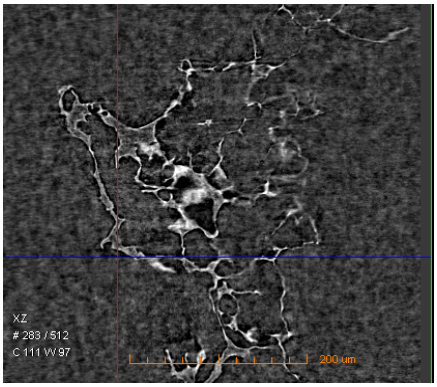

(a) XZ cross section-1

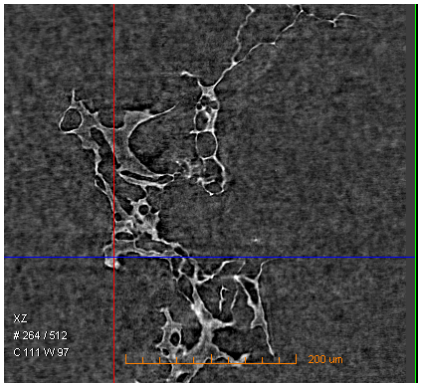

(b) XZ cross section-2

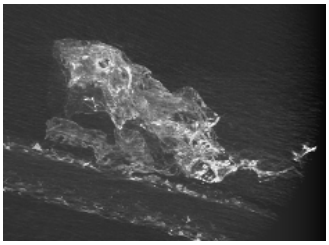

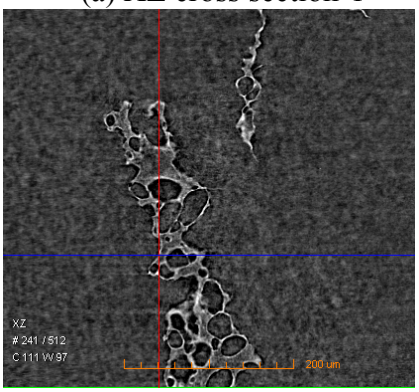

(c) XZ cross section-3

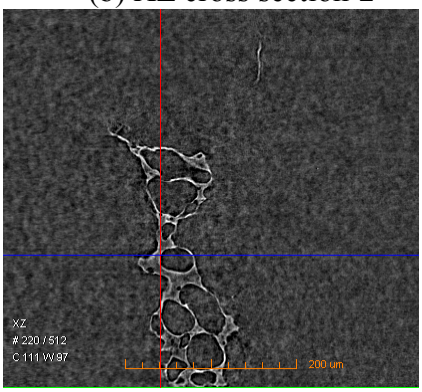

(d) XZ cross section-4

Another example, L/S: 1/1, 250-500 µm (scale bar: 100 µm)

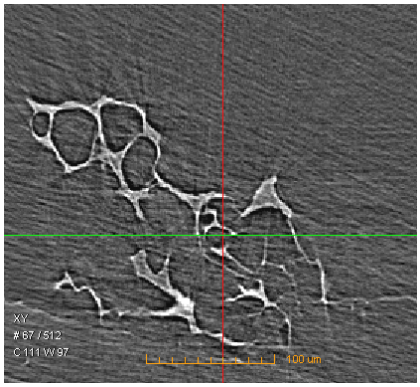

(a) XY cross section

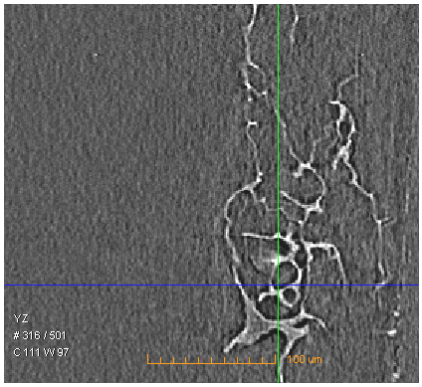

(b) YZ cross section

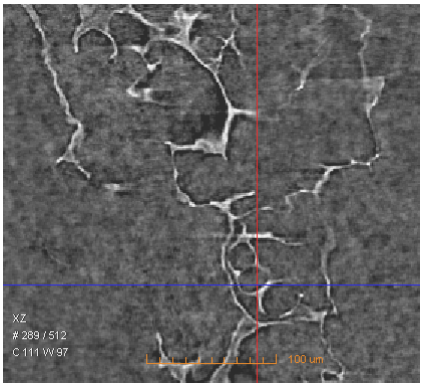

(c) XZ cross section

L/S: 0.5/1, 63-125 µm (scale bar: 100 µm)

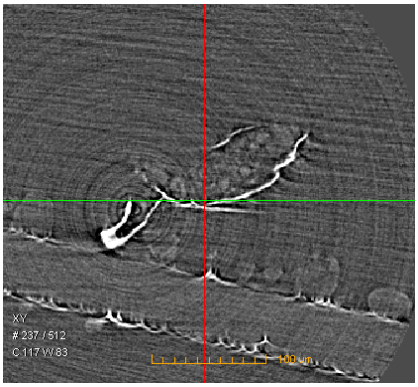

(a) XY cross section

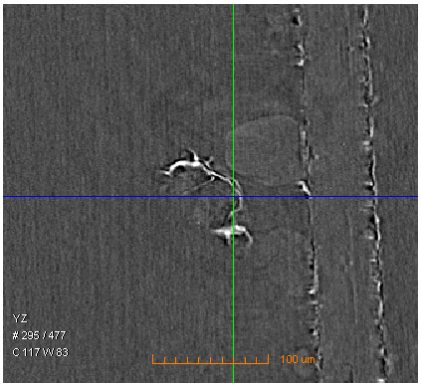

(b) YZ cross section

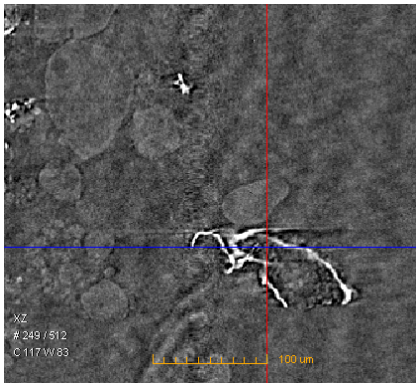

(c) XZ cross section

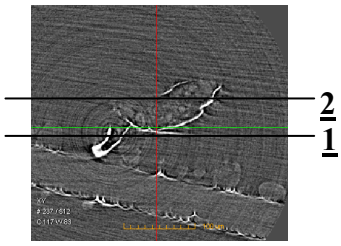

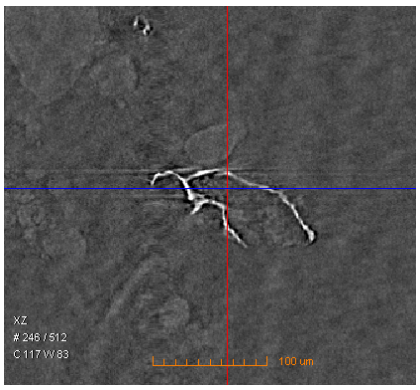

(a) XZ cross section-1

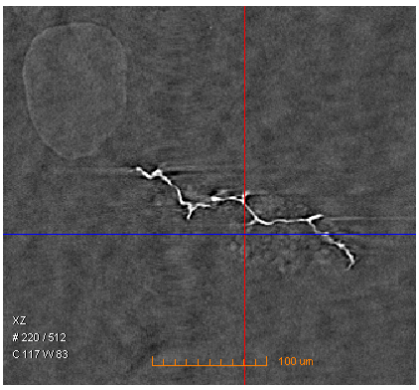

(b) XZ cross section-2

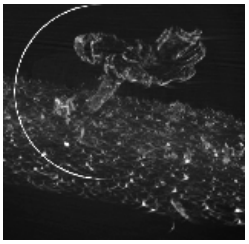

L/S: 0.5/1, 125-250 µm (scale bar: 100 µm)

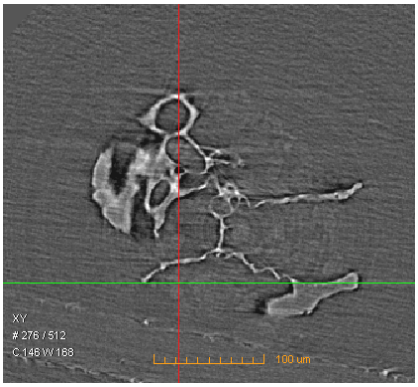

(a) XY cross section

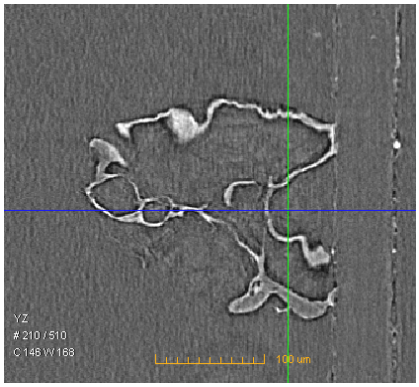

(b) YZ cross section

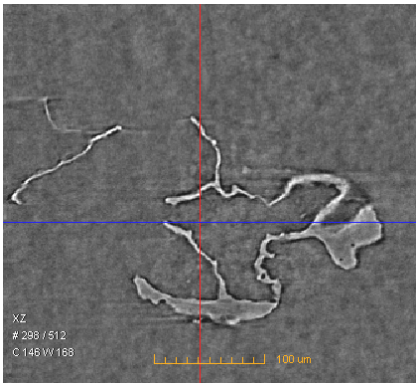

(c) XZ cross section

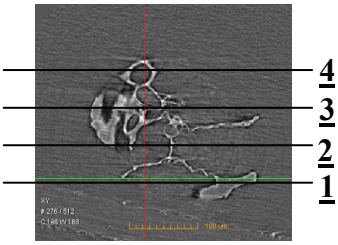

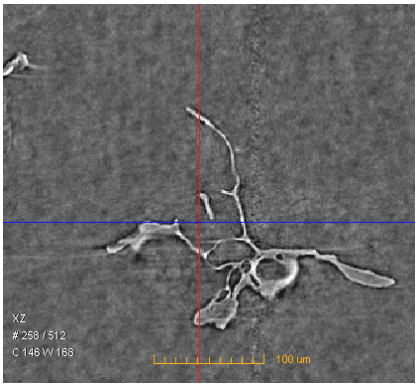

(a) XZ cross section-1

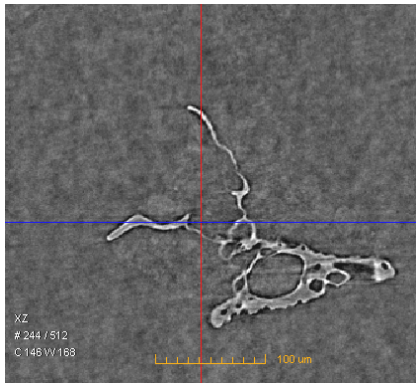

(b) XZ cross section-2

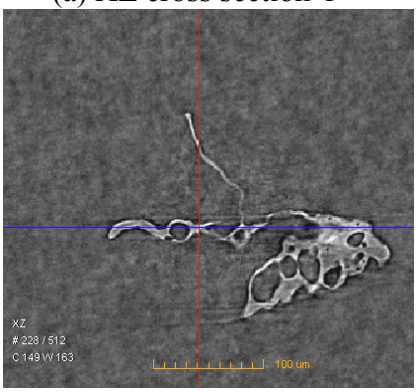

(c) XZ cross section-3

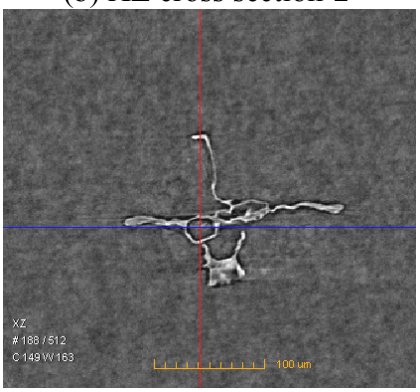

(d) XZ cross section-4

L/S: 0.5/1, 250-500 µm (scale bar: 200 µm)

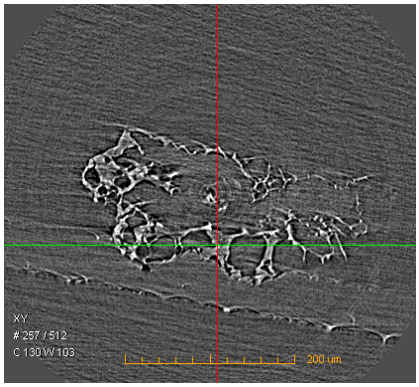

(a) XY cross section

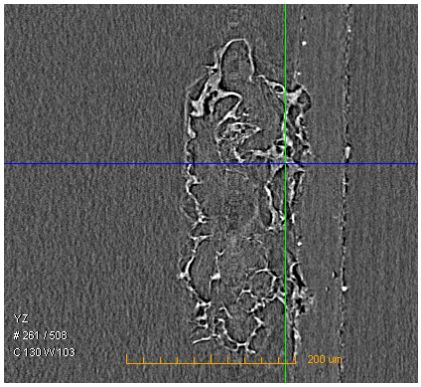

(b) YZ cross section

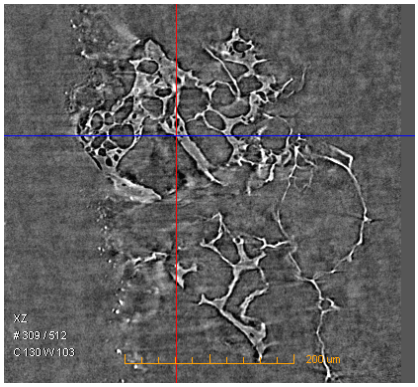

(c) XZ cross section

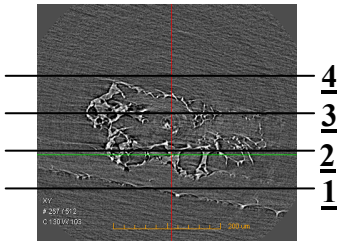

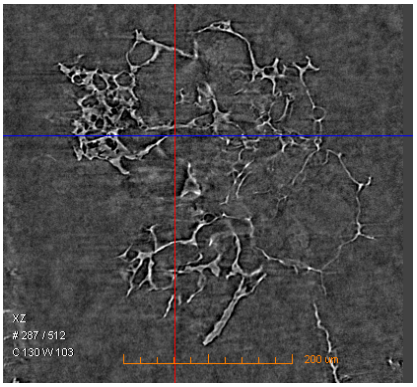

(a) XZ cross section-1

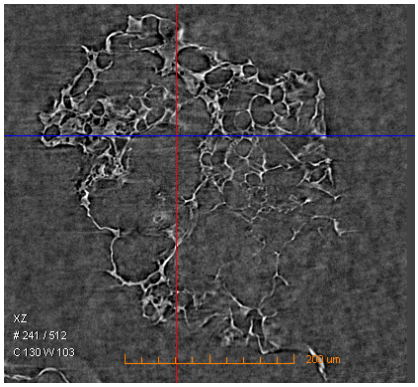

(b) XZ cross section-2

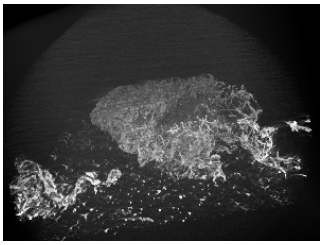

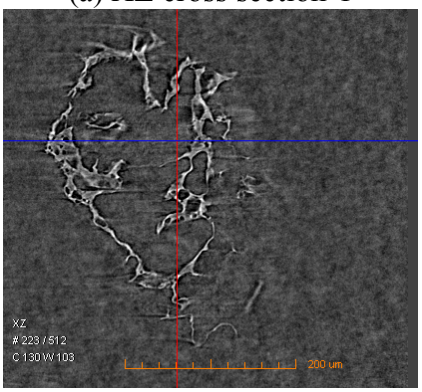

(c) XZ cross section-3

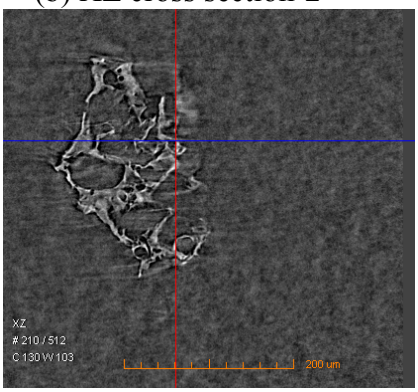

(d) XZ cross section-4

C

Published Version of:

Granulation of Hydrophobic Powders

(Chapter 3)

Powder Technology 189 (2009) 253–262

Contents lists available at ScienceDirect

Powder Technology

journal homepage: www.elsevier.com/locate/powtec

Granulation of hydrophobic powders

Karen P. Hapgood *, Batool Khanmohammadi

Monash Advanced Particle Engineering Laboratory, Department of Chemical Engineering, Monash University, VIC 3800 Australia

ARTICLE INFO

Available online 24 April 2008

Keywords:
Hydrophobic powder
Non-wetting
Solid-spreading
Nucleation
Wet granulation
Liquid marble

ABSTRACT

Granulation of hydrophobic powders is frequently required in the pharmaceutical industry. The structural complexity of new drug molecules mean that is increasingly common for entire classes of drug compounds to be highly hydrophobic. This creates considerable difficulty in understanding, controlling and trouble-shooting these industrial granulation processes.

There have been many recent advances in granulation theory. Essential to this theory is that wetting and spreading of the fluid through the powder particles is a prerequisite for good granulation. The possibility of a fine, hydrophobic powder spreading over the surface of the liquid during nucleation has been identified theoretically based on surface chemistry and as a potential nucleation mechanism. Recently, investigation confirmed that nucleation can occur by spreading of the sub-micron particles around the template drop to form a "liquid marble". The hollow granule structure formed by the "solid-spreading" nucleation mechanism suggests the possibility of using the controlled, open granule structure to manufacture designer structured agglomerates with advantageous properties, including controlled granule structure and size and excellent ideal flow and handling properties. This paper describes single drop solid-spreading nucleation experiments where single fluid droplets are placed onto loosely packed powder beds of hydrophobic powders and the formation of the powder shell observed. Experimental results and observations for some model systems are presented, together with a preliminary framework for liquid marble formation.

1. Introduction

Wet granulation is a particle size enlargement process where small particles are agglomerated using a liquid binder to form larger granules. Traditional reasons for granulating a material include improving flow and handling properties, increasing bulk density, reducing dust formation, and reducing segregation of materials [1]. More recently, granulation is motivated by a desire to *design structured agglomerates* for specialty products such as pharmaceuticals, controlled dissolution detergents and "instant" food powders such as sauces [2]. Problems during granulation of specialty products can cause enormous downstream processing problems and product that does not meet regulatory and quality specifications.

Great progress has being made in understanding and controlling granulation mechanisms (e.g. [3–6]) focusing on producing granules with a consistent, reproducible size distribution. This understanding has been applied to many industrial granulation processes, including pharmaceuticals [7], and detergents [8,5] to improve their performance. However, granulation of poorly wetting powders has not been addressed in the above works but is commonly performed in pharmaceutical, minerals and fertilizer granulation.

Granulation of hydrophobic powders is frequently required in the pharmaceutical industry. The structural complexity of new drug molecules mean that is increasingly common for entire classes of drug compounds to be poorly wetting (contact angles approx 70–90°) or highly hydrophobic (contact angle ≥90°). The poor wetting properties can create considerable difficulty in understanding, controlling and trouble-shooting these industrial granulation processes.

A surfactant is often added to the granulation fluid and/or powders to improve the wetting characteristics of the formulation but this is not possible in some applications such as iron ore granulation or certain pharmaceutical formulations due to either the cost of the surfactant or chemical interactions that may occur. For these industries, the current body of granulation theory is often not applicable, as it is inherently assumed in all current granulation research that the liquid must wet the powder in order for granulation to be successful. We review below the state of knowledge of hydrophobic powder granulation.

2. Literature review

2.1. Granulation of hydrophobic powders

The contact angle is defined as the internal angle formed by a liquid drop placed on a solid surface at the three phase contact line [9]. Measuring contact angles on powders are generally difficult and the reliable experimental methods have been recently reviewed [10]. In this paper, a hydrophobic powder system is defined as a powder or

* Corresponding author.
E-mail addresses: Karen.hapgood@eng.monash.edu.au (K.P. Hapgood), Batool.khanmohammadi@eng.monash.edu.au (B. Khanmohammadi).

0032-5910/$ – see front matter © 2008 Elsevier B.V. All rights reserved.
doi:10.1016/j.powtec.2008.04.033

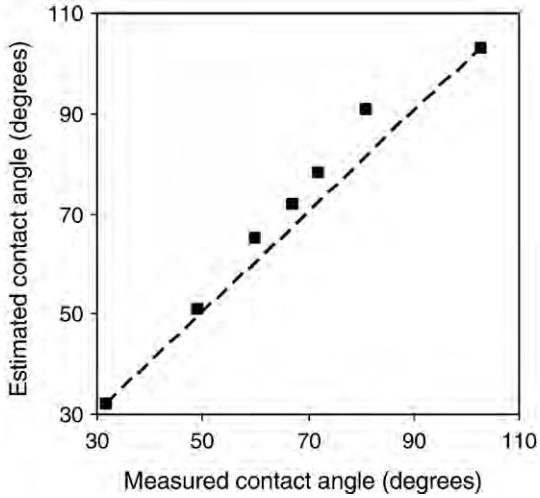

Fig. 1. Comparison of measured contact angles for lactose–salicylic acid combinations [13] versus the values predicted by Eq. (1).

combination of powders which have a contact angle with the granulating fluid greater than 90°.

The contact angle of the system directly affects the characteristics of the granulated product [11] measured the contact angles of neat pharmaceutical powders and powder combinations with water using the h–ε method [12]. The calculated contact angles were independent of particle size and cake porosity. For combinations of a hydrophobic drug powder and a hydrophilic excipient, the contact angle depended on the particle sizes. For the large particle size mixtures the hydrophobic material dominated the contact angle but for smaller particle sizes, a linear relationship was obtained between the cosine of contact angle and proportion of components [13] used water in a fluidized bed to granulation increasing proportions of a hydrophobic powder (salicylic acid with a contact angle of θ=103°) with a hydrophilic powder (lactose with contact angle θ=30°). The mean granule size decreased linearly as the mixture contact angle increased. One approach to estimating the average contact angle of a powder mixture is to use Cassie and Baxter's approach [9] of an average contact angle θ_{av}:

$$\cos\theta_{av} = f_1 \cos\theta_1 + f_2 \cos\theta_2 \quad (1)$$

where f_1 is the fraction of the powder mixture with contact angle equal to θ_1, and f_2 is the fraction of the powder mixture with contact angle equal to θ_2. Fig. 1 shows how Eq. (1) tends to overestimate the contact angle compared to the measured contact angles for lactose–salicylic acid mixtures [13]. There are a number of limitations with this approach (for example, see [14]) but Eq. (1) gives a result within 15% of more detailed surface analysis which this makes Eq. (1) useful in practical situations.

In addition to the demonstrated effect of contact angle on granule size [13], contact angle also directly affects granulation kinetics [15] granulated sand powders of varying contact angle (θ=38°, 58°, 75°, and >90°) with 1% CMC solution in a fluidized bed. As the contact angle increased, the rate of granule growth slowed, until barely no growth was achieved at a contact angle greater than 90°. These granules were observed to grow by coating of the granulating fluid on the particle surface, rather than by coalescence. A plot of the growth rate (based on gradient of each data set) versus adhesion tension was found to be linear [15]. Only one granulating fluid was used in these experiments, and further investigations would be required with several fluids to establish a general relationship between adhesion tension and granule growth kinetics.

Conventional granulation theory assumes that the liquid spreads over the solid particles. However, it is known that hydrophobic powders may spread around the drop during agitation and/or rolling of fluid drops on a hydrophobic powder. Spreading coefficients have been used by the pharmaceutical industry for many years to predict whether adequate wetting of the pharmaceutical powders will occur. The spreading coefficient λ is the difference between the works of adhesion and cohesion [16] and indicates whether spreading (i.e. further replacement of the solid–vapour interface with a solid–liquid interface) is thermodynamically favourable. There are three possibilities in spreading between a solid and a liquid:

a) The liquid may spread over the solid (λ_{LS}) and create a surface film;
b) The solid may spread or adhere to the liquid (λ_{SL}). The latter case will only occur if solid movement is physically possible, such as when the solid is in a powdered form. This is called *solid-spreading nucleation* [17].
c) Both the liquid and solid have high works of cohesion, and the solid–liquid interfacial area will be minimized (i.e. no spreading occurs). This final case represents non-wetting.

Granules formed by a fine layer of hydrophobic powder spread over the surface of a larger drop is "solid-spreading nucleation" [17].

A few studies of solid-over-liquid spreading (i.e. λ_{SL} driven) have been published but have been investigated on powder compacts [18] or large particles [16] rather than on loose powders of small particle size. Four articles discuss the effect of spreading coefficients on wet granulation [19,20,16,21] but these discuss the case where the drops are smaller than the particles.

Solid-spreading nucleation where the powder is fine compared to the size of the liquid drops has been observed [22–24], although the spreading coefficients were not measured to prove that the solid-over-liquid spreading coefficient λ_{SL} was the driving force. Some reports of "beading" of granulation fluid on hydrophobic powders have been published [25] where granulation produced wet patches and lumps. Granulation was improved using a foamed binder addition method [26,25] with the same granulating fluid, which may exploit pickering stability [9] or other interfacial effects present in foam to initiate contact between the hydrophobic particles, and presents an interesting area for future study.

It is also possible that the observed motion of particles over the surface of the fluid drop is driven by a force unrelated to the spreading coefficient λ_{SL}. Alternative explanations for the observed particle motion include (see Fig. 2):

a) Bulk motion within the drop caused by drop deformation and recoil motion after impact, which drives a corresponding surface flow around the drop entraining particles [27,28].
b) Particle motion towards low shear zones at the top of the drop to escape a high-shear region at the point of maximum drop deformation at impact [29].
c) Lateral capillary forces or other colloidal interfacial effects known to physically stabilize emulsions.

Without detailed characterization of the powder and liquid surface energies, including polar and dispersive components, the spreading coefficient driving force theory cannot be confirmed. This work plus a

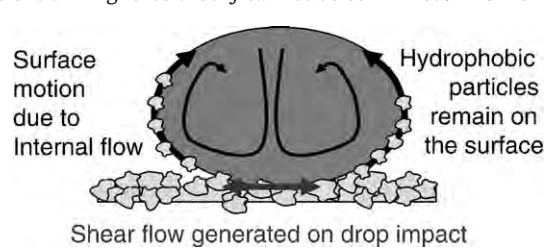

Fig. 2. Alternate explanations for the movement of particles around the surface of the drop include surface flow as a result of shear flow at the impact point and/or bulk flow within the drop following impact and deformation.

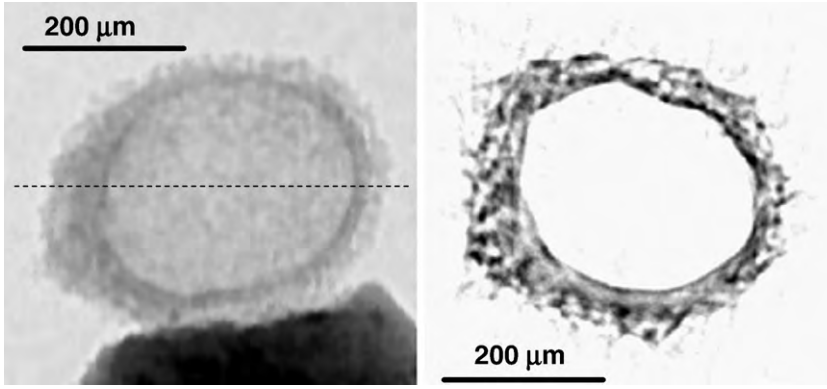

Fig. 3. X-ray transmission image (left) of a dried hollow granule formed from a liquid marble and reconstructed cross-section (right) showing hollow core [17].

review of underlying physics of the powder–fluid motion is currently underway.

2.2. Hydrophobic "liquid marbles"

Hydrophobic powders can be used in combination with water to produce stable and structurally strong spherical structures [30,31] described as "liquid marbles" formed from water droplets covered with hydrophobic lycopodium grains, which roll and bounce like glass marbles but deform and flex like a fluid. The hydrophobic particles sit at the air–water interface due to the high contact angle, and lateral capillary forces (created by deformation of the liquid surface) cause the particles to self-assemble into a powder film on the drop surface. The film of particles on the exterior form a powder shell which prevents the liquid from wetting the supporting surface and allows two liquid marbles to collide and rebound without coalescence. Two groups [17,32] have independently applied the liquid marble approach to produce designer particle assemblies for industrial applications.

Forny et al. [32] report "powder encapsulation" of fluid, where a hydrophobic fumed silica powder forms a powder shell encapsulating a water droplet core. They used two different vertical axis mixers — a high-shear mixer with knife blades and a triaxe mixer with rotating gyrating paddles. Two alternate methods were used to add water to the silica powder: direct loading of the liquid and powder into the mixer prior to commencing mixer operation; and by atomization over 3–4 min. In the lower shear triaxe mixer, atomization was required to form liquid marbles but they collapsed quickly to form a foam or mousse. The high-shear mixer was more successful and liquid marbles formed very quickly (approx 10 s). Using the most hydrophobic silica powder and high-shear processing conditions, up to 98% w/w water was able to be encapsulated with powder in the high-shear mixer. Formation of stable silica covered drops was most effective at the speeds of 12,000 min^{-1} or higher in a high-shear mixer with knife-edged impeller blades. Below this speed, the water formed a puddle at the base of the bowl and could not be successfully dispersed through the powder. Atomization into the high-shear mixer was not attempted. As the hydrophobicity of the silica powder decreased, the system became less stable, requiring higher impeller speed and more powder to encapsulate the same volume of liquid. Less hydrophobic silica powders were also more sensitive to shear conditions and collapse of the liquid marbles into a foam or mousse was reported [32]. The time for collapse reduced as the impeller speed and applied shear increased.

Liquid marbles and dry powder encapsulation are examples of particle design where the powder shell is used to protect the fluid interior [17] have extended the "liquid marble" approach by *drying* the liquid marbles to remove the interstitial fluid. The result is a spherical, hollow, granule (see Fig. 3) as demonstrated by micro X-ray tomography after drying of the granules. Between 70 and 78% w/w water was atomized over 7–8 min into a 2 L vertical axis high-shear mixer containing 70% w/w of a sub-micron hydrophobic powder (contact angle >90°). The granules were shown to be robust and survive handling and even milling in a screened comill.

Farber et al. [17] is the first to use a high loading of *hydrophobic* drug powder formulated with standard, *hydrophilic* pharmaceutical excipients. The presence of hydrophilic excipients components such as 20% w/w microcrystalline cellulose and 4% hydroxypropyl cellulose binder did not prevent liquid marble formation or self-assembly of the particles at the drop interface. The excipients stabilized the powder shell to allow the hollow structure to be preserved during drying. Even the presence of 1% sodium lauryl sulfate, a surfactant, as a powder did not prevent formation of liquid marbles, since the hydrophobic model drug powder constituted 90% of the batch on a volume basis. The work by [32] and [17] suggests how liquid marbles convert a normally problematic physiochemical property of hydrophobicity into a particle design advantage and show that liquid marbles can be produced using conventional granulation equipment. The work by Farber et al. [17] demonstrates that liquid marbles can be exploited as a precursor to hollow granules. This opens the way for a new generation of "designer granules".

Research into formation of hollow granules is an emerging field in melt granulation [33] and hydrophobic granulation [17,6]. Hollow

Table 1
Powder properties summary

Powder property	Salicylic acid	2-Ethoxybenzamide (EB)	Hydrophobic glass ballotini			
			AC	AE	AG	AH
D_{10} (μm)	69	1.89	139.3	88.65	47.36	47.10
D_{50} (μm)	131.6	4.67	190.86	121.12	65.58	65.22
D_{90} (μm)	501.6	12.74	261.49	165.20	90.44	89.83
Surface mean d_{32} (μm)	Not measured	3.76	185.25	117.6	63.47	63.11
Volume mean d_{43} (μm)	Not measured	7.02	196.59	124.64	67.57	67.18
Malvern specific surface area (m^2/kg)	Not measured	1600	32.4	20.8	94.5	95.1
True particle density (g/cm^3)	1.43	1.27	2.48	2.44	2.47	2.46
Molecular formula	2-(HO)$C_6H_4CO_2H$	$C_2H_5OC_6H_4CONH_2$	SiO_2	SiO_2	SiO_2	SiO_2

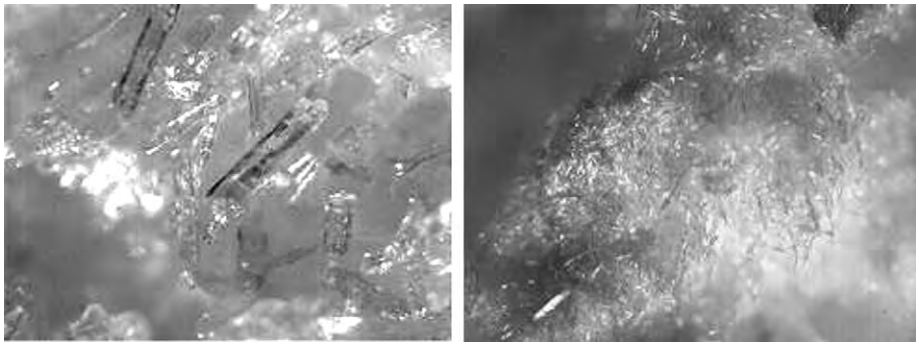

Fig. 4. Optical microscope images of salicylic acid needles (left) and 2-ethoxybenzamide (right).

granules formed by solid-spreading nucleation can be used to produce "designer particles" with pre-specified desirable properties, such as:

- Simultaneous control of granule size and structure — granule size is controlled by the drop size under low spray flux conditions and the liquid marble structure is self-assembled during the granulation process.
- Ability to easily handle a high loading of a hydrophobic drug.
- Spherical granules with excellent flow properties.
- Fast, mass-transfer limited drying due to the thin powder shell structure, which eliminates the diffusion-controlled, falling rate drying period.
- Highly porous granules due to hollow interior suggests good particle rearrangement and compression characteristics for tabletting plus reproducible dissolution due to the consistent granule and tablet structure.
- Potential to load one soluble drug in the fluid interior and granulate with a second hydrophobic drug to form the outer shell.

These properties make the design of hollow granules ideal for high-value applications in the pharmaceutical, food and cosmetics industries.

To design a hollow granule design requires a sound understanding of:

1. Controlling mechanisms of liquid marble formation via solid-spreading nucleation,
2. Formulating to produce strong stable liquid marbles,
3. Maximizing granule strength and stability to avoid collapse of the structure [17,32].
4. Granulation mechanism and kinetics linked with the granule growth regime map [3,4]

These main areas of research will ultimately lead to an extension of granulation theory to encompass the granulation of highly hydrophobic powders via solid-spreading nucleation. This paper presents the first steps towards this aim, by studying the nucleation behaviour of a single drop on a bed of hydrophobic powder.

3. Experimental

A loosely packed powder bed was formed by lightly sieving the powder into a petri dish and scraping level to produce a smooth powder surface. A loosely packed bed approximates the powder state in an agitated granulator [34]. A 100 μl Hamilton precision syringe with a 22 gauge needle was positioned just above the bed surface. Drops (4 μl volume) were allowed to detach and gently fall 1–2 mm before landing on the bed surface. This distance was selected to minimize drop bouncing and rolling, and is not intended to represent the typical length scale of the granulation process. A Stereo microscope (SMZ Series) with a 3MP camera operating at 30 frame/s was used to film a single drop impinging on to the powder surface.

3.1. Materials

Glass ballotini spheres (Potters Industries Pty Ltd.) in four size grades (AC, AE, AG, AH) were used. In order to make the glass beads hydrophobic, SIGMACOTE solution (chlorinated organopolysiloxane in heptane, Sigma-Aldrich Pty Ltd.) was used. Glass beads are an ideal model powder but other more realistic powders are also required. Two hydrophobic drug powders were used: Salicylic acid (99%ACS Reagent, Sigma-Aldrich Pty Ltd.) with a contact angle of 103° [11] and 2-Ethoxybenzamide (97% Sigma-Aldrich Pty Ltd.) which has been used elsewhere as a model hydrophobic drug [35]. The particle size distribution was analysed by dry laser diffraction using a Malvern Mastersizer 2000, although salicylic acid was measured by sieving. The true density of the particles was measured using Helium pycnometry (Micromeritics Accupyc 1330). Particle properties are summarized in Table 1 and Fig. 4 shows optical microscope images of the needle-shaped salicylic acid and ethoxybenzamide particles. We note that although the finest particle size specifications is for the AH ballotini grade, the particle size distributions were essentially identical to the AG grade.

Several different binder fluids were used: distilled water, four grades of poly-ethylene glycol (PEG200, PEG300, PEG400, and PEG600), glycerol and a 1% mass sodium dodecyl sulfate (SDS) solution. A summary of binder properties is given in Table 2.

4. Results

Experiments initially focused on screening material combinations to find suitable systems for further study. Table 3 summarizes the experimental observations and some pictures of liquid marbles are shown in Fig. 5. Water was able to form a liquid marble with all the powders tested, and glycerol was able to form liquid marbles with all powders except ethoxybenzamide. The addition of 1%SDS surfactant to the water eliminated liquid marble formation by reducing the contact angle below 90° allowing the drops to penetrate into the powder.

Table 2
Granulating fluid properties at 20 °C

Granulating fluid	Density ρ_L (g/mL)	Surface tension γ_{LV} (mN/m)	Viscosity μ (mPa s)	Manufacturer
Distilled water	1	72.0[a]	1	N/A
1% SDS	~1	35[d]	~1	Sigma-Aldrich
Glycerol	1.25[b]	63.7[a]	950	Fluka
PEG200	1.127[b]	43.7[c]	60[b]	Sigma-Aldrich
PEG300	1.125[b]	43.7[c]	95[b]	Fluka
PEG400	1.126[b]	43.7[c]	120[b]	Sigma-Aldrich
PEG600	1.128[c]	43.7[c]	152.9[c]	Fluka

a — Data from (a) [18]. (b) Sigma-Aldrich. (c) [22] and (d) [36].

Table 3
Summary of liquid marble formation experiments

Powder	Fluid	Liquid marble?	Comments
Salicylic acid	PEG200	No	Drop penetration — no powder shell.
	PEG300	No	Drop penetration — no powder shell
	PEG400	No	Drop penetration — no powder shell
	PEG600	No	Drop penetration — no powder shell
	Distilled water	Yes	Stable liquid marble formed
	Glycerol	Yes	Stable liquid marble formed
	Water + 1% SDS	No	Drop penetration — no powder shell
2-Ethoxybenzamide (E.B.)	PEG200	No	Liquid marble formed and sank simultaneously
	PEG300	No	Liquid marble formed and sank simultaneously
	PEG400	No	Liquid marble formed and sank simultaneously
	PEG600	No	Liquid marble formed and sank simultaneously
	Distilled water	Yes	Stable liquid marble formed
	Glycerol	No	Liquid marble formed and sank simultaneously
	Water + 1% SDS	No	Drop penetration — no powder shell
Hydrophobic glass ballotini (AC)	PEG200	No	Drop penetration — no powder shell
	PEG300	No	Drop penetration — no powder shell
	PEG400	No	Drop penetration — no powder shell
	PEG600	No	Drop penetration — no powder shell
	Distilled water	Yes	Stable liquid marble formed
	Glycerol	Yes	Stable liquid marble formed
	Water + 1% SDS	No	Drop penetration — no powder shell
Hydrophobic glass ballotini (AE)	PEG200	No	Drop penetration — no powder shell
	PEG300	No	Drop penetration — no powder shell
	PEG400	No	Drop penetration — no powder shell
	PEG600	No	Drop penetration — no powder shell
	Distilled water	Yes	Stable liquid marble formed
	Glycerol	Yes	Stable liquid marble formed
	Water + 1% SDS	No	Drop penetration — no powder shell
Hydrophobic glass ballotini (AG)	PEG200	Yes	Stable liquid marble formed
	PEG300	No	Drop penetration — no powder shell
	PEG400	No	Drop penetration — no powder shell
	PEG600	No	Drop penetration — no powder shell
	Distilled water	Yes	Stable liquid marble formed
	Glycerol	Yes	Stable liquid marble formed
	Water + 1% SDS	No	Drop penetration — no powder shell
Hydrophobic glass ballotini (AH)	PEG200	Yes	Stable liquid marble formed
	PEG300	No	Droplet covered with powder; then sank
	PEG400	No	Droplet covered with powder; then sank
	PEG600	No	Droplet covered with powder; then sank
	Distilled water	Yes	Stable liquid marble formed
	Glycerol	Yes	Stable liquid marble formed
	Water + 1% SDS	No	Drop penetration — no powder shell

There are some interesting observations noted in Table 3. First, water and glycerol had the two highest surface tensions (of the three fluids that were used) and were able to form liquid marbles with almost all the powders tested. Based on the introduction, we expect that interfacial tension will be an important parameter in liquid marble systems, although with only three data points we cannot draw any conclusion at this stage. Second, there appears to be a viscosity effect, where low viscosity PEG200 was able to form a liquid marble with AG and AH ballotini, but PEG300 and upwards were unsuccessful. However, the most viscous fluid tested so far, glycerol, was able to form liquid marbles which suggests that viscosity is a secondary effect compared to the surface chemistry of the powder–binder system.

Third, there appears to be a particle size effect, where formation of liquid marbles using PEG200 was only successful on the two finest ballotini grades – AG and AH – which had identical particle size distributions as noted earlier. This implies either that the driving force (currently not known) is not strong enough to carry the largest ballotini particles around the drop surface, or that there is a drop to particle size ratio criterion for liquid marble formation.

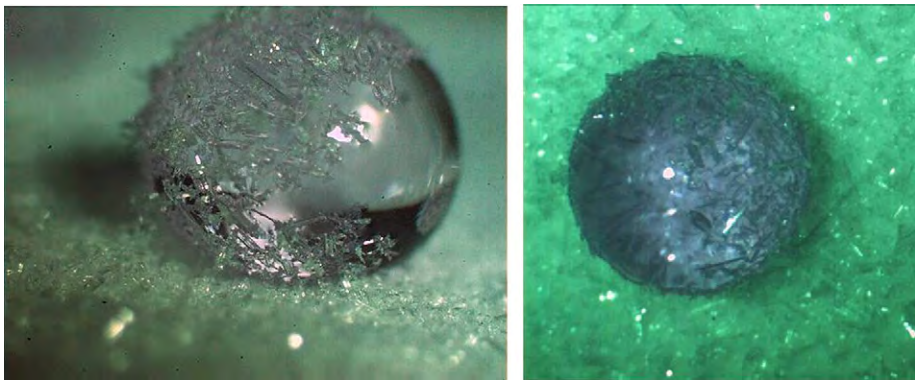

Fig. 5. Example of liquid marbles formed by solid-spreading nucleation of salicylic acid powder over a water droplet approximately 2 mm diameter.

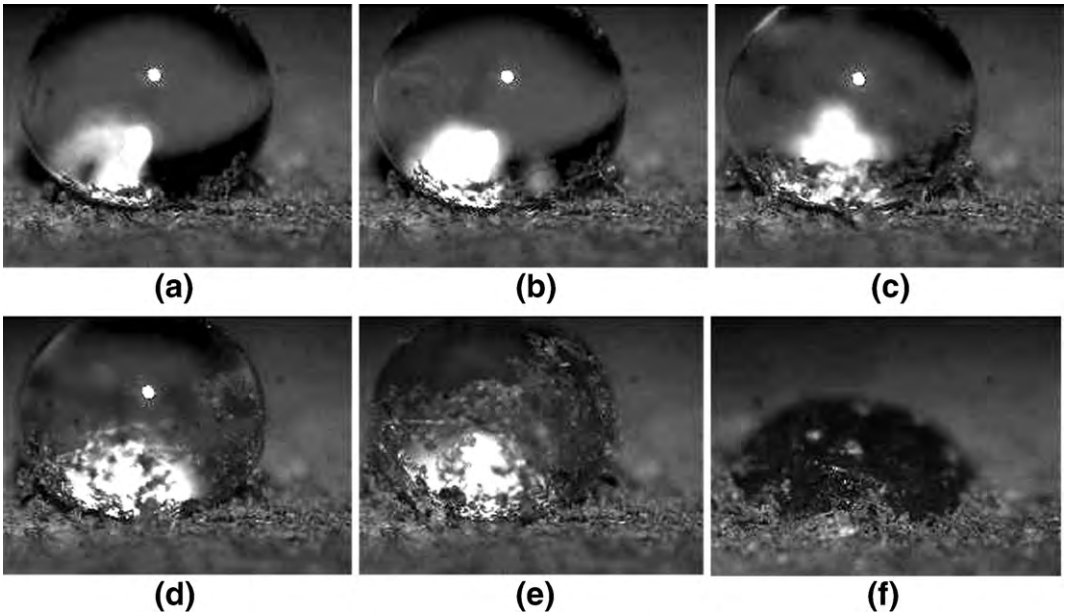

Fig. 6. Water droplet (~2 mm diameter) on cinnamon powder showing initial stages of liquid marble formation, after (a) impact; (b) 1.4 s; (c) 3 s; (d) 6 s; (e) 10 s; followed by penetration into the powder bed (f) after 3 min.

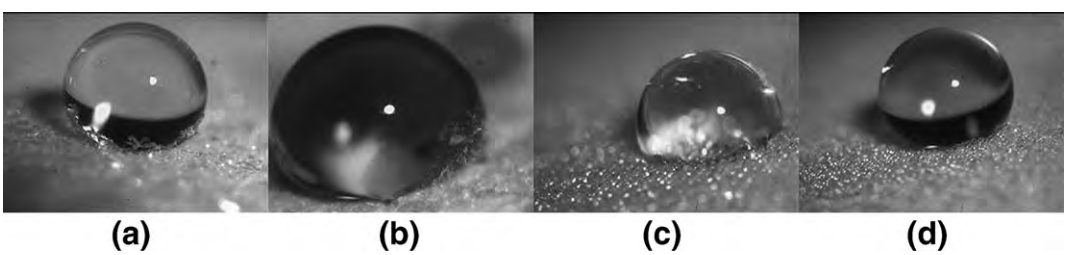

Fig. 7. Careful placement of a water droplet (d_d ~2 mm) on (a) salicylic acid, (b) EB, (c) AE glass ballotini, (d) AG glass ballotini shows no liquid marble formation.

Finally, it appears to be possible to temporarily form liquid marbles from systems with contact angles less than 90° — a number of combinations in Table 3 were observed to initially form a powder layer on the drop exterior but then penetrate completely into the powder bed. This is shown in Fig. 6 for water on food-grade cinnamon powder. Cinnamon in a naturally-derived material which contains many sub-components. We postulate that a soluble component at the surface of the ground cinnamon particle slowly leaches into the fluid, eventually reducing the contact angle to below 90°, causing a switch in behaviour. However, this explanation does not explain the behaviour for several other powder–fluid combinations, such as the ethoxybenzamide powder with PEG and glycerol. Further investigation, including contact angle measurements of the powders, is underway.

The experiments in Table 3 were performed by allowing the drop to fall a short distance of approximately 1–2 mm. An increased tendency to form a liquid marble was observed when the drop rolled or deformed during impact. A second series of experiments was performed where the drops of water and glycerol were placed extremely gently onto the powder bed to avoid bulk motion within the drop interior due to impact or rolling. Fig. 7 shows that there is no surface coverage when a water drop is carefully placed on several particles, presumably because no bulk motion is created within the droplet to entrain particles in the surface flow. The same behaviour was also observed for careful placement of glycerol droplets.

Alternatively, the particles can be spread over the uncovered droplet by shaking the petri dish. Fig. 8 shows a much higher level of surface coverage compared to the careful placement experiment shown in Fig. 7. Moreover, if the droplet is allowed to roll on the surface, the droplet will become covered with particles, as described by [30,31] and shown in Fig. 8(b).

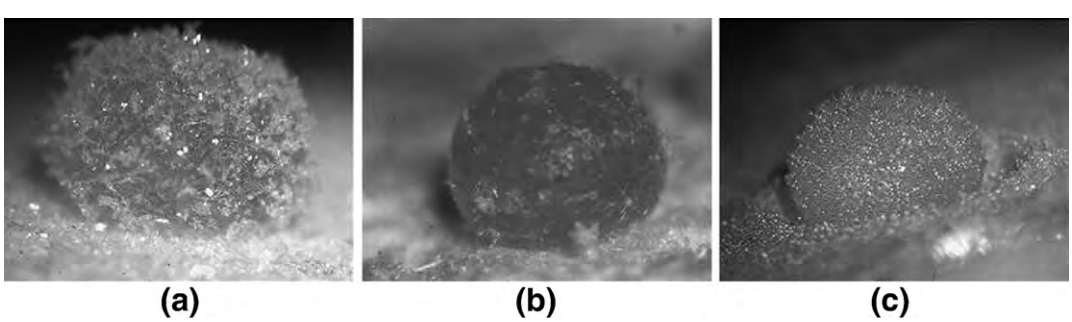

Fig. 8. Effect of rolling or shaking on surface coverage. (a) Water on salicylic acid after shaking, (b) water on EB after rolling and (c) glycerol after shaking on AH ballotini (d_d is ~2 mm).

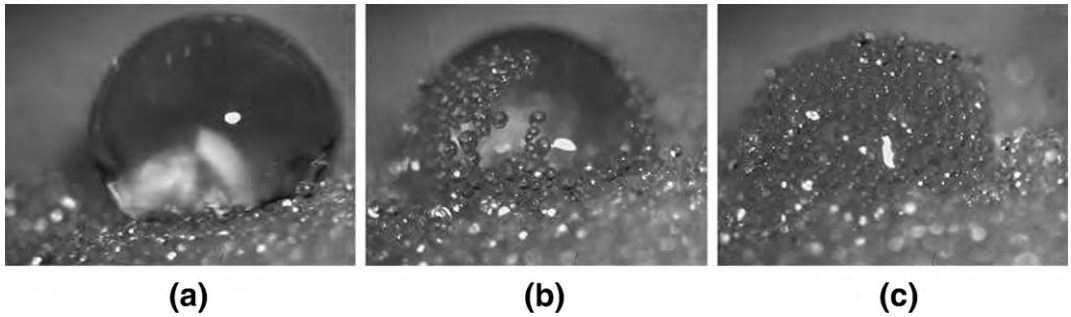

Fig. 9. Liquid marble formation using water drop (~2 mm diameter) and hydrophobic AC ballotini powder from (a) 0 cm height, (b) 15 cm height and (c) higher than 30 cm level.

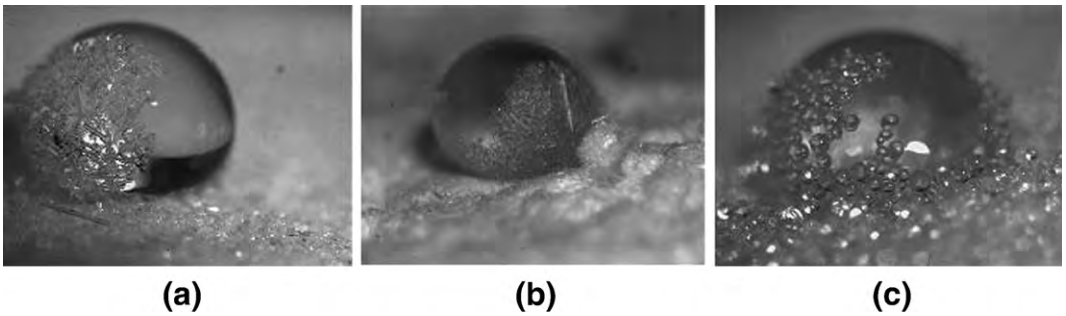

Fig. 10. Partly formed powder sheets due to lateral capillary forces. Water droplet (d_d ~2 mm) on (a) Salicylic acid, (b) EB, (c) hydrophobic AC ballotini.

To test whether bulk motion is responsible for the formation of the powder shell, the drop release height was increased to 15 cm and 30 cm. These heights are more representative of the spray height in a granulation process, although the drop sizes used here are much larger than typically found in an atomized spray. Fig. 9 shows the gradual increase in surface coverage for a water-AC ballotini system as the drop height is increased. The images in Fig. 9 were taken after the system had stabilized and no further powder movement was observed. Since the physiochemical properties of these experiments are constant, the kinetic energy of the drop appears to determine the extent of shell formation. In practical granulation situations, we presume that the drop surface is instantly covered with powder due to the highly agitated powder motion in the fluidized bed or mixer granulator.

When the drop is only partially covered with powder, the powder is not evenly distributed over the powder surface, but instead accumulates to form a sheet powder (refer to Fig. 10). Individual particles move across the drop surface until they aggregate into a film. This phenomena is caused by attractive lateral capillary immersion forces [32].

5. Discussion

The solid-over-liquid spreading coefficient λ_{SL} [16] may provide a quantitative method to predict whether a given formulation will form liquid marbles. However, our results also suggest that bulk motion of the drop, due either to rolling or impact, is required for solid-spreading nucleation to occur. It is also possible that solid-spreading motion is driven entirely by a physical flow mechanism (refer to Fig. 2), where the degree of surface coverage is proportional to the size of the bulk flow generated within the drop, and that the spreading coefficients are not applicable to liquid marble formation. Surface energy measurements by inverse gas chromatography are underway to determine whether λ_{SL} can be used as a predictive tool.

All of the hollow granules formed in these studies eventually collapsed into hemispheres (see Fig. 11). Only multi-component formulations can produce inter-particulate bonds to stabilize hollow granules once the template drop has been removed during drying. To date, only one investigation [17] into liquid marbles and solid-spreading nucleation has used a multi-component formulation of powders. All other studies have used a single fluid on a neat hydrophobic powder [31,32]. This is also an area requiring significant further investigation.

In order for a stable, spherical, liquid marble to form from a single drop via solid-spreading nucleation, we outline a series of steps that must occur:

1. A single drop must be formed that is much larger than the size of the powder particles (i.e. $d_d \gg d_p$) [37–39] but small enough to form a spherical drop rather than a distorted pool or puddle i.e. Bond number $B_0 = \rho_L g R^2/\gamma_{LV} < 1$ [31].
2. The drop must land on the powder and survive the impact without breaking or shattering into smaller droplets i.e. Weber number $We = \rho_L d_d v^2/\gamma_L < 1000$ [40] and Ohnesorge number $Oh = \mu/(\rho_L \gamma_{LV} R)^{0.5} > 0.05$ [41].
3. The fluid must have a contact angle θ greater than 90° with the powder to prevent penetration of the drop into the powder bed [9,34].

Fig. 11. Water–salicylic acid granule that has collapsed into a hemisphere during air drying. Granule diameter is approximately 2 mm.

4. The powder must spread around the air–liquid interface of the drop to form a shell — driven either through impact induced surface flows [27,28] or by spreading coefficients [16] as discussed earlier.
5. The powder must be able to self-assemble into a sufficiently dense layer to prevent contact of the drop interior with a supporting surface [32].

If any of these conditions are not fulfilled, a liquid marble will not be formed. In addition, in order to maintain small individual drop templates, the dimensionless spray flux must be low [42]. Under low spray flux conditions the granule size would be controlled by the atomized drop size i.e. the drop controlled nucleation regime [43].

Fig. 12 proposes a schematic flow sheet summarizing the formation of stable liquid marbles, incorporating several dimensionless groups

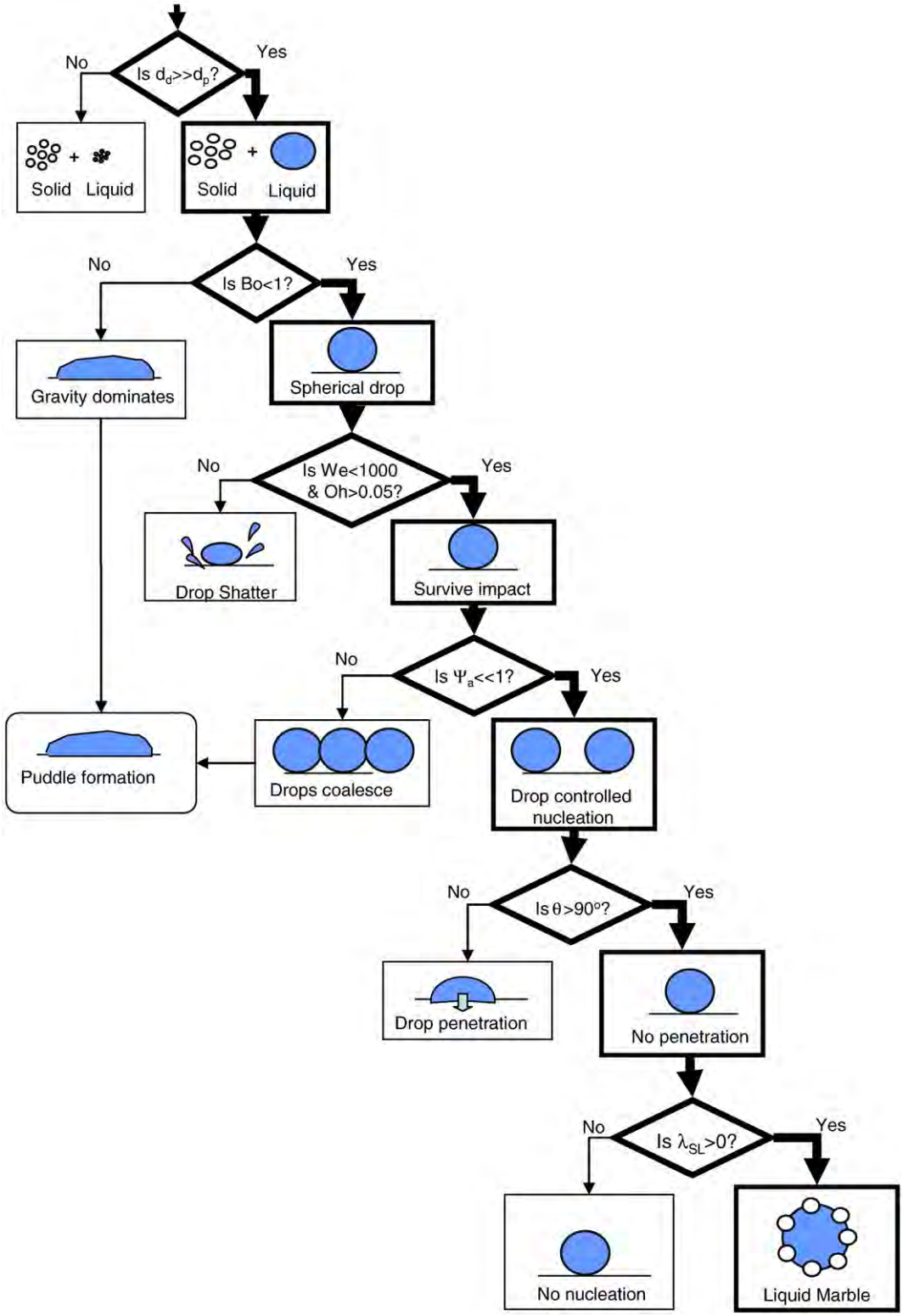

Fig. 12. Schematic flowsheet summarizing the steps and dimensionless groups controlling the formation of liquid marbles during granulation.

identified by previous workers [37,38,31,17] combined with ratios and dimensionless groups that form part of the framework for granulation theory [34,42].

For a stable, spherical hollow granule to form from a single drop, the following additional steps must occur:

6. In an agitated powder mass, the assembled liquid marble must be sufficiently strong to withstand the stresses experienced within in the agitated bed and subsequent standard powder handling operations.
7. The concentration and distribution of hydrophilic excipients must not negatively affect hollow granule formation, strength or stability.
8. The multi-component powder shell must be sufficiently strong to be self-supporting in order to avoid collapse during drying to form a hollow sphere and subsequent standard powder handling operations.

The controlling groups for these final three steps to form hollow granules are currently unknown but are expected to be complex functions of powder and liquid physiochemical properties and packing arrangements of multi-component particles. This area is the subject of further ongoing research by the authors.

6. Conclusion

We report here the first stage of ongoing work studying the granulation of hydrophobic powders by the solid-spreading nucleation mechanism [17]. Several combinations of hydrophobic powders and fluids have been shown to exhibit solid-spreading nucleation and to form "liquid marbles" [30,31]. The liquid marble structure seems superficially consistent with the long established spreading coefficients [16], although we also propose an alternate mechanism where bulk motion within the drop creates a corresponding surface flow which entrains particles, creating a shell.

Preliminary experiments suggest that some bulk fluid motion is required for shell formation to occur, and that smaller particle size, lower fluid viscosity and higher kinetic energy during impact all favour the formation of a powder shell. Some unexpected behaviour was reported, where a powder shell initially began to form but was not stable and the drop then penetrated into the powder bed. Finally, a framework for liquid marble formation was proposed by outlining the sequential steps and the possible controlling groups for each step. However, the ultimate aim of this ongoing research project is to follow the lead of [17] and dry the liquid marbles to produce hollow granules suitable for pharmaceutical drug delivery and other specialty applications.

Nomenclature

Bo	Bond Number representing dimensionless ratio of gravity forces to surface tension forces acting on a drop ($B_0 = \rho g R^2 R^2/\gamma_{LV}$)
d_d	Diameter of the droplet (m)
d_p	Diameter of the particle (m)
F	Fraction of powder component in Eq. (1) (−)
G	Gravitational acceleration (9.8 m^2/s)
Oh	Ohnesorge number representing dimensionless ratio of viscosity and surface tension ($Oh = \mu/(\rho_L \gamma_{LV} R)^{0.5}$)
R	Drop radius ($= d_d/2$)
V	Velocity of the fluid drop (m/s)
We	Weber number representing dimensionless ratio of inertia to surface tension ($We = \rho_L d_d v^2/\gamma_{LV}$)
γ_{LV}	Surface or interfacial tension of the fluid in contact with the vapour (mM/m)
λ_{LS}	Spreading coefficient for the liquid over the solid (−)
λ_{SL}	Spreading coefficient for the solid over the liquid (−)
μ	Fluid viscosity (mPa s)
θ	Contact angle between the solid and liquid phases (degrees)
ρ_L	Density of the liquid phase (kg/m^3)
ρ_S	Density of the solid particles (kg/m^3)
Ψa	Dimensionless spray flux, a measure of spray density and drop overlap in the spray zone (−).

Acknowledgements

The authors gratefully acknowledge the valuable contributions of Dr. Leslie Yeo, Dept Mechanical Engineering in the early stages of this project. The authors would also like to acknowledge the Monash University Engineering Faculty and Australian Research Council Discovery Projects program (DP0770462) for providing financial support for this work as well as the Monash Graduate Research School for providing scholarship support for B. Khanmohammadi.

References

[1] J.D. Litster, B.J. Ennis, The science and engineering and granulation processes, Kluwer Academic Publishers, Dordrecht, 2004.
[2] P.C. Knight, Structuring agglomerated products for improved performance, Powder Technology 119 (1) (2001) 14–25.
[3] S.M. Iveson, J.D. Litster, et al., Nucleation, growth and breakage phenomena in agitated wet granulation processes: a review, Powder Technology 117 (1–2) (2001) 3–39.
[4] S.M. Iveson, P.A.L. Wauters, et al., Growth regime map for liquid-bound granules: further development and experimental validation, Powder Technology 117 (2001) 83–97.
[5] P.R. Mort, Scale-up of binder agglomeration processes, Powder Technology 150 (2) (2005) 86–103.
[6] K.P. Hapgood, B. Khanmohammadi, Granulation of hydrophobic powders via solid spreading nucleation, AIChe Annual Meeting, AIChE, San Francisco, 2006.
[7] R. Plank, B. Diehl, et al., Quantifying liquid coverage and powder flux in high-shear granulators, Powder Technology 134 (3) (2003) 223–234.
[8] R. Boerefijn, M.J. Hounslow, Studies of fluid bed granulation in an industrial R&D context, Chemical Engineering Science 60 (14) (2005) 3879–3890.
[9] D. Myers, Surfaces, interfaces and colloids: principles and applications, VCH Publishers Inc., New York, 1991.
[10] M. Lazghab, K. Saleh, et al., Wettability assessment of finely divided solids, Powder Technology 157 (1–3) (2005) 79–91.
[11] C.F. Lerk, A.J.M. Schoonen, et al., Contact angles and wetting of pharmaceutical powders, Journal of Pharmaceutical Sciences 65 (6) (1976) 843–847.
[12] P.M. Heertjes, N.W.F. Kossen, Measuring the contact angle of powder–liquid systems, Powder Technology 1 (1) (1967) 33–42.
[13] M.E. Aulton, M. Banks, Influence of the hydrophobicity of the powder mix on fluidised bed granulation, Powder Advisory Centre, Basel, Switzerland, 1979.
[14] R.E.J. Johnson, R.H. Dettre, Wettability and contact angles, in: E. Matijevic (Ed.), Surface and Colloid Science, Wiley Interscience, 1969, pp. 85–153.
[15] M. Hemati, R. Cherif, et al., Fluidized bed coating and granulation: influence of process-related variables and physicochemical properties on the growth kinetics, Powder Technology 130 (1–3) (2003) 18–34.
[16] R.C. Rowe, Binder–substrate interactions in granulation: a theoretical approach based on surface free energy and polarity, International Journal of Pharmaceutics 52 (1989) 149–154.
[17] L. Farber, K. Hapgood, et al., Hydrophobic Nucleation in Particle Agglomeration, World Congress of Particle Technology, vol. 5, Florida, AIChE, Orlando, 2006, April 2006.
[18] L. Zajic, G. Buckton, The use of surface energy values to predict optimum binder selection for granulations, International Journal of Pharmaceutics 59 (1990) 155–164.
[19] D. Zhang, J.H. Flory, et al., Wettability of pharmaceutical solids: its measurement and influence on wet granulation, Colloids and Surfaces A: Physicochemical and Engineering Aspects 206 (1–3) (2002) 547–554.
[20] O. Planinsek, R. Pisek, et al., The utilization of surface free-energy parameters for the selection of a suitable binder in fluidized bed granulation, International Journal of Pharmaceutics 207 (1–2) (2000) 77–88.
[21] I. Krycer, D.G. Pope, An evaluation of tablet binding agents. Part I. Solution binders, Powder Technology 34 (1983) 39–51.
[22] K.P. Hapgood, Nucleation and binder dispersion in wet granulation, Department of Chemical Engineering, University of Queensland, Brisbane, Australia, 2000.
[23] K.P. Hapgood, S.M. Iveson, et al., in: A.D. Salman, M.J. Hounslow, J.P.K. Seville (Eds.), Granule Rate Processes, Granulation, Handbook of Powder Technology, vol. 11, Elsevier, London, 2006, p. 11.
[24] S.J.R. Simons, R.J. Fairbrother, Direct observations of liquid binder–particle interactions: the role of wetting behaviour in agglomerate growth, Powder Technology 110 (2000) 44–58.
[25] R. Flores, C. Keary, et al., Advantages of foam granulation and process miniaturization for small quantities of micronized drugs, Annual Meeting of the American Association of Pharmaceutical Scientists, TN, AAPS, Nashville, 2005, November 6–10.
[26] C.M. Keary, P.J. Sheskey, Preliminary report of the discovery of a new pharmaceutical granulation process using foamed aqueous binders, Drug development and industrial pharmacy 30 (8) (2004) 831–845.

[27] L. Mahadevan, Y. Pomeau, Rolling droplets, Physics Fluids 11 (1999) 2449–2453.
[28] H. Fujimoto, A. Tong, et al., Numerical and experimental study on oblique collision of water droplet with a solid substrate, Proc. 2005 International Mechanical Engineering Congress and Exposition, IMECE05., 2005
[29] D.T. Leighton, A. Acrivos, Measurement of shear-induced self-diffusion in concentrated suspensions of spheres, Journal of Fluid Mechanics 177 (1987) 109–131.
[30] P. Aussillous, D. Quere, Liquid marbles, Nature 411 (6840) (2001) 924–927.
[31] P.J. Aussillous, D. Quere, Properties of liquid marbles, Proceedings Royal Society A 462 (2067) (2006) 973–999.
[32] L. Forny, I. Pezron, et al., Storing water in powder form by self-assembling hydrophobic silica nanoparticles, Powder Technology 171 (1) (2007) 15–24.
[33] M.A. Ansari, F. Stepanek, Formation of hollow core granules by fluid bed in situ melt granulation: modelling and experiments, International Journal of Pharmaceutics 321 (1–2) (2006) 108–116.
[34] K.P. Hapgood, J.D. Litster, et al., Drop penetration into porous powder beds, Journal of Colloid and Interface Science 253 (2) (2002) 353–366.
[35] K. Takano, N. Maruyama, et al., Fluidized bed binderless granulation of hydrophobic drugs with fine lactose powder, Advanced Powder Technology 14 (2003) 369–381.
[36] M.S. Kalekar, S.S. Bhagwat, Dynamic behavior of surfactants in solution, Journal of Dispersion Science and Technology 27 (7) (2006) 1027–1034.
[37] T. Schæfer, C. Mathiesen, Melt pelletization in a high shear mixer IX. Effects of binder particle size, International Journal of Pharmaceutics 139 (1996) 139–148.
[38] T. Schæfer, C. Mathiesen, Melt pelletization in a high shear mixer VIII. Effects of binder viscosity, International Journal of Pharmaceutics 139 (1996) 125–128.
[39] G.I. Tardos, M.I. Khan, et al., Critical parameters and limiting conditions in binder granulation of fine powders, Powder Technology 94 (1997) 245–258.
[40] S. Agland, S.M. Iveson, The Impact of Liquid Drops on Powder Bed Surfaces, CHEMECA, vol. 99, IEAust/IChemE/RACI, Newcastle, Australia, 1999, September 25–29.
[41] D. Bartolo, C. Josserand, et al., Retraction dynamics of aqueous drops upon impact on non-wetting surfaces, Journal of Fluid Mechanics 545 (2005) 329–338.
[42] J.D. Litster, K.P. Hapgood, et al., Liquid distribution in wet granulation: dimensionless spray flux, Powder Technology 114 (1–3) (2001) 32–39.
[43] K.P. Hapgood, J.D. Litster, et al., Nucleation regime map for liquid bound granules, AIChE Journal 49 (2) (2003) 350–361.

D

Published Version of:

Liquid marble formation:

Spreading coefficients or kinetic energy?

(Chapter 4)

Powder Technology 196 (2009) 126–132

Contents lists available at ScienceDirect

Powder Technology

journal homepage: www.elsevier.com/locate/powtec

Liquid marble formation: Spreading coefficients or kinetic energy?

Nicky Eshtiaghi [a,*], Jacques S. Liu [a], Wei Shen [b], Karen P. Hapgood [a,*]

[a] Monash Advanced Particle Engineering Laboratory, Dept. of Chemical Engineering, Monash University, Victoria 3800, Australia
[b] Australasian Pulp and Paper Institute, Dept. of Chemical Engineering, Monash University, Victoria 3800, Australia

ARTICLE INFO

Article history:
Received 12 November 2008
Received in revised form 18 June 2009
Accepted 13 July 2009
Available online 20 July 2009

Keywords:
Hydrophobic powder
Granulation
Nucleation
Kinetic energy
Liquid marble
Powder shell formation
Spreading coefficients

ABSTRACT

A liquid marble is a network of self-assembled hydrophobic powder around a droplet. The mechanism and driving force leading to the formation of liquid marbles have not been investigated. In this study, the solid–liquid spreading coefficient (λ_{SL}) is calculated and the effect of the impact of kinetic energy on liquid marble formation for various fluids and particles is investigated. Single drops of fluid were produced using a syringe and released from different heights onto loosely packed powder bed. The degree of powder coverage over liquid droplet after impact was photographed and analyzed using image analysis. The results show that the spreading coefficients do not predict liquid marble formation, but instead that powder coverage of the drop is proportional to the applied kinetic energy. As the kinetic energy is increased, the percentage of coverage of liquid droplet by powder increases, and as the particle size decreases the percentage of coverage also increases. These results demonstrate that good powder coverage is assisted by increasing the kinetic energy of impact, which increases the size of the initial fluid-powder contact area and causes internal fluid flow within the droplet during impact and rebound, which entrains the particles and forms the powder shell. The knowledge that the level of agitation applied is an important factor in whether liquid marble is successfully produced, is expected to facilitate progress in creating liquid marbles as precursors to a wide range of structured powder–liquid products in cosmetics, pharmaceuticals and other advanced materials.

1. Introduction

Liquid marbles are uniquely structured granules, where a self-assembled network of hydrophobic powder forms a shell around the exterior of a droplet of fluid [1]. Liquid marbles are a novel approach for producing structured fluid-filled particles in the food, cosmetics and pharmaceutical industries [2–4].

There are now several papers on the formation of liquid marbles, but there are no studies currently published on *why* liquid marbles form. Two different mechanisms have been tentatively proposed to date in the literature:

1. The first suggested mechanism is that liquid marble formation is a surface energy phenomena, driven by the solid-over-liquid spreading coefficient (λ_{SL}) [2,4].
2. The second proposed mechanism is that kinetic energy [2,3] is responsible, based on observations of the role of mixing intensity during the manufacture of a large quantity of liquid marbles.

A previous study [2] of liquid marble formation on a loosely packed bed of hydrophobic powder made two critical observations. When a droplet was placed gently onto the powder bed (to avoid fluid flow within the drop interior due to impact or rolling), almost no coverage of the droplet with powder with powder occurred. This implies that the spreading of the powder over the liquid may not be driven by surface tension or spreading coefficients. However, when the drop was released from a height or rolled on the powder surface, an increased tendency to form a complete liquid marble was observed. These preliminary results [2] suggested that bulk motion of the drop due to the kinetic energy of either rolling or impact, is critical for liquid marble formation. This agreed with other observations of liquid marble formation at pilot scale [3], where the use of higher mixer impeller speed to increase the level of agitation and overall kinetic energy applied during mixing was found to be crucial to effectively encapsulating the water in a shell of hydrophobic powder.

In order to form a stable, spherical, liquid marble from a single drop, a series of steps was proposed [2] as part of a framework. The final step in liquid marble formation was provisionally shown as needing a positive value of the solid-over-liquid spreading coefficient (λ_{SL}). The spreading coefficient is defined as the difference between the works of adhesion and cohesion [5,6]. Spreading coefficients define that spreading (i.e. further replacement of the liquid–vapor interface with a liquid–solid interface) will occur if it is thermodynamically favorable [6], as indicated by a positive value of the spreading coefficient. Two spreading coefficients are theoretically possible [5] — the liquid may spread over a solid, denoted as λ_{LS}, or the solid may spread over the liquid, denoted as λ_{SL}. For liquid marble

* Corresponding authors.
E-mail addresses: Nicky.Eshtiaghi@eng.monash.edu.au (N. Eshtiaghi), Karen.hapgood@eng.monash.edu.au (K.P. Hapgood).

0032-5910/$ – see front matter © 2009 Elsevier B.V. All rights reserved.
doi:10.1016/j.powtec.2009.07.002

formation, we are most interested in how a hydrophobic powder covers a liquid droplet, which is theoretically described by λ_{SL}.

$$\lambda_{SL} = -\Delta G_{SL} = \gamma_{SL} + \gamma_{SV} - \gamma_{LV}. \quad (1)$$

A negative value for ΔG_{SL} and a corresponding positive value for λ_{SL} mean that the spreading process occurs spontaneously and the solid will freely spread over liquid. Thus, if $\lambda_{SL}>0$ then the solid–liquid interaction is sufficiently strong to promote the spreading of solid over liquid, while if $\lambda_{SL}<0$ then the solid will not spread over liquid.

Spreading coefficients for phase 1 over phase 2 can be calculated from their dispersive component (indicated by superscript d) and polar component (indicated by superscript p) of the total surface energy (based on Wu's harmonic mean method) [5,6]:

$$\lambda_{12} = 4\left[\frac{\gamma_1^d\gamma_2^d}{\gamma_1^d + \gamma_2^d} + \frac{\gamma_1^p\gamma_2^p}{\gamma_1^p\gamma_2^p} - \frac{\gamma_1}{2}\right]. \quad (2)$$

Eq. (2) can be used to calculate the solid-over-liquid spreading coefficient λ_{SL}, by defining phase 1 as the solid, and phase 2 as the liquid.

Wu's harmonic mean method is an empirical approach where the forces are divided into polar forces and dispersive forces, and has little fundamental basis. It is intended to be applied only to pure fluids, not to aqueous solutions where adsorption of the polymer at the interface has a significant effect on the local surface energy. Despite this the approach has been widely used to predict solid–liquid spreading interactions, including cases of powder spreading over liquids, with apparent success (for example, see [17,18]). In addition, some of these papers, apply the theory to aqueous solutions such as PVP and HPC solutions [17,18] which is theoretically invalid, although again their experimental results appear to indicate a causal link between spreading coefficients and granule wetting, strength and/or structure.

The solid–liquid spreading coefficient has been proposed as a quantitative method to predict whether a given powder–liquid combination will form a liquid marble [4]. In this paper, we test the hypothesis that the solid–liquid spreading coefficient λ_{SL} predicts liquid marble formation, by calculating the λ_{SL} spreading coefficient using literature values of surface energy and comparing these results to the corresponding experimental observations of liquid marble coverage while holding the kinetic energy as close as possible to zero. The second part of the paper then systematically varies the kinetic energy of the drop at impact and examines the effect on the degree of liquid marble powder coverage, as well as the effect of varying powder size and liquid properties.

2. Experimental

2.1. Spreading coefficient experiments

For the spreading coefficient experiment, we used 100 μm polytetrafluoroethylene (PTFE) spheres with droplets of different fluids: distilled water, glycerol (99%, Sigma Aldrich Riedel-de Haen), 6% w/w polyvinylpyrrolidone (PVP(40T), Sigma Aldrich Pty Ltd) and 2% w/w hydroxypropylmethylcellulose (HPMC, Premium LV, E3, The DOW Chemical Company). Each droplet was released from either 0 cm or 10 cm onto a powder bed using 1 cc syringe. PVP and HPMC solution viscosities were measured using a rotational viscometer (Visco Basic Plus, Fungilab, Barcelona).

2.2. Kinetic energy experiments

In order to investigate powder motion mechanism, kinetic energy experiments consisted of two phases — firstly using liquids with different viscosities and secondly using powders with different particle sizes. A loosely packed powder bed of PTFE 100 (Sigma Aldrich Pty Ltd.) was prepared by sifting the powder through a coarse sieve and collecting the powder in a petri dish. The powder surface was levelled by gently scraping the powder surface with a flat edge. The resulting powder bed was 1.2 cm high (level with the top of the petri dish) and 61% porosity. Droplets were dispensed from a 1 cc syringe using an 18 g needle with 0.02 mL volume. The syringe needle was oriented horizontally, parallel to the powder bed so that droplet volume would be better controlled. The droplet would have to pool on top of the needle aperture before falling, and so it was possible to pull back on the plunger to prevent multiple droplets being released.

In these experiments 6 mixtures of water and glycerol (99%, Sigma Aldrich Riedel-de Haen) solution — 0%, 20%, 40%, 60%, 80% and 100% glycerol solutions — were chosen (see Table 1 for properties). Droplets of each solution were released from various heights from 2 cm to 25 cm onto a loosely packed powder bed using a 100 μL Hamilton syringe with a 22 gauge needle. In this set of experiments 2 mL of food dye (Queen Fine Foods Pty Ltd) was added to initial 10 mL glycerol–water mixture to increase contrast when taking photos. This affected the actual concentration of glycerol. We refer to the fluids by their names before adding the dye (20%, 40%, etc) but the true concentration (including the dye) has been given in the Table 1. The data shown in Table 1 have been interpolated from water–glycerol solution data, assuming that the dye has the same viscosity as the water. This is a reasonable method to estimate the solution viscosity. The presence of the food dye reduced the surface tension of the fluids. Table 1 summarises the surface tensions of the fluids as measured using a dynamic surface tensiometer (Nima Technology, DST 9005) with a platinum DuNouy Ring (ring diameter 20.6 mm and wire diameter 500 μm).

The kinetic energy of the droplets was calculated from the potential energy of the droplet. By keeping the droplet volume constant at 0.02 mL and accounting for differences in fluid density, the kinetic energy can be varied by changing the release height of the droplet. We assume that the potential energy of the droplets is transformed completely into kinetic energy and this kinetic energy is used upon contact with the powder bed to deform the droplet such that the coverage of the droplet is attained via internal flow of the droplet dragging particles onto it. Kinetic energy losses via powder packing rearrangement, including formation of a crater in the powder bed have not been taken into account.

The effect of powder size was investigated using a similar methodology. Four different size grades of PTFE powder (Sigma Aldrich Pty Ltd) — 100, 35, 12, and 1 μm grades — were used to produce 1.2 cm high loosely packed powder beds with 61%, 75%, 78%, and 87% porosity for 100, 35, 12, and 1 μm particle size, respectively. For these experiments, drops of a water solution (10 mL distilled water plus 2 mL dye) were dispensed using the same 100 μL syringe onto the powder beds, and the liquid marble images were analyzed as above.

2.3. Image analysis method

After the drop had landed, the fractionally covered liquid marbles were then photographed using a stereo microscope (SMZ series) with a 3 MP camera at 1024×768 resolutions using Motic camera imaging software. Two images per droplet were taken directly

Table 1
Physical properties of fluids (including food dye) at 20 °C.

Fluid	Actual composition including food dye (% glycerol v/v)	Surface tension (mN/m)	Viscosity (mPa s) [7]
Water	0	71.4	1.0
Glycerol 20%	0.17	70.6	1.54
Glycerol 40%	0.33	69.2	2.68
Glycerol 60%	0.50	66.3	5.26
Glycerol 80%	0.67	64.6	9.8
Glycerol 100%	0.83	45.8	509

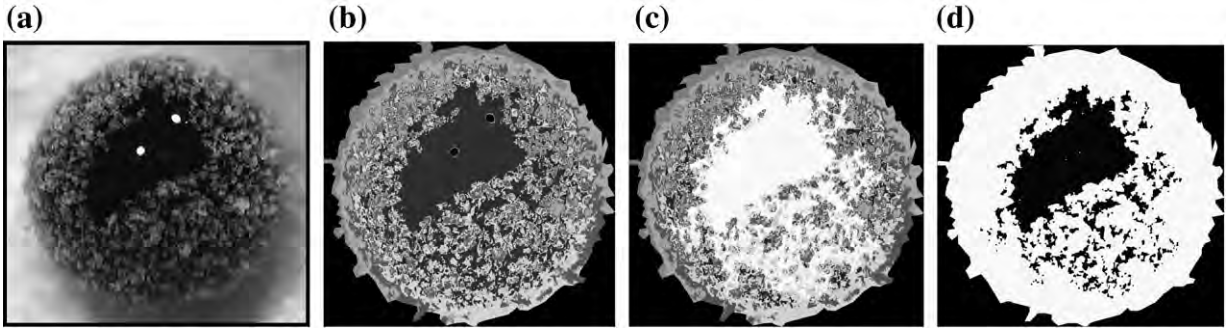

Fig. 1. Image processing for 20%glycerol–water droplet on PTFE 100 µm from 10 cm height: (a) original photo (b) clustered image after segmentation (c) after threshold and (d) final image after binary processing.

overhead: one with the upper surface of the droplet in focus to capture the fine details of the droplet (see Fig. 1a) and the other with the outermost circumference of the droplet in focus. This latter image was used to trace the border of the droplet in NIH Image J software (V1.38X) so that the region of interest could be saved and applied to the former image.

After the two images were acquired, the image processing and analysis phase were performed. Firstly, the background was changed to black and foreground to white and the image was then segmented using "*k*-means clustering" (see Fig. 1b). Reflections of the fiber optic lighting globes were manually edited out (compare white versus black spots in Fig. 1b and c). The image was then converted to a threshold image with a setting of 0–5 (see Fig. 1c) and the percentage coverage in the region of interest was calculated for images including fine details of gaps in the powder sheet (see Fig. 1a versus c).

A fine crack in the powder sheet which we refer to as a "vein" was not a point of interest but affected the percentage coverage results. For this reason, the image processing was continued from the above step to eliminate the veins. The threshold image was converted to a binary image. The resulting image will have the covered region in black and the rest of the image in white (see Fig. 1d). The image was then inverted and dilated twice and eroded once such that the uncovered vein like region diminished. If veins still exist they are either likely to be large enough to be important, or they are cut off from the main uncovered region and only present as small islands which can be omitted by the "particle analysis" tool in Image J. Then, the percentage coverage in binary images was calculated using Image J.

Five repetitions of kinetic energy experiment were made for each combination. Fig. 1 shows the process of image J analysis for a mixture of 20% glycerol–water droplet which was released from 10 cm above a powder bed of PTFE 100 µm. The percentage of coverage for this system varied from 69.7% before deleting veins (Fig. 1c) to 81.4% after deleting veins (Fig. 1d).

3. Results and discussion

3.1. Spreading coefficients theory

According to Rowe [5], the sign of the spreading coefficient λ_{SL} can be used to predict whether the solid powder would spread on the liquid surface or not. The surface energies of all the powders and fluids used in these experiments are summarised in Table 2. Results for the calculated values of λ_{SL} using Eq. (2) are tabulated in Table 3.

Rowe [5] proposed that spontaneous spreading of solid powder should occur when λ_{SL} is positive. Table 3 shows that $\lambda_{SL}>0$ for pure liquids on PTFE which means that the spreading of solid powder over liquid should be spontaneous. On the other hand, all combinations of PTFE and pure liquids have $\lambda_{LS}<0$, which predicts that the spreading of the liquid over the solid should be thermodynamically unfavorable. Predictions of powder behaviour based on pure liquids and PTFE are in contradiction with the experimental observations for drops placed gently on the powder bed from a height of 0 cm. These drops show no powder coverage (Table 3). Since no consideration of external forces is given in the derivation of equations (1) and (2), the zero release height experiment simulates the condition where the drop is under no external force. Thus, if liquid marble formation was solely a surface chemistry effect, with positive λ_{SL} it would be expected that a liquid marble would spontaneously form. Therefore, we find that Eq. (2) proposed by Rowe [5] does not predict the spreading of powder over a liquid surface and therefore cannot be used to predict liquid marble formation.

Apart from pure fluids, two polymer binder solutions were also studied for their interactions with powders. It is known that for polymer–water solutions the dispersive and polar components cannot be determined using Eq. (2) because of the possible adsorption of polymers on the surfaces of the polymer solutions. The spreading of powder over these polymer surfaces could not be experimentally observed. Literature surface tension data of PVP (6%) and HPMC (2%) solutions [9] show that these polymers quite significantly influence the surface tension of water (Table 2). PVP and HPMC reduce the polar component of water by 50.6% and 41.2%, respectively, and change the dispersion component of water by 30.3% and −15.6%, respectively. Teflon powder shows no tendency of spreading on any of the liquids. The non-spreading behaviour of Teflon power over these polymer solutions further suggests that comparing surface free energy values of the liquid and solid phases (through λ_{SL}) is not a valid predictive indicator for solid powder spreading over liquid surface.

Table 3 also shows variations in the amount of powder coverage when the drops were released from a 10 cm height. Although there is some variation in the amount of coverage due to local powder packing, the viewing angle, rolling on landing, etc., the amount of powder coverage appears to decrease as the fluid viscosity (provided in Table 2) increases. The viscosity effect is more systematically investigated in the Section 3.2.

An obvious reason for the inability of λ_{SL} to predict powder spreading over a liquid surface is that Eq. (2) does not correctly capture the physical process of powder spreading over a liquid surface. When hydrophobic powder spreads over a liquid surface, solid powder particles do not increase their surface area as they spread.

Table 2
Summary of dispersive, polar and total surface energies.

Powder or fluid	Dispersive surface energy (mJ/m^2)	Polar surface energy (mJ/m^2)	Total surface energy (mJ/m^2)	Fluid viscosity (mPa s)
Water	21.8 [8]	51.0 [8]	72.8 [8]	1.0 [7]
Glycerol	37.0 [8]	26.4 [8]	63.4 [8]	509 [7]
6% PVP solution [9]	28.4	25.2	53.6	2.2
2% HPMC solution [9]	18.4	30.0	48.4	3.1
PTFE [10]	18.0	0.0	18.0	–

Table 3
Calculated spreading coefficients for several fluid droplets on 100 μm PTFE (15× magnification, and 1200 μm scale bar for all photos).

Fluid	λ_{SL}	λ_{LS}	Released from Height = 0cm	Released from Height = 10 cm
Water	3.44	-106.16	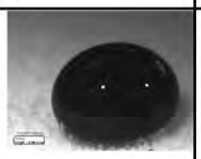	
Glycerol	12.44	-78.36		
PVP (6%)	-	-		
HPMC (2%)	-	-		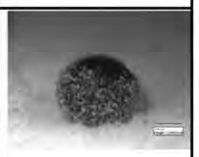

Instead, powder aggregates merely disintegrate when they expand their coverage over the liquid surface [20]. In this process, inter-particle attraction forces must be overcome in order for powder particles to spread over a liquid surface. However, the inter-particle attraction forces cannot be equated to the work of cohesion of the solid surface [20]. Therefore λ_{SL}, which is a comparison of liquid–solid adhesion and solid "cohesion", does not reflect the physical process of powder spreading correctly. This is an area of ongoing research effort [20].

3.2. Effect of kinetic energy on droplet coverage

An alternative mechanism for liquid marble formation is that powder motion around the shell is driven entirely by kinetic energy [2,3]. Pilot scale studies of dry water formation showed that increased agitation promoted liquid marble formation [3]. Other studies have shown that an impinging drop undergoes flow circulation in the droplet interior and consequent surface flow was observed and modelled [11,12]. We believe that this flow within the droplet is responsible for liquid marble formation [2], and that the driving force is the kinetic energy applied to the system [2,3].

If the kinetic energy of drop impact on a solid surface is sufficiently high, the drop will first deform and flatten on impact, increasing the maximum radius of the droplet and thus increasing the area of contact between the solid surface and the drop. After the drop has deformed and flatten, the surface tension will cause the drop to recoil back towards a spherical shape. Both the deformation at impact and the recoil after impact create internal flow within the droplet interior, which drives a corresponding surface flow around the drop entraining particles [11,12]. When a fluid drop lands on a hydrophobic powder surface, it does not penetrate into the powder pores but "sees" an effectively solid powder surface [13]. As soon as the drop touches the powder, a small section of the powder will adhere to the base of the drop. This is the initial step in forming the powder shell of a liquid marble. As the drop deforms and flattens, the contact area between the fluid and powder will increase, and more powder will adhere to the base of the drop. The overall surface area of the drop also increases since the drop is no longer spherical. This process of increasing contact area and increasing powder pickup continues until the maximum drop deformation is reached, and drop recoil commences. During drop recoil, the droplet returns to a spherical shape. The total surface area of the drop decreases back to its original spherical minima, and internal flow is created within the drop as the flattened shape recoils back to spherical. This internal flow creates a corresponding surface flow in the droplet, moving generally from the base of the drop towards the top. The combination of all of these processes — the increased powder–liquid contact area during deformation, the upward flow of fluid at the drop surface due to the recoils motion, and the temporary increase and then retraction of the drop surface area — all contribute to the formation of a liquid marble.

Since all these processes are enhanced by increasing the kinetic energy of impact, it follows that the degree of liquid marble powder coverage will be proportional to the kinetic energy of the drop as it lands on the hydrophobic powder surface. Although there is some evidence to support this hypothesis from preliminary results [2] and pilot scale studies [3], this hypothesis has not been rigorously tested.

3.3. Effect of kinetic energy and fluid viscosity on droplet coverage

The first series of experiments focused on investigating the relationship between the kinetic energy imparted upon droplet and its coverage by powder on a flat loosely packed bed, and the second phase concentrated on particle size effect. Fig. 2 shows the relationship between kinetic energy and percentage coverage for six water–glycerol solutions on 100 μm PTFE powder. The X-scale error bars are representative of the maximum errors in height measurements (±0.5 mm) and the subsequent variation in kinetic energy calculation. The *Y*-scale error bars represent one standard error of the mean for 5 samples per droplet.

Fig. 2 shows that increasing the kinetic energy causes an exponential increase in the powder coverage for water droplets on 100 μm PTFE powder. Initially, the liquid marble coverage increases

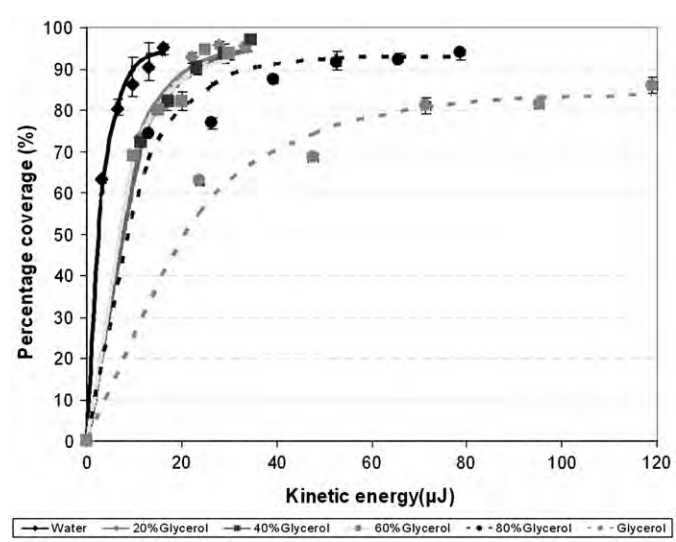

Fig. 2. Kinetic energy and viscosity effects on liquid marble powder coverage for water and glycerol solutions on 100 μm PTFE powder.

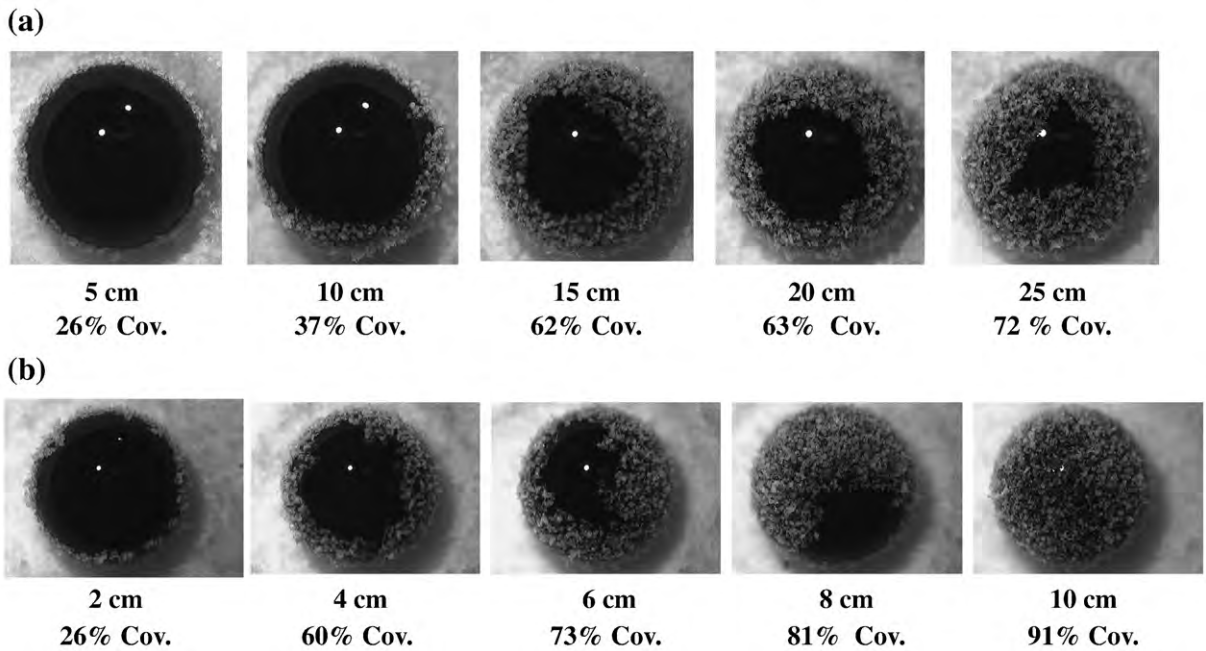

Fig. 3. Percent PTFE 100 powder coverage as a function of the drop release height for: (a) glycerol droplet and (b) water droplet.

rapidly with each increment in the applied kinetic energy. However, as the coverage gets closer to 100%, the rate of coverage slows and eventually appears to plateau at a maximum value between 85%–95% of complete coverage. Compared with the same data series for water, glycerol liquid marbles have a much lower coverage for a given kinetic energy. For example, powder coverage for a glycerol droplet is around 50% less than for a water droplet the same size released from the same height of 10 cm (see Fig. 3). The strongest glycerol solution used in these experiments had a viscosity 500 times the viscosity of water which significantly impairs the deformation and recoil of the drop upon impact. This consequently gives lower coverage because so much of the kinetic energy is dissipated by viscous forces. In addition, the higher concentration glycerol solutions also have lower surface tensions (refer to Table 1) which reduce the drop recoil forces [14,15]. Subsequently, higher kinetic energy is needed to expand the drop-powder surface area at contact and also to produce good bulk fluid motion during deformation and recoil of the viscous drops. Thus, the percentage of coverage for glycerol droplet is much lower than for a water droplet at same given kinetic energy.

The liquid marble coverage data shown in Fig. 2 are related to kinetic energy using the following empirical equation.

$$\text{Coverage}(\%) = A\left(1 - e^{-bE}\right) \tag{3}$$

where A is the maximum extent of liquid marble coverage (%), b represents the ease of liquid marble formation (%coverage/unit energy) and E is the kinetic energy of impact. High values of b mean that only a small increment in kinetic energy is required to produce a considerable increase in liquid marble coverage. The values of the parameters A and b were determined by fitting Eq. (3) to each data set shown in Fig. 2 and minimising the sum square of errors. The results are summarised in Table 4, which shows that the maximum liquid marble coverage A is a strong function of the fluid viscosity. Fig. 4 plots the maximum coverage A as a function of the fluid viscosity, and shows that the maximum coverage achieved falls sharply as the viscosity increases due to increasing fluid resistance to motion.

Figs. 2 and 4 show that the higher the viscosity of the solution, the lower the degree of coverage. Table 4 also shows that the maximum extent of coverage A decreases as surface tension decreases due to the loss of driving force for drop recoil. Note that the surface tension of the fluids used varies over a narrow range (see Table 1) compared to the several orders of magnitude variations in fluid viscosity. This again supports the conclusion that surface energy effects are not the main factor in determining the liquid marble powder coverage, as Fig. 4 shows large differences in coverage where there are differences in viscosity but comparatively small changes in surface tension. The 20%, 40% and 60% glycerol data all overlap because the viscosity differences of these three solutions are relatively small (see Table 1 which shows viscosity varies between 1 and 5 mPa s). Fluids with higher viscosity and lower surface tension require higher kinetic energy input to produce the same liquid marble coverage.

The proposed model for liquid marble formation by kinetic energy involves deformation and an increase in surface area of the droplet upon impact followed by recoil which drives fluid flow. Thus we expect that kinetic energy, surface energy and viscosity will all be important factors in determining liquid marble coverage. Plots of the coverage versus various combinations of dimensionless groups relevant to drop deformation and recoil [13,15,16], including the modified Weber number, Ohnesorge number, Capillary number and Bond number did not produce an improved analysis or show a more general trend, and generally looked similar to Fig. 2. The reason for the failure of dimensionless analysis in this case is not understood. The conventional analysis of drop impact required high speed dynamic imaging of the drops to determine the maximum spreading diameter, which can then be shown to be related to various functions of We and Re (e.g. [13,15,16]). We do not have this data available, and impact on the deformable powder bed creates a “crater” where the drop sinks below the top surface of the bed, which makes capturing the required images much more difficult compared to studying drop impacts on

Table 4
Summary of the ease of formation, b, and maximum extent of coverage, A, for liquid marbles formed using 100 μm PTFE powder.

Fluid	Maximum coverage A (%)	Ease of formation b (%/μJ)
Water	95	0.3
20% Glycerol	96	0.13
40% Glycerol	96	0.12
60% Glycerol	94	0.13
80% Glycerol	93	0.1
100% Glycerol	84	0.045

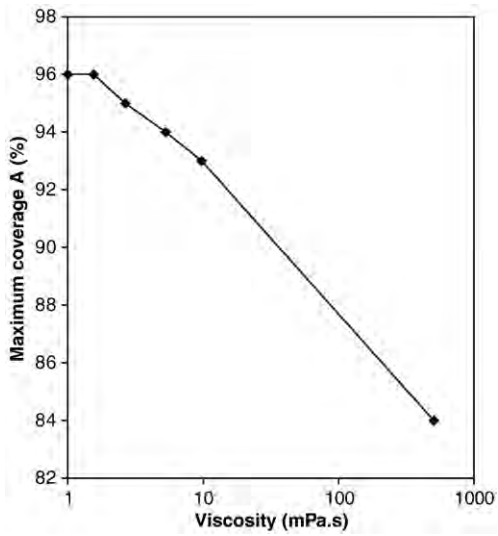

Fig. 4. The effect of fluid viscosity on maximum extent of coverage for water and glycerol solutions on 100 μm PTFE powder.

solid, immovable surfaces. Although we expect that the percentage coverage should be a function of the Weber and Reynolds numbers, our data do not support a simple overarching dimensionless relationship between liquid marble powder coverage and dimensionless groups.

3.4. Effect of particle size on droplet coverage

The effect of particle size was investigated by repeating the experiments for different particle sizes of PTFE. Fig. 5 shows that the same exponential relationship between kinetic energy and percentage of coverage was found, but the smaller particle sizes exhibit less coverage (see Table 5 and Fig. 5). This is contrary to what is expected — a smaller particle is lighter and should be more easily carried by internal flows of the droplet. We believe that particle agglomeration confounded the effect of particle size. Aside from PTFE 100 μm, all the smaller particle size grades formed agglomerates which were clearly larger than the stated particle size and in some instances formed aggregates even greater than 100 μm. Fig. 6 clearly demonstrates these agglomeration phenomena. These agglomerates hindered liquid

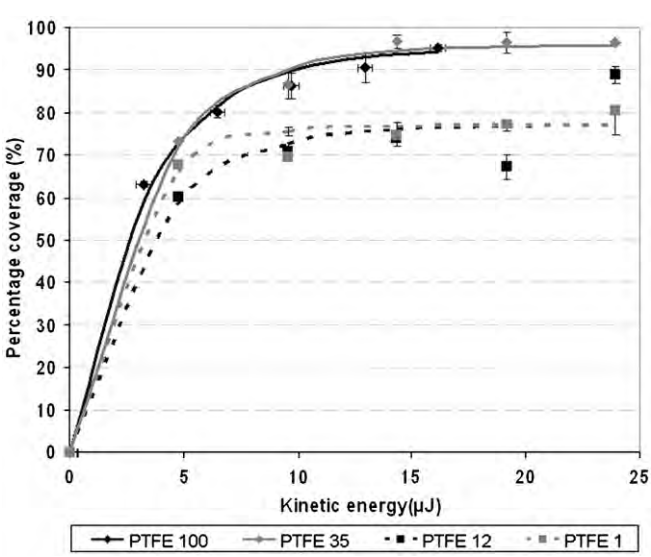

Fig. 5. Particle size effect on liquid marble powder coverage for water droplets on PTFE powders.

Table 5
The ease of formation and maximum coverage of water liquid marbles as a function of PTFE particle size.

PTFE particle size (μm)	Maximum coverage *A* (%)	Ease of formation *b* (%/μJ)
100	95	0.3
35	96	0.3
12	77	0.3
1	77	0.4

marble formation as they resisted movement due to their higher mass. Thus our results show that the percentage of coverage increases as primary particle size of the powder increases, due to the lower level of agglomeration for the coarser powders tested.

Fig. 6a clearly shows PTFE 1 μm particles containing agglomerates much larger than the theoretical 1 μm particle size. As shown in Fig. 6d for PTFE 100 μm, all of the particles are similar in size and no agglomeration is observed. We expect that the trend of increasing coverage for larger apparent particle size would be reversed for powders where the particles remained well dispersed, although agglomeration of fine particles is well known and extremely common. Kendall (1994) reported that cohesion forces (van der Waals force) for particle with 1 μm size can be up to million times greater than gravity forces depending on the particle size and roughness of the surface in contact [19]. The strong cohesion forces between the finer particles would result in the aggregation of the powders, as shown in Fig. 6a, b, and may also increase the adhesion between the particles and the bulk of the powder bed. The inter-particle attraction between the particles in the bed would also resist the separation of aggregates and the formation of the powder shell around the liquid marble. More kinetic energy would be required to break the strong cohesion forces between particles as the primary particle size decreases, further retarding the extent of liquid marble coverage.

The results in Fig. 5 appear to show a critical height/kinetic energy where any additional kinetic energy input yields similar coverage. It may be that there is actually 100% coverage but due to minor image analysis bias 100% is not reported. Alternatively it may be that there is a limiting coverage amount of *A* due to the powder properties, including powder packing causing gaps in the self-assembled powder

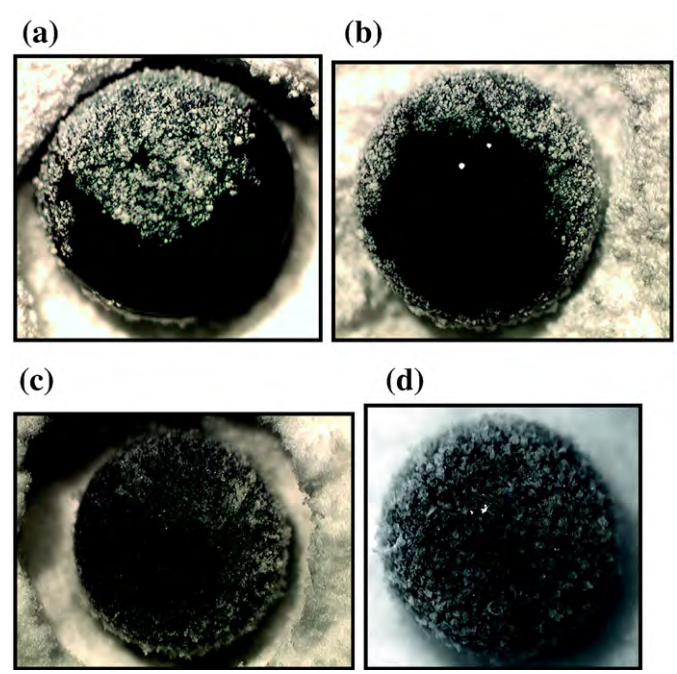

Fig. 6. Water droplet released from 10 cm height on (a) 1 μm (b) 12 μm (c) 35 μm and (d) 100 μm PTFE powder bed (droplet size and image magnification are constant).

layer, hydrophobic or static repulsion and limitations in the level of droplet deformation that can be achieved.

Differences in particle packing within the petri dish may also have contributed to the unexpected trend in liquid marble coverage as a function of particle size. Often droplets impacting onto the powder bed cause the bed to deform and a "crater" is created. This reduces the overall amount of kinetic energy available for droplet coverage. As particle size decreases, the propensity for crater formation increases, due to the much lower bulk densities of the powder beds, which allow significant bed rearrangement and void collapse. Further investigation into the effects of particle size, aggregate size and powder bed structure is required to determine which is the most important effect.

In addition to the agglomeration issues already noted, the smaller particles were also less opaque compared to the larger 100 μm PTFE powder. If the liquid marbles were only covered in a thin monolayer, the image analysis had more difficulty detecting the opacity (whiteness) of the particles, even if the liquid marble was fully covered. The small focal plane of the camera also aggravated this. Fine uncovered veins in the unfocused regions would be blurred and appear larger than they actually are and these dark areas left exposed would be counted as uncovered regions upon image analysis. This decreases the reported coverage from the true coverage, and this effect may have contributed to the measured maximum coverage and the parameter A being consistently less that 100%, even when visual inspection of the liquid marbles appeared to show 100% coverage. An example of this is shown in Fig. 6c, where the side liquid marble can be seen to be well covered by a thin layer of powder, which is more difficult to see compared to the thicker layers on the top of the droplet.

4. Conclusions

By calculating solid–liquid and liquid–solid spreading coefficients for several liquid marble formulations confirmed that the spreading coefficient theory [5,6] is inconsistent with experimental observations of liquid marble formation. An exponential relationship was found between increasing kinetic energy and the percentage of liquid marble coverage. The kinetic energy from impact causes an increase in drop surface area and the drop deformation and recoil create fluid flow which entrains the powder and forms the powder shell. By increasing the drop release height and therefore increasing kinetic energy, the liquid marble powder coverage increases, and the maximum extent of liquid marble coverage falls as viscosity increases and surface tension decreases. As particle size increased, higher coverage of the droplet was observed but these results were most likely confounded by the effects of agglomeration and/or powder bed rearrangement on impact. The results of this study are the first to study the formation mechanisms of liquid marbles and are an important step in understanding how to create liquid marbles as a precursor to producing a wide range of structured powder–liquid products and advanced materials.

Acknowledgements

This work was financially supported by the Chemical Engineering Department and Faculty of Engineering at Monash University, and by the Australian Research Council Discovery Projects program (DP0770462). Scholarship support for N. Eshtiaghi was provided by the Monash Graduate Research School. Thanks to Leslie Yeo for initial discussions on kinetic energy effects.

References

[1] P. Aussillous, D. Quere, Liquid marbles, Nature 411 (2001) 924–927.
[2] K.P. Hapgood, B. Khanmohammadi, Granulation of hydrophobic powders, Powder Technology 189 (2009) 253–262 (special issue on granulation).
[3] L. Forny, K. Saleh, I. Pezron, P. Guigon, L. Komunjer, Influence of mixing characteristics for water encapsulation by self-assembling hydrophobic silica nanoparticles, Powder Technology 189 (2009) 263–269 (special issue on granulation).
[4] K.P. Hapgood, L. Farber, J.N. Michaels, Agglomeration of hydrophobic powders via solid spreading nucleation, Powder Technology 188 (2009) 248–254.
[5] R. Rowe, Binder-substrate interactions in granulation, a theoretical approach based on surface free energy and polarity, International Journal of Pharmaceutics 52 (1989) 149–154.
[6] S. Wu, Polar and non polar interactions in adhesion, Journal of Adhesion 5 (1973) 39–55.
[7] D.R. Lide, Ed., CRC Handbook of Chemistry and Physics; CRC Press/Taylor and Francis: Boca Raton, 2008.
[8] P. Luner, M. Sandell, The wetting of cellulose and wood hemicellulloses, Journal of Polymer Science. Part C 28 (1969) 115–142.
[9] L. Zajic, G. Buckton, The use of surface energy values to predict optimum binder selection for granulations, International Journal of Pharmaceutics 59 (1990) 155–164.
[10] W.A. Zisman, Influence of constitution on adhesion, Industrial and Engineering Chemistry 55 (10) (1963) 19–39.
[11] L. Mahadevan, Y. Pomeau, Rolling droplets, Physics of Fluids 11 (1999) 2449–2453.
[12] H. Fujimoto, N.J. Hatta, Deformation and rebounding processes of a water droplet impinging on a flat surface above Leidenfrost temperature, Journal of Fluids Engineering 118 (1996) 142–149.
[13] D. Kannangara, H. Zhang, W. Shen, Liquid–paper interactions during liquid drop impact and recoil on paper surfaces, Colloids and Surfaces A: Physicochemical and Engineering Aspects 280 (1–3) (2006) 203–215.
[14] S. Middleman, Modeling Axisymmetric Flows, Dynamics of Films, Jets, and Drops, Academic Press, Inc., San Diego, 1995.
[15] T. Mao, D.S. Kuhn, H. Tran, Spread and rebound of liquid droplets upon impact on flat surfaces, AIChE 43 (9) (1997) 2169–2179.
[16] H. Park, W.W. Carr, J. Zhu, J.F. Morris, Single drop impaction on a solid surface, AIChE Journal 49 (10) (2003) 2461–2471.
[17] I. Krycer, D.G. Pope, An evaluation of tablet binding agents. Part I. Solution binders, Powder Technology 34 (1983) 39–51.
[18] R.C. Rowe, Binder–substrate interactions in granulation: a theoretical approach based on surface free energy and polarity, International Journal of Pharmaceutics 52 (1989) 149–154.
[19] K. Kendall, Molecules and mechanics, Science 263 (5154) (1994) 1720–1725.
[20] T.N. Nguyen, N. Eshtiaghi, K.P. Hapgood, W. Shen, An analysis of the thermodynamic conditions for solid powder particles spreading over liquid surface, submitted for publication to Chemical Engineering Science.

E

Published Version of:

Formation of hollow granules from liquid marbles: Small scale experiments

(Chapter 6)

Powder Technology 197 (2010) 184–195

Contents lists available at ScienceDirect

Powder Technology

journal homepage: www.elsevier.com/locate/powtec

Formation of hollow granules from liquid marbles: Small scale experiments

Nicky Eshtiaghi, Jacques J.S. Liu, Karen P. Hapgood *

Monash Advanced Particle Engineering Laboratory, Department of Chemical Engineering, Monash University, Melbourne VIC 3800, Australia

ARTICLE INFO

Article history:
Received 18 February 2009
Received in revised form 31 August 2009
Accepted 13 September 2009
Available online 22 September 2009

Keywords:
Hollow granule
Liquid marble
Non-wetting
Hydrophobic granulation
Dry water

ABSTRACT

Research into formation of hollow granules from liquid marbles is an emerging field in hydrophobic granulation. A liquid marble is formed by a network of self-assembled hydrophobic powder around a droplet, and this paper investigates the conditions required for forming hollow granules from a liquid marble precursor.
Single drops of fluid were produced using a syringe and placed onto loosely packed powder beds of hydrophobic powders. Liquid marbles formed from several powder/liquid combinations were dried at several conditions to investigate the drying conditions required for formation of a stable hollow granule.
The formation of stable hollow granules was found to depend on drying temperature and binder concentration. For HPMC and PVP binder, formation of hollow granule is proportional to binder viscosity and for HPC binder, this relationship is constant. Different combinations of powder and binder at both drying temperatures – 60 °C and 100 °C – had mixed success rates in forming hollow granules, but generally the success rate was improved by using higher drying temperatures, smaller particles or higher viscosity binder fluids.

1. Introduction

Hollow granules can be formed from hydrophobic powders by "solid spreading nucleation" [1] where the powder spreads around a template drop and the interior liquid is subsequently dried to form a hollow granule. The nuclei formed by solid spreading are also known as "liquid marbles" [2,3] and "dry water" [4], and are used in cosmetic [4] and pharmaceutical formulations [1].

The pre-specified structural properties of hollow granules allow simultaneous control of granule size and structure, excellent flow, good compression for tabletting and fast dissolution rate. These granules are ideal for pharmaceutical products with a high concentration of a hydrophobic drug. Research into formation of hollow granules via either melt granulation [5] or via hydrophobic liquid marbles [1,6] is an emerging field in hydrophobic granulation.

Solid spreading nucleation can be used to create hollow pharmaceutical granules suitable for compression into tablets [1]. Powder shell formation experiments were performed in a 2 L high-shear mixer with 70 mass% of a submicron hydrophobic powder (contact angle >90°) and 78% w/w water, which was atomized over 7–8 min into the mixer. In addition, 20% microcrystalline cellulose and 4% hydroxypropyl cellulose binder were added as hydrophilic excipient components plus 1% sodium lauryl sulfate as a surfactant. By drying the liquid marbles to remove internal fluid, stable spherical hollow granules were formed. The presence of excipients and surfactants did not prevent liquid marble formation or self-assembly of the particles at the drop interface since the hydrophobic model drug powder constituted 90% of the batch on a volume basis. Moreover, the excipients stabilized the powder shell to allow the hollow structure to be preserved during drying [1]. Apart from this one paper, there are no further studies on hollow granule formation from liquid marble precursors.

Bhosale et al. [7] studied the strength of liquid marble formed with PTFE (7–12 μm) and 2 types of fumed silica powder, which had been treated with hexamethyldisilazane and dimethyldichlorosilane. Bhosale et al. suggested that high surface area nano-particle materials like Aerosil create more uniform powder shells through uniform coverage of the liquid–vapor interface. They found that nano-powder shells form an "elastic" membrane that makes these liquid marbles mechanically robust in comparison with conventional liquid marbles made from larger particles. We expect that liquid marbles formed from nano-particles may be able to withstand higher compressive stresses during drying, and may be more likely to form a hollow granule.

Dandan and Erbil [8] determined the evaporation rate of graphite liquid marble and found that graphite liquid marbles had a much longer lifetime than a pure water droplet of the same size. The presence of graphite retarded the evaporation of water and extended the time required for the liquid to be completely evaporated. Increasing the relative humidity of the medium increases the evaporation resistance. For larger droplets, the lifetime was determined by diffusion controlled evaporation [8]. In comparison to the study of Bhosale et al. [7], they found the graphite liquid marble evaporation rate was 7% lower compared to PTFE liquid marbles, which indicated that the liquid marble lifetime is extended by using small particles (e.g. graphite 10–20 μm) rather than larger particles (e.g. PTFE 5–7 μm).

* Corresponding author. Tel.: +61 3 9905 3428; fax: +61 3 9905 5686.
E-mail address: Karen.Hapgood@eng.monash.edu.au (K.P. Hapgood).
URL: http://www.eng.monash.edu.au/chemeng/people/academics/askh.htm

0032-5910/$ – see front matter © 2009 Elsevier B.V. All rights reserved.
doi:10.1016/j.powtec.2009.09.013

Polymeric binder is required to avoid the liquid marble collapsing after drying, as the binder forms solid bridges between the particles during drying which give strength to the powder shell. The physical properties of the binder and the drying temperature are both expected to be important in avoiding granule collapse. Drying of liquid marbles is expected to show some similarities with drying of liquid drops containing solutes. Fundamental studies of the phenomena occurring during the droplet drying process were reported by Charlesworth and Marshall [9]. They developed a technique where an individual droplet was suspended in a controlled air stream, and the weight and temperature were recorded during drying in parallel with visual observations of the appearance and size of the droplet (see Fig. 1). They used an aqueous solution of an inorganic salt droplet in relatively slow rates of evaporation (moderate air temperatures and velocities). The first period of drying was characterized by evaporation from a free liquid surface which is similar for all droplets regardless of the solute or drying conditions. After further drying, crystals formed at the bottom of droplet and gradually formed a crust around the droplet. After completion of the crust formation, drying depended on the solutes and the surrounding air temperature. Charlesworth and Marshall [9] categorized these features into two main sections: air temperature above or below the boiling point of solution. In this study, we are interested in drying a single droplet in air at a temperature below the boiling point of solution. For this case, three different sub-categories were defined [9] (see Fig. 1):

a) If the crust is rigid and porous, the air–liquid interface retreats between pores and the appearance does not change (I)
b) If the crust is rigid but non-porous, fracture phenomenon occurring on the crust allows air to enter the particle and the air–liquid interface returns to the crust surface under the influence of capillary forces. There are three possible conditions after fracturing:

   I. If fracture remains open, further formation of solid occurs out from particle surface (IIb) or within the crust structure (IIa)
   II. If the fracture closes, the supply of air would be disrupted and the liquid interface once more retreats into the crust interstices. As the amount of liquid decreases, successfully smaller pores are emptied (crystal grows (IIc))

c) Crust is pliable and impervious. Rupture by implosion could eventually occur as the skin thickens and stiffens (III).

Charlesworth and Marshall's [9] study as summarized in Fig. 1 is also presumed to be applicable for liquid marble drying, as the outer shell of powder in a liquid marble can be assumed to be similar to the first step of drying from a liquid surface. After further drying and shrinkage, a solid shell-like crust is produced. The permeability of the powder shell and binder matrix will determine whether there are enough pores to allow the interior liquid to be vaporized freely, and thus which of the cases shown in Fig. 1 will occur for the drying of liquid marbles.

Walton and Mumford [10] also classified the various types of particle morphology produced at two different temperatures (70 °C and 200 °C). They used a single droplet drying technique with a droplet containing dissolved solids under controlled air temperature, humidity and velocity in a simulated spray dryer. Their study demonstrated that both the chemical and physical natures of the material are important in determining particle morphology and the pliable or plastic nature of the skin is related to its chemical and/or physical structures [10]. Polymeric materials tended to form a shriveled thin-walled hollow particle. Particles with a polymeric skin decreased in size without any rupture of the skin surface during initial drying period suggesting that the skin is porous. By increasing the concentration of solute in droplet, the particle diameter tended to stabilize as the particle skin (crust) adopted a more permanent structure, and resulted in a decrease in particle distortion, surface rupture and internal bubble nucleation.

At lower drying temperatures after complete drying, particles tend to shrivel and deform, and some signs of internal bubble nucleation and particle inflation appeared [10]. An increase in drying temperature from 70 °C to 200 °C increased the rate of heat and mass transfer experienced by both droplet and particle increased. This resulted in shorter drying times and more violent drying behavior which produced particles with a greater tendency to inflate, shrivel and in some cases explode. At 200 °C, internal bubble nucleation was rapidly formed and the bubbles expanded to violently distort, and eventually rupture. This caused the particle to collapse, shrive and then re-inflate. This cycle was repeated three or four times until the internal moisture had evaporated (see Fig. 2).

In some cases, evaporation of a residual liquid inside partially dried particles caused the liquid to foam and bubble causing internal blistering within the larger parent particle [10]. After drying, the hardened foam gave a blistered appearance to particle. High surface

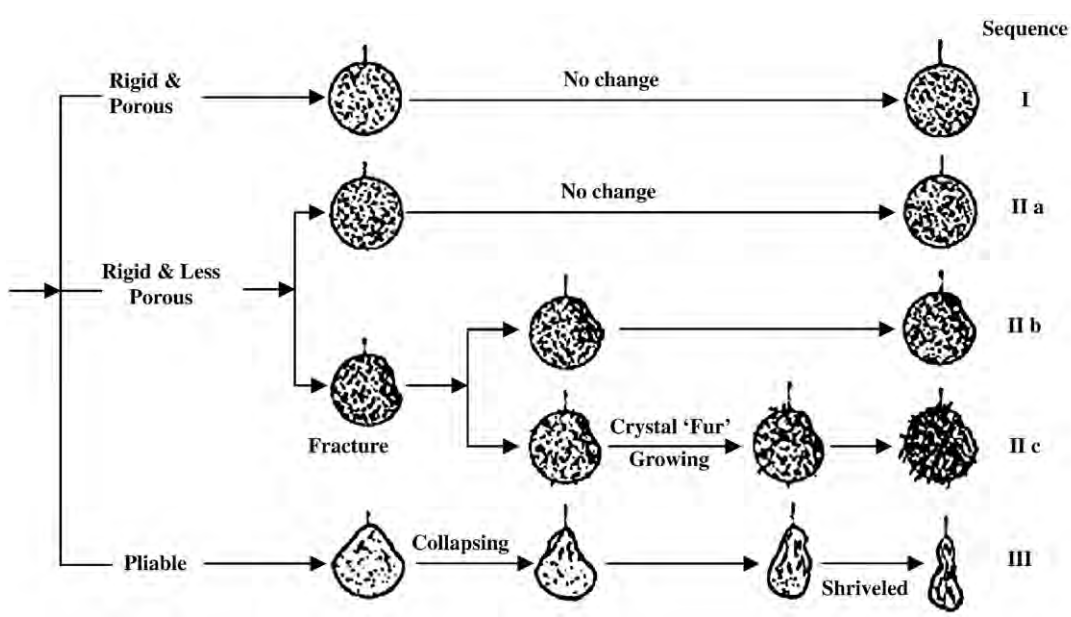

Fig. 1. Selected structures formed after drying of a single droplet below the boiling point of the solution [8].

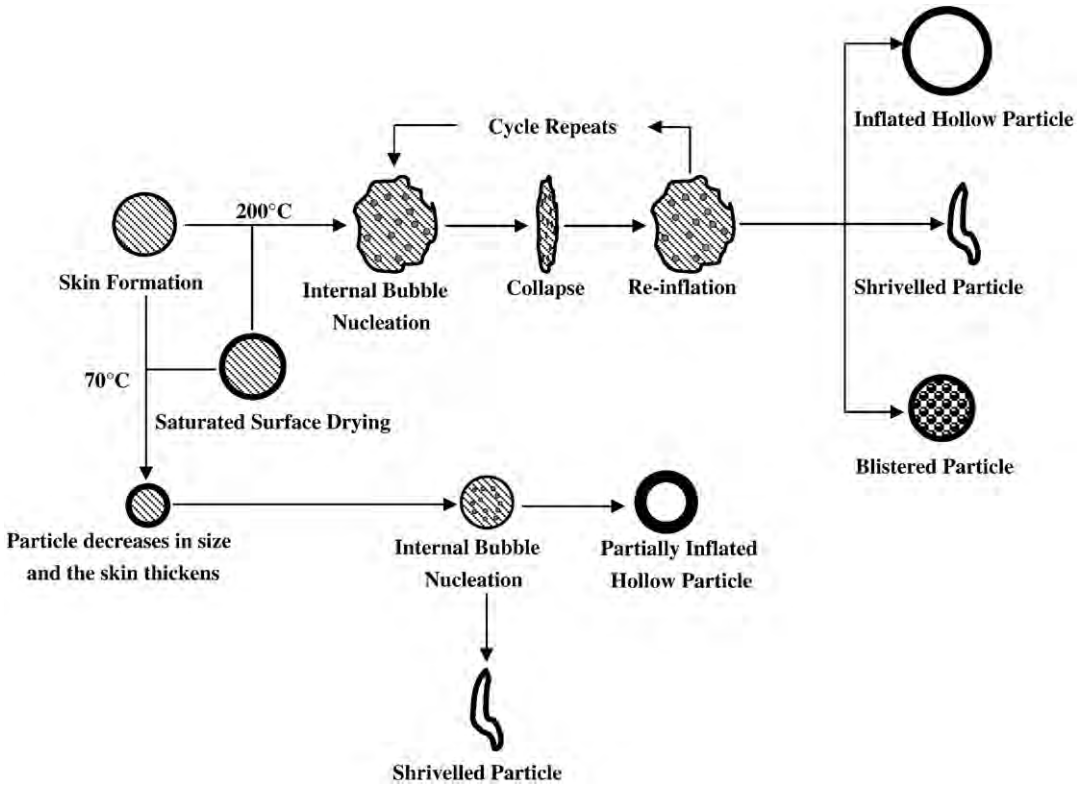

Fig. 2. Selected different particle morphologies formed after drying of a single droplet at 70 °C and 200 °C [10].

area powders with good gas absorption properties increased the internal porosity of the particles by adsorption of gases during drying. The internal structure of these particles showed much larger vacuoles [10].

This paper will investigate what happens to the liquid marble as the template drop is removed during drying for a variety of powder–fluid combinations and a range of drying temperatures. The aim is to identify the right powder–binder combination and the right drying temperature to produce stable hollow granules from liquid marble nuclei.

2. Materials and methods

Glass ballotini spheres ($d_{50}=65$ μm, AH/AG grade, $\rho=2.5$ g/cm^3, Potters Industries Pty Ltd.) were used to form liquid marbles. In order to make the glass beads hydrophobic, SIGMACOTE solution (chlorinated organopolysiloxane in heptane, Sigma Aldrich Pty Ltd.) was used. Two additional hydrophobic powders were used: Polytetra fluoroethylene (PTFE) with four different particle size grades (1, 12, 35, and 100 μm, $\rho=2.1$ g/cm^3, Sigma Aldrich Pty Ltd.), and fumed silica Aerosil R974 with primary particle size of 12 nm (Degussa, Germany).

Several different binder solutions were used: PVP (poly-vinyl pyrrolidone (40T), Sigma Aldrich Pty Ltd.), HPMC (Hydroxy Propyl Methyl Cellulose, Premium LV, E3, The DOW Chemical Company), and HPC (Hydroxy Propyl Cellulose, 100,000 Mw, Sigma Aldrich Pty Ltd.). Concentrations between 2 and 18% on a weight basis were used. Fluid viscosities were measured using a rotational viscometer (Visco Basic Plus, Fungilab, Barcelona).

Liquid marbles were prepared by releasing a droplet from a 1 mL syringe with an 18 g needle approximately 2 cm above a loosely packed powder bed. The droplets were then agitated using the syringe needle tip on the surface of the powder bed to form a multilayered liquid marble. At least 10 liquid marbles were dried for each individual combination of temperature, powder and binder. To try to estimate the liquid to solid for each powder–liquid combination, the average weight of 10 liquid marbles was measured using an analytical balance, and compared to the average weight of 10 drops of the fluid. The powder shells were very light, approximately 0.1 mg each, and the random variations during weighing were the same or larger than the weight of the powder shell. We were unable to obtain sensible results for the L:S ratio and this data is therefore not reported.

Several drying methods have been used: air drying at 24 °C and 31% humidity, freeze drying at −50 °C and 300 mm Hg (Bench Top Freeze Dryer, OPERON Co., Ltd.) and oven drying in a fan-forced 60 L laboratory oven (S.E.M. (SA) Pty. Ltd.) at 60 °C, 80 °C, and 100 °C and an overall air flow rate of 20 L/min. This gives an air flow rate of 12 cm/min. Based on the inlet air temperature and humidity, the RH in the oven was approximately 3%RH at 60 °C and less than 1%RH at 80 °C and 100 °C. Liquid marbles were dried for at least 12 h to ensure complete drying.

Once dried, the granules were removed from drier and classified visually into categories and counted. To minimize inconsistency, all analysis for each powder/binder combination was performed on the same day. Pictures of the hollow granules were taken with a stereo microscope (SMZ series) with a 3 MP Motic camera. The internal structure of selected granules was analyzed using an XUM X-ray microscopy.

The effects of changing the drying temperature, powder type and size, binder type and binder concentration were studied to determine the best drying conditions. The matrix of data was first analyzed for each binder solution at different drying temperatures to find the most suitable temperature for drying liquid marbles regardless of binder and powder type. Then, the effects of binder and powder type at two selected drying temperatures (60 °C and 100 °C) were examined.

3. Results

During experiments we observed that if the liquid droplet was covered with only a thin or mono layer of powder, all the liquid

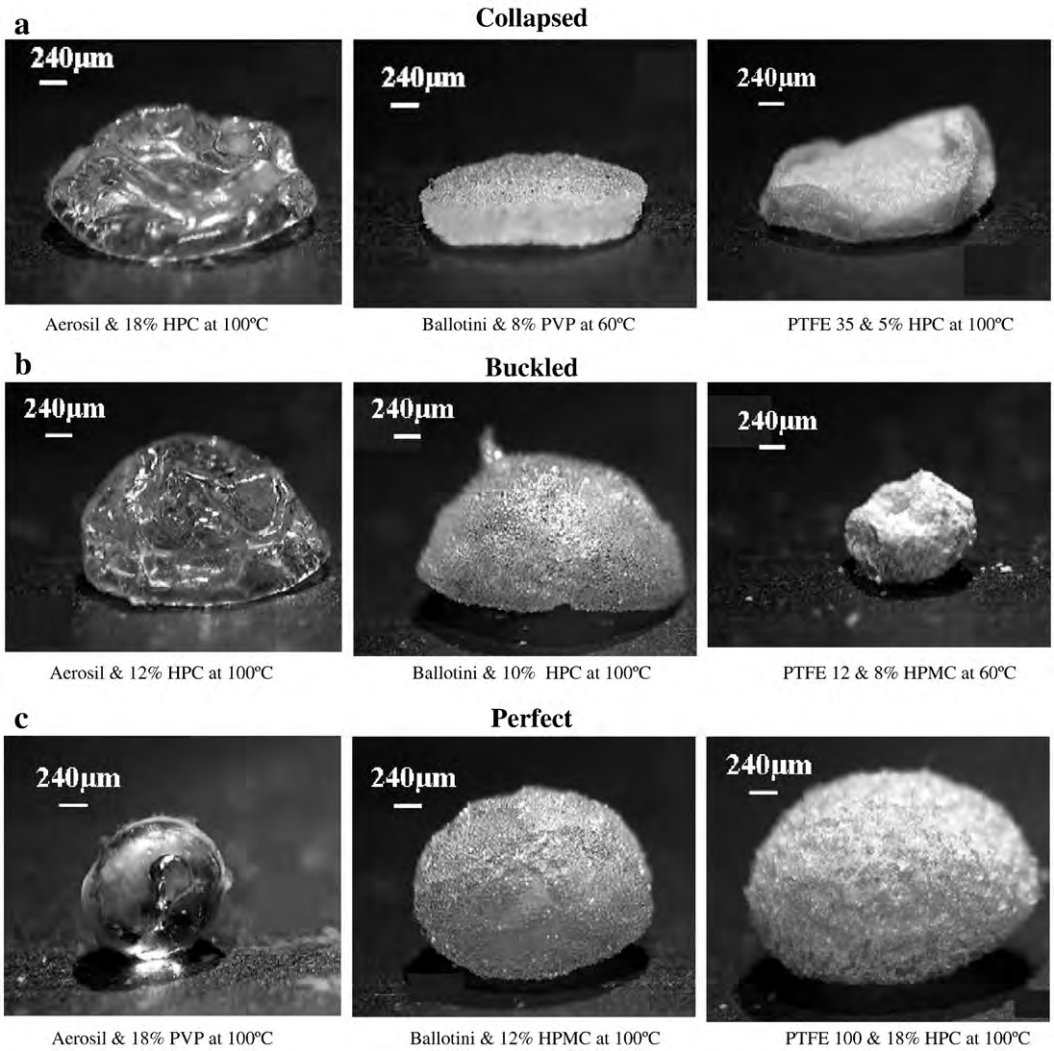

Fig. 3. Formed hollow granule structure of Aerosil R974, hydrophobic glass ballotini (AG) and PTFE powder (a) collapsed (b) buckled and (c) perfect.

marbles collapsed during drying regardless of temperature, binder and powder type. Survival of hollow granules was generally observed when there was a thick powder layer around the droplet. In practice during granulation in high-shear mixers, it can be assumed that all droplets will have a multi-layer of powder as a result of the frequent collision with powders in the highly agitated powder motion in granulator. Moreover, anecdotal observations suggested that the smaller the droplet size, the higher the chance of hollow granule survival. This is consistent with previous reports of collapsed granules occurring mainly in the larger granule sizes [1]. Drop sizes in a granulation process are much smaller, typically 100–500 μm, so the liquid marble survival results in this study represent a worst case scenario.

In our analysis we consider two criteria: "survivability" and "quality" of the hollow granules. "Survivability" refers to the propensity of the liquid marbles to form hollow granules, i.e. to avoid collapse during drying. "Quality" of the hollow granules refers to their shape. A variety of different shapes were observed after drying: collapsed granules which often formed an annular blood cell shape;

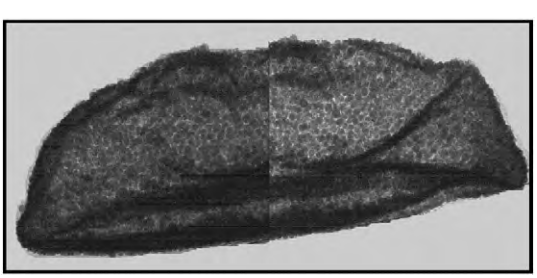

Fig. 4. X-ray microscopy image of a buckled hollow hemisphere granule (3 mm diameter) made from hydrophobic glass ballotini and 10% HPC dried at 60 °C.

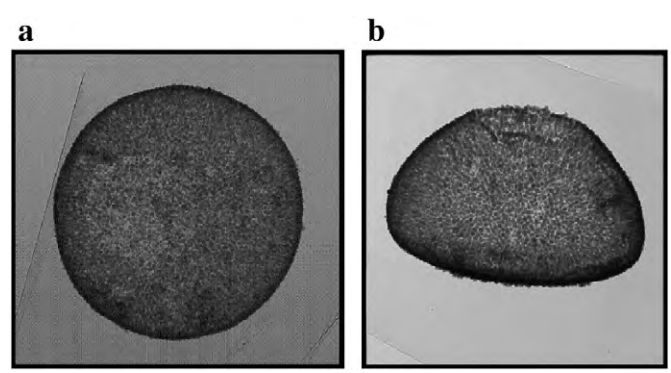

Fig. 5. X-ray microscopy image of hollow spherical granule (2–3 mm diameter). Hydrophobic glass ballotini and 10% HPC dried at 100 °C (a) top view, (b) side view.

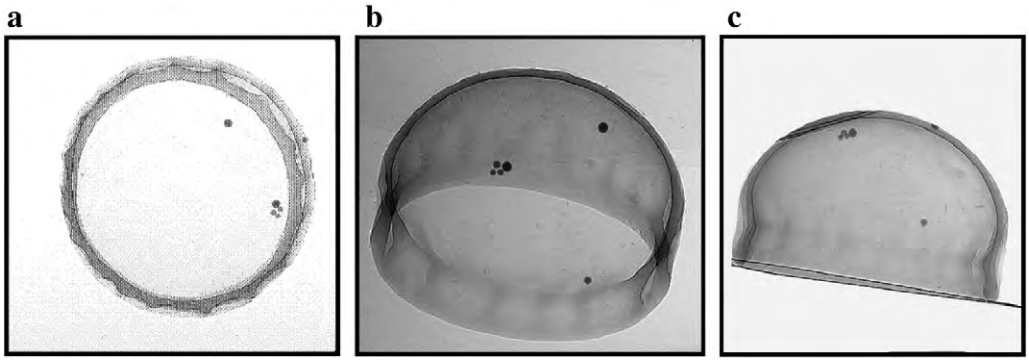

Fig. 6. X-ray microscopy image of hollow hemispherical granule (2–3 mm diameter) of Aerosil R974 and 8% HPC from, (a) top view, (b) bottom view, and (c) side view.

buckled hemispherical granules with one or more depression; and perfect hemispherical granules.

Fig. 3 shows several examples of each type. In a few cases, perfect spherical granules were formed. The success of a given drying condition is a combination of how well the drying condition supports both survivability and quality.

X-ray microscopy was used to confirm that the spherical or hemispherical granules formed after drying were hollow, as shown in Figs. 4–6. Fig. 6 clearly shows the hollow structure as the absence of particles in the interior of the shell is obvious. X-ray microscopy was conducted only on glass ballotini and Aerosil granules as a confirmation of visual observations. The remaining granules are assumed to be hollow or collapsed based on the shape of the exterior.

A systematic set of experiments was performed with different binder types and powders, at a range of different drying temperatures. Table 1 summarizes the overall results of these experiments, and indicates the dependency of stability and shape of the hollow granules on the drying temperature, and powder/binder combinations.

From Table 1, PVP polymer was not able to stabilize glass ballotini liquid marbles at any tested drying temperature, but HPMC polymer was successful at 100 °C and HPC above 80 °C. Maintaining a hollow granule throughout the drying process appears to be aided by higher drying temperatures. All the tested binders were able to make hollow granules with Aerosil at drying temperatures above 60 °C. The results in Table 1 imply that the ability to form hollow granules after drying depends on both binder type and drying temperature.

The stability of the hollow granule appears to depend on the powder used as indicated by Walton and Mumford [10], as different drying temperatures are required for each powder to ensure hollow granule survival. For example, glass ballotini hollow granules survive above 80 °C while Aerosil granules survive as long as the drying temperature is above 60 °C. Moreover, by increasing the temperature from 60 °C to 100 °C the shape of hollow granule gradually improves until a perfect hemisphere is reached (see Table 1). This result shows that the final quality of the hollow granules depends on the drying temperature. At higher drying temperatures, quick removal of the interior liquid improves the stability of hollow structure. The receding surface of the drying droplet does not generate as much capillary stress on the particle shell. It may also form a rigid porous shell at higher drying temperatures (as per case Ia in Fig. 1) and form a pliable shell (see case III in Fig. 1) at lower drying temperatures [9].

To find a general trend for drying liquid marbles it is necessary to examine a matrix of data for different binder/powder combinations at two selected temperatures– 60 °C and 100 °C – which had shown reasonable hollow granule formation after drying in the preliminary drying studies in Table 1.

Each binder–HPMC, PVP, HPC– is discussed individually below before analyzing the overall trends observed during the experiments.

3.1. HPMC binder

As the HPMC binder concentration increased, the survivability of the liquid marbles improved as well as the quality of the hollow granules. As shown in Fig. 7, by increasing HPMC concentration from 5% to 18% the proportion of perfect hollow granules increased from 19% to 72% and the percentage collapsed was reduced from 58% with 5% HPMC to 0% with 18% HPMC. This result is consistent with the previous study reported by Walton and Mumford [10] as they reported that by increasing the concentration the particle distortion and surface rupture decreased. The formation rate for buckled granules was unaffected over the concentration tested. Data in Fig. 7 is a combination of result for all powders– Aerosil, glass beads and PTFE – at both drying temperatures — 60 °C and 100 °C.

Fig. 8 illustrates how increasing the concentration of HPMC affected the quality of hollow granules formed from Aerosil. The 12% HPMC granule (left) is almost a hemisphere and has a hole in the base. In contrast, the granule formed from 18% HPMC (right) is noticeably more spherical and has no hole in the base. Some of the produced hollow granules produced with 18% HPMC had odd striped patterns on their surface (see Fig. 9). The striated surface may be the first step toward buckling. As the overall shape of these hollow granules was still hemispherical, these hollow granules were classed as hemispherical rather than buckled.

Table 1
Preliminary drying studies for hydrophobic glass ballotini and Aerosil R974.

Powder and binder		Freeze drying (at −50 °C, 300 mm Hg)	Air drying (at 24 °C, 31%H)	60 °C	80 °C	100 °C
Hydrophobic glass ballotini	5% PVP	Collapsed	Collapsed	Collapsed	Collapsed	Collapsed
	5% HPMC	Collapsed	Collapsed	Collapsed	Collapsed	Buckled hemisphere
	5%HPC	Collapsed	Collapsed	Collapsed	Perfect and buckled hemisphere	Perfect hemisphere
Aerosil R974	5% PVP	Collapsed	Collapsed	Perfect hemisphere	Perfect hemisphere	Perfect hemisphere
	5% HPMC	Collapsed	Collapsed	Perfect hemisphere	Perfect hemisphere	Perfect hemisphere
	5%HPC	Collapsed	Collapsed	Perfect hemisphere	Perfect hemisphere	Perfect hemisphere

Table 2
Survivability of hollow granules for different concentrations of HPMC, HPC, and PVP binders.

Binder type	Binder concentration (wt.%)	Binder viscosity (mPa s)	Survivability (%)
HPMC	5	12	43
	8	41	79
	10	83	89
	12	158	86
	18	855	100
PVP	5	2.1	17
	8	3.1	36
	10	4.0	36
	12	6.0	47
	18	11.1	52
HPC	5	108	45
	8	566	50
	10	785	41
	12	970	36
	18	5504	44

Increasing the drying temperature from 60 °C to 100 °C improved the success rate for hollow granule formation using HPMC binder across all powders (Fig. 10). For example, with 8% HPMC dried at 100 °C exhibited less collapsing compared to drying at 60 °C. It appears that increasing the drying temperature does not significantly affect the proportion of buckled granules. Fig. 10 shows a steady amount of buckled hollow granules across HPMC 8% to 18%, while the amount of collapsed granules decreases and the number of perfect granules increases. Thus, increasing the drying temperature considerably improves both the survivability and quality of hollow granules formed with HPMC as a binder.

Increasing the drying temperature at higher HPMC concentrations (12 and 18%) had a little effect on the quality or survivability (see Fig. 10). When the desired hollow granule is achieved at a lower temperature, there is no advantage in increasing the drying temperature further.

Fig. 11 shows the survivability and quality of HPMC granules as a function of the powder used. Data for all HPMC concentrations and both drying temperatures have been combined to show the overall trend in Fig. 11.

Overall, Aerosil is clearly the most successful powder in terms of survivability as well as the quality of formed hollow granule. The loosely aggregate floc-like structure of the nano-sized silica particles creates a highly porous shell and consequently increases the chance of survival (see case I in Fig. 1). These resilient Aerosil liquid marbles are consistent with reports by Bhosale et al. [7] that nano-sized Aerosil forms stronger liquid marbles compared to larger size particles. This is demonstrated in Fig. 11, where Aerosil produces a very high proportion of perfect hemispherical hollow granules compared to PTFE and glass beads as these liquid marbles will withstand higher compressive stresses and tensile loads [7], as experienced during drying.

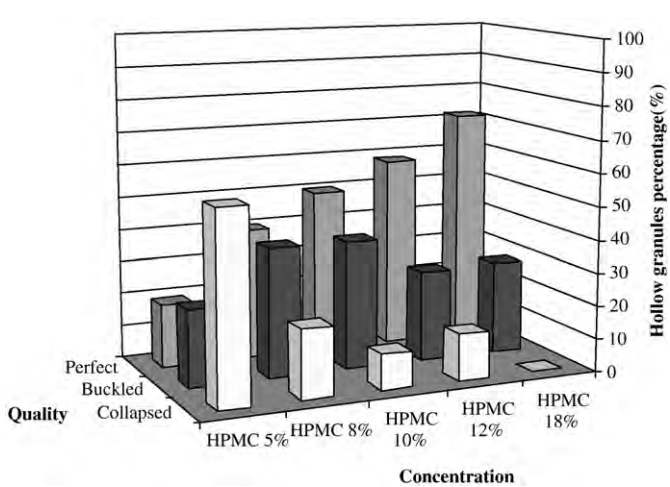

Fig. 7. Effect of increasing HPMC binder concentration. Graph combines data for all powders and both drying temperatures.

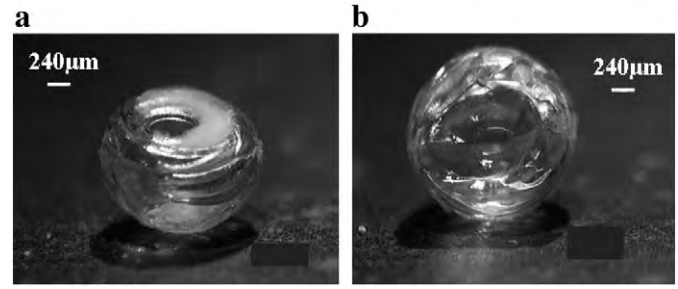

Fig. 8. Hollow granules formed at 100 °C from Aerosil R974 and (a) 12% HPMC, and (b) 18% HPMC.

It was expected that as particle size decreased, the chance of survival would increase as small particles are subjected to less gravity force due to the reduced weight of the small particles. However, for PTFE powder, the largest PTFE 100 μm powder was the most successful, then the 12 μm and 1 μm size grades, and finally the 35 μm size grade which was the least successful. The 12 and 1 μm size grades of PTFE may form better multilayered powder shells due to their cohesiveness and this would improve the survivability. The PTFE 100 may also provide good coverage as each particle was large and the particles were observed to pack fairly densely in the powder shell, leaving relatively only small regions of the droplet surface uncovered. The chance of survival of the liquid marbles will be high as powder creates a uniform particle layer in the liquid–vapor interface [7]. These factors would explain the apparent superiority of 100, 12, and 1 μm PTFE powders over the 35 μm size grade, which was neither large nor cohesive and could not achieve good liquid coverage.

3.2. PVP binder

Increasing the PVP binder concentration also increased the success rate for hollow granule formation. As shown in Fig. 12, increasing the concentration of PVP from 5% to 18% improved survivability. Increasing the binder concentration had only a slight effect on the quality of the granules formed, as there is no significant change in the number of perfect hollow granule across 5 to 18% PVP concentration.

Increasing the drying temperature from 60 °C to 100 °C improved PVP hollow granule survival by decreasing the number of collapsed granules and increasing number of buckled granules across all PVP concentrations (Fig. 13).

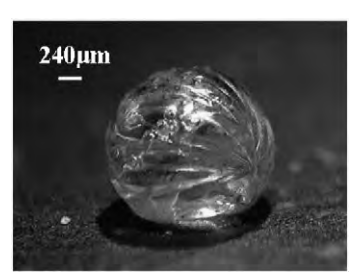

Fig. 9. Hollow granule formed with Aerosil R974 and 18% HPMC dried at 100 °C showing striated surface.

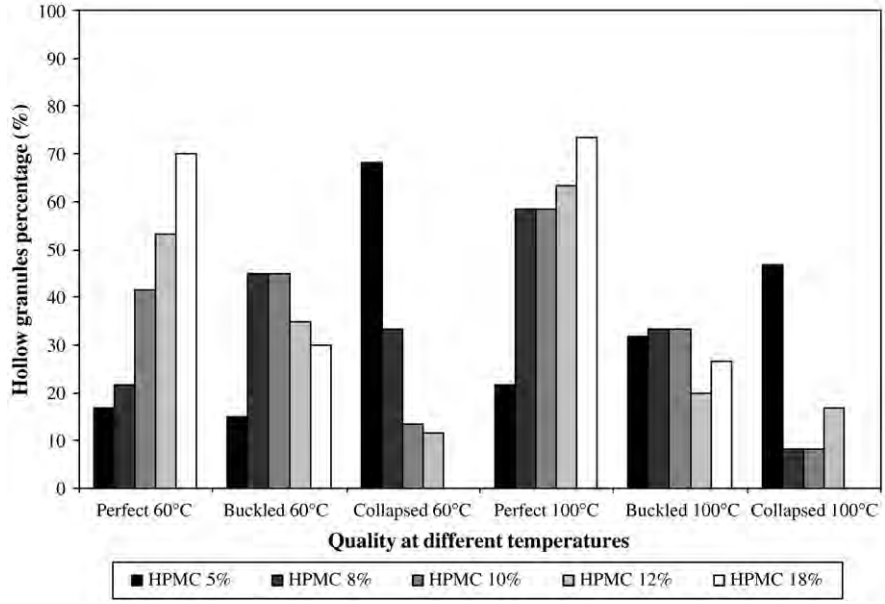

Fig. 10. Effect of HPMC concentration and drying temperatures on survivability and quality of hollow granules (graph includes data for all used powders).

From Fig. 14, Aerosil was the most successful powder (see lowest left image in Fig. 3) with PVP binder, and glass ballotini was the least successful. Hollow PVP granules are most likely to survive if the particle size is small — the nano-sized Aerosil R974 produced 100% perfect granules and the 1 μm and 12 μm grades of PTFE had high survival rates close to 50%. For glass ballotini neither increasing binder concentration nor increasing drying temperature could produce any form of hollow granule. The complete collapse under all conditions implies that some property of the glass powder – perhaps the higher density – is incompatible with PVP binder which corresponds with Walton and Mumford's [10] study that the final morphology of particles depends on the chemical and physical natures of the skin material. In summary, the survival of PVP hollow granules improves as the particle size decreases, the drying temperature increases and the concentration of PVP increases.

3.3. HPC binder

Fig. 15 summarizes whether a hollow granule survived during drying process as a function of HPC binder concentration across all used powders and drying temperatures. As the HPC concentration increases from 5% to 18%, the number of collapsed granules remains almost constant but the quality improves as shown by the decreasing number of buckled granules and increasing number of perfect hollow granules. Above 10% HPC concentration, it seems that the quality of the formed granules decreases while the number of collapsed granules remains constant. In other words, increasing HPC concentration above 10% causes previously perfect hollow granules to start buckling. This implies that there is a limit in increasing the concentration of binder (see Fig. 15) and that there is an optimum binder viscosity and/or surface tension which occurs at 8–10% HPC.

Figs. 16 and 17 summarize hollow granule survivability during drying, as a function of HPC concentration and temperature for ballotini and Aerosil. Higher HPC concentrations are expected to produce stronger hollow granules due to a stronger and denser network of solid bridges which form during the drying process. The lowest HPC concentration of 2% was not able to properly assemble

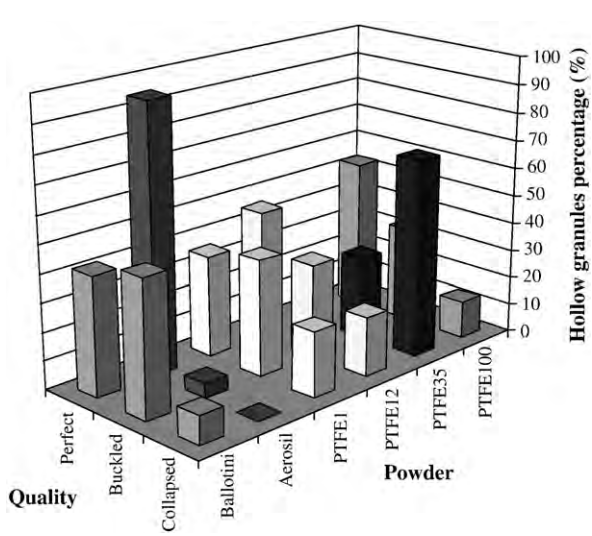

Fig. 11. Effect of powder type on hollow granule survivability and quality. Data for all HPMC concentrations and drying temperatures have been combined.

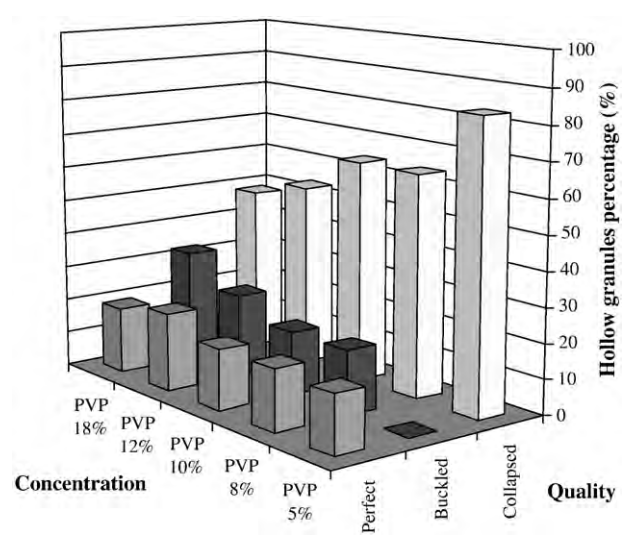

Fig. 12. Effect of increasing PVP binder concentration on survivability of hollow granule (graph includes data for all used powders and both drying temperature: 60 °C and 100 °C).

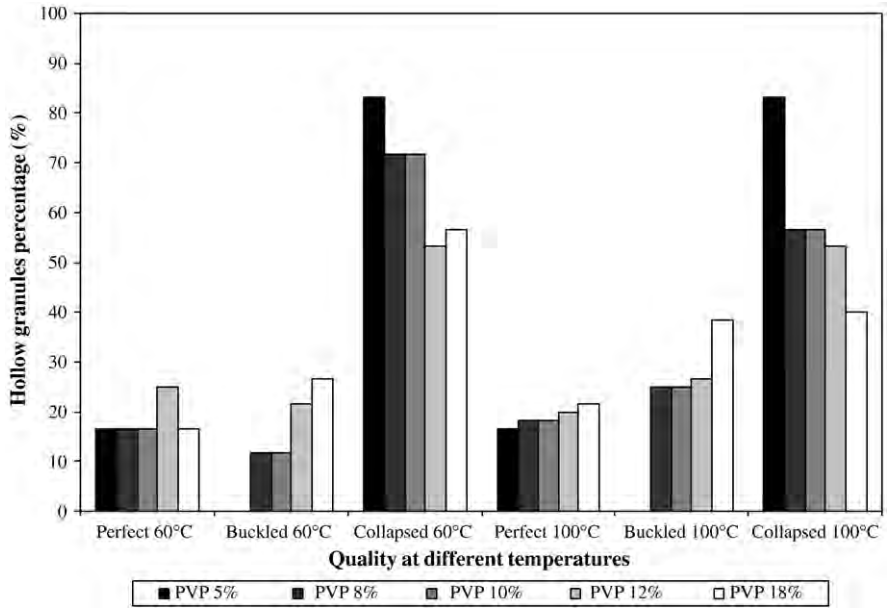

Fig. 13. Effect of increasing drying temperature on survival of hollow granules using PVP binder.

particles together to prevent collapsing the liquid marble during drying, even at the highest drying temperature (100 °C) with Aerosil (see Fig. 16). These figures show that there is a minimum concentration of HPC required to avoid granule collapse, and that the minimum HPC concentration varies for each different powder. For example, 5% HPC could stabilize hollow granules of Aerosil R974 (Fig. 16) at 60 °C, but a higher concentration of HPC (10%) was needed to maintain the hollow structure for glass ballotini (Fig. 17) at the same temperature. The reason for this phenomenon may be related to the particle size and density, as larger and denser glass particles would need higher binder concentration to provide enough interparticulate bonds to withstand the gravitational forces.

Increasing the concentration of HPC binder also affects the hollow granule shape. As can be seen in Fig. 17, by increasing the concentration of HPC binder, more "perfect" granules — including a full "base" are formed from glass ballotini. For instance, by increasing the HPC concentration from 8% to 10%, just over 50% of the hollow granules formed from glass ballotini had a full base at 100 °C. By further increasing the HPC concentration to 18%, all of the formed granules had a base (see Fig. 17). The reason why no bases were formed for Aerosil granules despite a wide range of HPC concentrations is not clear.

The survivability of hollow granule dried at lower temperatures can be increased if the HPC concentration is increased. From Fig. 17 for glass ballotini and up to 8% HPC in binder, all glass ballotini liquid marbles dried at 60 °C collapsed. By increasing the binder concentration from 8% to 10% and 12%, the hollow granule survival rate after drying at 60 °C increased 30% and 60%, respectively.

Figs. 16 and 17 show that the survivability and quality of the hollow granules are different for each powder. PTFE 100 μm powder performed the best with HPC binder in terms of survivability and the proportion of perfect hemispherical shaped granules, compared to the smaller PTFE grades (see Fig. 18). Fig. 18 also shows that Aerosil performs better than other powders, perhaps due to its nano-particle

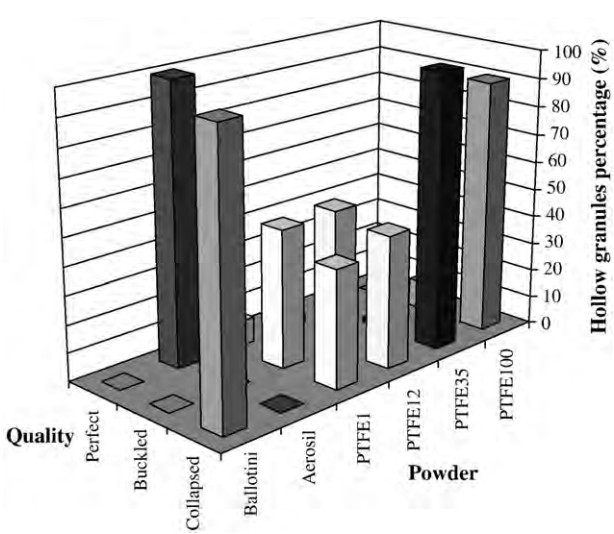

Fig. 14. Effect of powder type on survivability of hollow granule. Data from all PVP concentrations and both drying temperatures have been combined.

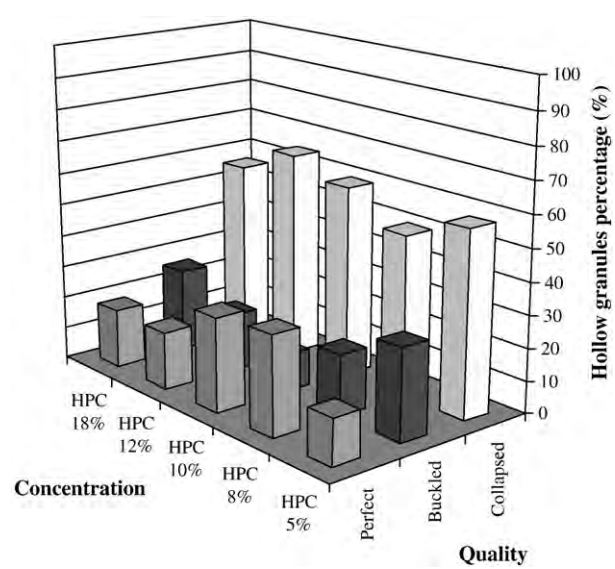

Fig. 15. Effect of HPC concentration on the hollow granule quality (graph combines data for all powders and both drying temperatures).

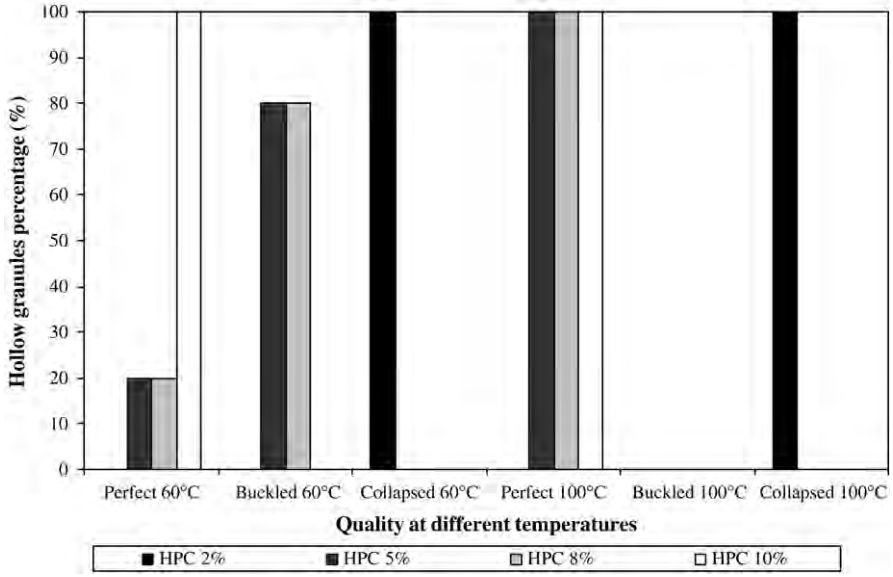

Fig. 16. Effect of HPC concentration on quality of Aerosil R974 hollow granule (graphs combines data for both drying temperatures).

size or the low density of the fractal particle aggregates. Although hydrophobic glass ballotini particles are smaller (65 μm) than PTFE 100 μm and lighter, hollow granule formation was less successful with glass ballotini which indicates the significance of careful powder selection.

In summary, Aerosil R974 was the most successful powder with HPC, and increasing HPC concentration improved the hollow granule quality. The effect of increasing the drying temperature was mixed.

4. Discussion

4.1. Comparing all three binders: HPMC, PVP and HPC

HPMC appeared to be the best binder as it worked well across the various powders and temperatures (see Fig. 19). HPC and PVP seemed to both perform poorly in comparison. However they seemed to complement each other in their response to different conditions: HPC performed well with the glass ballotini while PVP didn't, and vice versa with respect to the PTFE 1 and PTFE 12 powders.

In general, increasing temperature increases survivability in all cases (see Figs. 10 and 13) and improves significantly the quality of granules formed with HPMC (see Fig. 10). Temperature had no significant effect on the quality of hollow granules formed with PVP (see Fig. 13) and HPC (data not shown). There may be a viscosity effect involved, as the PVP was much less viscous than HPC and HPMC (see Table 2). For comparison, Fig. 20 shows the survivability of hollow granules as a function of viscosity for different concentrations of HPMC, PVP and HPC binders. As shown in Fig. 20, for PVP and HPMC there is a consistent proportional relationship between binder fluid viscosity and the proportion of formed hollow granule. In order for a liquid marble to collapse, the drop must deform which requires internal fluid flow. We propose that higher viscosity binder fluids resist this flow and therefore enhance liquid marble stability during drying. However, for HPC, the average survival rate remains relatively constant between 40 and 50% regardless of the HPC concentration or

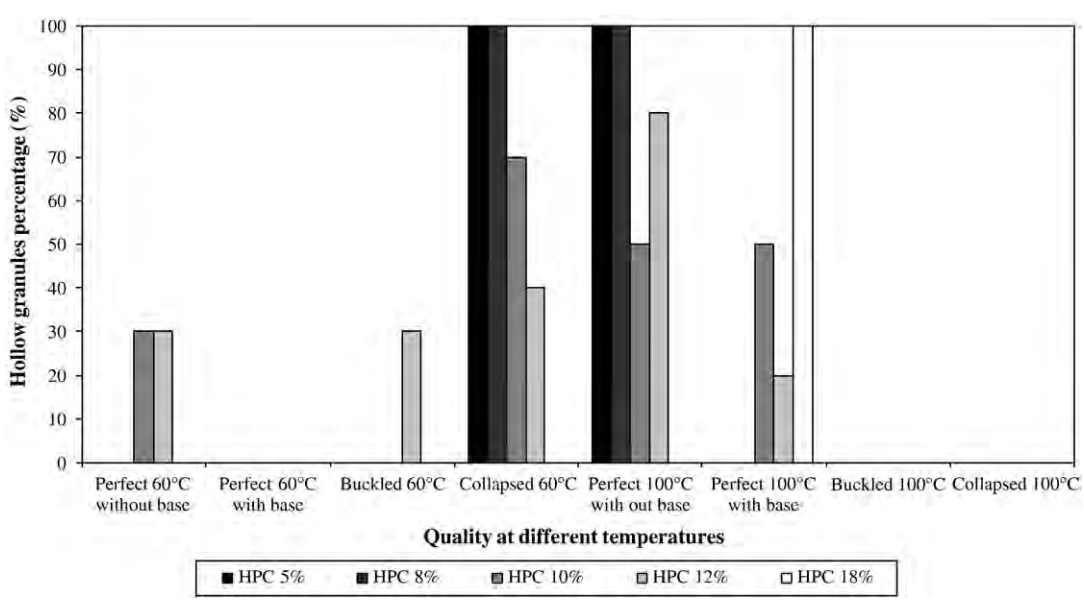

Fig. 17. Effect of HPC concentration on quality of glass ballotini hollow granules (graph combines data for both drying temperatures).

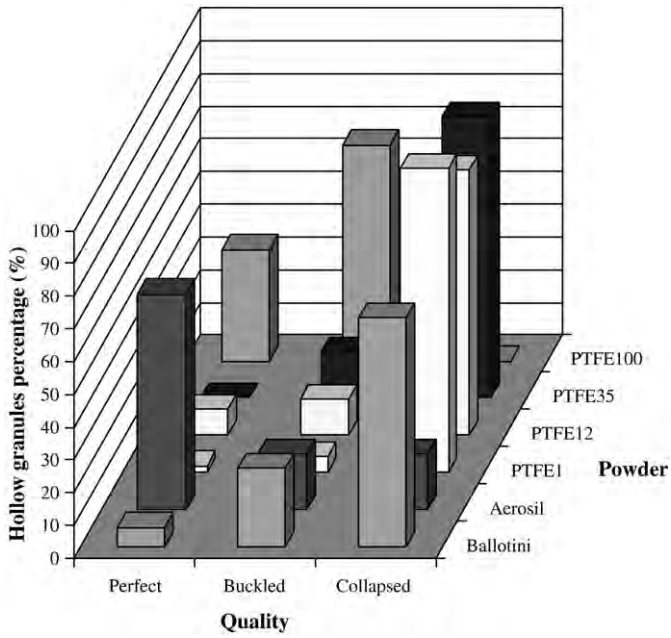

Fig. 18. Effect of powder type on survivability of hollow granules for HPC binder. Data from all HPC concentrations and both drying temperatures have been combined.

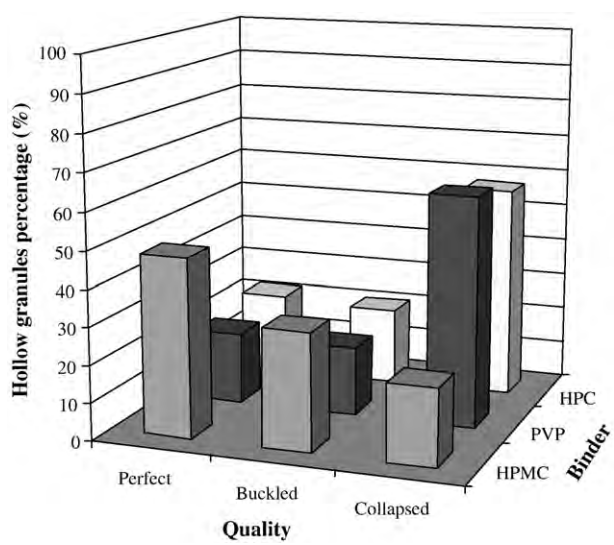

Fig. 19. Effect of changing binder on hollow granule formation. Graph includes data for all used powders and both drying temperatures (60 °C and 100 °C).

viscosity. This may be related to precipitation of HPC and decreasing solubility of polymer in water at higher temperature. HPC is freely soluble in water below 38 °C, forming a smooth, clear, colloidal solution and changes to a swollen floc at a temperature between 40 and 45 °C [12]. HPC precipitates out when the temperature increases above the cloud point, where the hydrogen bonds between water and the polymer chains become less favorable. The solubility of the HPC in water then decreases and a polymer-rich phase precipitates [11] which affect the uniformity of the polymeric bridges formed during drying. For example, the cloud point of a 250 ppm HPC solution is 43.5 °C [11] well below even the lowest drying temperature of 60 °C. As the polymer concentration decreases, the cloud point increases [11]. This may at least partly explain why increasing HPC concentration caused previously perfect hollow granules to start buckling, as the lower cloud point caused earlier precipitation of the HPC which adversely affected the survival rate.

Aerosil was the most successful powder for forming perfect hollow granules with all the binders tested (see Fig. 21). However, there were some exceptions at higher binder concentration (18% HPC and 18% HPMC) and at the highest drying temperature at 100 °C. The most successful combination was 12% HPMC binder using Aerosil R974 dried at 100 °C. The results for glass ballotini had mixed success. It was highly unsuccessful with PVP, moderately successful with the HPMC/HPC and did better at higher temperatures. PTFE powders had mixed success again but at least some of the grades worked with all binders.

Fig. 22 shows the effect of PTFE particle size on the hollow granule survival rate for the three tested binder fluids. For PVP, there is a critical particle size somewhere between 12 μm and 35 μm where only hollow granules formed from particles smaller than this size can survive. HPMC also shows a sharp drop in survival rate for PTFE35, although the survival rate then rebounds for the large PTFE 100 particles. In contrast, HPC shows a high success rate only for the largest PTFE particles.

When drying marbles formed with high binder concentrations, in some instances a higher drying temperature induced collapsing or buckling. At higher binder concentrations, the fluid viscosity could be quite high which causes the droplets to be slightly larger and thus more prone to deformation during the drying process. When dried at 60 °C, more shrinkage of the liquid marbles occurred (see Fig. 23) and this may have increased survivability, as opposed to 100 °C where shrinkage would occur less. Thus, the beneficial effects of drying at a lower temperature when using high concentrations of binder may be due to the enhanced shrinkage and strengthening of the liquid marble during drying. These points at least partly explain the unexpected lack of success at high binder concentrations and higher drying temperatures for both HPMC and HPC binders.

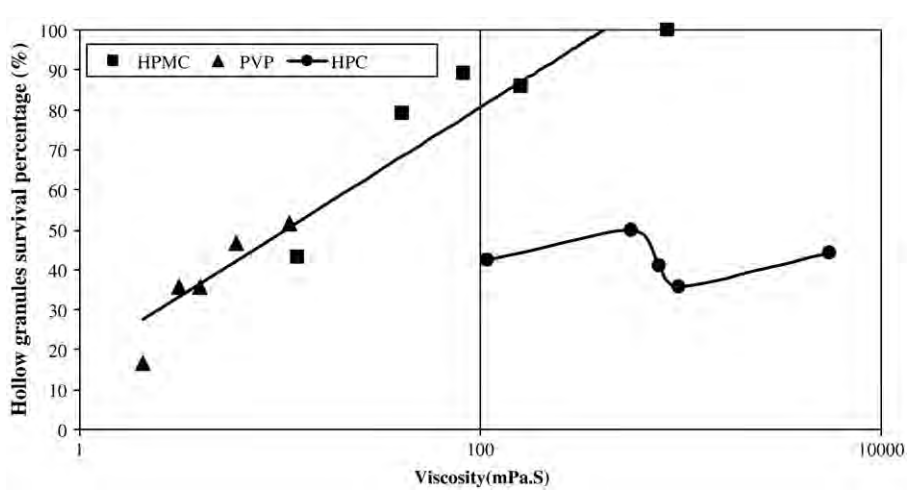

Fig. 20. Effect of binder viscosity on survivability of hollow granules.

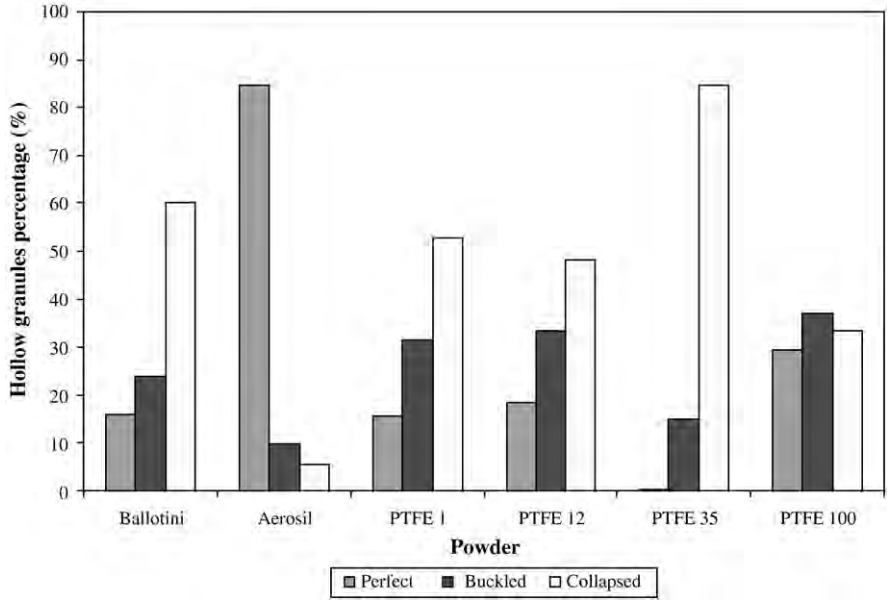

Fig. 21. Survivability and quality of all powder hollow granules. Data from all binders and both drying temperatures have been combined.

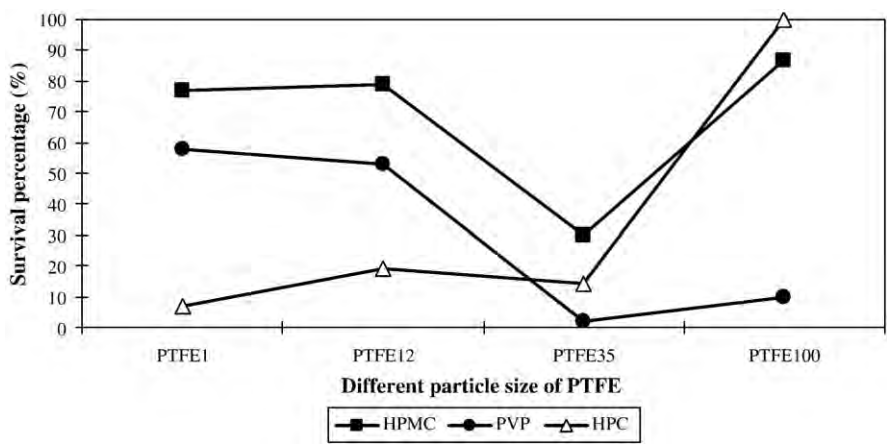

Fig. 22. Effect of PTFE particle size on hollow granule survivability.

4.2. Particle size effect

As drying continues the particles pack closely enough that inter-particle repulsions resist further shrinkage [13]. The binder, however, continues to vaporize through the holes between the particles [8]. The decrease in binder volume causes the receding of the drying surface into the droplet. Buckling of liquid marble can then occur because decreasing droplet pressure exerts a compressive capillary stress on the particle shell. When this stress becomes large enough to overcome the repulsive forces between the particles the outer shell undergoes buckling and wrinkling. It is clear inter-particle forces play an important role in determining droplet buckling, and any other ingredients in the particle shell can affect these forces and the buckling behavior of liquid marble. Polymers are an example of material that can significantly change the interaction between solid particles [13].

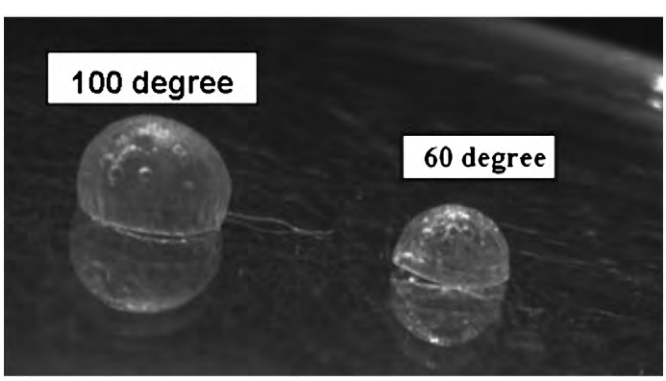

Fig. 23. Comparison of two perfect hollow hemisphere granules of Aerosil with 8% HPC, dried at 60 °C (1.5 mm diameter), and 100 °C (3 mm diameter). Spots on the granule surface are caused by trapped air bubbles.

Aerosil was the most successful powder with all of binders, presumably because the inter-particle forces between the nano-particles are high and able to resist the capillary stress. This is in agreement with the previous study by Bhosale et al. [7] who indicated that the loosely aggregate floc-like structure of the nano-sized silica particles creates a highly porous shell and consequently increases the chance of survival. This hypothesis also agrees with case I in Fig. 1 by Charlesworth and Marshall [9].

4.3. Shrinkage of liquid marble during drying

During drying of the liquid marbles, the droplet shrinks and the final granule size is smaller than the original droplet. The level of

shrinkage depends on the drying temperature. Fig. 23 shows two granules of Aerosil with 8% HPC dried at 60 °C and 100 °C. Although their initial primary droplet size was the same, it is clearly seen that the granule dried at 60 °C is smaller than granule size at 100 °C. The higher drying temperature creates a granule size more comparable with primary droplet size. This can be seen as an additional variable requiring control, or as an additional variable which can be used to manipulate the granule size. We expect that the granules shown in Fig. 23 would also have different granule strengths, due to both the physical size and the film thickness, although we have not performed any experiments to test this to date.

4.4. Implications of liquid marble drying behavior

We have previously postulated a series of steps for liquid marble formation and for hollow granule formation [1]. The final step was that "the multi-component powder shell must be sufficiently strong to be self-supporting in order to avoid collapse during drying to form a hollow sphere and subsequent standard powder handling operations" [1]. Qualitatively, the drying behavior of liquid marbles is in agreement with the types of drying behaviors observed by Charlesworth and Marshall [9] and shown in Fig. 1. All crust structures except IIC were observed during this study. We conclude that the optimal drying conditions for liquid marbles are driven by similar mechanisms for drying of solute drops, except that liquid marbles begin the drying process with a powder shell "crust" already in place. This observation should be of practical use during formulation and product development of cosmetic and pharmaceutical products based on liquid marbles and hollow granules.

5. Conclusion

The optimal condition for stabilizing liquid marbles during drying and formation of hollow granules were investigated for several types of powder and binder at different drying temperatures. Higher drying temperature, smaller or nano-size particles and higher binder concentration tend to promote the formation of perfect hollow granules. It was found that the survival rate was directly proportional to binder viscosity for HPMC and PVP. However; for HPC binder the survival rate was essentially constant regardless of HPC concentration. Different combinations of drying temperature, binder type, binder concentration, and powder type/grade could result in quite large changes in survival rate indicating the importance of careful formulation during hollow granule process development.

Acknowledgements

This project is financially supported by the Australian Research Council under Discovery Projects DP0770462. Scholarship support for N. Eshtiaghi was provided by the Monash Graduate Research School. We express our grateful thanks to Sherry Mayo for taking X-ray microscopy photo of our samples in Manufacturing and Material Technology Group of CSIRO lab.

References

[1] K.P. Hapgood, L. Farber, J.N. Michaels, Agglomeration of hydrophobic powders via solid spreading nucleation, Powder Technology 188 (2009) 248–254.
[2] P. Aussillous, D. Quere, Liquid marbles, Nature 411 (2001) 924–927.
[3] P. Aussillous, D. Quere, Properties of liquid marbles, Proceedings of Royal Society A 462 (2006) 973–999.
[4] L. Forny, K. Saleh, I. Pezron, P. Guigon, L. Komunjer, Influence of mixing characteristics for water encapsulation by self-assembling hydrophobic silica nanoparticles, Powder Technology, Special Issue on Granulation 189 (2009) 263–269.
[5] M.A. Ansari, F. Stepanek, Formation of hollow core granules by fluid bed in-situ melt granulation: modelling and experiments, International Journal of Pharmaceutics 321 (2006) 108–118.
[6] K.P. Hapgood, B. Khanmohammadi, Granulation of hydrophobic powders, Powder Technology 188 (2009) 248–254.
[7] P.S. Bhosale, M.V. Panchgnula, H.A. Stretz, Mechanically robust nanoparticle stabilized transparent liquid marbles, Applied Physics Letters 93 (2008) 034109/1-034109/3.
[8] M. Dandan, H.Y. Erbil, Evaporation rate of graphite liquid marbles: comparison with water droplets, Langmuir (2009), doi:10.1021/la900729d.
[9] D.H. Charlesworth, W.R.J. Marshall, Evaporation from drops containing dissolved solids, AIChE Journal 6 (1960) 9–23.
[10] D.E. Walton, C.J. Mumford, The morphology of spray-dried particles: the effect of process variables upon the morphology of spray-dried particles, Chemical Engineering Research & Design 77 (1999) 442–460.
[11] F.M. Winnik, Effect of temperature on aqueous solutions of pyrene-labled (hydroxypropyl) cellulose, Macromolecules 20 (1987) 2745–2750.
[12] R.J. Harwood, Hydroxypropyl cellulose, in: R.C. Rowe, P.J. Sheskey, S.C. Owen (Eds.), Handbook of Pharmaceutical Excipients, 5th edition, Pharmaceutical Press, London, 2006.
[13] Y. Sugiyama, R.J. Larsen, J. Kim, D.A. Weitz, Buckling and crumpling of drying droplets of colloid-polymer suspensions, Langmuir 22 (2006) 6024–6030.

F

Published Version of:

Producing hollow granules from hydrophobic powders in high shear mixer granulators

(Chapter 7)

Advanced Powder Technology 20 (2009) 558–566

Contents lists available at ScienceDirect

Advanced Powder Technology

journal homepage: www.elsevier.com/locate/apt

Original research paper

Producing hollow granules from hydrophobic powders in high-shear mixer granulators

Nicky Eshtiaghi [a], Benedicta Arhatari [b], Karen P. Hapgood [a,*]

[a] Monash Advanced Particle Engineering Laboratory, Department of Chemical Engineering, Monash University, Clayton, VIC 3800, Australia
[b] Department of Physics, La Trobe University, Bundoora, VIC 3086, Australia

ARTICLE INFO

Article history:
Received 30 April 2009
Received in revised form 20 August 2009
Accepted 23 August 2009

Keywords:
Hollow granule
Liquid marbles
Dry water
Hydrophobic
Granulation
Agglomeration
XRT

ABSTRACT

The formation of hollow granules from hydrophobic powders in a high-shear mixer granulator has been investigated by changing the binder/powder mass ratio and studying its effects on granule size and structure. In this study, a mixer granulator was filled with 100 g of hydrophobic fumed silica and then varying quantities of 5% Hydroxy Propyl Cellulose solution was slowly sprayed into granulator. A range of liquid to solid mass ratios between from 0.5:1 to 15:1 was used. Granules were then dried at 60 °C in a fan forced oven. This paper compares the particle size distributions, scanning electron microscopy (SEM) images and X-ray tomography (XRT) images of hollow granules as a function of the liquid to solid mass ratio. The granule mean size increased and the fraction of un-granulated (fine) particles decreased as the liquid to solid mass ratio increased. Simultaneously, the morphology and structure of the hollow granules changed from a spherical to a deformed structure which indicates the importance of choosing the optimal liquid to solid mass ratio. The optimal liquid to solid mass ratio for Aerosil R202 powder in this study was found to be between 3:1 and 6:1. The final granule shape and size distribution are dependent on the liquid to solid ratio if the liquid marble nucleation process starts with a preformed droplet template.

1. Introduction

A tablet with good characteristics such as good flow and compressibility, uniform concentration of active ingredients and excipients, and few fine particles is not made on a tablet press; it is made in granulation process [1]. Wet granulation is the process of collecting particles together by creating bonds between them using a binding agent. The granulation process combines one or more powders and forms granules that will allow the tabletting process to be predictable. Wet granulation is one of the most common ways to granulate. The granulation process can be very simple or very complex depending on the characteristics of the powders. If the active ingredient represents a high percentage of the blended material and is also hydrophobic like many drugs in the pharmaceutical industry, problems may then begin. In many processes surfactant is added to overcome the problematic characteristics of hydrophobic powders, but in some cases the surfactant is either not compatible or too expensive to be used [2].

Hollow granule formation is a new way to solve the problematic granulating behavior of hydrophobic powders. The dissolution rate of tablets made from hollow granules is rapid and the drying is fast due to the thin shell thickness [3]. These granules also show good compressibility characteristics during the tabletting process [3].

Hollow granules can form from hydrophobic powders by "solid spreading nucleation" [2,3] where the powder spreads around a template drop in the nucleation process and the interior liquid is subsequently dried to form a hollow granule. The nuclei formed by solid spreading are also known as "liquid marbles" [4,5] and "dry water" [6], and are used in cosmetic and pharmaceutical formulations. Liquid marbles and dry powder encapsulation are examples of particle design.

There are now several studies on producing liquid marbles and hollow granules at laboratory scale. McEleney et al. [7] studied the effect of powder density and particle size on the stability of the liquid marbles and reported the formation of a hollow granule shell after drying poly-methylmethacralate (PMMA) liquid marbles. In another study, Eshtiaghi et al. [8] reported three different granule shapes – perfect, buckled and collapsed – after drying liquid marbles in small scale experiments. The formation of perfect hollow granules was generally improved by increasing the binder viscosity, increasing the drying temperature and decreasing the particle size of the powder. In a laboratory scale study, Bhosale et al. [9] investigated the strength of liquid marbles formed with PTFE (7–12 μm) and two types of treated fumed silica powder. High surface area nanoparticle powders (e.g. Aerosil) created more uniform

* Corresponding author.
E-mail address: Karen.hapgood@eng.monash.edu.au (K.P. Hapgood).

0921-8831/$ - see front matter © 2009 The Society of Powder Technology Japan. Published by Elsevier B.V. and The Society of Powder Technology Japan. All rights reserved.
doi:10.1016/j.apt.2009.08.006

powder shells through uniform coverage of the liquid–vapor interface. They found that nano-powder shells form an "elastic" membrane that makes these liquid marbles mechanically robust in comparison with conventional liquid marbles made from larger particles, and that these liquid marbles formed from nano-particles are able to withstand higher compressive stresses during drying, and may be more likely to form hollow granules [9]. These studies did not investigate or attempt the production of hollow granules on a larger scale.

Although there are now several published papers on the production of liquid marbles and hollow granules via laboratory techniques [7–9], only two methods of mass producing of hollow granules are reported in the literature [2,5,10].

The first method for mass production of hollow granules is melt granulation [10] where a single granule is formed from a binder particle by sequential deposition of hydrophilic primary particles on its molten surface. If the first layer of particles forms a stable arch and does not collapse as the binder liquid from the core is drawn by capillary force to the shell region, a hollow core granule is formed.

The second method is via solid spreading nucleation in a high-shear mixer [2,6] and there are two related studies in this area. In one study, "Dry water" was produced by encapsulation of water with various grades of hydrophobic silica [6]. In this study, they found that by decreasing the hydrophobicity of powder, powder shell formation became more sensitive to intense mixing conditions. The liquid marbles became less stable and required lower impeller speed and more powder to encapsulate the same volume of liquid. Atomization into the high-shear mixer was not performed. In this study, the liquid marbles were the desired end product.

Stable hollow granules [3] were successfully produced by drying liquid marbles which were formed via solid spreading nucleation. The granules were produced in a 2 L granulator using a formulation of 70 wt.% hydrophobic drug powder, 20% microcrystalline cellulose and 4% hydroxypropyl cellulose binder as hydrophilic excipients and 1% sodium lauryl sulfate surfactant. The hollow granules were strong enough to withstand the downstream milling process as the excipients stabilized the powder shell to allow the hollow structure to be preserved during drying. Hapgood et al. [3] studied the effect of wet massing time on granule structure for two different liquid ratios and found that the granules tended to deform and elongate as the amount of fluid and/or wet massing time increased. There are no further studies on the effect of changing the binder liquid ratio on the morphology of the hollow granules. More investigation in this area is required.

The objective of this present work is to perform a systematic study of the effect of the binder fluid to powder mass ratio on the size distribution and internal microstructure of granules formed by a high-shear mixer granulation process.

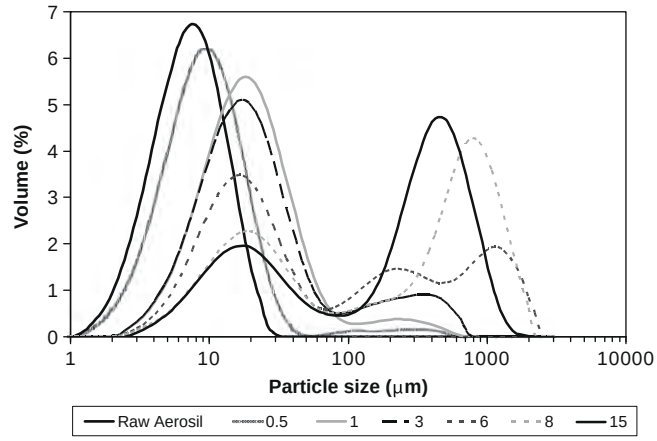

Fig. 2. Particle size distributions for un-granulated and granulated Aerosil with different HPC binder mass ratio in high-shear mixer granulator.

2. Materials and methods

Aerosil R202 (Degussa Co. Germany) is the commercial name for highly hydrophobic fumed silica which has been silanised to turn the surface hydrophobic. The original powder is very fluffy and somewhat dusty with a reported primary particle size of around 16 nm and a high 300 m^2/g BET surface area. However, it tends to self-agglomerate to form large and loose flocculated networks with a much larger particle size between 1 and 30 μm. Fig. 1 shows a SEM image of Aerosil particle aggregates and Fig. 2 shows the particle size distribution as measured by laser diffraction. HPC (Hydroxy Propyl Cellulose, 100,000 Mw, Sigma Aldrich Pty Ltd.) with 5% concentration was used as a binder solution. The viscosity of the 5% HPC solution was measured using a rotational viscometer (Visco Basic Plus, Fungilab, Barcelona) and found to be 108 mPa s.

Granules were prepared in high shear KG-5 (Series IV) laboratory scale granulator from the fumed silica and 5 mass% HPC. The metal mixing bowl was 20 cm in diameter and 13 cm height. A three bladed impeller was mounted at the base of the bowl, and the fluid was added through a nozzle port in the perspex lid. The ratio of binder fluid to powder mass (L:S) was varied between 0.5:1 and 15:1. The granulator bowl was loaded with 100 g of fumed silica and mixing was performed at constant impeller speed

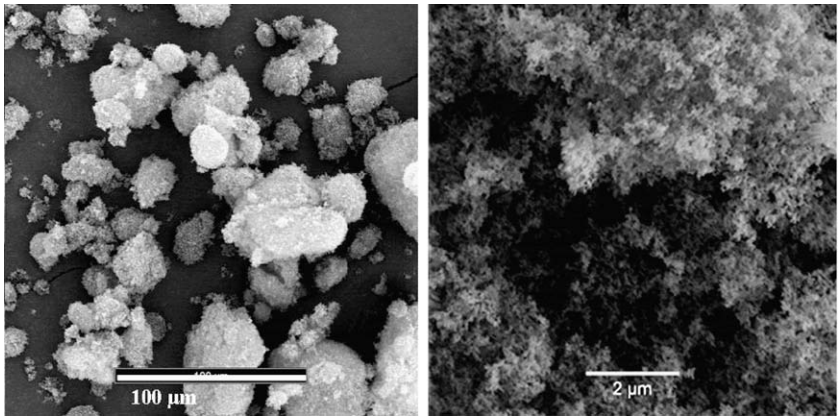

Fig. 1. SEM micrograph of un-granulated Aerosil R202.

of 155 rpm. At this impeller speed, the powder exhibited roping flow. The silica was dry mixed for 2 min in order to break down any weak, loose aggregates of primary particles.

The 5% HPC binder solution was then sprayed into the granulator using Unijet nozzle (400017) at 5.6 bar pressure and 90 g/min flow rate. The distance from the nozzle tip to the powder surface was approximately 3 cm and the spray width at this point was almost 1 cm. The droplet size distribution 3 cm below the nozzle was measured using a Malvern Spraytec with a 300 mm lens, which measures up to a nominal drop size range of 0.5–900 μm. The d_{50} drop size was 442 μm, with a broad distribution of (d_{10} = 145 μm, d_{90} = 763 μm). The total spray time varied with the liquid ratio. To reach a liquid ratio of 6:1 took 6.67 min of spraying while a liquid ratio of 15:1 was reached after 16.75 min of spraying. At the completion of the granulation step, approximately one third of the wet granulated powder was tray-dried in a forced-fan oven at 60 °C.

Particle size distributions were analyzed by laser diffraction using a Malvern Mastersizer 2000 with detectable particle size between 0.2 and 2000 μm. Analysis was performed in dry mode using 3 bar pneumatic transportation for un-granulated Aerosil powder and at 0.5 bar for analyzing the hollow granules. The vibrating feeder was set to 100% to obtain an obscuration between 1% and 6%. These conditions were chosen based on titration of the pneumatic transport pressure and vibrating feeder settings, to ensure reproducible data. The Aerosil R202 was quite difficult to measure reproducibly due to its aggregated initial state and sensitivity to electrostatic forces. A pneumatic pressure of 3 bars was found to be the optimum pressure for dispersing the un-granulated Aerosil. Below 3 bar, significant large aggregates of primary particles were found while increasing the pressure above 3 bar caused the Aerosil particles to re-aggregate. The pneumatic transport pressure used for analyzing the granules was 0.5 bar, which was again found to be the optimum which was able to disperse the particles in the laser beam without significant breakage of the granules.

Laser diffraction uses an assumption of constant density across the entire size range when reconstructing the particle size distribution of the sample. There are many cases where this assumption is questionable, including when analyzing "normal" granule size distributions where there is a mixture of porous granules and non-porous particles from the raw powder. In these experiments, the "un-granulated" fine Aerosil particles are also low-density, fractal aggregates of nano-particles with >90% void space. Thus, any density differences between the hollow granules and the raw aggregated powder is expected to be far less than would occur in a "normal" granulation experiment.

Granules were sieved into size fractions (1000, 500, 250, 125, 63 μm) and the microstructure of each sieve fraction was characterized scanning electron microscopy (SEM) and X-ray tomography (XRT). Representative granule samples were imaged using either JEOL 840A SEM equipment (back scattering at 20 kV acceleration voltage, 3e−10 probe current or at 15 kV and 1e−9 probe current), or JEOL 6300 FEG SEM equipment at 5 kV acceleration voltage. Back scattering and/or low acceleration voltages were required to overcome granule charging problems which occurred while taking some images.

Three dimensional X-ray images of granules were obtained using X-ray micro computed tomography machine (Xradia Inc. USA) with approximately 2 μm resolution. The X-ray sources operated at 40 kV. Each granule was scanned by acquiring 361 or 721 projections taken at 0.5° or 0.25° rotational increments. The distance between the source and sample was 80–125 mm, and the sample detector distance was fixed at 20–25 mm. Different exposure times and magnifications were used for scanning different mesh size granules to acquire sufficiently detailed images. After collecting a set of phase contrast projections (where each projection shows mainly the edge enhancement of the sample), these projections were processed with tomography reconstruction software to produce three dimensional phase contrast data.

The phase contrast projection data-set from some samples were then selected to apply a phase retrieval step. Phase retrieval is applied to each phase contrast projection image to obtain a phase map of the object in each projection. The resulting phase images are then tomographically reconstructed to produce a 3D phase map of the sample. Phase retrieval represents a considerable advance over phase contrast images in terms of obtaining a quantitative measure of the object reflective index, whereas phase contrast can obtain only qualitatively the object structure that can be seen typically in the edge enhancement This is a useful technique for imaging a transparent material (e.g. Aerosil) as transparent materials produce poor absorption contrast, and require an intermediate step of phase retrieval to acquire more detailed images.

3. Results

The effect of liquid–solid ratios ranging from 0.5:1 up to 15:1 on granule morphology and size distribution was investigated. The liquid ratio of 15:1 was the upper limit of liquid to solid ratio. After adding 1.5 kg of solution to 100 g of powder, the granulated mass showed behavior similar to a soft solid, where vibrating the powder bed would cause the bed to wobble like jelly due to attaching liquid marbles to each other. This was also the upper limit that could be handled in the 4 L mixer bowl as the bed swelled so dramatically that the granule flow was visibly constricted by the granulator lid.

Fig. 2 shows particle size distribution (PSD) for the granulated Aerosil as a function of liquid ratio. The particle size distribution of the un-granulated Aerosil R202 is shown for comparison. Prior to granulation, the raw Aerosil powder is aggregated between 1 and 30 μm. After 50 g of water has been added (i.e. L:S ratio of 0.5:1) the main un-granulated powder peak is mostly unchanged, but a small proportion of newly formed granules appear as a second peak between approximately 80 and 600 μm. The location of this main granule peak seems to coincide with median drop size of the spray, suggesting that these granules are being formed directly from the drop templates in the spray. Adding a further 50 g of liquid to reach a 1:1 liquid ratio shifts the un-granulated peak slightly to the right and the proportion of granules formed increases. The shift in the un-granulated peak suggests that the finest particles in the feed powder are being granulated first.

As the liquid to powder ratio increases to 6:1 the amount of un-granulated powder decreases sharply and two peaks are seen in the granule distribution – the first at approximately 200 μm and the second at approximately 1 mm. At 8:1 liquid ratio, the batch is more than half granulated and the main granule peak has shifted upwards to approximately 1 mm. Further liquid addition to the limit of 15:1 appears to show some breakage of the granules as relatively few granules larger than 1 mm remain. Overall, Fig. 2 shows that as the liquid to solid mass ratio increases, the proportion of granules (approx 100 μm–2 mm) steadily increases with a major granule peak around the mean droplet size (440 μm) while the amount of un-granulated Aerosil (<100 μm) steadily decreases. Table 1 summarizes the particle size distribution statistics as a function of liquid level.

Fig. 3 presents SEM images of the granules and Fig. 4 presents X-ray tomography (XRT) images as a function of both granule size and liquid ratio. The particle size distribution results in Fig. 2 are consistent with observations from the SEM images (Fig. 3). The sieve cut of 63–125 μm contains a mixture of un-granulated and granulated powder. As the binder:solid ratio increases from 0.5:1 to 15:1 (see Fig. 3a, d, g, j, n and s) the amount of un-granulated

Table 1
Mean values for un-granulated and granulated Aerosil with different HPC binder mass ratio in high-shear mixer granulator.

Liquid ratio	d_{10} (μm)	d_{50} (μm)	d_{90} (μm)	Surface mean d_{32} (μm)	Volume mean d_{43} (μm)
Un-granulated Aerosil	3	7	14	6	8
0.5:1	4	9	20	7	16
1:1	7	17	49	14	32
3:1	7	18	173	14	56
6:1	7	30	946	19	262
8:1	10	308	1107	32	436
15:1	11	264	702	34	305

powder in the 63–125 μm SEM images also visibly decreases, which is consistent with the size data in Fig. 2. For L:S ratios between 0.5:1 and 6:1, a second peak representing small granules appeared in Fig. 2. XRT images shown in Fig. 4a–c confirm that these small granules are indeed hollow.

We also observed that as the L:S ratio increased, the liquid marbles tended to attach to each other and produce larger, irregularly shaped granules, which are not desirable (compare Fig. 3p with Fig. 3c). The granules gradually become elongated and deformed as the liquid level and average granule size increases, as observed in another liquid marble system [3]. Many of the granules shown appear to be partially collapsed or buckled in shape. This kind of structure is not seen in conventional granulation, but has been observed previously in solid spreading nucleation systems [2,8].

Fig. 3 shows the gradual evolution in granule size up to a maximum of approximately 500 μm. Although the laser diffraction results in Fig. 2 shows that there are granules above 1 mm in size, these samples generally broke during the SEM or XRT sample preparation procedure, which indicates that they are loose aggregate of particles. Only at the two highest liquid ratios tested – 8:1 and 15:1 – could images of the largest granules be taken. An XRT image of a 1 mm loose aggregate formed at 8:1 liquid ratio is shown in Fig. 4s. The structure of this fragile granule is clearly different to all the other granules shown and the granule was not hollow.

The XRT images in Fig. 4 demonstrate that most of the hollow granules formed across all L:S ratios have a complex and almost foam-like internal shape structure. As the L:S ratio increases, this structure stretches and finally produces a filament-shaped granule. These stretched granules are clearly seen in SEM images (see Fig. 3b, e, h, k, o and t) and XRT images (for example see Fig. 4w and x). Only a few spherical hollow granules containing only one hollow cavity were found and an example is shown in Fig. 7. These granules were mostly in the 63–125 μm sieve cut and can be seen as small round granules in the top row of Fig. 3, although the example shown in Fig. 7 is a larger 250–500 μm example. This is in contrast to previous work on hollow granules [3], where single

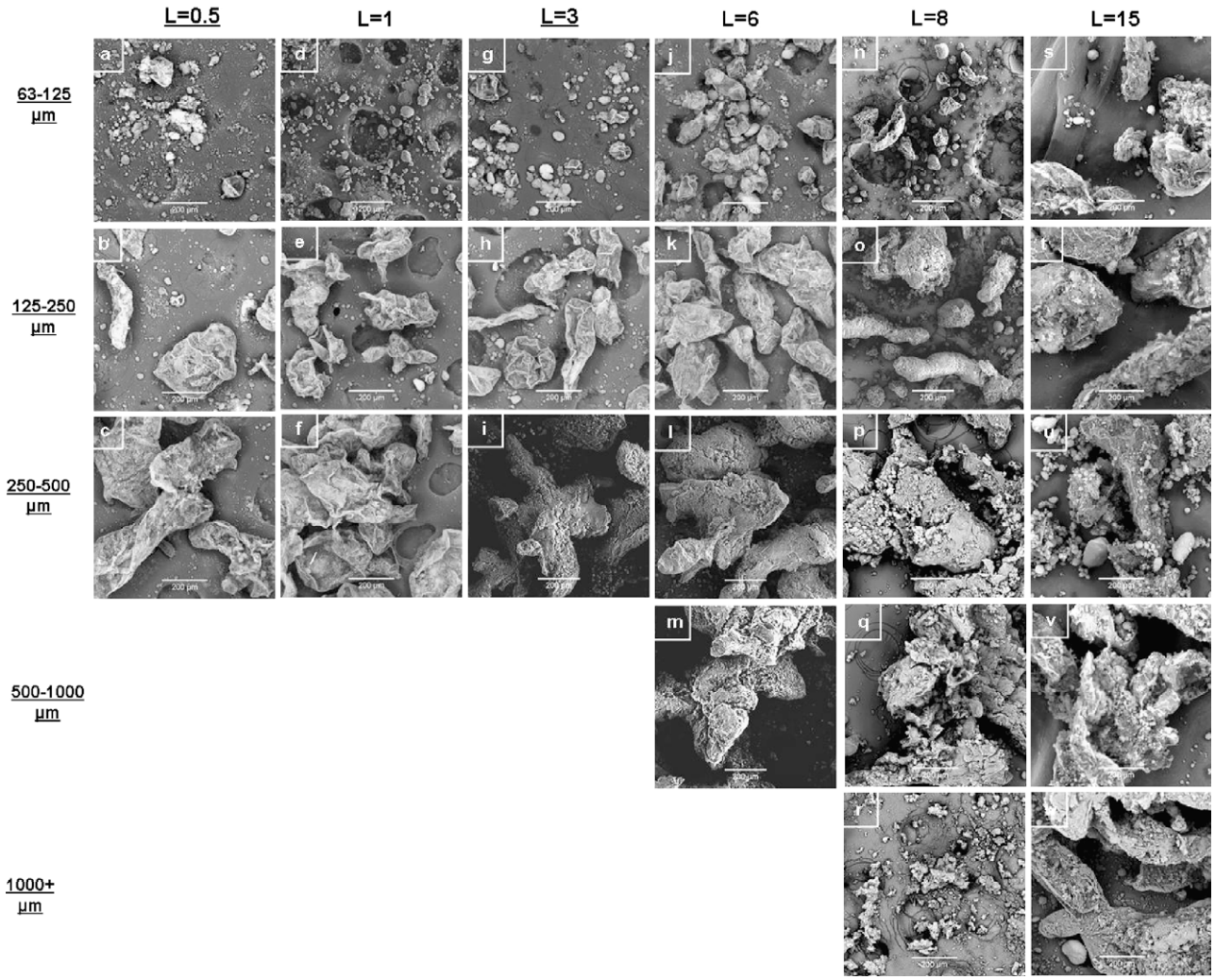

Fig. 3. SEM micrograph for 63–1000 μm mesh cut of granulated Aerosil with different HPC binder mass ratio in high-shear mixer granulator (scale bar is 200 μm).

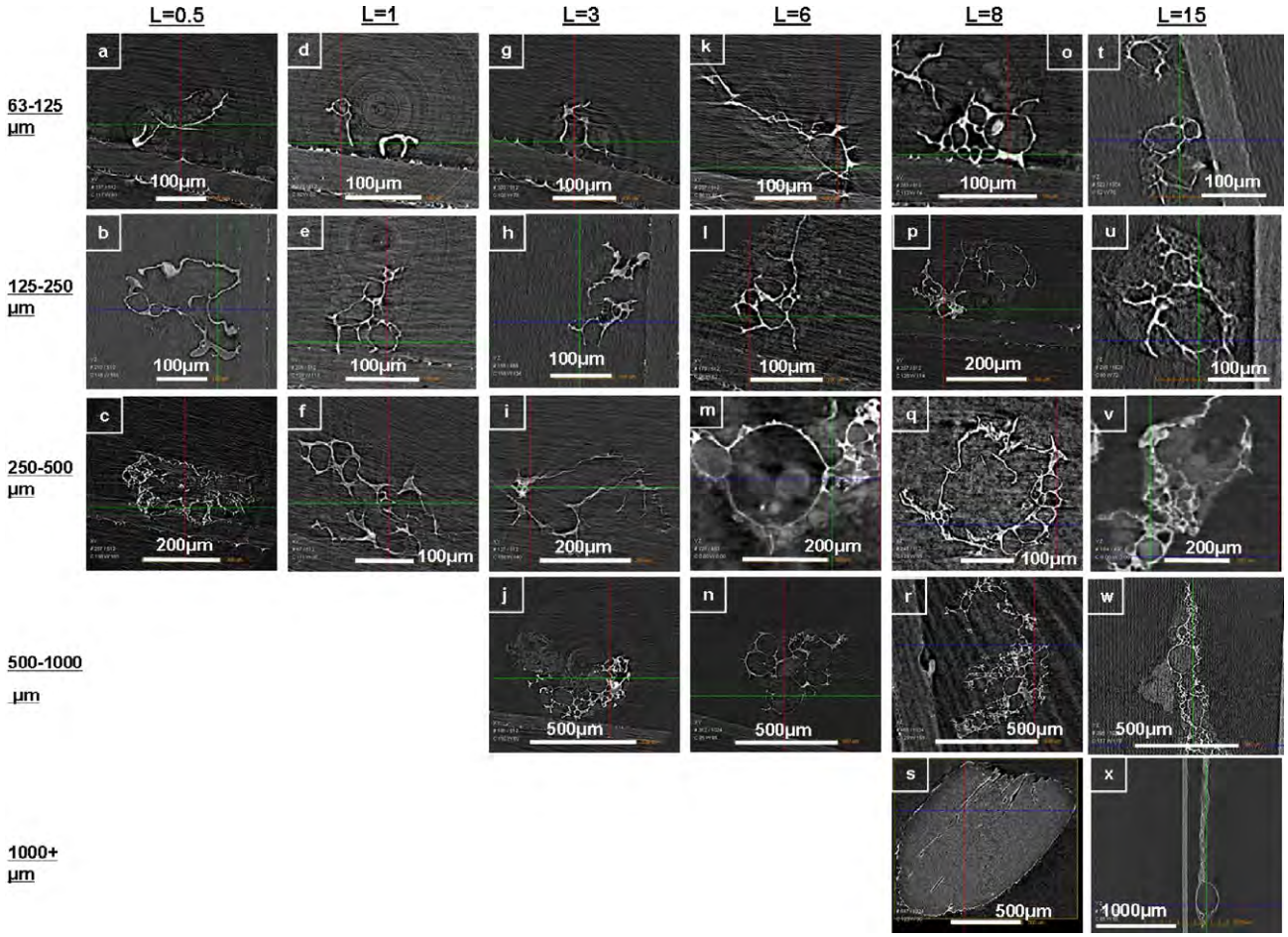

Fig. 4. X-ray tomography of the granule internal structure as a function of liquid binder mass ratio and granule size.

cavity spherical granules were commonly found and the even the larger granules only contained 2–4 hollow cavities rather than the complex foam structure observed here. The reasons for the differences in structure are unknown and could be related to the formulation, the processing conditions, or both.

The maximum granule size at the highest L:S ratio of 15:1 decreases from 1000 µm to around 500 µm (see Fig. 2) which is indication of granule breakage. We expected to see loose aggregate granules above 1 mm but the X-ray image of this mesh cut (Fig. 4x) at 15:1 liquid:solid ratio indicates the existence of hollow granules. The corresponding SEM image for this mesh cut (Fig. 3w) also reveals large granules, and is quite different in appearance to Fig. 3r which shows the same sieve cut at a lower liquid ratio of 8:1. The appearance of at least some hollow granules greater than 1 mm at the highest L:S ratio of 15:1 may be related to the availability of enough binder fluid to granulate all the particles. However, none of these examples of granules greater than 1 mm are suitable for drug delivery as they are either loose aggregate of the primary particles or flattened and stretched filament of hollow granules (see Fig. 4s and x, respectively).

As granulation proceeds, we see increased coalescence of the granules as the L:S ratio is increased. The granules tended to coalescence in layers or sheets to form large granules (typically 500 µm and larger) with a foam-like internal structure. Figs. 5 and 6 show XRT cross sectional images of foam sheet for 500 µm mesh cut of 3:1 and 15:1 L:S mass ratio, respectively. We expect these granules will have different strengths as their shell thicknesses are quite different. The foam formation is most likely caused by compression and squeezing of the liquid marbles during processing, perhaps even in the highly turbulent spray zone. The Aerosil R202 powder has an extremely low bulk density and the roping flow pattern in the granulator was significantly disrupted as it passed beneath the overhead nozzle. Preliminary experiments with smaller batches showed that it was possible for the force of the spray to blast the powder out of the way and land directly on the metal base of the bowl. Forny et al. [11] have shown that there is a threshold energy per unit mass, above which a phase inversion to form a "mousse" can occur. In our experiments, no bulk phase inversion of the batch occurred, and the patches of foam-like structure could either be coalescence of liquid marbles or localized areas of phase inversion to form a mousse. Alternatively, the foam structure may be related to foaming and bubbling during drying which can occur due to the evaporation of a residual liquid inside partially dried particles [12]. Walton and Mumford [12] reported high surface area powders with strong gas absorption properties had higher internal porosity after drying due to adsorption of absorbed gases.

To maximize the number of spherical, single cavity granules and minimize the formation of foam sheets, choosing the optimal L:S ratio is important. For the process examined in this paper, the optimum L:S ratio appears to be between 3:1 and 6:1. The size distribution data in Fig. 2 shows a reasonable conversion of dry powder to hollow granules, while the granules morphology shown in Figs. 3 and 4 show minimal occurrences of all undesirable effects

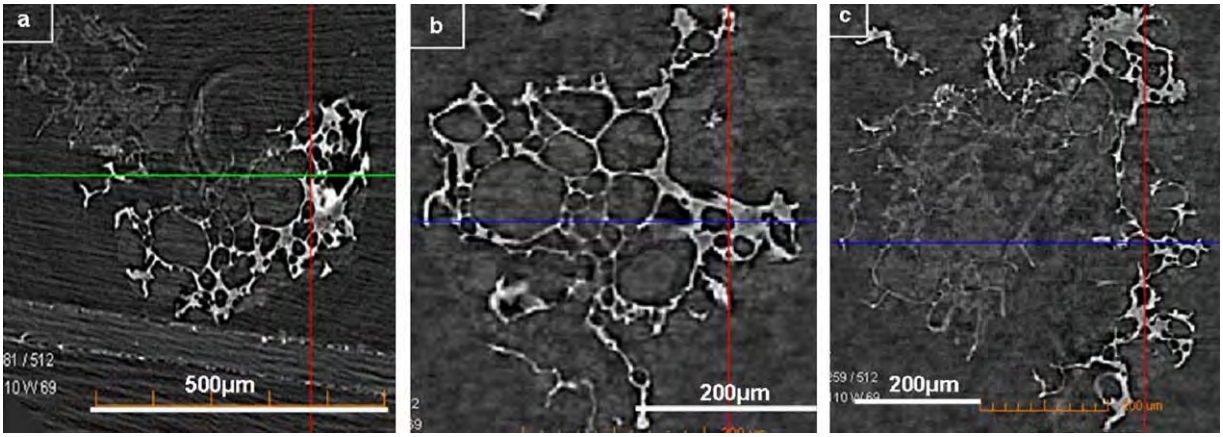

Fig. 5. (a) X-ray tomography of 3:1 binder: powder granules, (b) bottom cross sectional area of image a, (c) top cross sectional area of image a.

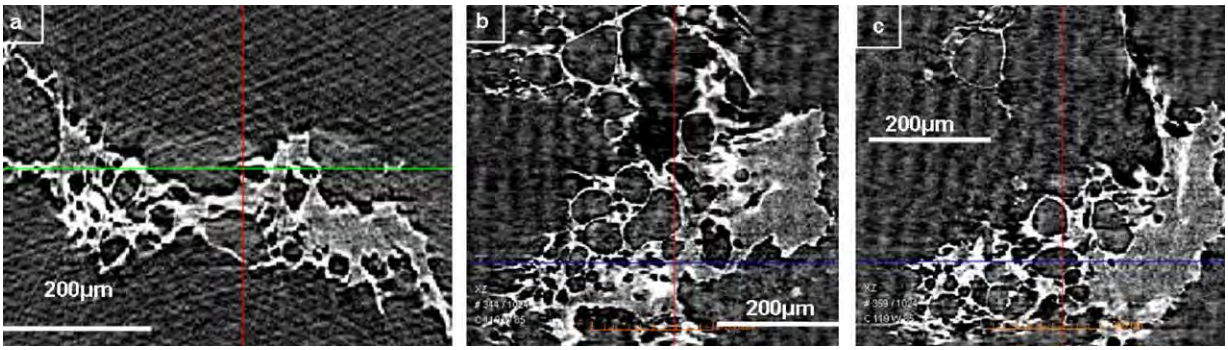

Fig. 6. (a) X-ray tomography of 15:1 liquid: powder granules (b) bottom cross sectional area of image a, (c) top cross sectional area of image a.

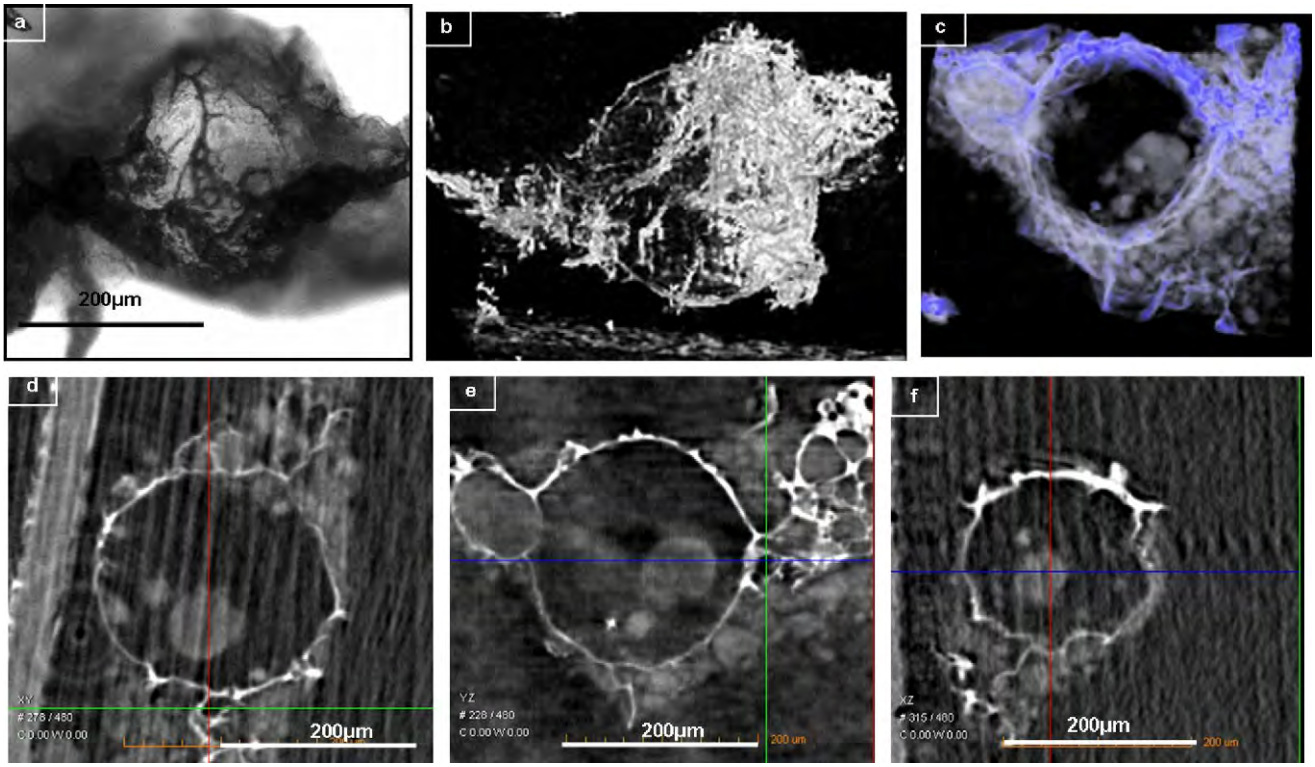

Fig. 7. XRT image of 6:1 L:S ratio. (a) Three dimensional microscope image, (b) three dimensional X-ray tomography phase contrast image, (c) three dimensional X-ray tomography phase retrieval image, (d) XY cross sectional area, (e) YZ cross sectional area and (f) XZ cross sectional area.

such as foam sheet formation, stretched filament granule, and also considerable amount of un-granulated fine particles are less illustrated in this range.

There are some interesting features hidden in X-ray tomography images when they are reanalyzed as phase retrieval images instead of phase contrast images. All images in Fig. 4 are phase contrast images except Fig. 4m and v. Fig. 7 demonstrates phase retrieval image of L:S mass ratio of 6:1 for 250–500 μm mesh cut. A spherical hollow granule is shown, which appears to be filled with smaller spherical powder aggregates. The internal aggregates may be formed during granulation, or perhaps are related to erosion of the interior of the granule shell during drying, transportation, sampling, or sample characterization, or can be related to internal blistering occurred during drying [12]. This internal blistering produces small particles or blisters within the larger parent particle. The bright outlines surrounding the circumference of the spherical granule in Fig. 7d–f (and the small foam sheet around the granule in Fig. 7e) indicate a denser wall structure formed from Aerosil and HPC binder, while the faded white color within the granule is consistent with lower density un-granulated Aerosil.

The phase retrieval images also help to interpret some features observed in the SEM images. Many of the granules shown in the SEM micrograph images in Fig. 3 have multiple small, spherical attachments on the surface. For example, see Fig. 3p and u. From the SEM images, it is not clear whether these attachments were small hollow granules or small aggregates of the primary particles. By comparing SEM and X-ray images (see Fig. 8) the low-density circles on the outside of the granule outline are clearly not hollow. We conclude that these small exterior attachments are mostly aggregate of un-granulated Aerosil particles.

4. Discussion

The work presented here has shown that stable hollow granules can be produced from liquid marbles formed from hydrophobic Aerosil R202 and 5% HPC binder in a high-shear mixer granulator. The formulation used here is far simpler than the formulation reported previously [3] although the granule structure is far more irregular and complex than the earlier reports. This may be due to the extremely high liquid ratios used; differences in the formulation used, or due to the processing conditions including the high-shear mixer design. In comparison, the maximum liquid to solid ratio in the previous report of hollow granule formation from liquid marbles was only 0.78:1 [3]. The smaller liquid ratio may have made their system simpler to control, as even the larger granules contained a single hollow cavity [3] rather than the complex foam structure found in this work. In addition, the formulation used in the previous study contained several different components with different functionality, including a surfactant and water absorbing cellulose [3]. This more complex formulation changes the interactions between the solid and liquid and may have contributed to producing spherical, single cavity granules. The dramatic differences in granule structures indicate the importance of performing X-ray tomography experiments during hollow granule formulation design.

Our experimental results show Aerosil R202 powder, which is the most hydrophobic commercial pharmaceutical grade, can encapsulate up to 15 times of its own weight of 5% HPC solution, which is extraordinary. Previous studies on a similar system of Aerosil R202/R812S and pure water in a high-shear mixer granulator were able to encapsulate 24 times the powder weight [6]. This was not attempted in this study due to the volume restriction of used granulator. Forny et al. [6] reported that the formation of liquid marble becomes less sensitive to mixing conditions as the hydrophobicity of the Aerosil powder increases, and that liquid marbles can be produced at using any impeller design at the correct speed. We were able to encapsulate fluid 15 times of powder weight without producing a bulk mousse. We note that the mixing conditions and rotational speeds used in this study were different from previous study [6]. This demonstrates that liquid marbles can be formed in any equipment using highly hydrophobic Aerosil as long as the mixing condition remains in roping regime [13]. The roping regime ensures good mixing from top to bottom of the powder in the granulator. If powder mixing is poor, the binder will accumulate in bottom of granulator and fewer liquid marbles will form. Poor mixing can occur if the powder flow is in the bumping flow regime [13] or if the powder circles the exterior wall of the granulator due to low mass and high centrifugal forces (e.g. high Froude number). We found that centrifugal flow is easy to induce when using a low-density, highly aerated powder like Aerosil.

Forny et al. [6] reported that changing the liquid to solid ratio does not affect on the shape or size distribution of the formed granules. In contrast, our study showed that the shape and the size distribution of granules were influenced by L:S ratio. The discrepancy between our observations and previous work may be related to liquid addition method, as we atomized the liquid into the high-shear mixer but in previous work the bulk of water was added into mixer. By spraying liquid, the granulation process starts with a preformed droplet, but by adding bulk of liquid then mixing, the

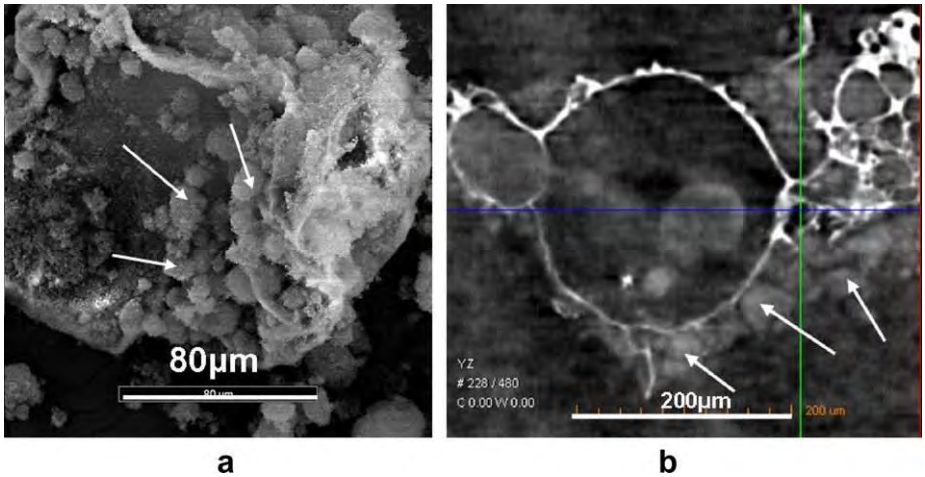

Fig. 8. Images of 6:1 binder ratio (a) SEM micrograph image (b) X-ray tomography image.

process of nucleation starts in mechanical dispersion regime [14]. These two methods of adding liquid indicates two different nucleation mechanisms for forming the drop templates for the liquid marble. These different methods in turn cause changes in the granule shape and particle size distribution in response to changes in the operating variables.

In the melt granulation method for producing hollow granules, Ansari and Stepanek [10] reported that the un-granulated fine particle fraction dropped as L:S ratio increased, but the granule size was only affected slightly. We also found that the proportion of un-granulated particles decreases as the L:S ratio increases, in contrast to Forny et al. [6] who used an almost identical formulation. This may imply that nucleation of liquid marbles from a preformed droplet template determines how the granulation process will proceed, regardless whether solid spreading nucleation [3] or melt granulation [10] is being used.

Although, the mechanism of hollow granule formation in our study and Ansari's study [10] was different, the "solid spreading" nucleation stage of both processes starts with a preformed droplet template. Both studies found that the granule morphology was affected by the L:S ratio. This was not seen in Forny's study [6] even though also had a "solid spreading" nucleation process.

The SEM and XRT data showed that as the hollow granule size increases, they tend to become buckled, which has also been reported previously [2,7–9]. As reported in our previous study [8] using a similar formulation, 80% of Aerosil (R974) and 5% HPC granules buckled at 60 °C drying temperature and only 20% of granules had perfect hemispherical shape. In this study, we also see the same buckled and spherical shaped hollow granules, but had expected to see more spherical granules due to the smaller droplet size of the binder (less than 500 μm). The previous work used much larger, 3 mm diameter single droplets and liquid marble quality was improved as droplet size decreased [8]. Also, the Aerosil R202 used in this study had higher surface area compared to Aerosil R974 [6] which may produce a more uniform shell and more robust liquid marbles during drying [9]. The probability of buckling during drying appears to increase as more liquid marbles attach to each other due to longer residence times in the mixer, or perhaps during sample handling while wet. These larger granules will experience more compressive stresses during drying [9]. This may be because the irregular shape and higher mass of the large granules creates stresses that break the wet bridges between particles during drying. Symmetric spherical granules are inherently more mechanically robust because the spherical shape is a somewhat self-supporting. Irregularly shaped granules would require much more concentrated binders to support the same mass of powder.

The intention of this study was to determine the optimum conditions for producing perfect spherical hollow granules but as can be seen from Fig. 3 most of the granules are buckled with many depressions and twists on the exterior surface. The appearance of a buckled surface was also seen in small scale experiments during drying of liquid marbles [7–9]. For PVP and HPMC solutions, success rate of hollow granule formation was proportional to the binder fluid viscosity [8]. However, for HPC solutions, the average survival rate remained relatively constant regardless of the HPC concentration/viscosity [8]. This may imply that the shear experienced by granules during the longer residence time in the granulator is important in determining the extent of granule buckling and deformation in granulator. Specifically, higher liquid ratios and longer spray times mean that the total shear experienced by the granules is also higher. Consequently, the proportion of deformed or buckled hollow granules as well as filament and foam-like granule increases. These large scale experiments had less success in producing high quality hollow granules compared to small scale experiments [8] even though we used a higher surface area Aerosil and smaller droplet size. Both of these were expected to produce more robust spherical hollow granules. Choosing the optimal L:S ratio is very important in terms of maximizing the chance of survival of spherical hollow granules and minimizing the portion of un-granulated fine material. In addition, shorter residence times may be better for producing spherical hollow granules, although further experiments with different types of powders are required to test this. In all cases, the existence (or not) of hollow granules should be confirmed with XRT.

5. Conclusion

The effect of liquid to solid mass ratio on hollow granule formation in high-shear mixer granulator has been studied. The final granule size was found to be increasing as the liquid to solid mass ratio increased. As the liquid to solid ratio increased, the amount of un-granulated fine particles decreased but the proportion of flattened and stretched filament granules increased which indicates the importance of choosing an optimal liquid to solid ratio. The optimal L:S ratio for Aerosil R202 in this study was found to be between 3:1 and 6:1. In this L:S range, more of the raw fine particles were granulated and fewer flattened hollow granules were produced. The final granule shape and size distribution were dependent on liquid to solid ratio when the liquid marble nucleation process began with a preformed droplet template from an atomized spray. When there is no droplet template at the start of process (e.g. mechanical dispersion of a large bulk of fluid, [6]), the final shape and size of granules is independent of liquid to solid ratio and formation of liquid marbles occurs in a mechanical dispersion regime.

Acknowledgements

This project is financially supported by Australian Research Council under Discovery Projects DP0770462. Scholarship support for N. Eshtiaghi was provided by Monash Graduate Research School.

References

[1] M.D. Tousey, The granulation process 101, basic technologies for tablet making, Pharmaceutical Technology Journal, Tableting & Granulation Yearbook (2002) 8.
[2] K.P. Hapgood, B. Khanmohammadi, Granulation of hydrophobic powders, Powder Technology 188 (2009) 248–254.
[3] K.P. Hapgood, L. Farber, J.N. Michaels, Agglomeration of hydrophobic powders via solid spreading nucleation, Powder Technology 188 (2009) 248–254.
[4] P. Aussillous, D. Quere, Liquid marbles, Nature 411 (2001) 924–927.
[5] P. Aussillous, D. Quere, Properties of liquid marbles, Proceedings of Mathematical, Physical, and Engineering Sciences 462 (2006) 973–999.
[6] L. Forny, K. Saleh, I. Pezron, P. Guigon, L. Komunjer, Influence of mixing characteristics for water encapsulation by self-assembling hydrophobic silica nanoparticles, Powder Technology 189 (2009) 263–269 (special issue on granulation).
[7] P. McEleney, G.M. Walker, I.A. Larmour, S.E.J. Bell, Liquid marble formation using hydrophobic powders, Chemical Engineering Journal 147 (2009) 373–382.
[8] N. Eshtiaghi, S. Liu, K.P. Hapgood, Formation of hollow granules from liquid marbles: small scale experiments, Powder Technology, accepted for publication.
[9] P.S. Bhosale, M.V. Panchgnula, H.A. Stretz, Mechanically robust nanoparticle stabilized transparent liquid marbles, Applied Physics Letters 93 (2008) 034109/1–034109/3.
[10] M.A. Ansari, F. Stepanek, Formation of hollow core granules by fluid bed in-situ melt granulation: modelling and experiments, International Journal of Pharmaceutics 321 (2006) 108–118.
[11] L. Forny, I. Pezron, Kh. Saleh, Dry water: from physico-chemical aspects to process related parameters, in: Ninth International Symposium on Agglomeration and Fourth International Granulation Workshop, Sheffield, UK, 2009.
[12] D.E. Walton, C.J. Mumford, The morphology of spray-dried particles: the effect of process variables upon the morphology of spray-dried particles,

Transactions of the Institution of Chemical Engineers. Part A, Chemical Engineering Research & Design 77 (1999) 442–460.
[13] J.D. Litster, K.P. Hapgood, J.N. Michaels, A. Sims, M. Roberts, S.K. Kameneni, Scale-up of mixer granulators for effective liquid distribution, Powder Technology 124 (2002) 272–280.
[14] K.P. Hapgood, S.M. Iveson, et al., Granule rate processes, in: A. Salman, M. Hounslow, J.P.K. Seville (Eds.), Granulation, Handbook of Powder Technology, vol. 11, Elsevier Science, London, 2007.

G

Published Version of:

Phase retrieval tomography in the presence of noise

Phase retrieval tomography in the presence of noise

B. D. Arhatari,[1,a)] W. P. Gates,[2] N. Eshtiaghi,[3] and A. G. Peele[1]
[1]*Physics Department, La Trobe University, Victoria 3086, Australia*
[2]*Civil Engineering Department, Monash University, Victoria 3800, Australia*
[3]*Chemical Engineering Department, Monash University, Victoria 3800, Australia*

(Received 13 July 2009; accepted 4 January 2010; published online 4 February 2010)

We describe the use of single-plane phase retrieval tomography using a laboratory-based x-ray source, under conditions where the retrieval is not formally valid, to present images of the internal structure of an Aerosil granule and a hydrated bentonite gel. The technique provides phase images for samples that interact weakly with the x-ray beam. As the method is less affected by noise than an alternative two-plane phase retrieval method that is otherwise formally valid, object structure can be observed that would not otherwise be seen. We demonstrate our results for phase imaging in tomographic measurements. © *2010 American Institute of Physics*. [doi:10.1063/1.3298930]

I. INTRODUCTION

In conventional or absorption, tomography, the distribution of x-ray attenuation by the object can be calculated using filtered backprojection[1] from contact, or radiological, measurements of the intensity as modulated by the sample for a set of different projections through the sample.[2] This can become a problem for materials with low electron density due to the weak attenuation of x-rays where noise in the experimental system can swamp the signal due to absorption. In such cases it has been recognized that measurement of the propagated beam exiting a sample will exhibit contrast due to diffraction from the spatial distribution of the real and imaginary parts of the refractive index of a material. The imaginary part of the refractive index is colloquially associated with absorption imaging while the real part can dominate what is referred to phase contrast imaging.[3] Standard filtered backprojection methods[2] can be applied to the projections acquired in phase contrast imaging to provide a qualitative picture of the sample due, typically, to edge enhancement of the sample image.[4] *Phase contrast* methods have been widely used by synchrotron researchers due to the highly coherence of the source.[5] However, laboratory-based x-ray tube systems with sufficiently small source sizes have also been used to demonstrate phase contrast imaging.[6,7]

There are several approaches to phase retrieval currently used.[8–11] We consider here methods that rely solely on the free-space propagation of x-rays that exit a sample as this allows sample imaging with a minimum of additional equipment. There are also several algorithms that have been explored for free-space propagation[8–10] and the particular method chosen will depend on the imaging regime in which the data has been acquired. This will include factors such as the x-ray energy used, the properties of the sample and the experimental geometry. An important class of algorithms, in the context of free-space propagation methods, are those where the assumption is made that the sample is homogeneous.[10,12] For more general samples multiple planes of image data at different propagation distances must be collected in order to solve the phase retrieval problem. Under the assumption of sample homogeneity a single plane of data will typically suffice and hence these methods are often referred to as single-plane methods.

In phase retrieval tomography, the intensity data measured at the detector is subjected to a phase retrieval step that provides a map of the real part of the projected refractive index through the sample. Those projections can in turn be operated on using filtered backprojection to obtain the three-dimensional (3D) distribution.[8,13] Alternatively, algorithms have been demonstrated that combine the phase retrieval and filtered backprojection steps into a single operation that produce a 3D map of the sample distribution in the real part of the refractive index.[14–16] In some of that work,[16,17] it was shown that, although violating the assumption of homogeneity, useful results could still be obtained for nonhomogeneous samples when using a single-plane method.

In this paper, we will further explore the use of a particular single-plane approach under conditions that violate the assumption of sample homogeneity in the context of phase imaging using a laboratory source. We demonstrate that notwithstanding the lack of sample homogeneity high-quality images amenable for 3D sample segmentation can be obtained. In addition, due to the different noise characteristics of the single-plane method compared to some multiple-plane methods, more useful images can be obtained using the single-plane approach for nonhomogeneous samples. Some experimental results of this type of phase retrieval will be demonstrated.

II. PHASE RETRIEVAL, NOISE, AND HOMOGENEITY

A well-studied multiple-plane phase retrieval method[3] can be written as

$$\varphi(\boldsymbol{r}) = -k\nabla^{-2}\left(\nabla\cdot\left\{\frac{1}{I(\boldsymbol{r})}\nabla\left[\nabla^{-2}\frac{\partial I(\boldsymbol{r})}{\partial z}\right]\right\}\right), \tag{1}$$

where $k=2\pi/\lambda$, λ is the wavelength, $\boldsymbol{r}$ is the position in a plane, I is the intensity, z is the propagation distance, and φ is the retrieved phase. Note that in the Fourier domain, the Laplacian has a simple expression given by ∇^{-2}

[a)]Electronic mail: b.arhatari@latrobe.edu.au.

$=-\mathbb{F}^{-1}(1/\boldsymbol{u}^2)\mathbb{F}$ and the grad term by $\nabla=-\mathbb{F}^{-1}\boldsymbol{u}\mathbb{F}$ so that

$$\varphi(\boldsymbol{r}) = -k\mathbb{F}^{-1}\frac{1}{\boldsymbol{u}^2}\boldsymbol{u}\mathbb{F}\frac{1}{I(\boldsymbol{r})}\mathbb{F}^{-1}\boldsymbol{u}\frac{1}{\boldsymbol{u}^2}\mathbb{F}\frac{\partial I(\boldsymbol{r})}{\partial z}, \tag{2}$$

where $\mathbb{F}$ is the Fourier transform operator and $\boldsymbol{u}$ is the Fourier variable conjugate to the position coordinates. Two intensity images taken at different propagation distances separated by dz are needed for this method in order to obtain the intensity derivative, $\partial I/\partial z$, hence its classification as a multiple-plane, or in this case two-plane, scheme. It is readily seen that low spatial frequencies in the intensity derivative and in the filtered intensity derivative divided by the intensity will be enhanced by the 1/u filtering term that appears twice in the solution to the phase. Consequently, any noise signal that has power at low spatial frequencies will be enhanced in the retrieved phase.

The phase retrieval for a single-plane method is written[12,14] (in the weakly absorbing limit)

$$\varphi(\boldsymbol{r}) = -k\delta\mathbb{F}^{-1}\left(\frac{1}{\mu + z\delta\boldsymbol{u}^2}\mathbb{F}\left[\frac{I^z(\boldsymbol{r})}{I^{in}(\boldsymbol{r})} - 1\right]\right), \tag{3}$$

where μ and δ are the attenuation coefficient and the decrement of the real part of the refractive index, respectively, I^z is the intensity at a distance z and I^{in} is the intensity entering the sample. It can be seen here that low spatial frequencies will now be suppressed by the appearance of the absorption term, μ, in the denominator.

To better compare the noise performance of the two approaches, consider the case when μ varies insignificantly in $\boldsymbol{r}$ direction. So that $\partial\mu/\partial r \approx 0$ and Eq. (2) can be simplified as

$$\varphi(\boldsymbol{r}) = -\frac{k}{I}\mathbb{F}^{-1}\frac{1}{\boldsymbol{u}^2}\mathbb{F}\frac{\partial I(\boldsymbol{r})}{\partial z}. \tag{4}$$

Figure 1 shows the simulation result of applying the two- and single-plane phase retrieval of Eqs. (2) and (3) to a Gaussian shaped phase object with maximum phase shift of 4.7 rad. The noise is composed of random numbers with a standard deviation of a percentage of the mean intensity. We chose experimental and materials parameters for an experiment similar to those described below to illustrate the noise behavior here. The x-ray energy was 11.5 keV. We used a polyimide sample ($C_{22}H_{10}N_2O_4$) with $\delta=2.36\times10^{-6}$ and $\mu=355\ \mathrm{m}^{-1}$. The noise is 1%. The separation distance, dz, for the two-plane method and the propagation distance, z, for the one-plane method are shown in the first column of Fig. 1. The plots are taken horizontally in the middle of the field of view $1000\times1000\ \mu\mathrm{m}^2$ of each image. Figure 1 shows that the single-plane algorithm is more stable to noise and increasing distance can be used to reduce the noise effect in both single- and two-plane phase retrieval methods.

If we consider measured intensity that is entirely comprised of noise, $n(\boldsymbol{r})$, then it is readily shown[18] that the characteristic features in the retrieved phase obtained from Eq. (4) can be described by

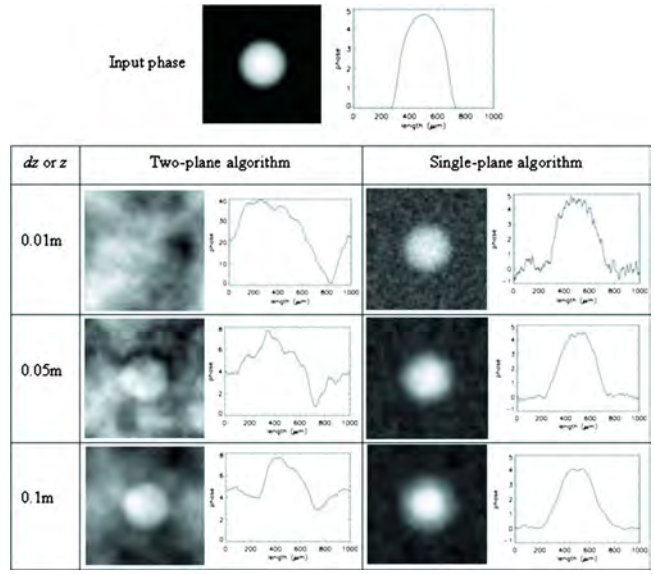

FIG. 1. (Color online) Simulation results of phase reconstruction of a phase object with 1% noise using the two-plane [Eq. (2)] and single-plane [Eq. (3)] algorithms, respectively. The input phase is shown on the top part. The distance shown is dz for the two-plane method and z for the single-plane method. For each method and distance an image of the retrieved phase and a lineout horizontally through the center showing magnitudes is shown. Additionally, it is also apparent that the same amount of noise will give less effect for the single-plane approach than for the two-plane approach.

$$\varphi^2_{\mathrm{noise}}(\boldsymbol{r}) = -\mathbb{F}^{-1}\frac{k\sqrt{2}}{I\cdot\boldsymbol{u}^2}\frac{\mathbb{F}n(\boldsymbol{r})}{dz}, \tag{5}$$

where the superscript symbol 2 denotes that the phase is retrieved using the two-plane method described in Eqs. (2) and (4). It can be similarly shown that the phase retrieved from a noise signal using the single-plane method of Eq. (3) is given by

$$\varphi^1_{\mathrm{noise}}(\boldsymbol{r}) = -\mathbb{F}^{-1}\frac{k\delta}{\mu + z\delta\boldsymbol{u}^2}\mathbb{F}n(\boldsymbol{r}), \tag{6}$$

where the superscript symbol 1 denotes the single-plane method.

For a noise distribution of pseudorandom numbers, $n(\boldsymbol{r})$, the Fourier transform, is also composed of random numbers. Equation (5) then shows that the distribution of spatial frequencies in the retrieved phase arising from noise is strongly peaked at the origin due to the effect of the division by $\boldsymbol{u}^2$. Thus this type of phase retrieval behaves as a low pass filter with a strong peak around the origin.[18] The result is that low frequency noise is amplified, which causes a low frequency contamination in the phase retrieved product, as confirmed in simulation results (Fig. 1 left column). Equation (5) also shows that a large separation distance between the two measurement planes, dz, is critical for reducing the magnitude of noise as can be seen from the lineouts in the left column of Fig. 1.

For the single-plane method Eq. (6) shows that the distribution of spatial frequencies in the retrieved phase arising from noise will have a similar distribution to the original random number noise, provided the attenuation term, μ, in the denominator, $\mu+z\delta\boldsymbol{u}^2$ dominates significantly. As the

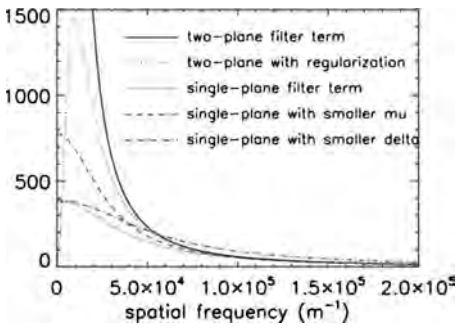

FIG. 2. Plot showing the filter term from Eq. (5), $k/(zu^2)$ (thick solid line) and from Eq. (6) $(k\delta)/(\mu+z\delta u^2)$ (thin solid line) as a function of spatial frequency. The dotted line shows Eq. (5) with a Tikhonov regularization parameter. The dashed and dashed-dotted lines are for Eq. (6) but where the attenuation term, μ, and the phase term, δ, have been decreased by a factor of 2, respectively.

propagation distance, z, increases the filter acts more like a low pass filter but where the attenuation component will always limit the amplification at the origin (Fig. 1 right column). It can also be seen from the lineouts in Fig. 1 that the magnitude of the retrieved phase due to noise for the single-plane method is, in this case, less than that for the two-plane method.

A Tikhonov regularization parameter, α, that handles division by $u=0$ in Eq. (5) can also act to provide noise suppression by substituting[19]

$$\frac{1}{u^2} \rightarrow \frac{u^2}{(u^2+\alpha^2)^2}. \tag{7}$$

Tikhonov regularization has been pointed out before in the context of the division by zero effect that the filter term introduces in various forms of phase retrieval[10] but it is worth considering here in relation to the effects of noise and the quality of the retrieval.

Figure 2 shows the comparison of the filter terms for Tikhonov regularization, for the two-plane approach and for the single-plane approach. For realistic parameters it can be seen that the single-plane approach will limit low frequency noise effects compared to the two-plane approach. Violating the homogeneity assumption will have a similar effect to using the wrong materials parameters, δ and μ in Eq. (3). The effect of this on the filter term can be seen in Fig. 2. It can be seen that even a gross change (factor of two in the absorption coefficient or δ value) has relatively little effect on the filter term in the phase retrieval. Additionally, while having the wrong δ and μ for nonhomogenous samples will give incorrect magnitudes in the retrieved phase. The relatively small errors at low frequency mean that, in general, the retrieved shape of an object will be preserved. On the other hand, varying the Tikhonov regularization parameter, α, for the two-plane approach, will suppress very low frequency terms as shown in Fig. 2 (dotted line). Increasing the value of the regularization parameter will shift the maximum peak to higher frequencies and will suppress more of the low frequency terms. Therefore, Tikhonov regularization is more likely to introduce artifacts into the retrieved shape of an object.

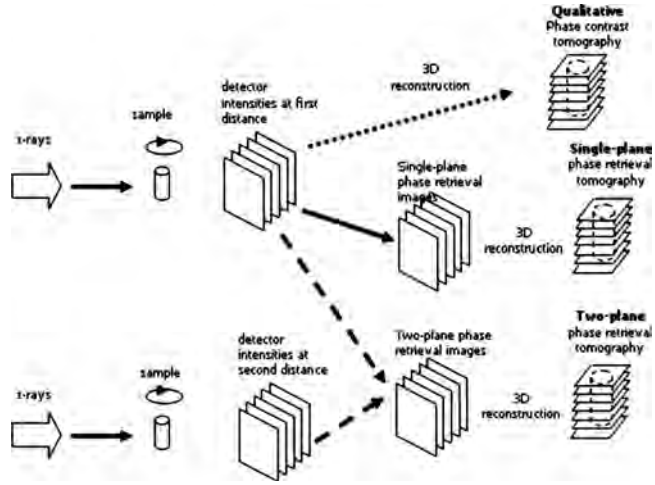

FIG. 3. Process diagram to produce qualitative-(dotted arrow), single-plane-(solid arrow) and two-plane-(dash arrow) tomography results. In qualitative phase tomography phase contrast images at one distance are collected and tomographically reconstructed to produce an edge-enhanced image. In single-plane phase tomography phase contrast images at one distance are collected, single-plane phase retrieval is applied (even though the requirement for sample homogeneity is violated) and the resulting phase images are tomographically reconstructed to produce a phase map of the sample. In two-plane phase tomography phase contrast images at two distances are collected, two-plane phase retrieval is applied and the resulting phase images are tomographically reconstructed to produce a phase map of the sample.

Overall, violating homogeneity is thus expected to have a relatively benign effect on the retrieved phase in the single-plane approach compared to the noise and shape effects seen in the two-plane approach.

III. EXPERIMENTAL RESULTS

We present here two case studies comparing qualitative phase contrast tomography (i.e., no phase retrieval), single-plane phase retrieval tomography where we violate the assumption of object homogeneity and two-plane phase retrieval tomography. The three different cases are represented schematically in Fig. 3.

The first sample is an aerosil granule representing a weakly absorbing nonhomogeneous sample. The second sample is a hydrated bentonite gel representing an absorbing and nonhomogeneous sample.

A. Aerosil granule: Nonhomogeneous sample

Aerosil R202 (Degussa Co. Germany) is the commercial name for highly hydrophobic fumed silica. Fumed silica is an amorphous compound of silicon dioxide (sand) produced in high-temperature processes. Aerosil R202 is a fine, very light, and white powder with a particle size of around 16 nm and is widely used in the cosmetic and pharmaceutical industries. Granulation of hydrophobic powders is frequently required in the pharmaceutical industry.[20] Granulation is the process of collecting particles together by creating bonds between them by using a binding agent.[21] The poor wetting properties of hydrophobic powders can create considerable difficulty in understanding, controlling, and trouble-shooting these industrial granulation processes.[20] Hollow granule for-

mation is a new way to solve the problematic granulating behavior of hydrophobic powders.[21] The dissolution rate of tablets due to the presence of hollow granules will be rapid and the drying will be fast due to the thin shell thickness. These granules also show good compressibility characteristics during the tablet pressing process. Hollow granules can be formed from hydrophobic powders by spreading powder around a template drop and the subsequent drying of the interior liquid to form a hollow granule. This process is known as *liquid marble* or *dry water*.[20]

This sample represents a weakly absorbing nonhomogeneous material. 3D x-ray images of a hollow Aerosil granule were obtained using the x-ray microcomputed tomography machine (Xradia Inc. USA), located in the Physics Department, La Trobe University. An x-ray source with a Tungsten target was operated at 40 kV and a current of 150 μA. The source size is about 8 μm. The illuminating spectrum with such a source is not monochromatic, as is assumed in the phase retrieval formulae discussed above. We used an effective wavelength matched to the phase and absorption components in the formula using the procedure developed by Arhatari *et al.*[22] This approach works best for samples that are weakly absorbing. Consequently, we have applied the approach here to both a weakly (this sample) and strongly absorbing sample (the second sample) to investigate whether the beneficial effect in noise suppression still applies when the sample is both inhomogeneous and strongly absorbing.

The granule was scanned by acquiring 361 projections taken at 0.5° rotational increments. The distance between the source and sample was $z_{ss}=100$ mm, and the sample detector distances were $z_{sd}=20$ and 125 mm. In this point projection geometry the phase retrieval formulae are modified by replacing distances with effective distance[12] calculated by $z_{eff}=(z_{ss}z_{sd})/(z_{ss}+z_{sd})=16.7$ mm and 55.6 mm and by scaling images by the magnification, which was here 1.2 and 2.25. The exposure time was 60 s for each projection. A charge coupled device camera coupled with a scintillator and a 20× objective lens was used as the detector. The best resolution for this setup was about 1.2 μm. A data set of intensity projections at the two propagation distances was obtained and the three types of tomographic reconstructions described in Fig. 3 were calculated.

Figure 4 shows the result for qualitative phase tomography. The edge-contrast characteristic of phase contrast imaging in Fig. 4 shows that the Aerosil granule is spherical and hollow with a diameter of about 200 μm. It has a thin (2–4 μm) shell and there are spongelike structures outside the granule of similar density to the shell. The images at 16.7 mm show better resolution due to the source size demagnification by the geometric setup. Blurring from the finite source size starts to influence the images taken at 55.6 mm, as indicated by the thicker and blurrier shell features.

Phase retrieval tomography becomes an important technique for the study of the 3D morphology and structure of hollow granules within Aerosil, as qualitative phase contrast tomography (Fig. 4) does not completely show the information available from the sample. Accordingly, we performed two-plane phase retrieval for each projected set of data (taken at 16.7 and 55.6 mm with a separation in effective propagation distance of 38.9 mm) thus producing phase images for each projection. The resulting 3D reconstruction is shown in Fig. 5 in the same cross section planes as for Fig. 4. Figure 5 shows similar spherical wall structure as the image in Fig. 4, albeit indicating thicker walls. This is expected as Fig. 5 shows a map of the phase and Fig. 4 essentially shows a map of the Laplacian of the phase. Of more interest is the suggestion of an object inside the spherical shell. However, the images are contaminated by low frequency noise artifacts, as indicated by a layer of clouds on the image and these are at a similar level of intensity to the putative object.

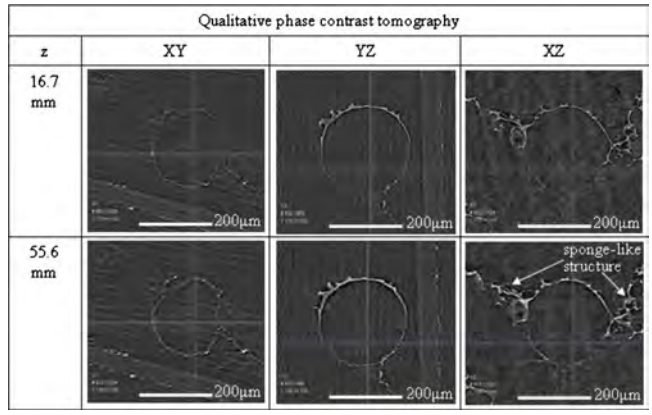

FIG. 4. (Color online) Qualitative phase contrast tomography of an Aerosil hollow granule, taken at effective propagation distances of 16.7 and 55.6 mm. Cross section planes XY, YZ, and XZ are indicated.

Finally we performed single-plane phase retrieval for each projected set of data at both propagation distances. We used the refractive index of silicon dioxide [density of 2.2 g/cm^3 at effective energy for the attenuation term of 10.5 keV and for the δ term of 11.5 keV (Ref. 22)] to calculate the phase in each projection. The resulting 3D reconstruction is shown in Fig. 6 in the same cross section planes as for Fig. 4. The single-plane algorithm clearly reveals better sample structure and also provides greater contrast. While the 16.7 mm result provides better high frequency contrast, it is more sensitive to noise, compared to the larger propagation distance of 55.6 mm as indicated by the presence of noise artifacts. This is in agreement with Fig. 1 (right column) that larger propagation distances will provide a lower noise magnitude in the retrieved result.

Of particular interest is that the putative object seen in Fig. 5 is clearly revealed in Fig. 6. The results of the single-plane phase retrieval (Fig. 6) are consistent with the features observed in a scanning electron microscopy (SEM) micro-

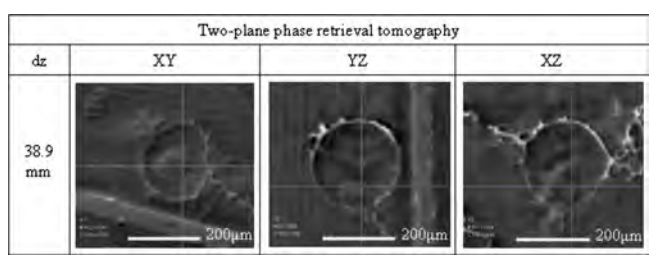

FIG. 5. (Color online) Phase retrieval tomography of an Aerosil hollow granule, based on the two-plane phase retrieval algorithm.

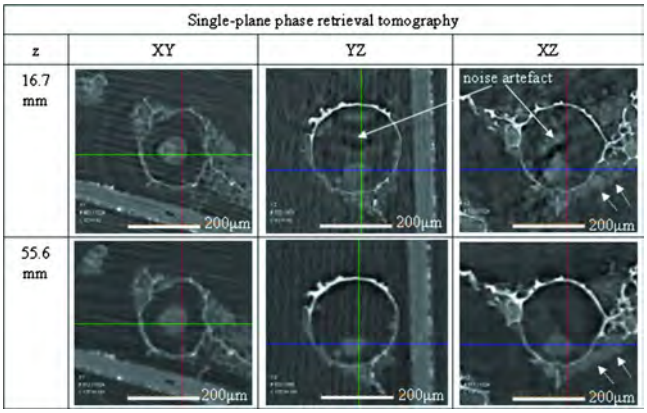

FIG. 6. (Color online) Single-plane phase retrieval tomography of an Aerosil hollow granule.

graph (Fig. 7). The micrograph shows multiple small, spherical attachments on the surface of the granule (indicated by arrows in Fig. 7). But it is not possible to tell from the micrograph whether the attachments are small hollow granules or small aggregates of the primary particles. The single-plane phase retrieval result confirms that the attachments (indicated by dot arrows in Fig. 6 right column) are not hollow. The bright outlines surrounding the granule shell indicates a denser wall structure formed from Aerosil and the binder (i.e., HPC-Hydroxyl Propyl Cellulose), while the weak white color is the agglomerated Aerosil. Aerosil powder tends to self-agglomerate to form a larger particle size between 1 and 50 μm. These facts and the images suggest that these small exterior attachments are aggregated Aerosil particles.[21]

This similarity between the external structures and the internal structures in Fig. 6 also suggests that the large spherical hollow granule contains smaller spherical aggregates of Aerosil powder. The internal aggregates may be formed during granulation or perhaps are related to erosion of the interior of the granule shell during drying, transportation, or other handling process.[21]

B. Hydrated bentonite gel: Nonweak absorption and nonhomogeneous sample

Bentonite is a naturally occurring material and is among the most important industrial minerals used in energy recovery, manufacturing, and environmental industries.[23] Bentonites are composed predominantly of the swelling clay mineral montmorillonite, but other minerals, such as quartz, feldspars, micas, and carbonates may also be present in the fine fraction. Swelling clay minerals like montmorillonite can take up several times their mass in water and swell to several times their volume, and when confined transmit water very slowly. Because of this, bentonites are useful as natural seals in dams, or as secondary barriers in landfills.[23] An important issue in the use of bentonites as hydraulic barriers is salinity induced loss of gel structure. When fully hydrated sodium saturated montmorillonite forms a gel which strongly attenuates water movement. However, because montmorillonite surfaces interact strongly with solutes, when exposed to saline water, or water containing a large proportion of divalent cations,[24] the gel structure collapses forming micron-sized pores which are not as effective at retaining water. While various spectroscopic and physical measures can be correlated with changes in the pore sizes, there are few direct measures available. Electron microscopy techniques have been developed[25] but are time consuming and can be subject to experimental artifact or beam damage. Scanning transmission x-ray spectromicroscopy[26] methods are useful for gaining high resolution images, but suffer from difficulty in gaining experimentally relevant information. For example, samples have to be of submicron to a few microns thick to provide quantitative results, providing obvious difficulty in studying gel structures. Thus, it is expected that 3D tomography can provide a visual indication of the changes in gel structure occurring when an intact bentonite sample is subjected to wetting by different liquids.

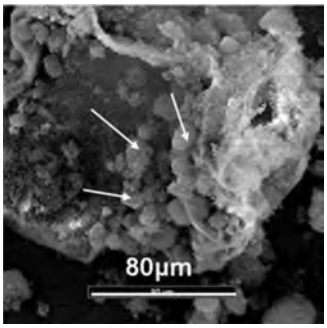

FIG. 7. SEM micrograph image of Aerosil granule attached by multiple small, spherical particles (Ref. 21).

A processed sodium bentonite powder from Miles, Queensland, Australia, (marketed as Trugel® by UniMin Australia) was used. We immersed a sample of bentonite within solutions of deionised water of 0.2*M* $CaCl_2$ to determine the effectiveness of 3D tomography to differentiate differences in pore features within the clay gels. In its bulk form, essentially all of the bentonite passes a 100 μm sieve, but this is composed of a range of particle sizes and different mineral phases.[27] The bulk material is composed of montmorillonite (69%), quartz (15%), opaline silica (7%), feldspar (8%), and minor amounts ($\sim$1%) of mica, zeolite, gypsum, and anatase. Importantly, the <0.2 μm (200 nm) fraction, which makes up 50% of the bulk material, is 97% montmorillonite with a small amount of opaline silica.

The clay-gel sample immersed in $CaCl_2$ was chosen to represent both a nonhomogeneous and absorbing sample. A similar setup as described above was used, except that a tube voltage of 100 kV and exposure time of 80 s was used for each projection. The number of projections acquired for this scan was 721 taken at 0.25° increments. A data set of intensity projections, at the same two effective propagation distances as before were obtained and the three types of tomographic reconstructions described in Fig. 3 were calculated.

Figure 8 shows the result for qualitative phase tomography. From the slice image, we can see that the sample consists mainly of particles within the 5–20 μm size range. Some of them are much larger, on the order of 200 μm, as seen in upper right of the YZ plane. As is typical for quali-

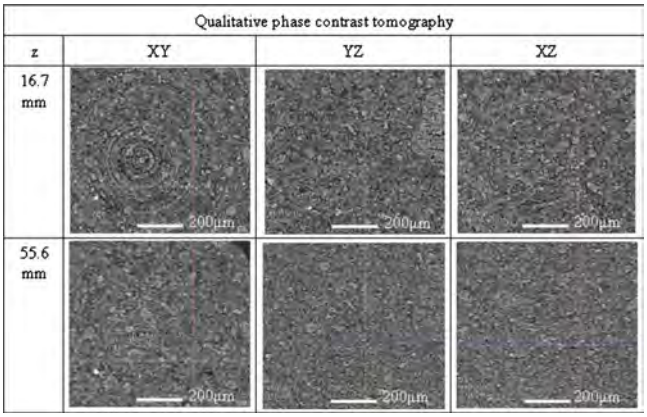

FIG. 8. (Color online) Qualitative phase contrast tomography of a hydrated bentonite gel immersed in 0.2*M* $CaCl_2$, taken at propagation distances of 16.7 and 55.6 mm. Cross section planes XY, YZ, and XZ are indicated.

tative tomography, edge enhancement from all the particles is well defined and the images at 16.7 mm have better resolution than those at 55.6 mm.

We performed two-plane phase retrieval for each projected set of data (taken at 16.7 and 55.6 mm with a separation in effective propagation distance of 38.9 mm) thus producing phase images for each projection. The resulting 3D reconstruction is shown in Fig. 9 in the same cross section planes as for Fig. 8. However, the images shown in Fig. 9 have very poor contrast, because the low frequency artifacts completely dominate the result.

Finally we performed single-plane phase retrieval for each projected set of data at both propagation distances. We used the refractive index of clay (with density of 1.3 g/cm^3) to calculate the phase in each projection. The resulting 3D reconstruction is shown in Fig. 10 in the same cross section planes as for Fig. 8. Notwithstanding the violation of weak absorption (as well as homogeneity) it can be seen that the resulting images provide well resolved and high contrast features that can potentially be used to segment the different regions of the image. As observed in the qualitative phase analysis, immersion of the bentonite in 0.2*M* $CaCl_2$ caused flocculation of the gel phase (best observed at the 55.6 mm distance in Fig. 10). The white specks (circled in the XY view) are most likely anatase grains, whereas the intermediate density particles (circled in the YZ view) are quartz grains. Individual flocs of clay are observed, as these are large incompletely hydrated particles, and the flocs are often separated by mineral free void spaces (represented in black). This result is expected for a material consisting of a mixture

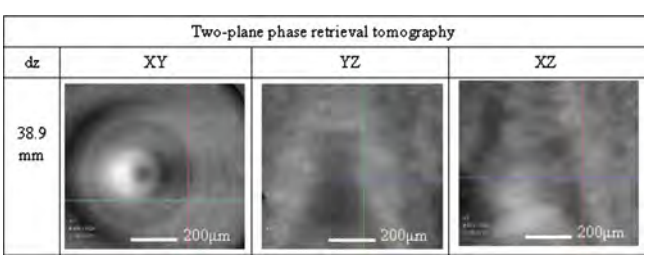

FIG. 9. (Color online) Two-plane phase retrieval tomography of a hydrated bentonite gel immersed in 0.2*M* $CaCl_2$.

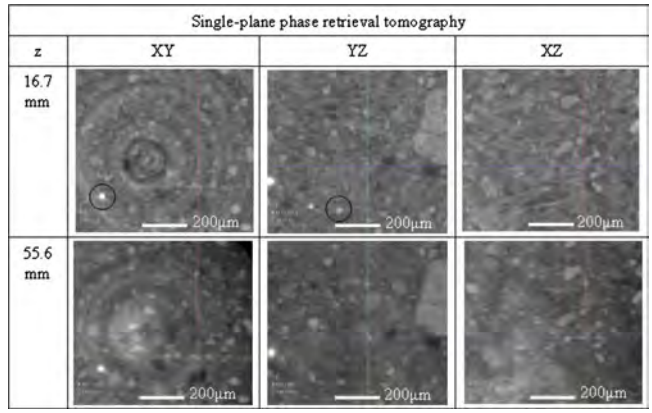

FIG. 10. (Color online) Single-plane phase retrieval tomography of a hydrated bentonite gel immersed in 0.2*M* $CaCl_2$.

of nonswelling dense mineral phases (e.g., quartz, feldspar, and other impurities) dispersed within a matrix composed predominantly of partially swollen and flocculated montmorillonite. The large particle at the upper right of the YZ plane shows a distinct boundary with the matrix material and has a greater density than most of the bentonite gel but also lower density than the many smaller quartz particles (e.g., circled particle in the YZ image). We interpret this particle as being an incompletely hydrated bentonite particle, as it is too large to be a single grain of any accessory mineral. These features are not observed in images of bentonite when it is immersed in deionised water.

IV. CONCLUSION

Single-plane phase retrieval tomography appears to be a powerful technique that can provide useful phase images of nonhomogeneous and either weakly or strongly absorbing materials, due to its nonsensitivity to noise. In particular, we have shown that these results can be successfully carried out using an x-ray laboratory-based source. The resulting images are far cleaner in terms of noise artifacts than the same data analyzed using the (formally valid) two-plane retrieval method. While such results are not quantitative due to the violations of the assumptions used in the methods the errors appear to be relatively small and well behaved in the sense that they do not produce image artifacts. Accordingly, data produced using this method will be very useful in segmenting samples into regions of different composition.

ACKNOWLEDGMENTS

The authors acknowledge the support of the Australian Research Council through the Centre of Excellence for Coherent X-ray Science and by an APDI fellowship (BDA), and Monash University for an Engineering Faculty New Staff Research Grant (WPG).

[1]G. T. Herman, *Image Reconstruction from Projections* (Springer-Verlag, Berlin, 1979).
[2]A. C. Kak and M. Slaney, *Principles of Computerized Tomographic Imaging* (IEEE, New York, 1988).
[3]D. M. Paganin, *Coherent X-Ray Optics* (Oxford University Press, New York, 2006).
[4]S. C. Mayo, T. J. Davis, T. E. Gureyev, P. R. Miller, D. Paganin, A.

Pogany, A. W. Stevenson, and S. W. Wilkins, Opt. Express **11**, 2289 (2003).
[5]A. Snigirev, I. Snigreva, V. Kohn, S. Kuznetsov, and I. Schelokov, Rev. Sci. Instrum. **66**, 5486 (1995).
[6]S. W. Wilkins, T. E. Gureyev, D. Gao, A. Pogany, and A. W. Stevenson, Nature (London) **384**, 335 (1996).
[7]B. D. Arhatari, A. P. Mancuso, A. G. Peele, and K. A. Nugent, Rev. Sci. Instrum. **75**, 5271 (2004).
[8]P. Cloetens, W. Ludwig, J. Baruchel, D. Van Dijck, J. Van Landuijt, J. Guigay, and M. Schlenker, Appl. Phys. Lett. **75**, 2912 (1999).
[9]K. A. Nugent, T. E. Gureyev, D. F. Cookson, D. Paganin, and Z. Barnea, Phys. Rev. Lett. **77**, 2961 (1996).
[10]L. D. Turner, A. G. Peele, B. Dhal, A. P. Mancuso, R. E. Scholten, C. Q. Tran, K. A. Nugent, J. P. Hayes, and D. Paterson, Opt. Express **12**, 2960 (2004).
[11]J. N. Clark, G. J. Williams, H. M. Quiney, L. Whitehead, M. D. d. Jonge, E. Hanssen, M. Altissimo, K. A. Nugent, and A. G. Peele, Opt. Express **16**, 3342 (2008).
[12]D. Paganin, S. Mayo, T. E. Gureyev, P. R. Miller, and S. W. Wilkins, J. Microsc. (Paris) **206**, 33 (2002).
[13]P. J. McMahon, A. G. Peele, D. Paterson, J. J. A. Lin, T. H. K. Irving, I. McNulty, and K. A. Nugent, Opt. Commun. **217**, 53 (2003).
[14]B. D. Arhatari, F. De Carlo, and A. G. Peele, Rev. Sci. Instrum. **78**, 053701 (2007).
[15]A. V. Bronnikov, Opt. Commun. **171**, 239 (1999).
[16]A. Groso, R. Abela, and M. Stampanoni, Opt. Express **14**, 8103 (2006).
[17]T. Weitkamp, A. Diaz, C. David, F. Pfeiffer, M. Stampanoni, P. Cloetens, and E. Ziegler, Opt. Express **13**, 6296 (2005).
[18]D. Paganin, A. Barty, P. J. McMahon, and K. A. Nugent, J. Microsc. **214**, 51 (2004).
[19]A. N. Tikhonov, Sov. Math. Dokl. **4**, 1035 (1963).
[20]K. P. Hapgood and B. Khanmohammadi, Powder Technol. **189**, 253 (2009).
[21]N. Eshtiaghi, B. D. Arhatari, and K. P. Hapgood, Adv. Powder Technol. **20**(6), 558 (2009).
[22]B. D. Arhatari, K. Hannah, E. Balaur, and A. G. Peele, Opt. Express **16**, 19950 (2008).
[23]W. P. Gates, A. Bouazza, and G. J. Churchman, Elements **5**(2), 105 (2009).
[24]D. A. Laird, Appl. Clay Sci. **34**, 74 (2006).
[25]D. Tessier and G. Pedro, Proceedings of the International Clay Conference, Denver, 1987 (unpublised).
[26]B. P. Tonner, T. Droubay, J. Denlinger, W. Meyer-Ilse, T. Warwick, J. Rothe, E. Kneedler, K. Pecher, K. Nealson, and T. Grundl, Surf. Interface Anal. **27**, 247 (1999).
[27]W. P. Gates, J. S. Anderson, M. D. Raven, and G. J. Churchman, Appl. Clay Sci. **20**, 189 (2002).